Thin Film Formation by Surface-Initiated ARGET Polymerization and UV-Hydrosilylation Methods

By

Bradley Alan Baker

Dissertation

Submitted to the Faculty of the

Graduate School of Vanderbilt University

in partial fulfillment of the requirements

for the degree of

DOCTOR OF PHILOSOPHY

in

Chemical Engineering

May 31, 2021

Nashville, Tennessee

Approved:

Paul E. Laibinis, Ph.D.

G. Kane Jennings, Ph.D.

Carlos Silvera-Batista, Ph.D.

William H. Fissell, M.D.

To the family and friends

who made this journey possible.

and

In memory of my Mother,

An unending source of knowledge, encouragement, and inspiration.

ACKNOWLEDGEMENTS

As long, winding roads oft are those less travelled, and yet those oft most enjoyed, such was the path that led me to the completion of this Ph.D. in Chemical Engineering. This road was paved by the many people I have come to know throughout my life and also my time in the Chemical and Biomolecular Engineering Department at Vanderbilt University. These people must be acknowledged for all they have contributed to helping me get to this point in my life.

I would like to offer my sincerest gratitude to my advisor, Dr. Paul E. Laibinis for his tremendous support, understanding, guidance, and insight throughout my time at Vanderbilt. His deep and sincere interest in all of the many facets and subtleties of my research helped challenge me to become a better thinker and researcher. I would like to further thank him for the academic freedom he both provided and encouraged in regards to exploring some of my ideas that were not a part of my initial research plans; I truly believe the work that came out of these opportunities was some of my best. I would like to thank Dr. G. Kane Jennings, who welcomed me into his research group's office, lab space, and weekly research meetings. His insight and support were invaluable in completing this journey. I would like to thank Dr. William H. Fissell for the opportunity to work on part of the artificial implantable kidney, a wonderfully challenging and incredibly impactful project. I would also like to thank Dr. Carlos Silvera-Batista for his positive outlook, encouragement, and the thorough introduction to colloidal science.

Throughout my time in the Chemical and Biomolecular Engineering Department here at Vanderbilt, I was privileged to work alongside of many wonderful labmates. They helped me reach the completion of this journey through their friendship, support, and wealth of scientific and experimental expertise. Specifically, I would like to thank Ian Njoroge, Xuanli Deng, Faustin Mwambutsa, Josh Passantino, Liudmyla Prozorovska, Marc Nabhan, and Kody Wolfe of the Jennings group who I have shared an office with over the past nearly six years. I would also like to thank Rabeb Layouni for the

TABLE OF CONTENTS

Page

List of Tables

List of Figures

Chapter I

INTRODUCTION:

Surface modification strategies involving polymer or molecular coatings provide the ability to tailor the interfacial properties of surfaces. The incorporation of specific moieties within these films allows control of these surface properties. Researchers have used polymer[1–4] and monolayer[5–9] coatings on flat, porous, and particle surfaces to achieve a myriad of functions including anti-corrosion barriers, nanoparticle stabilization, anti-fouling and anti-bacterial activity, chemical and bio-sensing abilities, selective adsorption, stimuli response (i.e. "smart" coatings), adhesion promoters, and wettability and frictional control.[1–9]

Surface-initiated polymerization is an especially useful method for producing robust, covalently-bound polymer surface coatings. This approach has seen wide use in modifying surfaces of various geometries (planar and porous substrates, nanoparticles, fibers, etc.) and on both organic and inorganic substrates.[2–4,10,11] In a typical surface-initiated polymerization scheme, the substrate is first modified to expose an appropriate initiator group, taking into account both the chemistry needed to stably attach this initiator-containing molecule to the substrate and also the chemistry needed to effectively initiate the desired polymerization reaction.[10,11] Next, the polymerization is conducted with the chosen monomer(s) to incorporate desired functionalities into the coatings and thus control their properties. Living polymerization reactions such as ring-opening polymerization (ROP), anionic polymerization, cationic polymerization, ring-opening metathesis polymerization (ROMP), reversible addition–fragmentation chain transfer polymerization (RAFT), atom transfer radical polymerization (ATRP), and activators regenerated by electron transfer polymerization (ARGET), among others, have been demonstrated for effectively modifying surfaces with grafted polymer films.[10–14]

Self-assembled monolayers (SAMs) are another widely used strategy for modifying substrates and tailoring their interfacial properties.[6,7] Molecules used for SAMs typically contain a headgroup that interacts/orients toward the substrate surface, and a tail group selected to provide the coating's function.[7] Common headgroup-substrate systems for these SAMs include thiols on gold, and chloro- and alkoxy-silanes on SiO_2, and possess tail groups that can be polar or non-polar depending on intended application and chemical compatibility.[6,7] These coatings form spontaneously due to favorable chemical interactions between the substrate and functional groups present in the assembling molecules. The resulting oriented films are often densely packed, have thicknesses defined by the extended length of the adsorbing molecule (i.e., a few nanometers or less), and can express a range of chemical functionality at their outer surfaces.[8] These changes in interfacial properties occur with minimal increases in thickness.[8] As with films formed by surface-initiated polymerization, SAMs can be applied to a large variety of substrates and geometries. In addition, SAMs have also found extensive use for 2-dimensional surface patterning and 3-dimensional nanofabrication.[5–9]

Surface-Initiated Polymerization by ATRP and ARGET

First reported by Matyjaszewski and Sawamoto in 1995 as a broadly useful living polymerization process for synthesizing bulk polymers, atom-transfer radical polymerization (ATRP) has quickly become one of the most commonly used approaches for generating surface-initiated polymer films.[2,3,11,13–15] ATRP is classified as a "controlled" radical polymerization due to its low likelihood of termination events which, as a result, leads to its favorable formation of well-defined polymers with low polydispersities. When conducted from a surface, ATRP offers the possibility for producing grafted polymer brushes of similar chain lengths.[11,13,14]

In a typical ATRP reaction (see Figure 1.1a), a transition-metal/ligand catalyst species reversibly activates/deactivates growing polymer chains by homolytically cleaving and reforming carbon-halide bonds at the ends of growing chains or initiator groups.[2,11,14] By this reversible sequestering process, the

deactivated or "dormant" polymer chains reduce the radical concentration of the growing polymer chains, thus dramatically decreasing the likelihood of bimolecular radical-radical termination events and afford ATRP's classification as a "controlled" radical polymerization reaction.[10]

ATRP from a surface employs three architectural considerations: the chemical initiator, its attachment to a surface, and the monomer that will form the polymer, each providing broad flexibility as detailed below. For example, a variety of chemical species — often benzyl-halides, α-halo esters, and other alkyl-halides — can be used for ATRP initiation.[10] . For surface-initiated polymerization, numerous attachment chemistries are available that allow the modification of most substrate materials to expose these initiating moieties.[10] For the reaction, typical ATRP monomers consist of olefins adjacent to a radical-stabilizing group such as in acrylates, methacrylates, acrylamides, methacrylamides, vinylimidazoles, and styrenes that each offer many chemical options for introducing other constituents.[3,10] Further contributing to its widespread adoption is that ATRP shows tremendous chemical compatibility toward numerous functional groups that can be present in the monomer.[16] This tolerance allows direct formation of bulk and grafted polymers of broad chemical constituencies and provides access to many functional polymer surfaces.[16]
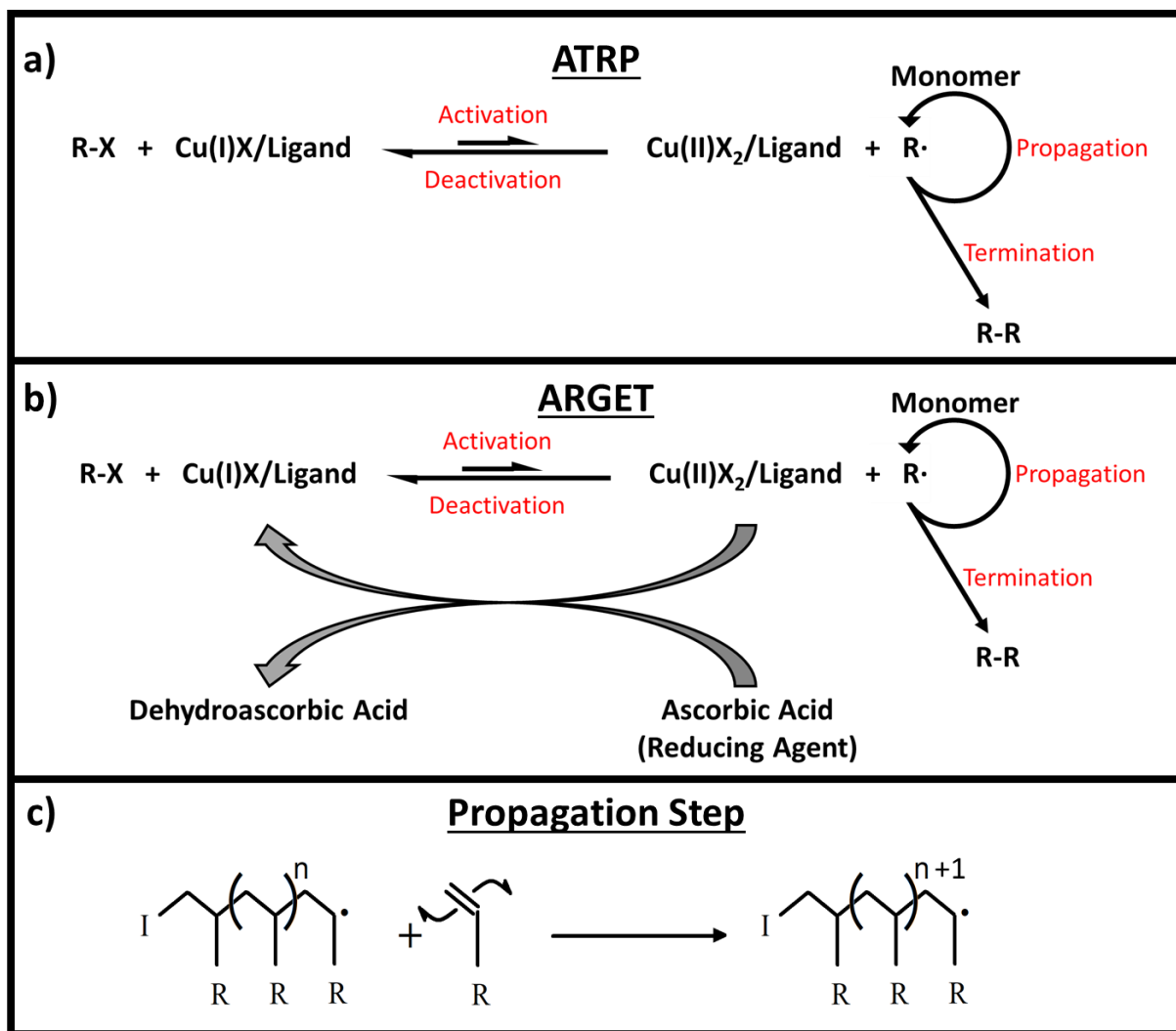
Figure 1.1. a) The mechanism for a typical ATRP reaction. The Cu(I)X species reversibly moderates the concentration of the propagating R• chain in order to limit termination reactions. b) The mechanism for ARGET polymerization. This variation of ATRP includes a reducing agent to produce/regenerate the catalyst species. c) The propagation reaction in ATRP and ARGET involving a radical with an olefinic monomer.

4

A significant operational drawback of ATRP is that this polymerization reaction requires rigorous deoxygenation as the required active catalytic Cu(I) species shown in Figure 1.1a readily oxidizes and forms an inactive Cu(II) state. Without the Cu(I) species, the polymerization reaction cannot progress.[16] As an alternative, Matyjaszewski and coworkers in 2006 reported their development of ARGET polymerization as an oxygen-tolerant variation of ATRP, that proceeded even in the presence of air.[16] In ARGET polymerization, a reducing agent such as ascorbic acid is used to form reactive Cu(I) species from air-stable Cu(II) precursors and maintain their activity throughout the polymerization reaction, as shown in Figure 1.1b.[10] With its removed requirement of stringent deoxygenation and its accommodation of aerobic conditions, ARGET provides a convenient alternative to traditional ATRP. Despite its operational ease-of-use, reports using ARGET in a surface-initiated manner for generating grafted polymers are limited compared to ATRP.[10,17,18]

The Need for Antifouling Surfaces

When synthetic surfaces come into contact with physiological fluids, the unwanted spontaneous adsorption of biological molecules present in these fluids (i.e. biofouling) will often occur. This non-specific adsorption often results due to favorable interactions between the surface and adsorbing species and/or high interfacial energies that can be present when a solid contacts water. This fouling represents a major obstacle in applications where the adsorption of unwanted molecules impedes the function of the substrate/device or it serves to nucleate further aggregating events (i.e., thrombosis). For applications ranging from medical implants and to devices that are exposed to marine environments, coatings are needed that can provide antifouling properties and retain them throughout the lifespan of the device to which they are attached.[17–25] Traditionally, coatings exposing polyethylene glycol (PEG) chains (as shown in Figure 1.2) have seen broad use in the prevention of fouling. The PEG chains interact with water forming a hydration layer that excludes direct contact between proteins and other species in the contacting phase with the surface, thereby reducing non-specific adsorption.[26] However, despite the prevalence of these coatings,

their deterioration under physiological conditions plagues the effectiveness of PEG coatings for long-term use, as discussed later in this chapter.[18,27–33] My research investigated various strategies for producing more robust, chemically-grafted antifouling polymer and monolayers coatings for devices such as these.
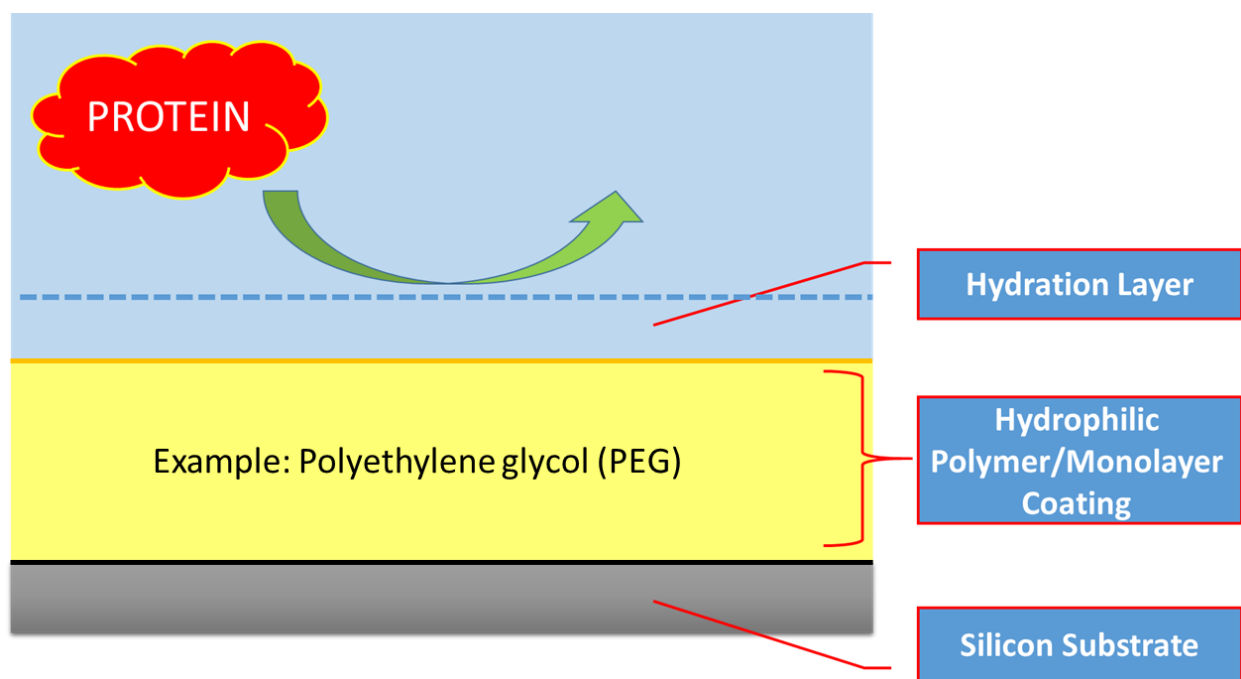
Figure 1.2. PEG-functionalization can prevent protein adsorption (i.e. fouling) to surfaces due to the ability of PEG to form a hydration layer. With the hydration layer presenting properties resembling the bulk water, the surface no longer provides sites for protein adsorption.

A targeted application for these more stable, fouling-resistant coatings is for an artificial implantable kidney (AIK) device currently being developed by our collaborator Dr. William Fissell at VUMC as a replacement for traditional dialysis treatments. The separation system within the AIK device, shown in Figure 1.3, is fabricated using microelectromechanical systems technology to produce silicon membranes composed of arrays of nanoslit pores with the needed geometry for effective hemofiltration.[19–21] Briefly, a multi-step series of sacrificial SiO_2 growth, polysilicon deposition, and etching steps is performed to manufacture the needed silicon nanofiltration membranes, where uniform slit shaped

nanoscale pores having <1% variation across a wafer can be prepared.[34] The development of an artificial implantable kidney with long-term operating ability would offer the hope of largely autonomous self-care at home to patients living with end-stage renal disease. The successful implementation of such a device would not only improve the quality of life but also greatly reduce the healthcare costs for patients that currently rely on traditional treatments.[21] The need for such a device is great as the United States Renal Data System reported that 444,337 US patients depended on dialysis at an annual cost of $88,195 per patient in 2015, equaling roughly $40 billion — 1% of the United States' federal budget — that year alone.[35]
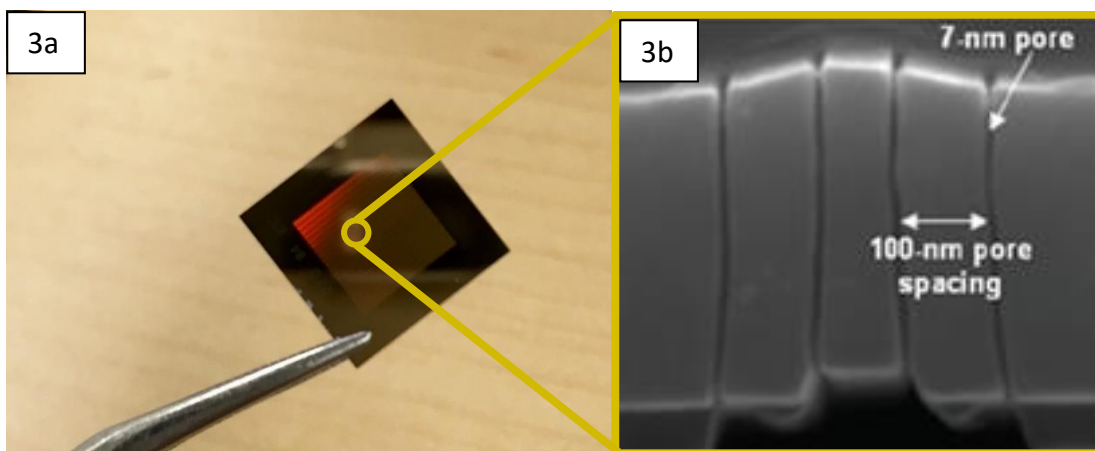
Figure 1.3. a) Optical image of a silicon nanopore membrane developed by the Fissell group at VUMC for as the sieving unit for an artificial implantable kidney device. b) Scanning electron microscopy image displaying the pore structure of these membranes.

To maintain needed permeability rates and selectivities for patients with end stage renal disease, fouling-resistance by the nanoslit membranes remains an obstacle for achieving long-term reliable operation by these AIK devices. In general, a key challenge in developing many implantable medical devices is maintaining their long-term operation during the regular exposure of their surfaces to tissues and blood. These conditions regularly lead to unwanted biofouling. For continuous application, such as for the AIK and other medical implants, coatings are crucially needed that provide antifouling properties and retain them throughout the lifespan of the implanted devices. My research focused on developing coatings

designed to offer sufficient fouling resistance and attachment chemistries that offered both synthetic ease and enhanced stability for improve their long-term viability within such devices.

Compounding the challenge of stability, as the device's pores utilize nanoscale geometries for their operation, any coatings present within the pore structures must be sufficiently thin as to not occlude the pores. Due to the geometry of these nanoporous devices, I had to evaluated how thin these coatings can be made while maintaining their stability and antifouling function. The methods developed in my research have allowed me to produce well-defined coatings with nanometer-scale thickness, a quality needed considering the confined nanopores of the AIK device. Figure 1.4 illustrates the desired properties of the coatings pursued during this dissertation.
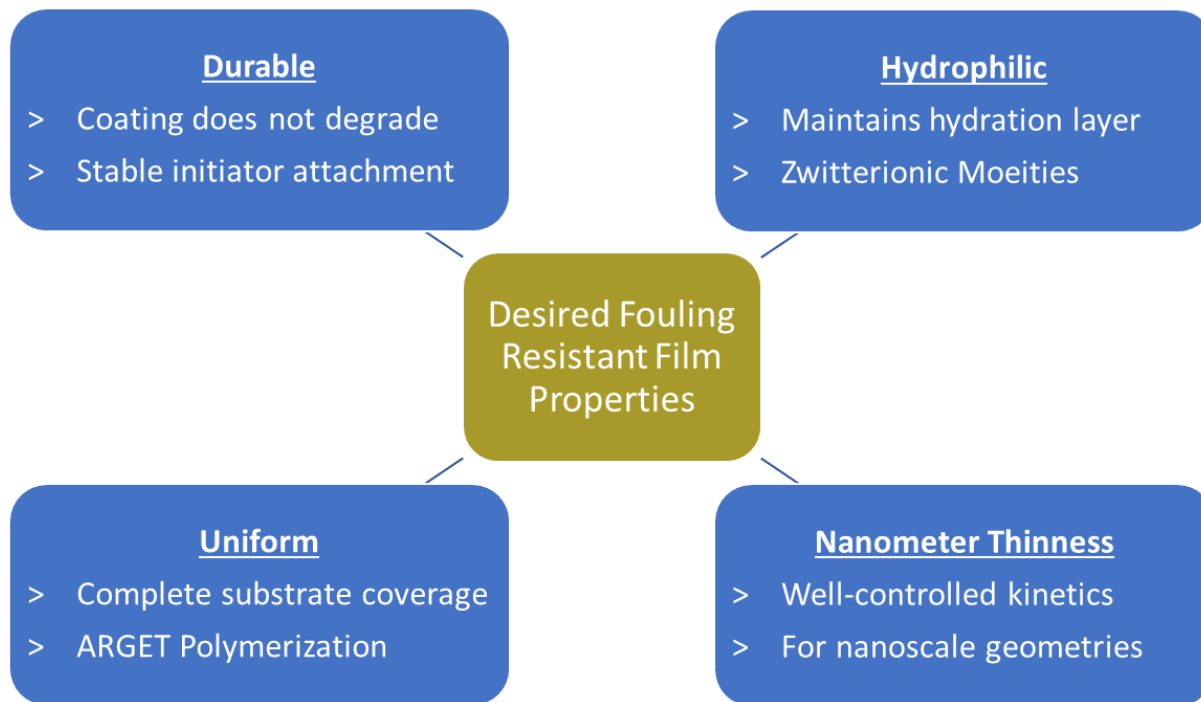
Figure 1.4. The properties of the fouling resistant films pursued in this research.

Fouling-Resistant Zwitterionic Polymer Films

The nanopore membranes currently used by the Fissell group are often surface-modified with a polyethylene glycol (PEG) coating to prevent fouling. Specifically, these coatings are composed of a monolayer of molecules referred to as "PEGsilane" consisting of 6-9 oxyethylene repeat units covalently attached to the silicon substrate via a siloxane linkage. While PEG coatings have seen broad use as anti-fouling coatings, they can deteriorate under physiological conditions via oxidation of PEG's polyether backbone or by hydrolysis of the siloxane (Si-O-Si) attachment.[18,27–33] For example, Sharma et al. observed a 50% loss in film thickness of one of their siloxane-bound PEG films after 3-4 weeks in PBS containing 5% CO_2 at 37 °C that simulated an in vivo environment.[27,28,30] Such degradation would be unacceptable for an implanted device. The degradation of PEG coatings may result from various failure modes. First, degradation of the PEG backbone itself has been reported from oxidation, as occurs for polyethers.[18,32,33] Additionally, PEG and other polymer coatings attached to surfaces via siloxane linkages are known to detach from their substrates in aqueous environments by hydrolysis.[10,17,36] To address the first issue, researchers hope to develop other potential non-fouling surface coatings using polar polymers with more stable backbones that avoid the possibility of polyether degradation.[36]

My research aims to develop antifouling coatings that employ zwitterionic functionality in place of PEGs. Surface coatings expressing zwitterionic functionality are of particular interest as they have been shown to exhibit exceptional antifouling properties.[17,18,36] These coatings are hypothesized to offer this exceptional antifouling property via formation of electrostatically-bound hydration layers (see Figure 1.5).[26,37] The strong binding of hydration layers make zwitterionic coatings more promising than many current surface modification schemes that similarly rely on hydration layers albeit by weaker hydrogen-bonding interactions. For example, Zhang et al. demonstrated that the zwitterionic polymers poly(sulfobetaine methacrylate) (pSBMA) and poly(carboxybetaine methacrylate) (pCBMA) can be grafted from the surfaces of glass and silicon via ATRP.[37] The resulting polymers exhibited high resistance to protein adsorption and low platelet adhesion when present at higher grafting densities. [10,37,38]
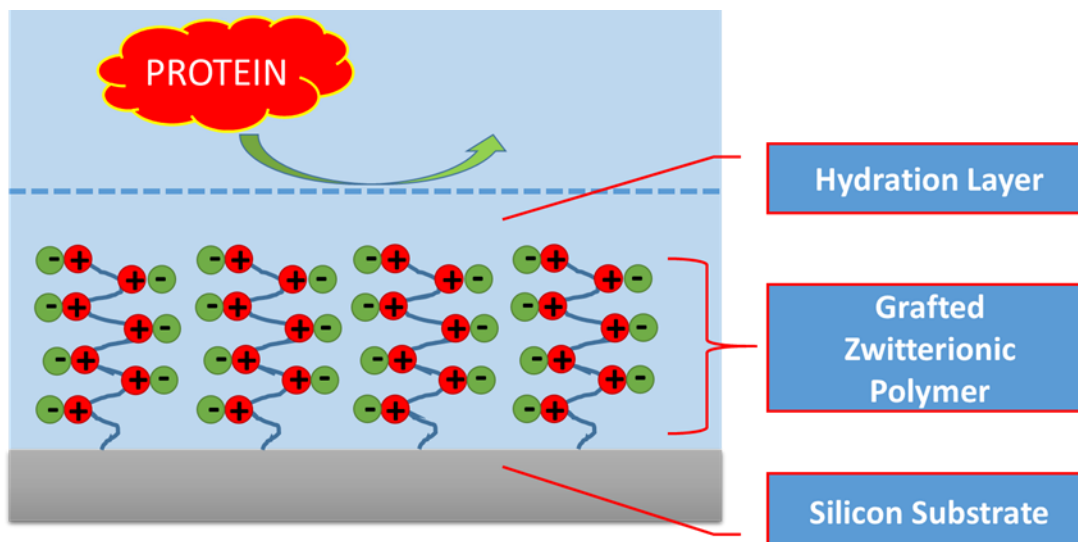
Figure 1.5. Hydration layer bound to surface via electrostatic interaction with grafted zwitterionic polymer coating.

My research involving surface-initiated polymerization primarily focused on the grafting of pSBMA via ARGET polymerization. Although well-controlled growth of pSBMA via ATRP has been reported,[10] such controlled growth of pSBMA via ARGET had not. In addition to SBMA, I also studied other zwitterionic monomers including sulfobetaine methacylamide (SBMAA), sulfobetaine acrylate (SBA), and sulfobetaine vinylimidazole (SBVI). Complementing these polymers, monolayers including g-PEGsilane and a zwitterionic silane were also grafted from silicon slides and characterized for comparison. The antifouling properties of the films were characterized via fluorescence microscopy, testing for the non-specific adsorption of FITC-labeled albumin. A goal was to identify the films that show high fouling resistance and then later graft them from the nanopore silicon filtration membranes being developed for the artificial kidney. Once again, the membranes include nanometer-sized pores, and the thickness of the surface coatings is highly important. As such, I investigated how thin these coatings could be made while retaining their ability to function as antifouling coatings. The zwitterionic polymer coatings I have produced using ARGET polymerization exhibited excellent fouling resistances with film thicknesses as low as 4-5 nm. Ultimately, ideal films should exhibit tightly-bound hydration layers via their zwitterionic moieties, complete substrate coverage with minimal defects, and minimal impedance of through-pore transport.
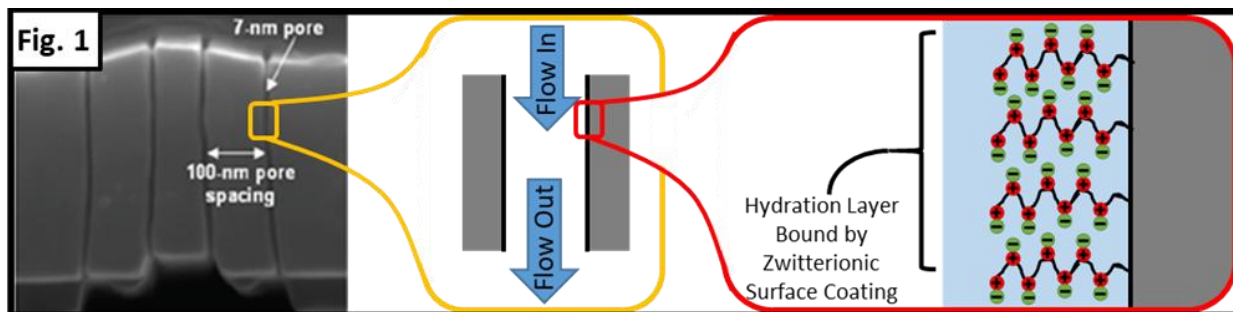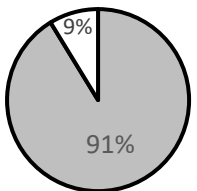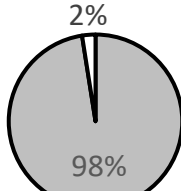
Figure 1.6. Illustration depicts structure of silicon nanopore membranes and the need for thinness of the zwitterionic polymer coatings on the pore walls.

A 2017 review by Zoppe et al. systematically catalogued the grafting of approximately 300 different monomers by various polymerization techniques including both ARGET and ATRP.[10] Table 1.1 summarizes commonly grafted polymers included in this database-like review, listing how many citations the review included for each monomer by a particular polymerization method.[10] The table shows the disparity in the number of papers employing ARGET as compared to ATRP. In this comprehensive review, only 13 of the approximately 300 listed monomers contained zwitterionic functionality. For these zwitterionic monomers, publications using ARGET polymerization represented only 4 of the >160 total ATRP and ARGET citations (see boxed area in Table 1.1).[10] Much of my research focused in this area where there are few examples of zwitterionic polymer films produced by ARGET polymerization.

Table 1.1. The number of papers investigating surface-initiated grafting of zwitterionic and nonionic polymers by ATRP and ARGET as catalogued by Zoppe et al. in 2017.

	Monomer	Citations Utilizing ATRP	Citations Utilizing ARGET	Comparison
Nonionic	methyl methacrylate **MMA**	217	27	
	N-isopropyl acrylamide **NIPAM**	206	18	
	2-hydroxyethyl methacrylate **HEMA**	164	17	
	2-(dimethylamino)ethyl methacrylate **DMAEMA**	141	19	
	poly(ethylene glycol) methyl ether methacrylate **PEGMEMA**	110	8	
	poly(ethylene glycol) methacrylate **PEGMA**	101	3	
Zwitterionic	sulfobetaine methacrylate **SBMA**	74	1	
	2-methacryloyloxyethyl phosphorylcholine **MPC**	50	3	
	carboxybetaine methacrylate **CBMA**	11	0	
	sulfobetaine methacrylamide **SBMAA**	11	0	
	sulfobetaine vinylimidazole **SBVI**	1	0	
	All Other Zwitterionic Monomers	10	0	

As many of these zwitterionic polymer surfaces exhibited advancing water contact angles in air of less than 15°, which is difficult to measure accurately using a goniometer, water contact angles were also measured under hexadecane. The increased interaction between the surface and the hexadecane environment (as compared to an air environment) effectively increases the contact angle to a more easily measured value. Further, as the high-energy zwitterionic surfaces could have a $\cos(\theta)$ value greater than 1, measurement of water contact angles in hexadecane allowed differentiation between surfaces that would otherwise show similar water contact angles of ~0° in an air environment. As wettability of many superhydrophilic polymer films are difficult to measure directly (i.e. possessing 0° or near-0° contact angles), an indirect method was developed to assess such films. To analyze these zwitterionic polymer coatings, I developed a model combining the Cassie, Fowkes, and Young equations, along with rate expressions to relate the surface properties of mixed copolymer surfaces to the composition of the monomer

solutions from which they were formed. These copolymer coatings were formed from a solution containing the zwitterionic monomer of interest and also a less hydrophilic co-monomer to effectively increase the contact angle to a more easily-measured value. This model allowed the estimation of the surface energy parameters of these zwitterionic polymer films, values that are difficult to obtain directly due to the challenges of quantifying the wettability of such hydrophilic surfaces. Surface energy values can provide a measure of a surface's ability to form a hydration layer – a key to prevent fouling.

UV-induced Attachment of Alkenes for Improved Stability of Attached Polymers and Monolayers

As mentioned above, siloxane-anchored films can degrade in aqueous environments.[18] However, Quintana has shown that polymers grafted from silane-based initiator surfaces can be protected.[18] They accomplished this stabilization by grafting a block of hydrophobic polystyrene from the initiator silane.[18] A block of polymer with the desired functionality was then grafted from the hydrophobic block.[18] In their study, pSBMAA films grafted directly from a silane-initiator surface showed a complete loss of the grafted polymer after 4 weeks in a simulated seawater environment.[18] Films that included a hydrophobic polystyrene block between the silane-initiator and the overlying grafted pSBMAA maintained approximately 80% of their original thickness after 3 months under the same conditions.[18] However, in situations like ours where pores are on the nanometer scale, film thickness can be an issue and such a strategy may not be viable due to the added thickness required to incorporate the hydrophobic block.

As an alternative to the reliance Si-O-Si linkages for attachment, I investigated an approach that employs more hydrolytically stable Si-C linkages to form monolayers and to provide sites for initiation. The method of grafting vinyl compounds from silicon utilizing a UV-induced silicon-carbon linkage has been demonstrated by the Buriak and Chidsey groups, among others.[39–46] As compared to Si-O-Si linkages, Si-C linkages are more stable and less susceptible to failure in aqueous environments as they avoid the hydrolytic instability associated with Si-O-Si linkages.[32,33,47,48] Figure 1.7 illustrates the general scheme for covalently attaching an alkene-containing molecule to a silicon substrate. In this method, silicon samples

13

is first exposed to a hydrofluoric acid solution to remove the native oxide layer and yield a hydrogen-terminated silicon surface. In a following step, the hydrogen-terminated silicon sample is exposed to the chosen alkene and irradiated with UV light. The UV irradiation leads to a homolytic dissociation of surface hydrogen atoms resulting in radical sites to which the alkene attaches.[39,49,50] By this scheme, monolayers of alkenes can be attached to surfaces that may be tailored to provide fouling-resistant properties or initiator groups from which polymers can be grown.
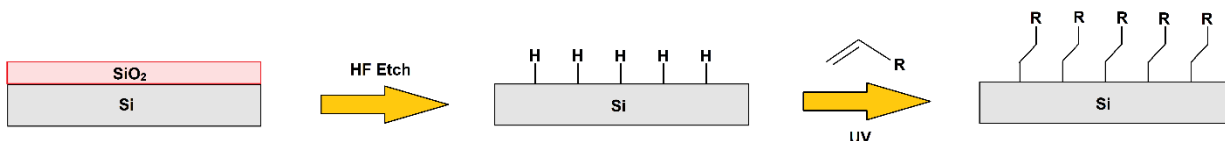
Figure 1.7. Reaction scheme for covalent attachment of alkenes to H-terminated silicon via UV.

Specifically, my research utilized the UV-induced hydrosilylation method to attach 4-vinylbenzyl chloride (VBC) to the silicon surface. This compound offered both the initiator and alkene groups required for polymerization and attachment via UV-induced hydrosilylation respectively; further, it has been attached to silicon in previous studies.[12,16,49,50] The chloride located at the benzylic position can be homolytically cleaved by the Cu(I)/ligand catalyst to generate the surface bound radicals necessary for ARGET and/or ATRP polymerization.[12,16,49,50] In my research, I demonstrated the ability of g-VBC to successfully function as an ARGET initiator surface to produce multiple zwitterionic polymer films including grafted pSBMA.

In addition to demonstrating g-VBC's use as an initiator to make zwitterionic polymer coatings, we also demonstrated the usefulness of g-VBC as a platform for nucleophilic substitution reactions, a synthetic strategy not yet reported in literature. A surface modification strategy utilizing nucleophilic substitution can provide researchers the ability to tailor interfacial properties by attaching moieties possessing desirable characteristics from surfaces. Figure 1.8 below illustrates the general scheme for the

studied routes to covalently attach the benzyl chloride group to a H-terminated silicon substrate and subsequently modify via substitution. Demonstrated here was the ability to utilize these grafted benzyl chloride moieties to perform substitution reactions with a variety of nucleophilic molecules to yield potentially useful surface coatings. First, substitution reactions of alkoxides with g-VBC to yield either hydrophilic PEG-terminated surfaces or hydrophobic alkyl-terminated surfaces were demonstrated. Also shown was the ability to perform a quaternization reaction to convert the g-VBC surfaces to ones possessing zwitterionic moieties. Another route was explored reacting dimethylamine with g-VBC surfaces to form tertiary-amine terminated surfaces; these were subsequently converted to zwitterionic surfaces upon reaction with 1,3-propanesultone. Finally demonstrated was a substitution reaction with NaN_3 to yield azide-modified surfaces potentially useful for "Click" chemistry.
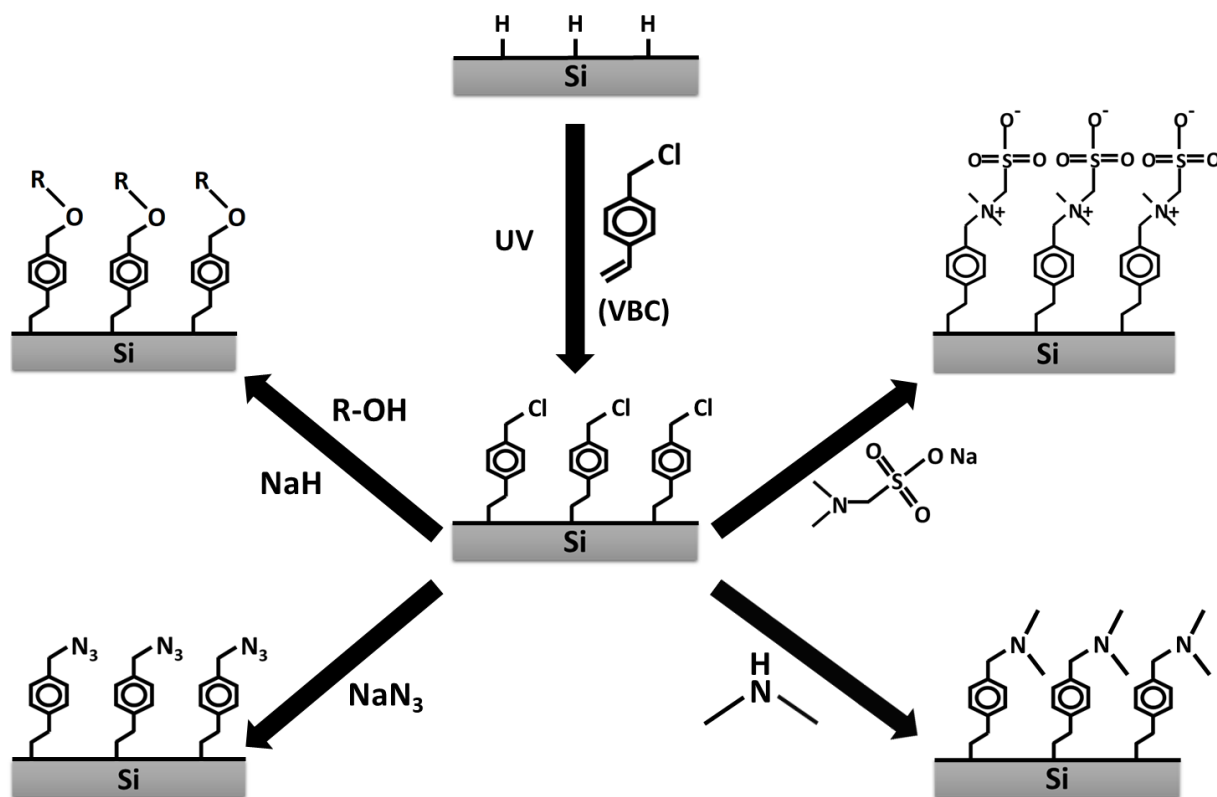
Figure 1.8. Strategy for introducing surface-bound benzyl chloride groups to a H-terminated silicon surface. VBC introduced onto the surface of the freshly HF-etched silicon substrate was then irradiated with UV to induce

attachment. Substitution reactions between the surface-bound benzyl chloride moiety and a chosen nucleophilic compound was then performed.

Novel Attachment Strategies of Azides to Silicon for "Click" Chemistry

With a desire to explore thin molecular films, I applied for and received the Dissertation Enhancement Grant through the Russell G. Hamilton Graduate Leadership Development Institute (GLDI) at Vanderbilt to allow me to explore a novel coating strategy that was complementary to the polymeric systems I had been developing. Specifically, this new approach involved the synthesis and characterization of a new class of single-layer zwitterionic films bound via a robust, hydrolytically-stable Si-C attachment chemistry. Up to this point, my dissertation research had focused primarily on polymeric coatings. This grant allowed me to broaden my research to include a new coating architecture (monomolecular vs polymeric) and new synthetic pathways utilizing "click" chemistry.

Copper(I)-catalyzed azide-alkyne cycloaddition (CuAAC) represents the most commonly used variety of "click" reaction and provides an efficient method for the linking of a diverse collection of organic moieties to one another, including at surfaces.[51–53] CuAAC has found wide use in many areas of research including solid-phase peptide synthesis,[52,54] cross-linking of polymers,[55] introducing/tailoring polymer architecture,[53–56] and surface modification.[51,56,57] For use in surface modification, once either an alkyne or azide group has been attached to a desired substrate (nanoparticles, flat surfaces, porous surfaces, CNT's, fibers, etc.), CuAAC can be an efficient strategy for introducing other functionalities, molecular species, biomolecules, or polymers with the corresponding azide or alkyne group to these solid supports/surfaces.[51,52,58,59]

Typically, azide-terminated monolayers are attached to silicon surfaces via silane chemistry[58,60,61] or via a multi-step modification of an existing hydrosilylation-derived monolayer.[62] For example, Zheng et al., Heise et al., and Balachander et al. all demonstrated the modification Si/SiO2 substrates with various bromide-terminated alkyltrichlorosilane compounds and subsequent conversion to azide-terminated

monolayers via substitution with sodium azide.[58,63,64]   Meanwhile, Paoprasert et al. and Vos et al. formed

azide-terminated monolayers directly onto Si/SiO2 substrates using azide-terminated trimethoxysilane

molecules that were deposited through a vapor or solution-phase process, respectively.[60,61]   In contrast,

others have investigated approaches that employ more hydrolytically stable Si-C linkages to form

monolayers and to provide sites for further modification via (CuAAC) and also copper-free "click"

reactions. Gouget-Laemmel et al. demonstrated formation of azide-terminated films from silicon by first

attaching undecylenic acid by hydrosilylation and then converting this acid-terminated monolayer to a NHS

ester using EDC coupling before finally obtaining the desired azide functionality by reaction with an azido-

PEG8-amine compound.[62]   While the method presented by Gouget-Laemmel et al. was successful, their

multi-step approach is more complicated than the more "straight-forward" approach to obtain azide-

modified silicon via a UV-hydrosilylation procedure that we developed.

After having gaining extensive experience in performing UV-induced attachment of 4-vinylbenzyl

chloride to H-terminated silicon to produce g-VBC coatings for ARGET initiation and substitution

reactions, these same g-VBC films were leveraged to develop a platform for novel monomolecular azide

films and serve as the basis for a series of "click" reactions. First, the substitution of g-VBC with sodium

azide was demonstrated to yield a surface enabling "click" chemistry to be performed. As a natural

progression upon the idea of converting a g-VBC surface to an azide surface, a novel strategy of attaching

4-vinylbenzyl azide (VBA) directly to H-terminated silicon via UV-induced hydrosilylation was

discovered. Figure 1.9 illustrates the general scheme for covalently attaching an organic azide to a H-

terminated silicon substrate via a one-step, UV-induced hydrosilylation reaction. "Click" chemistry, known

for its ease of use and high reaction conversion[65], allowed efficient introduction of various alkyne

molecules. In addition to traditional CuAAC "click" chemistry, this grafted VBA (g-VBA) surface also

allowed utilization of copper-free "click" chemistry, a technique that leverages ring-strained alkynes to

alleviate the need to include catalysts such as copper, for surface attachment.[66] To demonstrate the presence

of the attached azide and its usefulness for both of these variations of "click" chemistry, we investigated

the reactions between a collection of alkynes with the g-VBA surface and analyzed their products by water contact angles and ellipsometry. In addition to flat silicon substrates, we attached VBA to porous silicon (PSi) substrates where the inherent high surface area of PSi provided higher signals for FT-IR analysis. In addition to its usefulness for FT-IR, porous silicon has also been demonstrated to be a highly effective platform for sensing applications as the presence of captured target molecules can be quantified via analysis of changes in position of interference fringes obtained through reflectance experiments.[67] The biotin-streptavidin interaction system represents one of the most common coupling strategies for binding bioreceptor systems to surfaces for capturing analytes in biosensing applications.[9,67–71] To demonstrate the potential utility of our azide-modified porous silicon samples for biosensing applications, we demonstrated biotinylation of the substrates using a copper-free "click" reaction between an alkyne-containing biotin compound and the g-VBA surface.
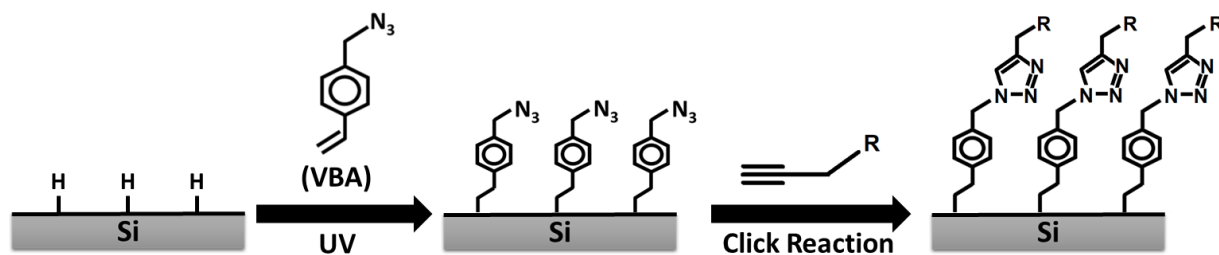
Figure 1.9. Strategy for introducing surface-bound azide groups to a H-terminated silicon surface. VBA was irradiated with UV to induce attachment to a freshly HF-etched silicon substrate. In a second step, "Click" chemistry between the surface-bound azide and an alkyne was performed.

References:

(1)   Edmondson, S.; Osborne, V. L.; Huck, W. T. S. Polymer Brushes via Surface-Initiated Polymerizations. *Chemical Society Reviews* **2004**, *33* (1), 14–22. https://doi.org/10.1039/b210143m.

(2)   Hui, C. M.; Pietrasik, J.; Schmitt, M.; Mahoney, C.; Choi, J.; Bockstaller, M. R.; Matyjaszewski, K. Surface-Initiated Polymerization as an Enabling Tool for Multifunctional (Nano-)Engineered Hybrid Materials. *Chemistry of Materials*. American Chemical Society January 14, **2014**, pp 745–762. https://doi.org/10.1021/cm4023634.

(3)   Radhakrishnan, B.; Ranjan, R.; Brittain, W. J. Surface Initiated Polymerizations from Silica Nanoparticles. *Soft Matter*. Royal Society of Chemistry April 18, **2006**, pp 386–396. https://doi.org/10.1039/b516508c.

(4)   Krishnamoorthy, M.; Hakobyan, S.; Ramstedt, M.; Gautrot, J. E. Surface-Initiated Polymer Brushes in the Biomedical Field: Applications in Membrane Science, Biosensing, Cell Culture, Regenerative Medicine and Antibacterial Coatings. *Chemical Reviews*. American Chemical Society November 12, **2014**, pp 10976–11026. https://doi.org/10.1021/cr500252u.

(5)   Gooding, J. J.; Mearns, F.; Yang, W.; Liu, J. Self-Assembled Monolayers into the 21st Century: Recent Advances and Applications. *Electroanalysis* **2003**, *15* (2), 81–96. https://doi.org/10.1002/elan.200390017.

(6)   Flink, S.; van Veggel, F. C. J. M.; Reinhoudt, D. N. Sensor Functionalities in Self-Assembled Monolayers. *Advanced Materials* **2000**, *12* (18), 1315–1328. https://doi.org/10.1002/1521-4095(200009)12:18<1315::AID-ADMA1315>3.0.CO;2-K.

(7)   Chechik, V.; Crooks, R. M.; Stirling, C. J. M. Reactions and Reactivity in Self-Assembled Monolayers. *Advanced Materials* **2000**, *12* (16), 1161–1171. https://doi.org/10.1002/1521-4095(200008)12:16<1161::AID-ADMA1161>3.0.CO;2-C.

(8)   Onclin, S.; Ravoo, B. J.; Reinhoudt, D. N. Engineering Silicon Oxide Surfaces Using Self-Assembled Monolayers. *Angewandte Chemie - International Edition*. John Wiley & Sons, Ltd October 7, **2005**, pp 6282–6304. https://doi.org/10.1002/anie.200500633.

(9)   Chaki, N. K.; Vijayamohanan, K. Self-Assembled Monolayers as a Tunable Platform for Biosensor Applications. *Biosensors and Bioelectronics*. Elsevier January 1, **2002**, pp 1–12. https://doi.org/10.1016/S0956-5663(01)00277-9.

(10)   Zoppe, J. O.; Ataman, N. C.; Mocny, P.; Wang, J.; Moraes, J.; Klok, H. A. Surface-Initiated Controlled Radical Polymerization: State-of-the-Art, Opportunities, and Challenges in Surface and Interface Engineering with Polymer Brushes. *Chemical Reviews* **2017**, *117* (3), 1105–1318. https://doi.org/10.1021/acs.chemrev.6b00314.

(11)   Edmondson, S.; Osborne, V. L.; Huck, W. T. S. Polymer Brushes via Surface-Initiated Polymerizations. *Chemical Society Reviews* **2004**, *33* (1), 14–22. https://doi.org/10.1039/b210143m.

(12)   Matyjaszewski, K. Atom Transfer Radical Polymerization (ATRP): Current Status and Future Perspectives. *Macromolecules* **2012**, *45* (10), 4015–4039. https://doi.org/10.1021/ma3001719.

(13)   Kato, M.; Kamigaito, M.; Sawamoto, M.; Higashimura, T. Polymerization of Methyl Methacrylate with the Carbon Tetrachloride/Dichlorotris-(Triphenylphosphine)Ruthenium(II)/ Methylaluminum Bis(2,6-Di-Tert-Butylphenoxide) Initiating System: Possibility of Living Radical Polymerization. *Macromolecules*. American Chemical Society September 1, **1995**, pp 1721–1723. https://doi.org/10.1021/ma00109a056.

(14)   Wang, J. S.; Matyjaszewski, K. Controlled/"Living" Radical Polymerization. Atom Transfer Radical Polymerization in the Presence of Transition-Metal Complexes. *Journal of the American Chemical Society* **1995**, *117* (20), 5614–5615. https://doi.org/10.1021/ja00125a035.

(15)   Tsujii, Y.; Ohno, K.; Yamamoto, S.; Goto, A.; Fukuda, T. Structure and Properties of High-Density Polymer Brushes Prepared by Surface-Initiated Living Radical Polymerization. *Advances in Polymer Science*. Springer, Berlin, Heidelberg **2006**, pp 1–45. https://doi.org/10.1007/12_063.

(16)   Matyjaszewski, K.; Hongchen, D.; Jakubowski, W.; Pietrasik, J.; Kusumo, A. Grafting from Surfaces for "Everyone": ARGET ATRP in the Presence of Air. *Langmuir* **2007**, *23* (8), 4528–4531. https://doi.org/10.1021/la063402e.

(17)   Blaszykowski, C.; Sheikh, S.; Thompson, M. A Survey of State-of-the-Art Surface Chemistries to Minimize Fouling from Human and Animal Biofluids. *Biomaterials Science* **2015**, *3* (10), 1335–1370. https://doi.org/10.1039/c5bm00085h.

(18)   Quintana, R.; Gosa, M.; Jańczewski, D.; Kutnyanszky, E.; Vancso, G. J. Enhanced Stability of Low Fouling Zwitterionic Polymer Brushes in Seawater with Diblock Architecture. *Langmuir* **2013**, *29* (34), 10859–10867. https://doi.org/10.1021/la402287a.

(19)   Kanani, D. M.; Fissell, W. H.; Roy, S.; Dubnisheva, A.; Fleischman, A.; Zydney, A. L. Permeability-Selectivity Analysis for Ultrafiltration: Effect of Pore Geometry. *Journal of Membrane Science* **2010**, *349* (1–2), 405–410. https://doi.org/10.1016/j.memsci.2009.12.003.

(20)   Fissell, W. H.; Dubnisheva, A.; Eldridge, A. N.; Fleischman, A. J.; Zydney, A. L.; Roy, S. High-Performance Silicon Nanopore Hemofiltration Membranes. *Journal of Membrane Science* **2009**, *326* (1), 58–63. https://doi.org/10.1016/j.memsci.2008.09.039.

(21)   Fissell, W. H.; Roy, S. The Implantable Artificial Kidney. *Seminars in Dialysis* **2009**, *22* (6), 665–670. https://doi.org/10.1111/j.1525-139X.2009.00662.x.

(22)   Chambers, L. D.; Stokes, K. R.; Walsh, F. C.; Wood, R. J. K. Modern Approaches to Marine Antifouling Coatings. *Surface and Coatings Technology* **2006**, *201* (6), 3642–3652. https://doi.org/10.1016/j.surfcoat.2006.08.129.

(23)   Yebra, D. M.; Kiil, S.; Dam-Johansen, K. Antifouling Technology - Past, Present and Future Steps towards Efficient and Environmentally Friendly Antifouling Coatings. *Progress in Organic Coatings*. Elsevier July 1, **2004**, pp 75–104. https://doi.org/10.1016/j.porgcoat.2003.06.001.

(24)   Maan, A. M. C.; Hofman, A. H.; Vos, W. M.; Kamperman, M. Recent Developments and Practical Feasibility of Polymer-Based Antifouling Coatings. *Advanced Functional Materials* **2020**, *30* (32), 2000936. https://doi.org/10.1002/adfm.202000936.

(25)   Francolini, I.; Vuotto, C.; Piozzi, A.; Donelli, G. Antifouling and Antimicrobial Biomaterials: An Overview. *APMIS* **2017**, *125* (4), 392–417. https://doi.org/10.1111/apm.12675.

(26)   Chen, S.; Li, L.; Zhao, C.; Zheng, J. Surface Hydration: Principles and Applications toward Low-Fouling/Nonfouling Biomaterials. *Polymer*. Elsevier Ltd October 29, **2010**, pp 5283–5293. https://doi.org/10.1016/j.polymer.2010.08.022.

(27)   Sharma, S.; Johnson, R. W.; Desai, T. A. Evaluation of the Stability of Nonfouling Ultrathin Poly(Ethylene Glycol) Films for Silicon-Based Microdevices. *Langmuir* **2004**, *20* (2), 348–356. https://doi.org/10.1021/la034753l.

(28)   Ostuni, E.; Chapman, R. G.; Holmlin, R. E.; Takayama, S.; Whitesides, G. M. A Survey of Structure-Property Relationships of Surfaces That Resist the Adsorption of Protein. *Langmuir*. American Chemical Society September 4, **2001**, pp 5605–5620. https://doi.org/10.1021/la010384m.

(29)   Han, S.; Kim, C.; Kwon, D. Thermal/Oxidative Degradation and Stabilization of Polyethylene Glycol. *Polymer* **1997**, *38* (2), 317–323. https://doi.org/10.1016/S0032-3861(97)88175-X.

(30)   Kane, R. S.; Deschatelets, P.; Whitesides, G. M. Kosmotropes Form the Basis of Protein-Resistant Surfaces. *Langmuir* **2003**, *19* (6), 2388–2391. https://doi.org/10.1021/la020737x.

(31)   Herold, D. A.; Keil, K.; Bruns, D. E. Oxidation of Polyethylene Glycols by Alcohol Dehydrogenase. *Biochemical Pharmacology* **1989**, *38* (1), 73–76. https://doi.org/10.1016/0006-2952(89)90151-2.

(32)   Nguyen, A. T.; Baggerman, J.; Paulusse, J. M. J.; Zuilhof, H.; van Rijn, C. J. M. Bioconjugation of Protein-Repellent Zwitterionic Polymer Brushes Grafted from Silicon Nitride. *Langmuir* **2012**, *28* (1), 604–610. https://doi.org/10.1021/la2031363.

(33)   Nguyen, A. T.; Baggerman, J.; Paulusse, J. M. J.; van Rijn, C. J. M.; Zuilhof, H. Stable Protein-Repellent Zwitterionic Polymer Brushes Grafted from Silicon Nitride. *Langmuir* **2011**, *27* (6), 2587–2594. https://doi.org/10.1021/la104657c.

(34)   Fissell, W. H.; Manley, S.; Dubnisheva, A.; Glass, J.; Magistrelli, J.; Eldridge, A. N.; Fleischman, A. J.; Zydney, A. L.; Roy, S. Ficoll Is Not a Rigid Sphere. *American Journal of Physiology-Renal Physiology* **2007**, *293* (4), F1209–F1213. https://doi.org/10.1152/ajprenal.00097.2007.

(35)   System, U. S. R. D. *2017 Annual Data Report*; 2017.

(36)   Blaszykowski, C.; Sheikh, S.; Thompson, M. Surface Chemistry to Minimize Fouling from Blood-Based Fluids. *Chemical Society Reviews* **2012**, *41* (17), 5599–5612. https://doi.org/10.1039/c2cs35170f.

(37)   Zhang, Z.; Chao, T.; Chen, S.; Jiang, S. Superlow Fouling Sulfobetaine and Carboxybetaine Polymers on Glass Slides. *Langmuir* **2006**, *22* (24), 10072–10077. https://doi.org/10.1021/la062175d.

(38)   Zhang, Z.; Chen, S.; Chang, Y.; Jiang, S. Surface Grafted Sulfobetaine Polymers via Atom Transfer Radical Polymerization as Superlow Fouling Coatings. *Journal of Physical Chemistry B* **2006**, *110* (22), 10799–10804. https://doi.org/10.1021/jp057266i.

(39)   Xu, F. J.; Kang, E. T.; Neoh, K. G. UV-Induced Coupling of 4-Vinylbenzyl Chloride on Hydrogen-Terminated Si(100) Surfaces for the Preparation of Well-Defined Polymer-Si Hybrids via Surface-Initiated ATRP. *Macromolecules* **2005**, *38* (5), 1573–1580. https://doi.org/10.1021/ma049225a.

(40)   Yu, W. H.; Kang, E. T.; Neoh, K. G.; Zhu, S. Controlled Grafting of Well-Defined Polymers on Hydrogen-Terminated Silicon Substrates by Surface-Initiated Atom Transfer Radical Polymerization. **2003**. https://doi.org/10.1021/jp034330s.

(41)   Buriak, J. M. Organometallic Chemistry on Silicon and Germanium Surfaces. **2002**. https://doi.org/10.1021/cr000064s.

(42)   Stewart, M. P.; Buriak, J. M. Photopatterned Hydrosilylation on Porous Silicon. *Angewandte Chemie - International Edition* **1998**, *37* (23), 3257–3260. https://doi.org/10.1002/(SICI)1521-3773(19981217)37:23<3257::AID-ANIE3257>3.0.CO;2-1.

(43)   Huck, L. A.; Buriak, J. M. UV-Initiated Hydrosilylation on Hydrogen-Terminated Silicon (111): Rate Coefficient Increase of Two Orders of Magnitude in the Presence of Aromatic Electron Acceptors. **2012**. https://doi.org/10.1021/la3035819.

(44)   Effenberger, F.; Götz, G.; Bidlingmaier, B.; Wezstein, M. Photoactivated Preparation and Patterning of Self-Assembled Monolayers with 1-Alkenes and Aldehydes on Silicon Hydride Surfaces. *Angewandte Chemie - International Edition* **1998**, *37* (18), 2462–2464. https://doi.org/10.1002/(SICI)1521-3773(19981002)37:18<2462::AID-ANIE2462>3.0.CO;2-R.

(45)   Terry, J.; Mo, R.; Wigren, C.; Cao, R.; Mount, G.; Pianetta, P.; Linford, M. R.; Chidsey, C. E. D. Reactivity of the H-Si (111) Surface. *Nuclear Instruments and Methods in Physics Research, Section B: Beam Interactions with Materials and Atoms* **1997**, *133* (1–4), 94–101. https://doi.org/10.1016/S0168-583X(97)00467-9.

(46)   Cicero, R. L.; Linford, M. R.; Chidsey, C. E. D. Photoreactivity of Unsaturated Compounds with Hydrogen-Terminated Silicon(111). *Langmuir* **2000**, *16* (13), 5688–5695. https://doi.org/10.1021/la9911990.

(47)   Sano, H.; Maeda, H.; Ichii, T.; Murase, K.; Noda, K.; Matsushige, K.; Sugimura, H. Alkyl and Alkoxyl Monolayers Directly Attached to Silicon: Chemical Durability in Aqueous Solutions. *Langmuir* **2009**, *25* (10), 5516–5525. https://doi.org/10.1021/la804080g.

(48)   Bhairamadgi, N. S.; Pujari, S. P.; Trovela, F. G.; Debrassi, A.; Khamis, A. A.; Alonso, J. M.; al Zahrani, A. A.; Wennekes, T.; Al-Turaif, H. A.; van Rijn, C.; Alhamed, Y. A.; Zuilhof, H. Hydrolytic and Thermal Stability of Organic Monolayers on Various Inorganic Substrates. *Langmuir* **2014**, *30* (20), 5829–5839. https://doi.org/10.1021/la500533f.

(49)   Xu, F. J.; Cai, Q. J.; Kang, E. T.; Neoh, K. G. Surface-Initiated Atom Transfer Radical Polymerization from Halogen-Terminated Si(111) (Si-X, X = Cl, Br) Surfaces for the Preparation of Well-Defined Polymer-Si Hybrids. *Langmuir* **2005**, *21* (8), 3221–3225. https://doi.org/10.1021/la0473714.

(50)   Xu, F. J.; Kang, E. T.; Neoh, K. G. Resist-Free Micropatterning of Binary Polymer Brushes on Si(100) via Surface-Initiated Living Radical Polymerizations. *Journal of Materials Chemistry* **2006**, *16* (28), 2948–2952. https://doi.org/10.1039/b604410g.

(51)   Liang, L.; Astruc, D. The Copper(I)-Catalyzed Alkyne-Azide Cycloaddition (CuAAC) "Click" Reaction and Its Applications. An Overview. *Coordination Chemistry Reviews*. December **2011**, pp 2933–2945. https://doi.org/10.1016/j.ccr.2011.06.028.

(52)   Castro, V.; Rodríguez, H.; Albericio, F. CuAAC: An Efficient Click Chemistry Reaction on Solid Phase. **2015**. https://doi.org/10.1021/acscombsci.5b00087.

(53)   Neumann, S.; Biewend, M.; Rana, S.; Binder, W. H. The CuAAC: Principles, Homogeneous and Heterogeneous Catalysts, and Novel Developments and Applications. *Macromolecular Rapid Communications* **2020**, *41* (1), 1900359. https://doi.org/10.1002/marc.201900359.

(54) Martens, S.; Holloway, J. O.; du Prez, Filip. E. Click and Click-Inspired Chemistry for the Design of Sequence-Controlled Polymers. *Macromolecular Rapid Communications* **2017**, *38* (24), 1700469. https://doi.org/10.1002/marc.201700469.

(55) Arslan, M.; Tasdelen, M. A. Click Chemistry in Macromolecular Design: Complex Architectures from Functional Polymers. *Chemistry Africa* **2019**, *2* (2), 195–214. https://doi.org/10.1007/s42250-018-0030-8.

(56) Arslan, M.; Tasdelen, M. A. Polymer Nanocomposites via Click Chemistry Reactions. *Polymers*. MDPI AG October 11, **2017**. https://doi.org/10.3390/polym9100499.

(57) Yáñez-Sedeño, P.; González-Cortés, A.; Campuzano, S.; Pingarrón, J. M. Copper(I)-Catalyzed Click Chemistry as a Tool for the Functionalization of Nanomaterials and the Preparation of Electrochemical (Bio)Sensors. *Sensors* **2019**, *19* (10), 2379. https://doi.org/10.3390/s19102379.

(58) Zheng, S.; Yang, Q.; Mi, B. Novel Antifouling Surface with Improved Hemocompatibility by Immobilization of Polyzwitterions onto Silicon via Click Chemistry. *Applied Surface Science* **2016**, *363*, 619–626. https://doi.org/10.1016/j.apsusc.2015.12.081.

(59) Li, N.; Binder, W. H. Click-Chemistry for Nanoparticle-Modification. *Journal of Materials Chemistry* **2011**, 16717-16734. https://doi.org/10.1039/c1jm11558h.

(60) Vos, R.; Rolin, C.; Rip, J.; Conard, T.; Steylaerts, T.; Cabanilles, M. V.; Levrie, K.; Jans, K.; Stakenborg, T. Chemical Vapor Deposition of Azidoalkylsilane Monolayer Films. *Langmuir* **2018**, *34* (4), 1400–1409. https://doi.org/10.1021/acs.langmuir.7b04011.

(61) Paoprasert, P.; Spalenka, J. W.; Peterson, D. L.; Ruther, R. E.; Hamers, R. J.; Evans, P. G.; Gopalan, P. Grafting of Poly(3-Hexylthiophene) Brushes on Oxides Using Click Chemistry. *Journal of Materials Chemistry* **2010**, 2651-2658. https://doi.org/10.1039/b920233a.

(62) Gouget-Laemmel, A. C.; Yang, J.; Lodhi, M. A.; Siriwardena, A.; Aureau, D.; Boukherroub, R.; Chazalviel, J. N.; Ozanam, F.; Szunerits, S. Functionalization of Azide-Terminated Silicon Surfaces

with Glycans Using Click Chemistry: XPS and FTIR Study. *Journal of Physical Chemistry C* **2013**, *117* (1), 368–375. https://doi.org/10.1021/jp309866d.

(63)   Heise, A.; Menzel, H.; Yim, H.; Foster, M. D.; Wieringa, R. H.; Schouten, A. J.; Erb, V.; Stamm, M. Grafting of Polypeptides on Solid Substrates by Initiation of N-Carboxyanhydride Polymerization by Amino-Terminated Self-Assembled Monolayers. *Langmuir* **1997**, *13* (4), 723–728. https://doi.org/10.1021/la960467g.

(64)   Balachander, N.; Sukenik, C. N. Functionalized Siloxy-Anchored Monolayers with Exposed Amino, Azido, Bromo, or Cyano Groups. *Tetrahedron Letters* **1988**, *29* (44), 5593–5594. https://doi.org/10.1016/S0040-4039(00)80820-5.

(65)   Hein, C. D.; Liu, X. M.; Wang, D. Click Chemistry, a Powerful Tool for Pharmaceutical Sciences. *Pharmaceutical Research*. Pharm Res October **2008**, pp 2216–2230. https://doi.org/10.1007/s11095-008-9616-1.

(66)   Jewett, J. C.; Bertozzi, C. R. Cu-Free Click Cycloaddition Reactions in Chemical Biology. *Chem. Soc. Rev.*, **2010**, 39, 1272-1279. https://doi.org/10.1039/b901970g.

(67)   Arshavsky-Graham, S.; Massad-Ivanir, N.; Segal, E.; Weiss, S. Porous Silicon-Based Photonic Biosensors: Current Status and Emerging Applications. *Analytical Chemistry*. American Chemical Society January 2, **2019**, pp 441–467. https://doi.org/10.1021/acs.analchem.8b05028.

(68)   Bã, M.-J.; Puchades, R.; Maquieira, Á. Chemical Surface Modifications for the Development of Silicon-Based Label-Free Integrated Optical (IO) Biosensors: A Review. *Analytica Chimica Acta* **2013**, *777*, 1–16. https://doi.org/10.1016/j.aca.2013.01.025.

(69)   Lowe, B. M.; Sun, K.; Zeimpekis, I.; Skylaris, C.-K.; Green, N. G. Analyst CRITICAL REVIEW Field-Effect Sensors-from PH Sensing to Biosensing: Sensitivity Enhancement Using Streptavidin-Biotin as a Model System. *Analyst* **2017**, *142*, 4173. https://doi.org/10.1039/c7an00455a.

(70)   Mooney, J. F.; Huntt, A. J.; Mcintosht, J. R.; Liberkot, C. A.; Walbat, D. M.; Rogers, C. T.; Prescott, D. M. *Patterning of Functional Antibodies and Other Proteins by Photolithography of Silane Monolayers (Self-Assembled Monolayers/Biotin/Streptavidin/Adsorption Isotherms)*; **1996**; Vol. 93.

(71)   Williams, E. H.; Davydov, A. v; Motayed, A.; Sundaresan, S. G.; Bocchini, P.; Richter, L. J.; Stan, G.; Steffens, K.; Zangmeister, R.; Schreifels, J. A.; Rao, V. Immobilization of Streptavidin on 4H-SiC for Biosensor Development. *Applied Surface Science* **2012**, *258*, 6056–6063. https://doi.org/10.1016/j.apsusc.2012.02.137.
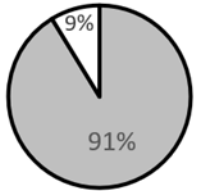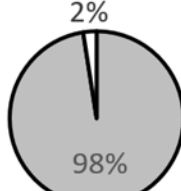
Chapter II

SURFACE-INITIATED POLYMER COATINGS BY ARGET

Introduction

Surface modification by a grafting-from approach can yield polymer film coatings with controllable interfacial properties.[1,2] Atom-transfer radical polymerization (ATRP) is a very commonly used approach for generating such polymer films.[1,3] One drawback of this approach is that ATRP requires rigorous deoxygenation for successful polymerization reaction as oxidation of the required active catalytic Cu(I) species forms an inactive Cu(II) state.[4] As an alternative, Matyjaszewski developed activators regenerated by electron transfer (ARGET) polymerization, a related polymerization reaction that can be performed even in the presence of air.[4] In ARGET, a reducing agent is used to form reactive Cu(I) species from air-stable Cu(II) precursors and maintain their activity.[4] As a result, ARGET provides a convenient alternative to traditional ATRP; however, despite its ease-of-use, reports of using ARGET for grafting polymers are fewer in comparison. A 2017 review paper by Zoppe et al. catalogued the grafting of approximately 300 different monomers by various polymerization techniques including both ARGET and ATRP.[1] Table 2.1 summarizes commonly grafted polymers included in this database-like review, listing how many citations the review included for each monomer by a particular polymerization method.[1] The table shows the disparity in the number of papers employing ARGET as compared to ATRP. In this comprehensive review, only 13 of the approximately 300 listed monomers contained zwitterionic functionality. For these zwitterionic monomers, publications using ARGET polymerization represented only 4 of the over 160 total ATRP and ARGET citations (see boxed area in Table 2.1).[1] My research focused in this area where there are few examples of zwitterionic polymer films produced by ARGET polymerization.

Table 2.1. The number of papers investigating surface-initiated grafting of zwitterionic and nonionic polymers by ATRP and ARGET as catalogued by Zoppe et al in the 2017 review paper.

	Monomer	Citations Utilizing ATRP	Citations Utilizing ARGET	Comparison
Nonionic	methyl methacrylate MMA	217	27	
	N-isopropyl acrylamide NIPAM	206	18	
	2-hydroxyethyl methacrylate HEMA	164	17	
	2-(dimethylamino)ethyl methacrylate DMAEMA	141	19	
	poly(ethylene glycol) methyl ether methacrylate PEGMEMA	110	8	
	poly(ethylene glycol) methacrylate PEGMA	101	3	
Zwitterionic	sulfobetaine methacrylate SBMA	74	1	
	2-methacryloyloxyethyl phosphorylcholine MPC	50	3	
	carboxybetaine methacrylate CBMA	11	0	
	sulfobetaine methacrylamide SBMAA	11	0	
	sulfobetaine vinylimidazole SBVI	1	0	
	All Other Zwitterionic Monomers	10	0	

Surface coatings expressing zwitterionic functionality are of particular interest as they can exhibit exceptional antifouling properties.[1,2,5–7] For practical applications, such as medical implants and devices exposed to marine environments, coatings are needed that can retain their antifouling properties throughout the lifespan of the device to which they are attached.[2,5,7] One application is an artificial implantable kidney device being developed as an alternative to dialysis led by our collaborator Dr. William Fissell at the Vanderbilt University Medical Center.[8,9] The need for such a device is great as the United States Renal Data System reported that 444,337 US patients depended on dialysis at an annual cost of $88,195 per patient in 2015.[10] In the device currently under development, silicon membranes with arrays of slit-shaped

nanopores provide the filtration (see Figure 2.1). To maintain requisite permeability rates and selectivities, fouling-resistance over long-term operation remains an obstacle for maintaining the reliability of these implantable devices for those with end stage renal disease.
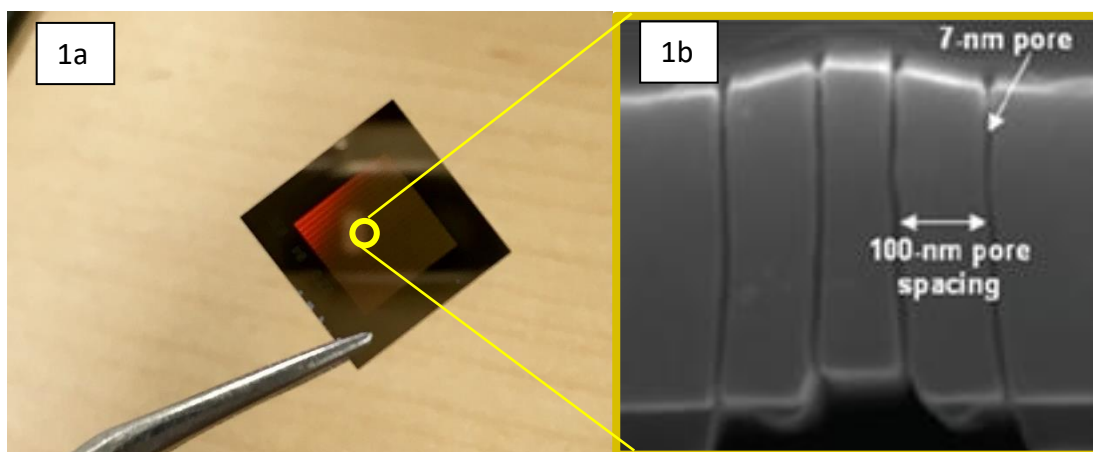
Figure 2.1. Depiction of the structure of silicon the nanopore membranes. a) Photograph of one of the 1 x 1 cm^2 silicon membanes nanopore membranes. b) SEM cross-sectional image of nanopore structure provided by the Fissell group at Vanderbilt University Medical Center.

The nanopore membranes currently used by the Fissell group are typically surface-modified with a polyethylene glycol (PEG) coating to prevent fouling. Specifically, these coatings are composed of a monolayer of molecules referred to as "PEGsilane" consisting of 6-9 oxyethylene repeat units covalently attached to the silicon substrate via a siloxane linkage. While PEG coatings have seen broad use as anti-fouling coatings, they are known to deteriorate under physiological conditions.[7,11–15] For example, Sharma et al. observed a 50% loss in film thickness of their siloxane-bound PEG after 3-4 weeks in PBS containing 5% CO_2 at 37 °C that simulated an in vivo environment.[12] Such degradation would be unacceptable for an implanted device such as this nanopore membrane.

The degradation of PEG coatings may result from various failure modes. First, degradation of the PEG backbone itself has been reported from oxidation, as occurs for polyethers.[11,12,14] Additionally, PEG

and other polymer coatings attached to surfaces via siloxane linkages are known to detach from their substrates in aqueous environments by hydrolysis.[7,16,17] To address the first issue, researchers hope to develop other potential non-fouling surface coatings using polar polymers with a more stable backbone that avoid the possibility of polyether degradation.[1,2,5] My research aimed to develop antifouling coatings that employ zwitterionic functionality in place of PEGs. Zwitterionic coatings are hypothesized to offer exceptional antifouling properties via formation of an electrostatically-bound hydration layer (see Figure 2.2).[5] The strong binding of hydration layers make zwitterionic coatings more promising than many current surface modification schemes that similarly rely on hydration layers albeit by weaker hydrogen-bonding interactions.
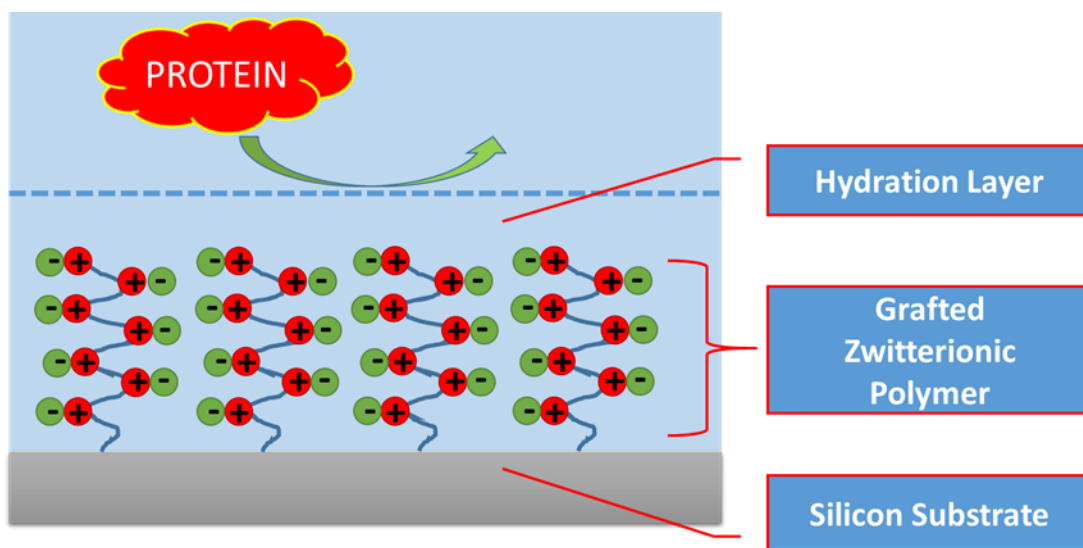
Figure 2.2. Hydration layer bound to surface via electrostatic interaction with grafted zwitterionic polymer coating.

For example, Zhang et al. demonstrated that the zwitterionic polymers poly(sulfobetaine methacrylate) (pSBMA) and poly(carboxybetaine methacrylate) (pCBMA) can be grafted from the surfaces of glass and silicon via ATRP.[18] The resulting polymers exhibited high resistance to protein adsorption and low platelet adhesion when present at higher grafting densities.[18]

My research, in part, focused on the grafting of pSBMA via ARGET polymerization. Although well-controlled growth of pSBMA via ATRP has been reported,[1,18,19] such controlled growth of pSBMA via ARGET had not. In addition to SBMA, I also studied other zwitterionic monomers including sulfobetaine methacylamide (SBMAA), sulfobetaine acrylate (SBA), and sulfobetaine vinylimidazole (SBVI). Complementing these polymers, monolayers including g-PEGsilane and zwitterionic sulfobetaine silane (SBSi) were also grafted from silicon substrates and characterized for the purpose of comparison. The antifouling properties of the films were characterized via fluorescence microscopy, testing for the non-specific adsorption of FITC-labeled albumin. A goal was to identify the films that showed high fouling resistance so that they could later be grafted from nanopore silicon filtration membranes being developed for the artificial implantable kidney. As the membranes include nanometer-sized pores, the thickness of the surface coatings is highly important. As such, I investigated how thin these coatings could be made while retaining their ability to function as antifouling coatings. Ultimately, an ideal film should exhibit a tightly-bound hydration layer due to its zwitterionic moieties, complete substrate coverage with minimal defects, and minimal impedance of through-pore transport.

Experimental Methods

Chemicals and Materials: Copper(II) bromide, L-ascorbic acid, tris(2-pyridylmethyl)amine (TPMA), α-bromoisobutyryl bromide (BIBB), (3-aminopropyl) trimethoxysilane (APTMOS), poly(ethylene glycol) methacrylate average molecular weight 360 (PEGMA), 2-(dimethylamino)ethyl acrylate (DMAEA), 2-hydroxyethyl methacrylate (HEMA), 2-(dimethylamino)ethyl methacrylate (DMAEMA), N-[3-(dimethylamino)propyl]methacrylamide (DMAPMAA), triethylamine (TEA), 4-Vinylbenzyl chloride (VBC), and 1,3-propanesultone were obtained from Aldrich. SBMA ([2-(methacryloyloxy)ethyl]dimethyl-(3-sulfopropyl)ammonium hydroxide) was obtained from both Aldrich and Fisher. N,N-Dimethyl-3-(trimethoxysilyl)propylamine (DMASi) and 2-[methoxy(polyethyleneoxy) 6-9 propyl]trimethoxysilane (PEGsilane) were obtained from TCI America and Gelest, respectively. All compounds were used as

received. The initiator-silane 2-bromo-2-methyl-N-3-[(trimethoxysilyl)propyl]-propanamide (BrTMOS) was synthesized as described previously.[19,20] Silicon wafers <100> were purchased from Pure Wafer and cut into 1x1 cm^2 pieces using a dicing saw.

BrTMOS Initiator Synthesis: The initiator molecule, 3-(trimethoxysilyl)propyl 2-bromo-2-methylpropanoate (BrTMOS), was synthesized as follows.[19,20] A stir bar and 3.49 mL (20.0 mmol) of APTMOS were placed in a 100 mL round bottom flask. The flask was sealed via septum and sparged with nitrogen. Subsequently, 50 mL of anhydrous THF and 2.79 mL of TEA (20.0 mmol) were added to the flask via syringe and then stirred for 30 min with nitrogen bubbled through it. Then, 3.00 mL of BIBB (24.0 mmol) was added dropwise to the solution via syringe over 30 min with continued stirring, nitrogen sparging, and chilling via ice bath. The reaction was then allowed to proceed overnight at room temperature. The precipitate was removed via frit filtration, and THF was removed from the remaining solution using rotary evaporation. The resulting yellowish oil was redissolved in 40 mL of CH_2Cl_2, washed twice with 0.01 N HCl, and washed twice more with ice-cold water. The organic phase was dried over anhydrous $CaCl_2$ before removal of the CH_2Cl_2 by rotary evaporation. The remaining product was re-dissolved in hexane and precipitate removed via gravity filtration. The hexane was removed via rotary evaporation, yielding the product as a light-yellow colored oil that was placed under vacuum for 12 h to remove remaining solvent.

Synthesis of Zwitterionic Monomers: Sulfobetaine methacrylamide (SBMAA) was synthesized based on a previously reported method.[21] First, 2.32 mL (12.8 mmol) of DMAPMAA and 10 mL of dried acetone were added to a RB flask, sealed via septum, and sparged for 30 min with N_2. In a separate RB flask, 1.50 g (12.3 mmol) of 1,3-PS was dissolved in 10 mL of dried acetone and sparged with N_2 for 30 min. The 1,3-PS solution was added to a stirred DMAPMAA solution dropwise via syringe over 30 min. The reaction was allowed to proceed overnight. The resulting solid product was collected via filtration and washed with

acetone before drying under reduced pressure.

Sulfobetaine vinylimidazole (SBVI) was synthesized based on the procedure reported by Ezzat et al.[22] To a RB flask, 3.00 g (24.5 mmol) of 1,3-PS was added, sealed, and sparged with N_2 for 30 min. Then, 20 mL of anhydrous THF was added to the flask via syringe, and the solution was sparged with N_2 for an additional 30 min. With stirring, 1.85 mL (20.5 mmol) of 1-vinylimidazole was injected to the flask dropwise over 30 min. After 2 days of stirring at 50 °C under N_2, the resulting solid product was collected via filtration and washed with THF and ether before drying under reduced pressure.

Sulfobetaine acrylate (SBA) was synthesized as follows. First, 5.18 mL (34.1 mmol) of DMAEA (caution: fatal if inhaled) and 30 mL of dried acetone were added to a RB flask, sealed via septum, and sparged for 30 min with N_2. In a separate RB flask, 4.00 g or 2.8 mL (32.8 mmol) of 1,3-PS was dissolved in 30 mL of dried acetone and sparged with N_2 for 30 min. The 1,3-PS solution was added to the stirred DMAEA solution dropwise via canula over 30 min. The reaction was allowed to proceed overnight. The crude solid product was collected via filtration and washed with acetone before drying under reduced pressure. The product was then further purified via recrystallization. Briefly, the lumpy, crude product was dissolved in ethanol (~100 mL ethanol per gram of crude product) with heating and stirring. The solution was hot filtered to remove undissolved materials, and then allowed to cool in the refrigerator. The recrystallized product was collected via vacuum filtration, thoroughly rinsing with acetone after the ethanol was removed. The product was then dried under vacuum, yielding a fine white powder.

Fabrication of BrTMOS-modified silicon slides: Silicon slides were exposed to a piranha solution (7:3 mixture of sulfuric acid and 30% hydrogen peroxide) for 30 minutes. Caution: piranha solutions can be quite dangerous if not following proper safety precautions. Slides were triple rinsed in DI water, and then in ethanol before addition to the BrTMOS solution. The piranha-cleaned slides were immersed into an initiator solution consisting of 250 µL (1.72 mmol) of BrTMOS dissolved in 10 mL of ethanol. Samples were allowed to react with the solution overnight. After removal from the BrTMOS solution, the slides

35

were rinsed with ethanol, dried with N_2, and placed in a 100 °C vacuum oven for 5 h. Initiator-modified slides were stored in foil-wrapped containers to prevent exposure to light.

Attachment of VBC via UV-Hydrosilylation: For modification of flat silicon, 1 x 1 cm^2 samples were placed in an 800 °C oven for 4 h. After cooling, the samples were soaked in a 2.5% solution of HF in a 7:3 ethanol-water mixture to remove the oxide, rinsed with DI water, and dried. For irradiation, samples consisted of 15 µL of VBC sandwiched between the silicon surface and a No. 1 thickness coverslide. Samples were irradiated with UV light in a DYMAX 5000-EC UV curing lamp system. Total exposure times were typically 100 s. After removal of the coverslides, the samples were immersed in acetone for 1 h and then dried before use.

Attachment of VBC via Thermal Hydrosilylation: For modification of flat silicon, 1 x 1 cm^2 samples were placed in an 800 °C oven for 4 h. After cooling, the samples were soaked in a 2.5% solution of HF in a 7:3 ethanol-water mixture to remove the oxide, rinsed with DI water, and dried. The H-terminated silicon samples were then immediately placed into individual 1 dram vials each containing enough neat VBC to cover the slide. The submerged samples were then placed in an oven at the desired temperature (typically 100-120 °C) for the desired period of time (typically 30-120 minutes). Exact temperature and exposure times will be discussed in the Results and Discussion section. Samples were then removed from the oven and allowed to cool. The samples slides were then removed from the liquid VBC, immersed in acetone for 1 h to remove unbound material, and then dried before use.

Surface initiated ARGET polymerization: A general procedure for surface-initiated ARGET polymerization is described here. For most 0.358 M monomer solutions, the procedure was as follows: the molar ratios of monomer:Cu(II):ligand:reducing agent were ~5000:1:5:30, unless otherwise specified, for

the N_2-sparged systems in a 1:1 methanol water mixture. Two stock solutions were used in the synthesis: $CuBr_2$/TPMA in methanol (18 mM in $CuBr_2$; 86 mM in TPMA) and ascorbic acid in methanol (25 mg per mL methanol). First, 5 mL of monomer solution was added to a 10 mL RB flask containing an initiator modified slide. The flask was sealed via septum, and N_2 was sparged through the solution for 30 min via syringe. Polymerization was initiated by injecting 100 µL (unless stated otherwise) of the ascorbic acid stock solution through the septum. Polymerizations were terminated by removal of the septum. The resulting polymer-grafted slides were submerged in 1:1 methanol/DI water, rinsed with DI water, and dried in a stream of N_2.

Later ARGET experiments used a modified procedure with lower monomer concentration and a higher reducing agent (ascorbic acid) concentration. A general procedure for the revised surface-initiated ARGET polymerization experiments is described as follows. For 0.018 M SBMA monomer solutions, the molar ratios of monomer:Cu(II):ligand:reducing agent were 250:1:5:160 in a 1:1 methanol water mixture. Two stock solutions were used in the synthesis: $CuBr_2$/TPMA in methanol (18 mM in $CuBr_2$; 86 mM in TPMA) and ascorbic acid in methanol (25 mg per mL methanol). In a 20mL vial, the following were added to form the monomer solution: 0.075g SBMA, 7.5 mL H_2O, 7.5 mL methanol, and 60 µL of $CuBr_2$/TPMA stock solution. This was sealed via septum and sparged with nitrogen for 30 minutes. Simultaneously, the initiator-modified silicon samplers were placed in individual 1 dram vials, sealed via septum, and sparged with nitrogen for 30 minutes. After the monomer solution was allowed to sparge for 30 minutes, 1.2 mL of the ascorbic acid stock solution was injected to the monomer solution before allowing the resulting solution to sparge for an additional 5 minutes. The monomer solution was then transferred to slide-containing vials via syringe to begin the surface-initiated ARGET polymerization. After the desired reaction time, samples were removed from the monomer solution, soaked in a 50:50 DI H_2O:methanol mixture to remove unbound materials, rinsed with additional methanol and water, and finally dried with compressed nitrogen.

PEGsilane Monolayers: PEGsilane monolayers were produced using a procedure described by Papra et

al.[23] Diced silicon slides were soaked in a 1:1 mixture of DI water and ethanol for at least 4 hours before rinsing with DI water and drying with a stream of nitrogen. Subsequently, slides were soaked in a piranha solution for 30 minutes. The piranha-cleaned slides were triple rinsed with DI water, ethanol, and then toluene before addition to the PEGsilane solution consisting of 22 µL of the PEGsilane and 12 µL of HCl in 15 mL of toluene for 18 h, then washed with toluene ethanol, and water, before drying in a steam of nitrogen.

SBSi Monolayers: SBSi was synthesized based on a method by Yeh et al.[24] To a N_2-sparged RB flask, 0.600 g (4.91 mmol) of 1,3-PS, 5 mL of dried acetone, and 1.00 mL (4.57 mmol) of DMASi were each injected via syringe. After 12 h reaction under N_2 with stirring, the resulting white solid product was collected by filtration, washed with acetone, and dried under reduced pressure for 1 h.

Piranha cleaned slides were placed in a solution containing 50 mg of SBSi, 20 mL of EtOH, and 40 µL of DI water for 12 h, rinsed with EtOH, and cured in an 80 °C vacuum oven for 30 min.

Analyses: Film thicknesses were measured using an M-2000VI spectroscopic ellipsometer (J.A. Woollam Co.). Each sample was measured at angles of incidence of 60° and 70°. CompleteEASE software was used to analyze the measurements using the built-in transparent Cauchy film on silicon substrate model. A refractive index of 1.45 was assumed based on previous work with these polymer films.[19]

Advancing and receding water contact angles were measured on static drops. Contact angles measured under hexadecane were obtained using a custom-made solvent vessel/sample platform.

Fluorescence Fouling Assay: Each sample was first soaked in PBS at room temperature for 1 h, and then incubated in a well of a twelve well plate containing 2 mL of a 0.5 mg/mL solution of FITC-albumin in PBS at 37 °C for 1 h. Slides were removed from solution, triple rinsed with PBS, triple rinsed with DI

water, then dried in a stream of N_2. Each sample was mounted on a microscope slide with SlowFade mounting medium and a coverslip, and then analyzed using a fluorescent microscope at various exposure times at 2x magnification. To evaluate changes in background fluorescence, untreated slides were mounted and evaluated at regular intervals at the same microscope settings. Images were analyzed in ImageJ to obtain the mean intensity and standard deviation across each slide for the green channel on a scale of 0-255. Data were normalized to the background fluorescence from blank samples not exposed to FITC-albumin.

Results and Discussion

The general strategy discussed in this chapter employed a "grafting-from" technique to synthesize polymer films from surfaces modified to provide initiator sites for ARGET polymerization. Figure 2.3 illustrates the reaction scheme used for grafting polymers (in this case pSBMA) from silicon surfaces.
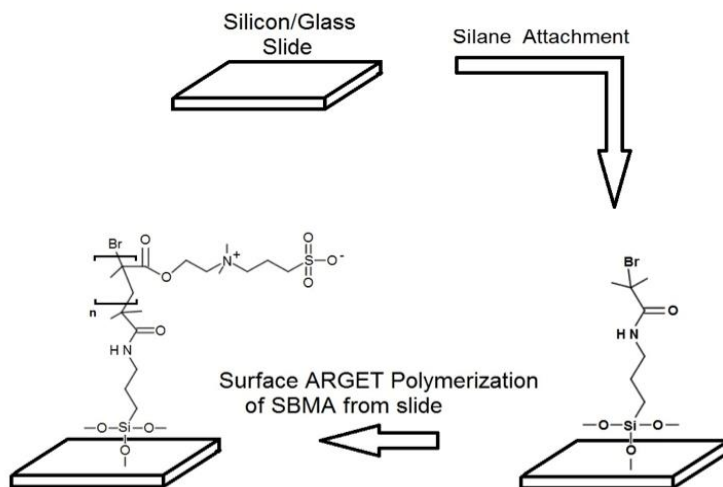
Figure 2.3. General scheme for forming a pSBMA coating on silicon via surface-initiated ARGET polymerization.

In the first step of this scheme, silicon slides were exposed to a piranha solution to generate surface hydroxyl groups to which BrTMOS could be covalently attached. After reaction with BrTMOS for 12 h, slides were incubated in a 100 °C vacuum oven to promote crosslinking of the silanes at the substrate surface.[25] Ellipsometric film thicknesses for the BrTMOS layers were typically 0.7 – 1.5 nm, consistent with its reported theoretical monolayer thickness of around 1.2 nm.[26] Advancing water contact angles on the slides increased from near-zero on freshly prepared piranha-cleaned surfaces to 60° - 70° after treatment with BrTMOS. The wetting and ellipsometry data agreed with literature values to suggest successful attachment of BrTMOS, providing the needed tertiary bromide initiation sites for grafting polymers from the surface.[26–28]

ARGET grafting of pSBMA

Initial attempts to graft pSBMA from g-BrTMOS slides using ARGET polymerization were unsuccessful. Typically, the polymerization solution turned cloudy and formed viscous, gel-like precipitates consistent with formation of bulk pSBMA in solution. Further, this phenomenon occurred even in the absence of an initiator-grafted slide. Slides removed from reaction vials before a solution turned cloudy showed no increase in ellipsometric film thickness and no change in water contact angle as compared to the initiator-grafted slides. For comparison, pSBMA films should exhibit water contact angles of ~10° or less.[18–20] Slides removed from cloudy SBMA solutions did exhibit water contact angles of ~10° but also showed uneven coating coverage upon visual inspection. Ellipsometric measurements on these slides showed an increase in thickness over the initiator grafted slides; however, rinsing with water easily removed the pSBMA films, returning their ellipsometric film thicknesses and their wetting properties to those of the initiator-modified surfaces. Based upon these observations, pSBMA found on these slides appeared to not be grafted from the slides. A hypothesis was that pSBMA formed in solution and then deposited physically onto the slides, preventing growth from surface initiator sites.

Grafting of Other Polymers from Slides

As my initial efforts to graft pSBMA from silicon slides by ARGET polymerization were unsuccessful, I examined other monomers, including HEMA and PEGMA, to ensure that my experimental procedures could successfully generate grafted polymer films. I focused on these uncharged monomers as they are reported to reliably undergo polymerization via ARGET and also yield antifouling coatings.[1,2,5,29–31] Under the same ARGET conditions used for the SBMA monomer, solutions of the HEMA and PEGMA monomers remained clear and free of precipitates, and the resulting grafted films did not rinse off.

The ability of ARGET to graft pPEGMA from the initiator-modified slides was demonstrated using the same methods shown previously. Figure 2.4 shows the effect of polymerization time on the thickness of films formed from PEGMA monomer solutions at two different concentrations. In Figure 2.4, a period of negligible growth was observed at shorter polymerization times, particularly at the lower monomer concentration. Similar "induction periods" have been reported by Matyjaszewski et al. to result from the reduction of Cu(II) to Cu(I) by the ascorbic acid competing against the oxidation of the Cu(I) to Cu(II) by oxygen within the air-containing system. A more rapid polymerization rate occurred *after* the oxygen in the reaction vial was consumed by this process.[32]
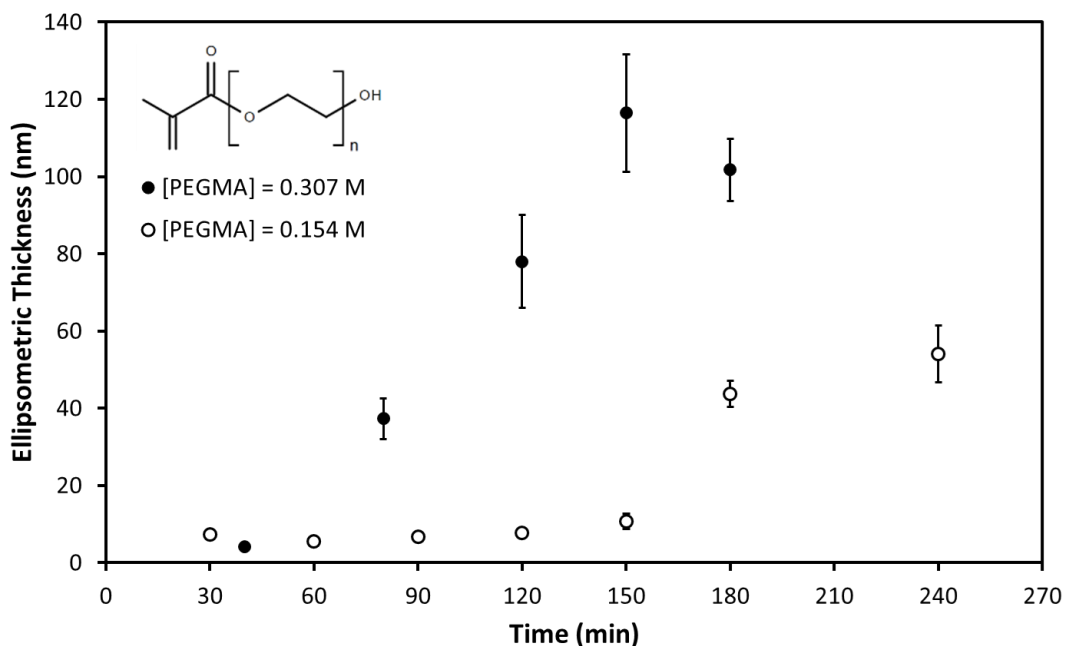
Figure 2.4. Ellipsometric thickness of g-pPEGMA films vs time formed at two different monomer concentrations from air-saturated solutions. These monomer solutions were not sparged with nitrogen, and [AA] = 7.7 mM. Also, note that film thicknesses of the initiator modified surfaces were not independently obtained for this experiment; consequently, film thickness values presented here also include the thickness of the underlying initiator layer.

To reduce the induction period and possibly improve the consistency of the resulting films, this experiment was repeated using N$_2$-sparged reaction vessels. As sparging with nitrogen was anticipated to significantly decrease the amount of oxygen in the reaction vials, I also reduced the concentration of ascorbic acid in the monomer solution. The resulting slides appeared more uniform, exhibited a mirror-like appearance, and had film thicknesses across individual slides with less variation than those without sparging. Figure 2.5 summarizes the ellipsometric film thickness results from this experiment. The resulting thicknesses were consistent with an overall first-order, linear growth process where a doubling in concentration leads to a doubling in polymerization rate. This behavior is expected for a growth rate described by $\frac{dT}{dt} = k_p * [R^·] * [M]$, where T is the film thickness, [M] is the monomer concentration of the solution, [R$^·$] is the concentration of active growing polymer chains, and k_p is a second-order rate constant for the polymerization. Under pseudo-first-order conditions where the Cu^I/Cu^{II} ratio, the active surface sites

for polymer growth, and the monomer concentration are assumed constant, the film thickness can be described by $T = k*[M]_o*t$ where k is a pseudo-first-order rate constant. For the grafting of pPEGMA, a rate constant of $k = 73 \pm 12 \frac{nm\ L}{mol\ hr}$ (95% confidence interval) was determined.
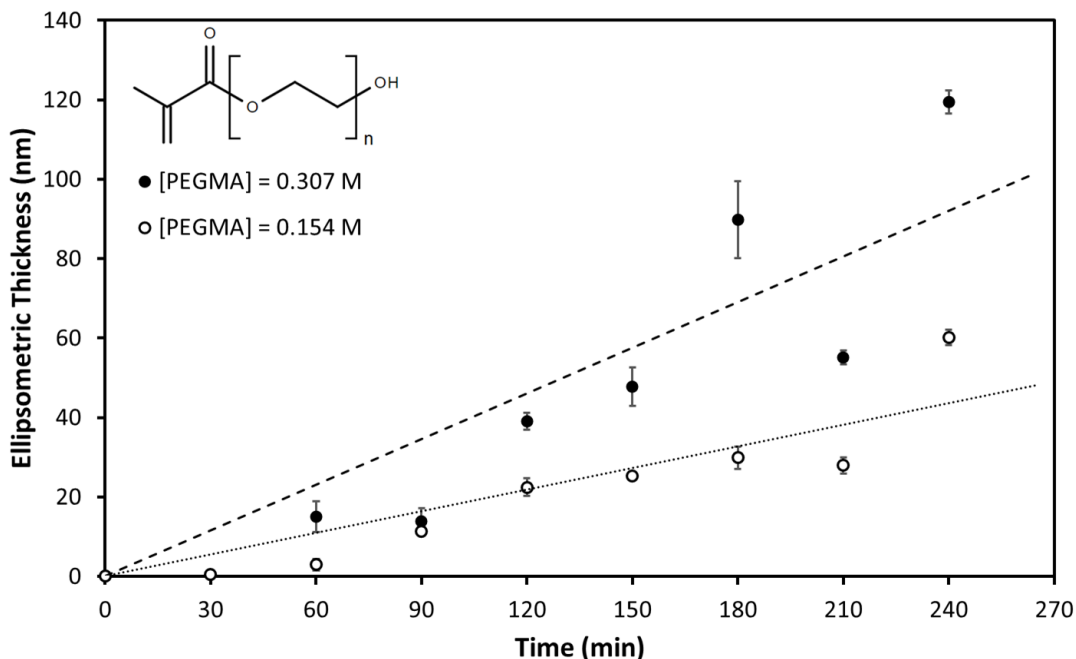
Figure 2.5. Ellipsometric thickness of g-pPEGMA films vs time formed at two different monomer concentrations in nitrogen-sparged reaction flasks. [AA] = 2.1 mM.

After successful growth of g-pPEGMA from initiator slides, g-pHEMA was also studied to examine whether the ARGET procedures that worked for grafting g-pPEGMA would also work with other monomers. Figure 2.6 shows the measured film thicknesses of g-pHEMA films with varying time and concentration. The g-pHEMA films were also grafted under nitrogen-sparged conditions. As with PEGMA, the g-pHEMA films appeared uniform visually. Variation in ellipsometric film thickness across each slide varied by less than ± 2 nm. A linear fit to the film thickness data yielded a rate constant k of $67 \pm 10 \frac{nm\ L}{mol\ hr}$ (95% confidence interval), a value similar to that for g-pPEGMA despite the HEMA monomer being smaller than the PEGMA monomer.
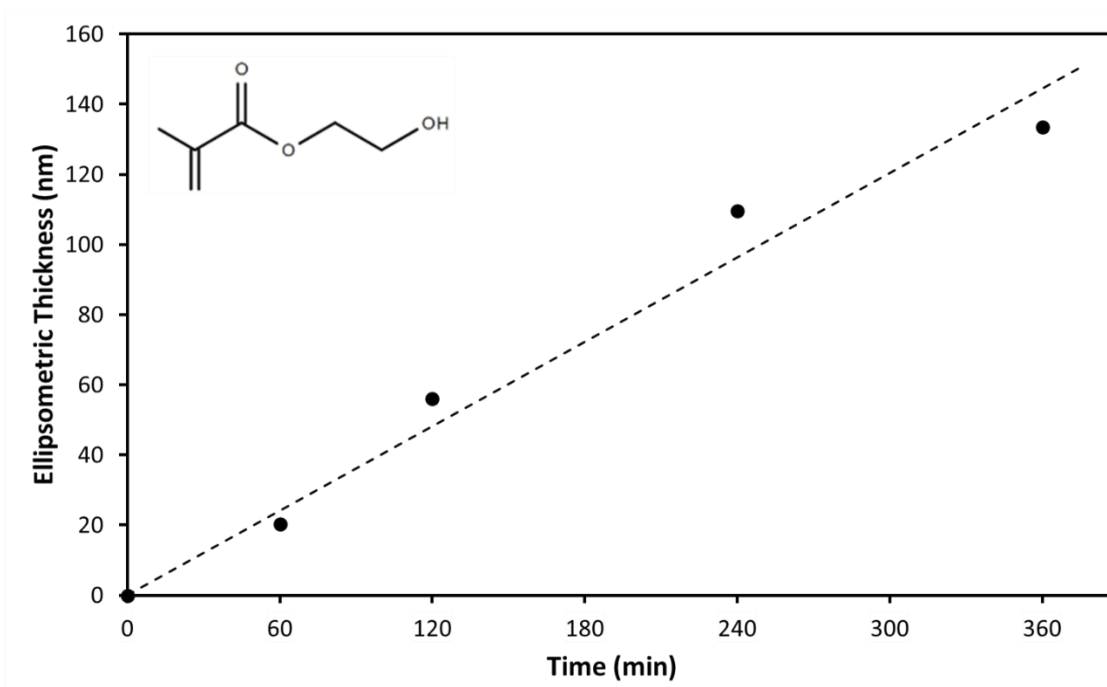
Figure 2.6. Ellipsometric thickness of g-pHEMA films vs time formed using a nitrogen-sparged 0.358 M monomer solution. [AA] = 2.1 mM.

Using the above ARGET procedure that yielded high-quality g-pHEMA and g-pPEGMA films, grafting of pSBMA was attempted once again. Unfortunately, these procedures, utilizing N_2-sparged solutions and associated lower ascorbic acid concentrations, continued to produce cloudy SBMA solutions resulting in precipitated films on the slides that could be removed by washing with water.

ARGET Polymerization of SBMA Revisited

As I was unable to obtain the SBMA monomer from Aldrich for a period of time after the initial experiments, I instead purchased the SBMA monomer from Fisher. Unexpectedly, SBMA obtained from Fisher could be grafted from silicon by ARGET without the previously experienced issues of solution cloudiness and precipitate formation. Using this SBMA from Fisher, the ARGET polymerization conditions were further refined to produce a system in which repeatable, controlled growth of g-pSBMA was realized.

Figure 2.7 shows the growth for an ARGET polymerization system in 9 and 18 mM solutions of SBMA. The data were consistent with first-order linear growth in which a doubling of monomer concentration leads to a doubling of polymerization rate. Assuming a constant Cu^I/Cu^{II} ratio, a constant number of active growing polymer chains, and a constant monomer concentration over the course of the polymerization, the growth could be described by $T = k*[M]_o*t$ where a rate constant k of $41 \pm 4 \frac{nm \, L}{mol \, hr}$ (95% confidence interval) was determined.
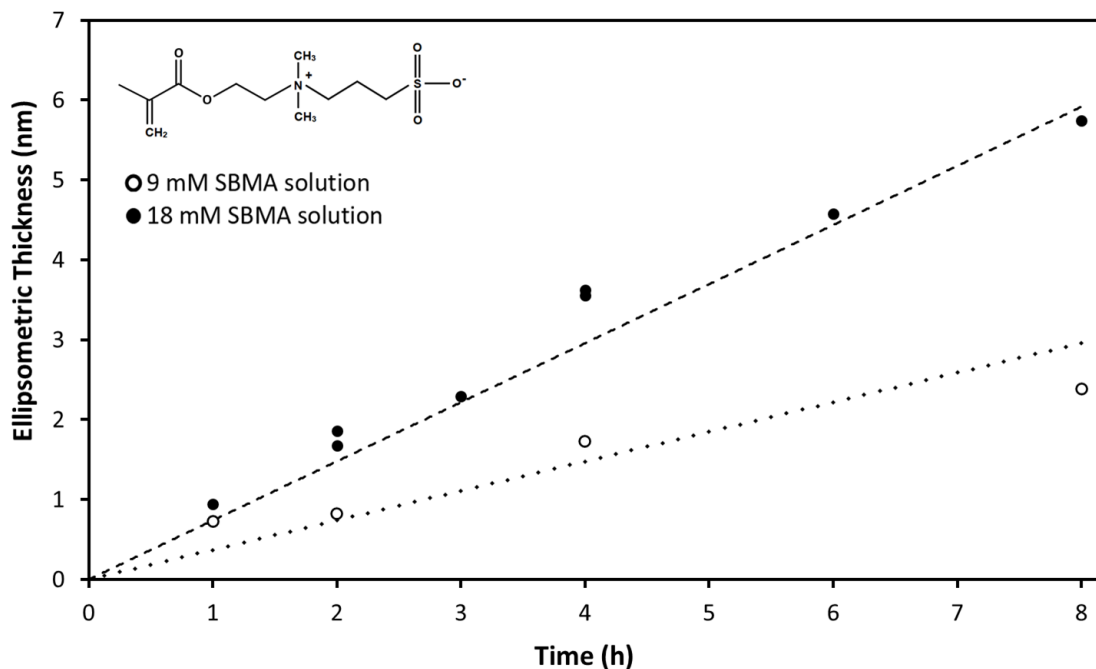
Figure 2.7. Ellipsometric thickness of g-pSBMA films vs time formed from 9 and 18 mM SBMA solutions using ARGET. The molar ratios of SBMA:CuBr$_2$:TPMA:AA were 125:1:5:160 and 250:1:5:160 for the 9 and 18 mM SBMA solutions respectively.

For applications involving the silicon nanopore membranes, the polymer thickness would need to be kept to a minimum in areas such as the pores walls. As g-pSBMA film should exhibit water contact angles of 10° or less,[18-20] I investigated the minimum thickness required to achieve such wetting values. Figure 2.8 shows the advancing contact angles of water in air for the samples in Figure 2.7 against their

ellipsometric thickness. The measured contact angles decreased from the 60-70° values of initiator modified slides to lower values as the zwitterionic polymer increased in thickness and covered the entire slide surface. Films with ellipsometric thickness of >4 nm had contact angles similar to values reported for thicker pSBMA films.[18–20]
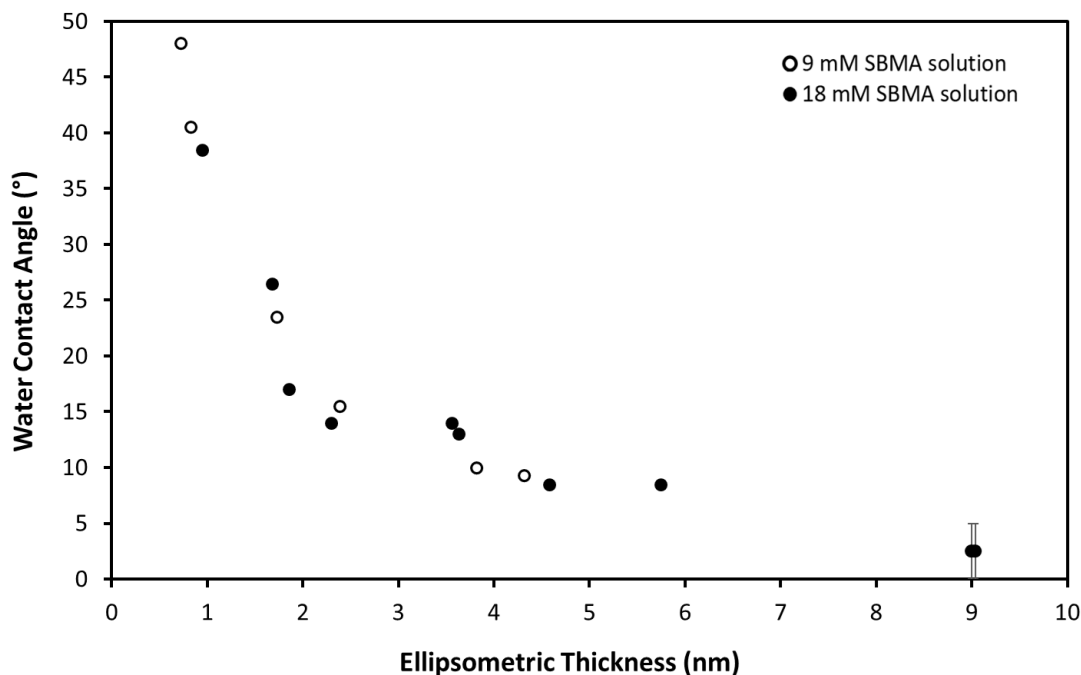
Figure 2.8. Advancing water contact angles vs ellipsometric thickness of g-pSBMA films grafted using ARGET. Note that the samples with film thicknesses of ~9 nm exhibited water contact angles ≤ 5°, and as a result, could not be accurately measured with our instrumentation Thus the samples were expressed in this figure as 2.5° ± 2.5° to represent the 0-5° range in which the water contact angle was likely to exist.

Based on these wetting results, I investigated whether the fouling resistance of these slides would improve with increasing thickness. Figure 2.9 plots the increase in fluorescence signal due to FITC-albumin adsorption on g-pSBMA films of varying thicknesses. Despite the scatter in the plot, the data showed the expected decrease in fouling with increasing film thickness. Possible sources of error that could have led to the scatter included inadequate washing procedures after FITC incubation or film heterogeneity.
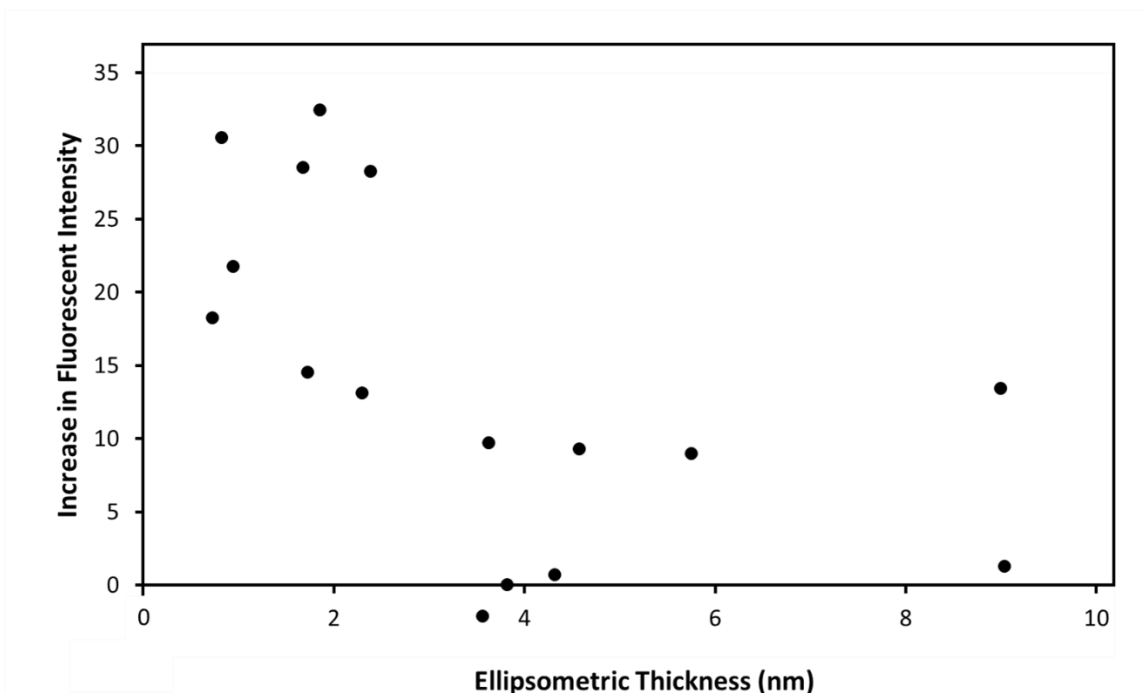
Figure 2.9. Fluorescence due to adsorbed FITC-albumin on g-pSBMA of various film thicknesses formed by ARGET. Intensity values normalized to average intensity of prior and subsequent blank slides. Exposure time = 5000 ms.

Figure 2.10 compares the increase in fluorescence to the water contact angles for the same samples shown in Figure 2.9. The expected trend of more hydrophilic samples exhibiting less increase in fluorescence due to adsorbed FITC-albumin was evident as these more wettable films should have been better able to form fouling-resistant hydration layers.
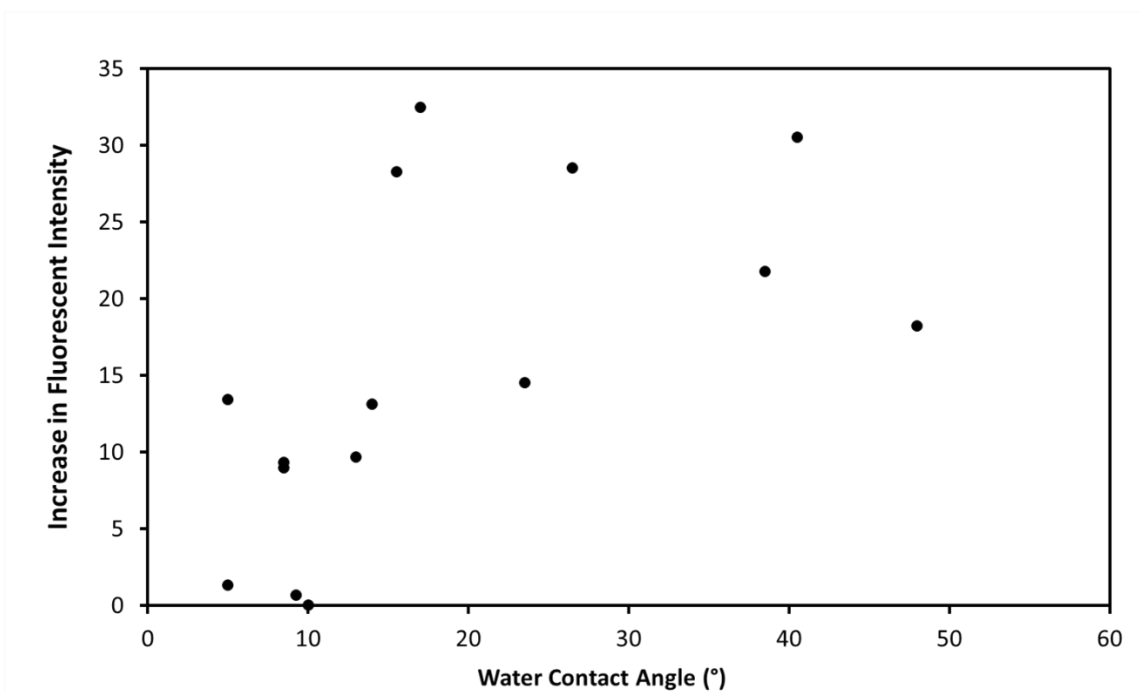
Figure 2.10. Fluorescence due to adsorbed FITC-albumin on g-pSBMA films formed by ARGET vs. their wettability by water. Intensity values taken at 5000 ms exposure normalized to average intensity of prior and subsequent blank slides.

Figure 2.11 compares the increase in fluorescence due to protein adsorption on g-pSBMA samples against that on g-BrTMOS and g-PEGsilane samples. In the figure, the fluorescence data for g-pSBMA was binned by thickness into 0-2 nm, 2-4 nm, and >4 nm ranges to allow easier comparison. As expected, samples with little to no grafted pSBMA film showed fouling similar to that of the initiator modified slides. With increasing thickness, the fouling resistance approached that of g-PEGsilane modified slides. The g-pSBMA films over 4 nm in thickness displayed promise, being those with performance most similar to that of the PEG-modified slides, with the expectation that they may exhibit slower rates of degradation.
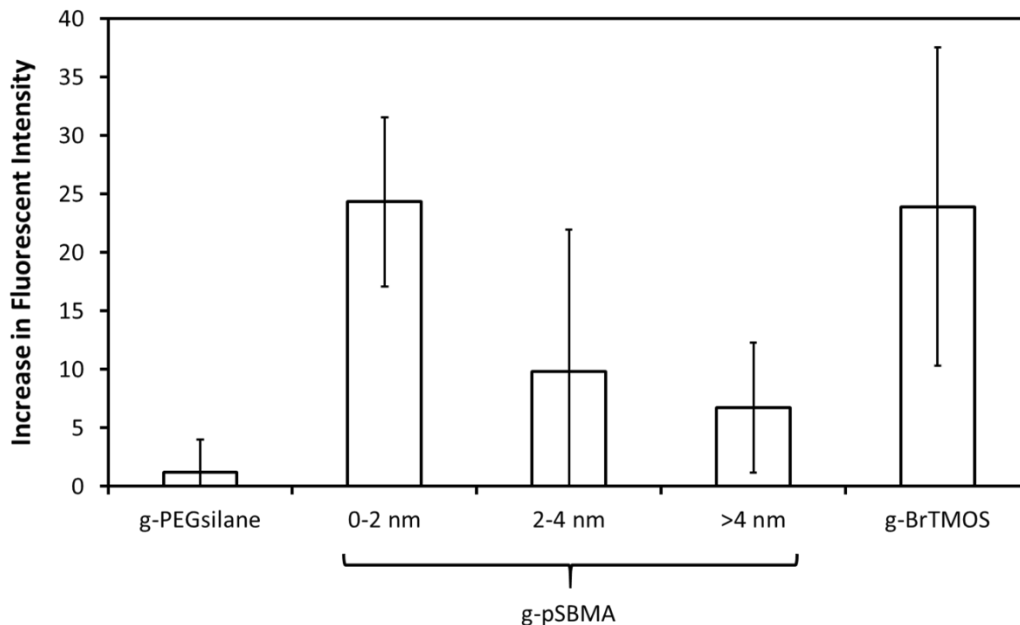
Figure 2.11. Increased fluorescence due to adsorption of FITC-albumin onto g-pSBMA films of different thickness ranges and onto initiator and PEG surfaces. Fluorescence measurements were normalized to the average intensity of prior and subsequent blank slides. Thicknesses of the g-BrTMOS and g-PEGsilane films were 1.1 ± 0.4 nm and 1.3 ± 0.2 nm, respectively. Exposure time = 5000 ms.

UV-Induced Attachment of Initiator-Alkene for Improved Stability of Attached Polymers

As mentioned previously, siloxane films often degrade in aqueous environments.[7,16,17,33,34] Quintana has shown that polymers grafted from silane-based initiator surfaces can, however, be protected.[7] They accomplished this stabilization by grafting a block of hydrophobic polystyrene from the initiator silane. A block of polymer with the desired functionality was then grafted from the hydrophobic polymer block. In their study, pSBMAA films grafted directly from a silane-initiator surface showed a complete loss of the grafted polymer after 4 weeks in a simulated seawater environment.[7] Films that included a hydrophobic polystyrene block between the silane-initiator and the overlying grafted pSBMAA maintained approximately 80% of their original thickness after 3 months under the same conditions.[7] However, in situations like ours where the silicon membrane's pores are on the nanometer scale, such a strategy may not be viable due to the required added thickness of the additional hydrophobic polymer layer.

As an alternative to the reliance Si-O-Si linkages for attachment, I also investigated an approach that employed more hydrolytically stable Si-C linkages to form monolayers and to provide sites for initiation. The method of grafting vinyl compounds from silicon utilizing a UV-induced silicon-carbon linkage has been demonstrated by the Buriak and Chidsey groups, among others.[35–42] As compared to Si-O-Si linkages, Si-C linkages are more stable and less susceptible to failure in aqueous environments as they avoid the hydrolytic instability associated with siloxane linkages.[16,17,33,34] Figure 2.12 illustrates the scheme for covalently attaching an alkene-containing molecule, in this case 4-vinylbenzyl chloride (VBC), to a silicon substrate. In this method, silicon samples were first exposed to a hydrofluoric acid (HF) solution to remove the native oxide layer and yield a hydrogen-terminated silicon surface. In a following step, the hydrogen-terminated silicon sample was simply exposed to the chosen alkene and irradiated with UV light. The UV irradiation induced homolytic dissociation of surface hydrogen atoms resulting in radical sites to which the alkene attached.[35,42,43] By this scheme, molecular films of alkenes were attached to silicon surfaces to provide initiator groups from which polymers were grown via ARGET.
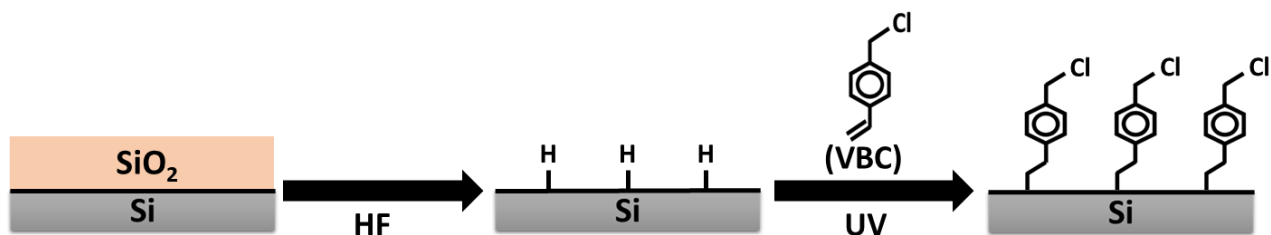
Figure 2.12. Reaction scheme for covalent attachment of alkenes such as VBC to H-terminated silicon via UV-hydrosilylation.

We leveraged this UV-induced linkage method to attach VBC to our silicon substrates as this compound offers both the desired initiator group and also the needed vinyl group for attachment to silicon via hydrosilylation.[35,44] Xu et al. previously demonstrated UV-induced hydrosilylation of VBC to H-terminated silicon and successfully utilized the resulting g-VBC surface as an ATRP initiator for grafting

of surface-initiated polymers from their silicon surfaces.[35,45] The chloride located at the benzylic position of VBC could be homolytically cleaved to by the Cu(I) catalyst to generate the surface bound radicals necessary for ARGET and/or ATRP polymerization of hydrophilic monomers such as HEMA, SBMA, and many others as will be shown here.[3,4,35,43,44]

In practice, I found that this UV-hydrosilylation process could be conducted in a very straight-forward manner. To do so, 15 µL of liquid VBC was simply deposited onto H-terminated silicon wafers, covered with a coverslip, and then exposed to a UV light source. As each UV-source's power and emission spectrum along with the coverglass's thickness and material (i.e. glass vs quartz) will all likely impact the hydrosilylation reaction progress differently, it is likely necessary to determine an ideal UV-exposure time for one's individual setup. With our DYMAX 5000-EC UV curing lamp system and No. 1 thickness glass coverslides, we determined 100 s exposure to be appropriate. Obtained g-VBC surfaces on flat silicon typically possessed advancing contact angles of approximately 75-85°, consistent with literature reports for g-VBC samples.[35] Longer times yielded minimal change in water contact angle or thickening/hardening of the VBC liquid (possibly a polymerization process) that would result in the coverglass becoming stuck to the sample surface, and thus longer exposure times were avoided. Shorter exposure times exhibited lower water contact angles which suggested lesser g-VBC coverage on the silicon substrate.

To demonstrate that the attachment was induced by the UV light source, and not purely some other factor such as heat, I assembled a crude mask made of strips of electrical tape on a glass coverslide (see Figure 2.13). This masked-coverglass was placed over H-terminated silicon slide during UV-hydrosilylation of VBC in place of the usual non-masked coverslides. The resulting g-VBC slide after ARGET polymerization of pHEMA exhibited dark blue stripes of polymer in the areas not masked by the electrical tape. This was consistent with areas of thicker pHEMA due to more densely grafted g-VBC in areas exposed to the UV light source.
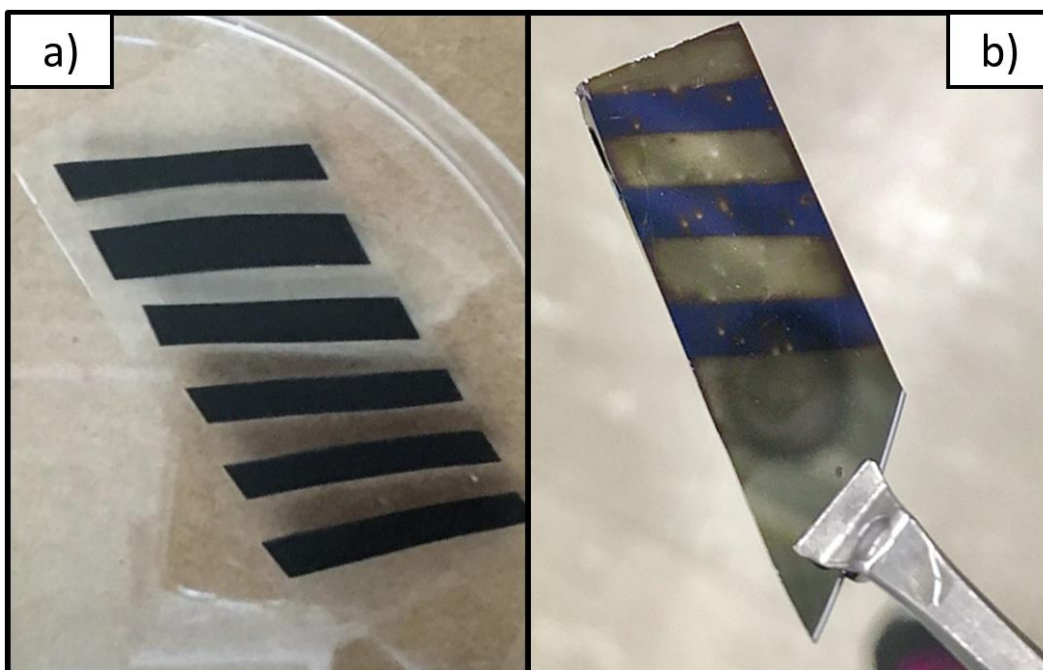
Figure 2.13. Early demonstration of UV-hydrosilylation. a) Crude mask made of strips of electrical tape on a glass coverslide. This was placed over H-terminated silicon slide during UV-hydrosilylation of g-VBC. b) The resulting g-VBC slide after ARGET polymerization of pHEMA. Note that the dark blue stripes represent the areas of thicker pHEMA on areas not masked by electrical tape during the VBC attachment step.

After successful ARGET grafting of pHEMA from these g-VBC initiator samples, I investigated the grafting of pSBMA from g-VBC. Figure 2.14 shows the thickness growth for the ARGET polymerization of SBMA from g-VBC compared to that previously grafted from g-BrTMOS initiator samples; in both cases, 18 mM SBMA solutions were utilized. The g-VBC-pSBMA samples exhibited faster initial growth and greater ellipsometric thickness for common exposure times as compared to the g-BrTMOS-pSBMA, albeit with less linear film growth. Ultimately, controlled growth of pSBMA from g-VBC was demonstrated based on these results.
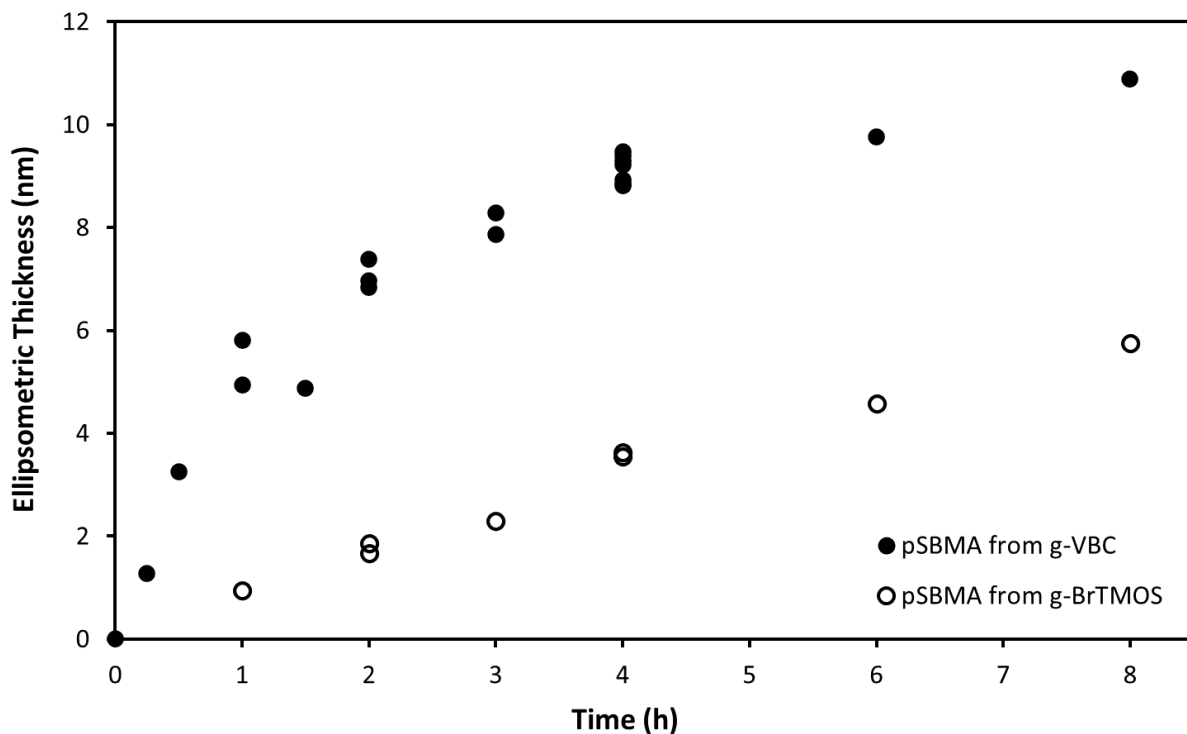
Figure 2.14. Ellipsometric thickness vs time of g-pSBMA films formed from 18 mM SBMA solutions using ARGET polymerization from two different initiators: g-VBC and g-BrTMOS. The molar ratios of SBMA:CuBr$_2$:TPMA:AA were 250:1:5:160 for the forming solutions.

Figure 2.15 shows the advancing water contact angles for the samples in shown Figure 2.14 against their ellipsometric thicknesses. The measured contact angles decreased from the 75-85° values of g-VBC initiator slides to lower values as the zwitterionic polymer increased in thickness, consistent with data demonstrated in previous g-BrTMOS-pSBMA experiments. As with g-BrTMOS-pSBMA films, the g-VBC-pSBMA films with ellipsometric thickness of >4 nm had contact angles less than 15° as expected for pSBMA coatings.
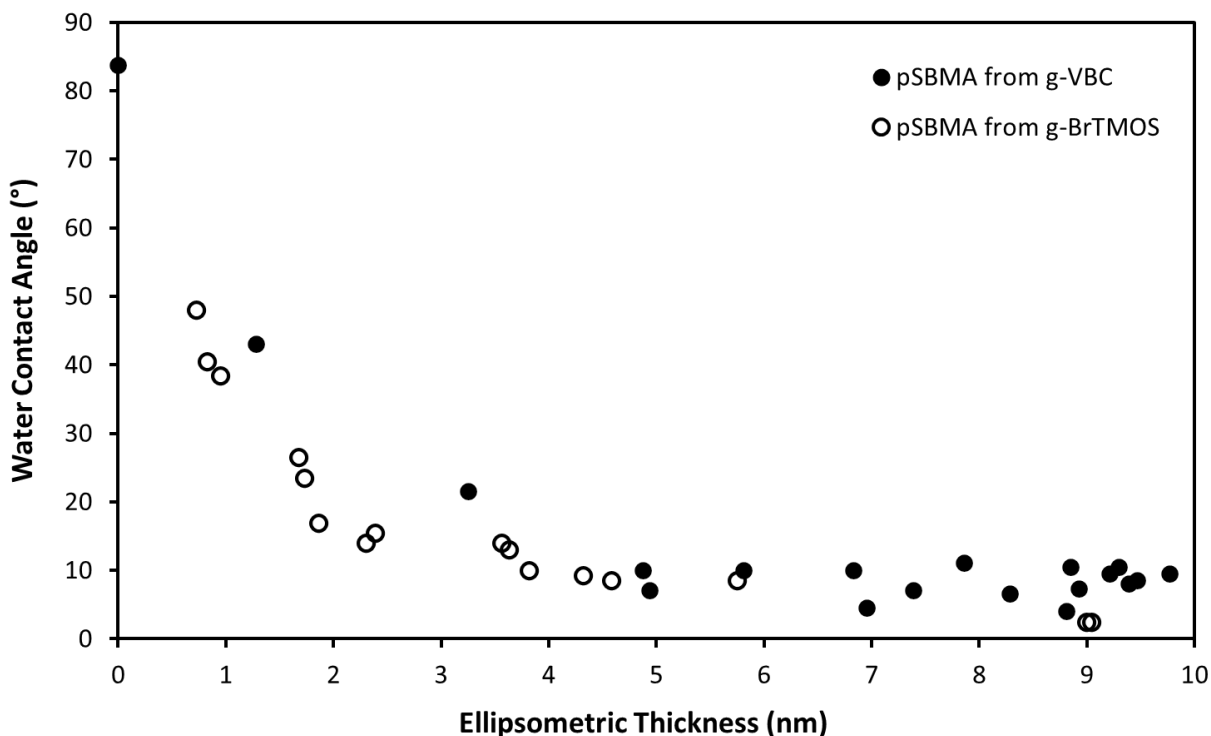
Figure 2.15. Water contact angle vs ellipsometric thickness of g-pSBMA films made by surface-initiated ARGET polymerization from two different initiators: g-VBC and g-BrTMOS.

Thermal Attachment of Initiator-Alkene for Improved Stability of Attached Polymers

In addition to UV-induced hydrosilylation of g-VBC, thermal hydrosilylation for attachment of g-VBC was also investigated. H-terminated silicon samples were submerged in VBC and placed in an oven at different temperatures (100°C and 120 °C) and for varying periods of time (30-120 minutes). Figure 2.16 shows the ellipsometric thickness growth for pSBMA films produced by ARGET polymerization from g-VBC initiator samples manufactured with varying temperature and exposure times; in all cases 18 mM SBMA solutions were utilized. As with the g-VBC produced via UV hydrosilylation, the thermally attached g-VBC also successfully initiated ARGET polymerization of pSBMA. Ultimately, controlled growth of pSBMA from thermally attached g-VBC was demonstrated based on these results.
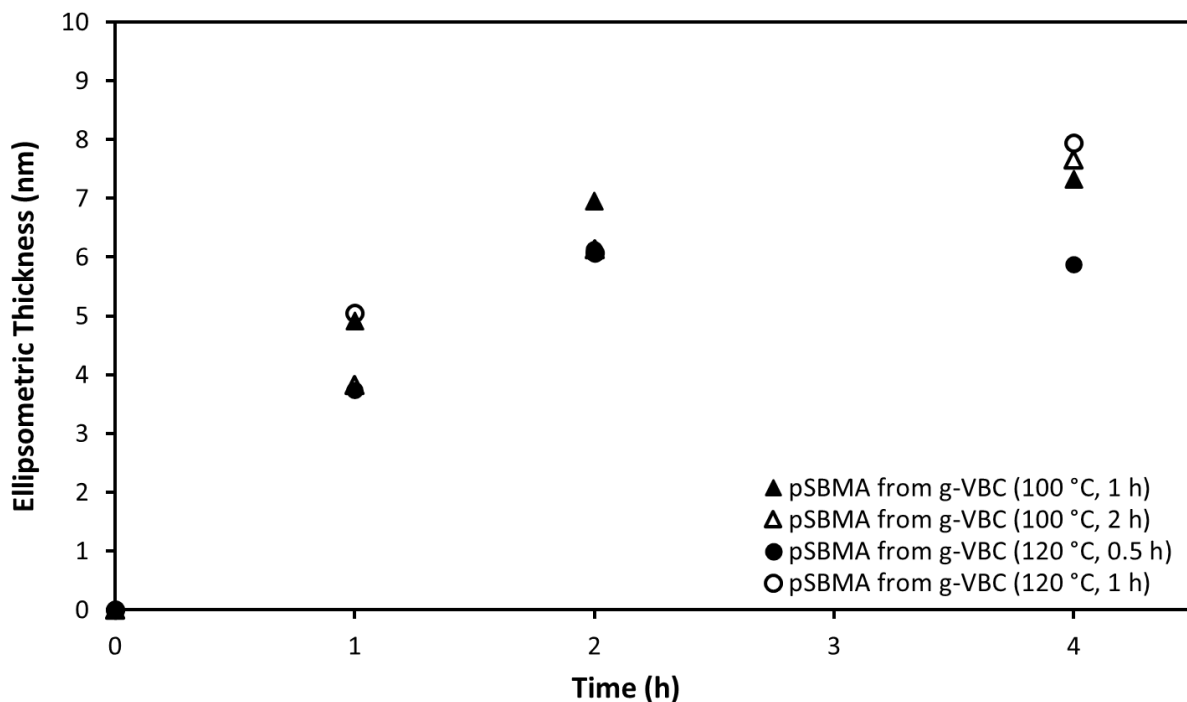
Figure 2.16. Ellipsometric thickness vs time of g-pSBMA films formed from 18 mM SBMA solutions using ARGET polymerization from g-VBC surfaces formed via thermal hydrosilylation. The molar ratios of SBMA:CuBr$_2$:TPMA:AA were 250:1:5:160 for the forming solutions.

Figure 2.17 shows the advancing water contact angles for the samples in shown Figure 2.16 against the added ellipsometric thicknesses of the grafted pSBMA. The measured contact angles decreased from the 70-85° values of g-VBC initiator slides to lower values as the zwitterionic polymer increased in thickness, consistent with data demonstrated in previous g-VBC-pSBMA experiments. Compared with pSBMA films grafted from g-VBC produced via UV hydrosilylation, pSBMA films from g-VBC produced via thermal hydrosilylation seemed to require a slightly higher ellipsometric thickness before exhibiting contact angles less than 15°. Regardless, the greater quantity of VBC needed for thermal attachment (where the sample is submerged in the liquid VBC), proved less practical than the UV method.
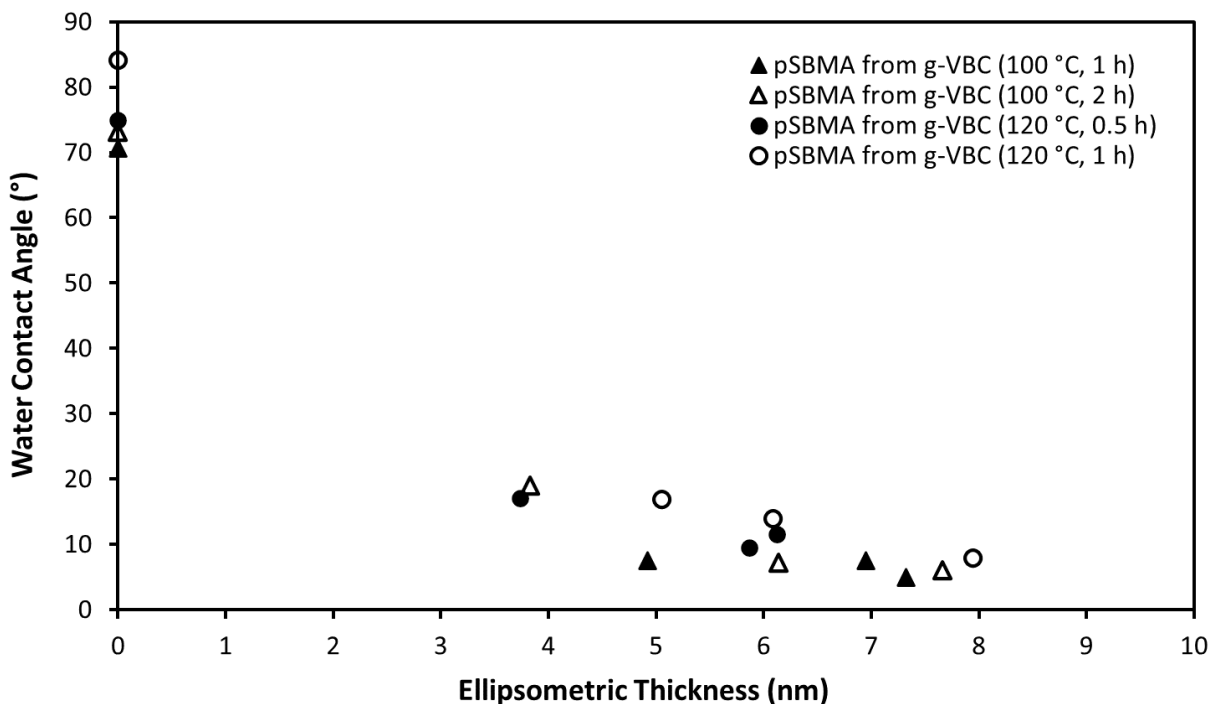
Figure 2.17. Water contact angles vs ellipsometric thickness of g-pSBMA films formed from 18 mM SBMA solutions using ARGET polymerization from g-VBC surfaces formed via thermal hydrosilylation. The molar ratios of SBMA:CuBr$_2$:TPMA:AA were 250:1:5:160 for the forming solutions.

Grafting of Other Zwitterionic Polymers and Monolayers

In addition to SBMA, I examined four other grafted zwitterionic coatings as potential antifouling candidates, three of which were polymers and one a monolayer. A zwitterionic monolayer generated by sulfobetaine-silane (SBSi) was studied as a means by which a surface could be functionalized with zwitterionic moieties while minimizing thickness of the added film. Figure 2.18 shows the approach used to synthesize SBSi via ring-opening reaction of N,N-dimethyl-3-(trimethoxysilyl)propylamine (DMASi) with 1,3-propanesultone (1,3-PS). This SBSi compound was attached by self-assembly to piranha-cleaned silicon slides. The resulting g-SBSi modified slides exhibited an ellipsometric thickness of 0.6 ± 0.1 nm and a high degree of hydrophilicity with water contact angles measuring $< 5°$ in air.
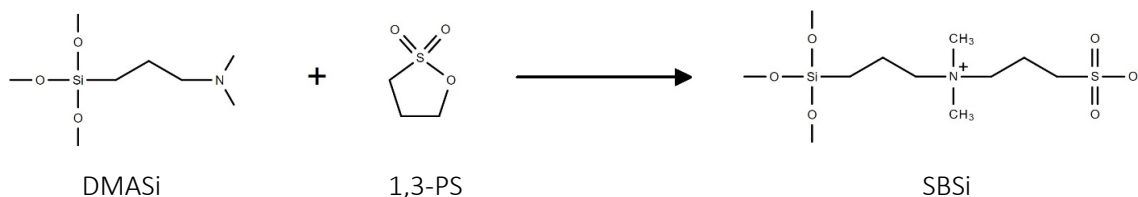
Figure 2.18. Reaction scheme for synthesis of SBSi.

As a result of the zwitterionic-silane's hydrophilic nature, the coating was expected to provide resistance to fouling. Figure 2.19 compares the increase in fluorescence due to adsorbed FITC-albumin on g-SBSi films to that on g-PEGsilane and initiator (g-BrTMOS) modified samples. The g-SBSi samples performed similar to the g-PEGsilane samples and exhibited a fluorescence close to that of the background. Like g-PEGsilane, g-SBSi showed significantly less increase in fluorescence than the g-BrTMOS slides. Based upon these results, it is expected that the g-SBSi will show a high resistance to fouling and not be susceptible to degradation processes that affect polyethers. Thin monolayers based on SBSi may be useful for coating the walls of the nanopore membranes, a location where coating thickness will likely need to be minimized.
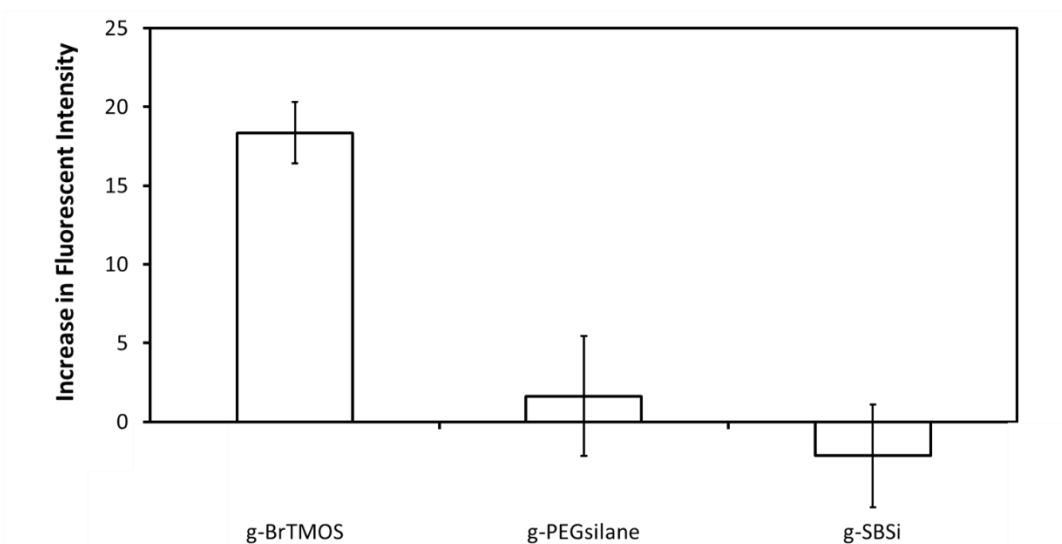
Figure 2.19. Fluorescence due to adsorption of FITC-albumin onto g-pSBSi, g-PEGsilane, and initiator modified surfaces. Fluorescence measurements were normalized to the average intensity of prior and subsequent blank slides. Exposure time = 5000 ms.

In addition to pSBMA, I examined the grafting of three other zwitterionic polymers. The first of these was sulfobetaine vinylimidazole (SBVI), a monomer that was synthesized by ring-opening reaction of 1-vinylimidazole with 1,3-propanesultone (1,3-PS) (see Figure 2.20).
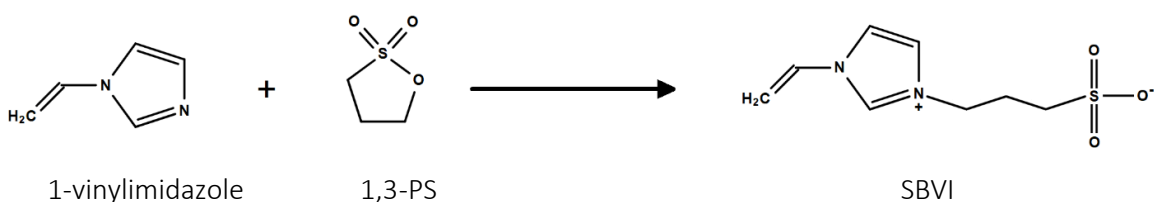
Figure 2.20. Reaction scheme for the synthesis of SBVI.

Efforts to graft g-pSBVI via ARGET did not yield films with wetting properties consistent with fouling resistant surfaces. The grafted films visually appeared non-uniform and exhibited water contact angles of ~40°. The grafted polymer appeared to not fully cover the underlying initiator layer. In contrast, grafted pSBVI as thick as 62 ± 3 nm was produced via ATRP. These films exhibited a more consistent

surface appearance and advancing contact angles for water of ~8°. Although these very hydrophilic pSBVI films formed by ATRP exhibited the favorable wetting properties associated with fouling resistant coatings, we discontinued work with this monomer as a polymer requiring the rigorous deoxygenation techniques needed for ATRP was not practical for our purposes.

Another zwitterionic monomer, sulfobetaine methacrylamide (SBMAA), was synthesized via ring-opening reaction of N-[3-(dimethylamino)propyl]methacrylamide (DMAPMAA) with 1,3-PS (see Figure 2.21). Efforts to graft g-pSBMAA via ARGET yielded films that were consistently highly wettable (water contact angles less than 15°). These films possessed a mirror-like, uniform surface appearance. Figure 2.22 shows the thickness growth for the ARGET polymerization of SBMAA from g-BrTMOS formed from both 18 mM and 36 mM SBMAA solutions. Worth noting was that compared to pSBMA grafted from g-BrTMOS, pSBMAA required a higher monomer concentration to obtain films of comparable thickness Ultimately, controlled growth of pSBMAA from g-BrTMOS was successfully demonstrated based on these results.
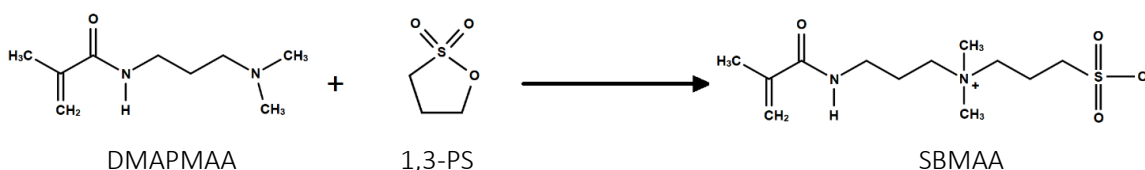
Figure 2.21. Reaction scheme for synthesis of SBMAA.
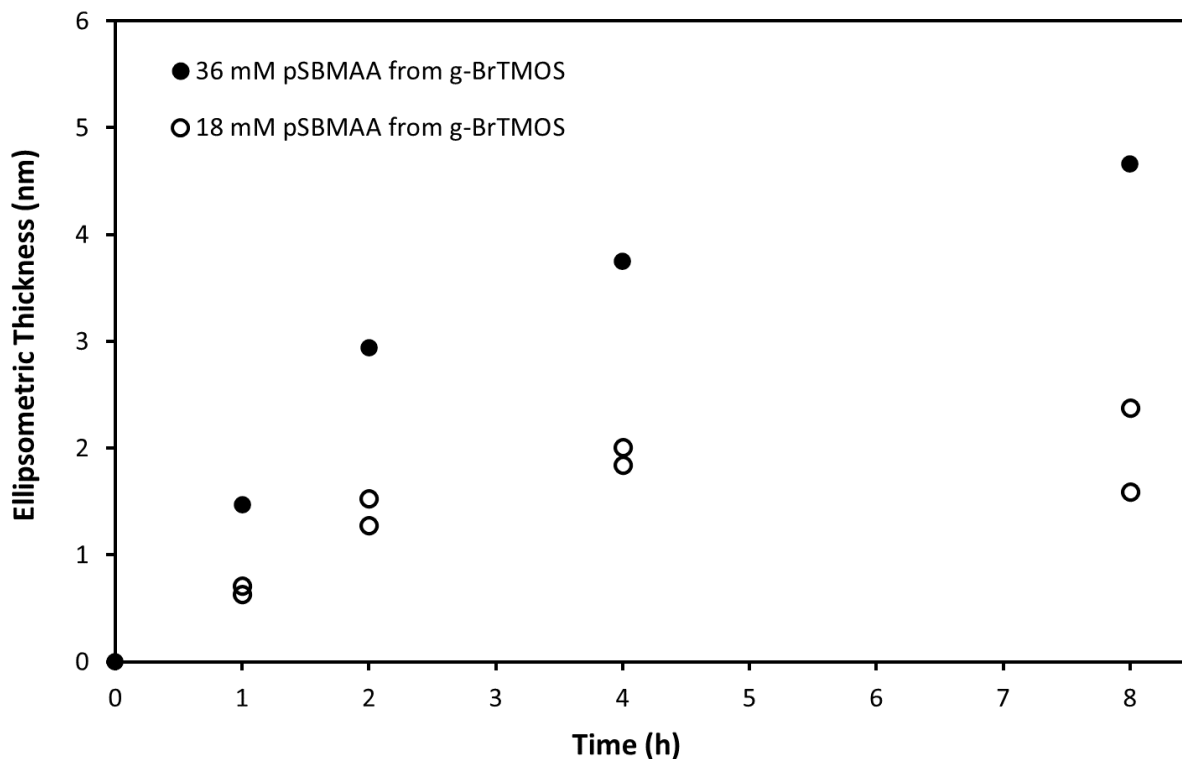
Figure 2.22. Ellipsometric thickness vs time for g-pSBMAA films formed from 18 and 36 mM SBMAA solutions using ARGET from g-BrTMOS initiator surfaces. The molar ratios of SBMAA:CuBr$_2$:TPMA:AA were 250:1:5:160 and 500:1:5:160 for the 18 and 36 mM SBMAA solutions respectively.

Figure 2.23 shows the advancing water contact angles for the samples in shown Figure 2.22 against the increase in ellipsometric thicknesses due to added pSBMAA. The measured contact angles decreased from the higher values of g-BrTMOS initiator slides to lower values as the zwitterionic polymer increased in thickness, similar with data demonstrated in previous g-BrTMOS-pSBMA experiments. Compared to g-BrTMOS-pSBMA films, the g-BrTMOS-pSBMAA films exhibited contact angles under 15° at lower ellipsometric thicknesses than the g-VBC-pSBMA coatings. The g-BrTMOS-pSBMAA films with ellipsometric thickness of >2 nm demonstrated contact angles less than 15°.
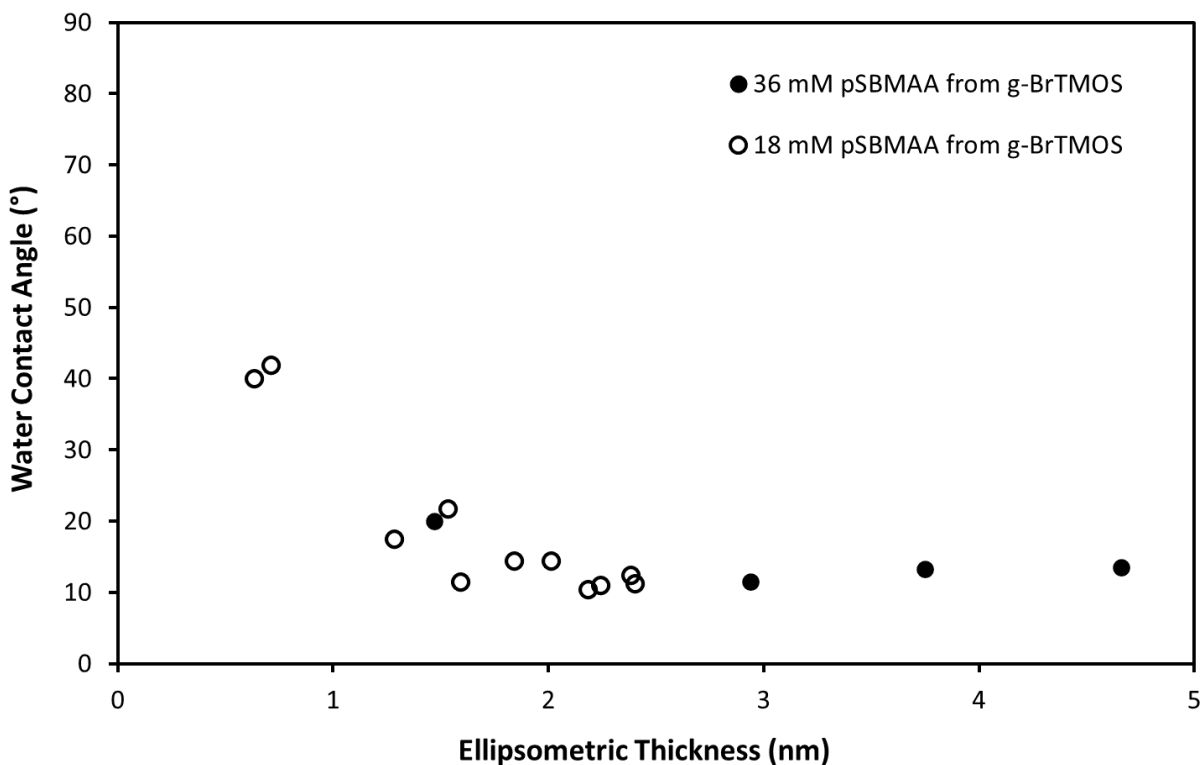
Figure 2.23. Water contact angle vs ellipsometric thickness of g-pSBMAA films formed from 18 and 36 mM SBMAA solutions using ARGET from g-BrTMOS initiator surfaces. The molar ratios of SBMAA:CuBr$_2$:TPMA:AA were 250:1:5:160 and 500:1:5:160 for the 18 and 36 mM SBMAA solutions respectively.

In addition to studying pSBMAA grafted from the g-BrTMOS initiator, I also examined pSBMAA grafted from g-VBC. Figure 2.24 shows the thickness growth for the ARGET polymerization of SBMAA from g-VBC formed from both 36 mM and 72 mM SBMAA solutions. The g-VBC-pSBMAA samples showed similar growth in ellipsometric thickness for a common monomer concentration (36 mM) as compared to the g-BrTMOS-pSBMAA. Ultimately, controlled growth of pSBMAA from g-VBC was demonstrated based on these ellipsometry results.
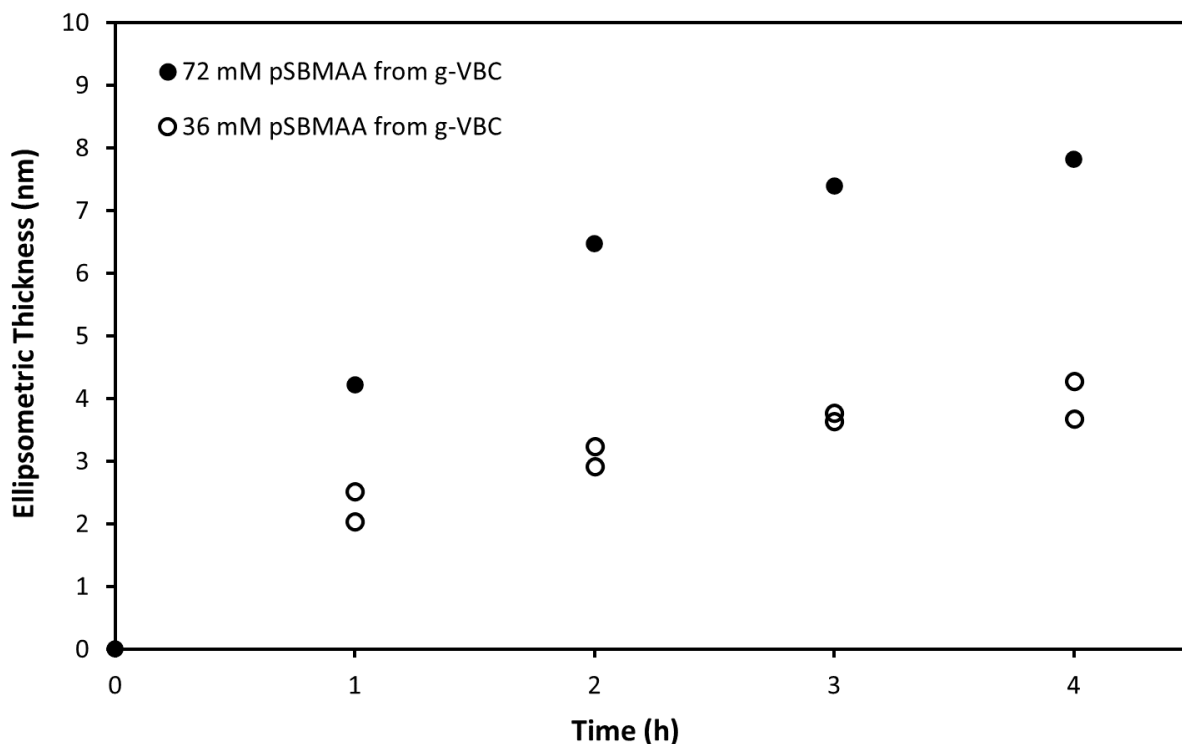
Figure 2.24. Ellipsometric thickness vs time of g-pSBMAA films formed from 36 and 72 mM SBMAA solutions using ARGET from g-VBC initiator surfaces. The molar ratios of SBMAA:CuBr$_2$:TPMA:AA were 500:1:5:160 and 1000:1:5:160 for the 36 and 72 mM SBMAA solutions respectively.

Figure 2.25 shows the advancing water contact angles for the samples in shown Figure 2.24 against the increase in ellipsometric thicknesses due to added pSBMAA. The measured contact angles decreased from the 75-85° values of g-VBC initiator slides to lower values as the zwitterionic polymer increased in thickness, similar with data demonstrated in previous g-BrTMOS-pSBMAA experiments. Compared to g-BrTMOS-pSBMAA films, the g-VBC-pSBMAA films did not exhibit the desired contact angles of under 15° within the thickness range studied here (approximately 0-8 nm); meanwhile, the g-BrTMOS-pSBMAA films with ellipsometric thickness of >2 nm did demonstrate contact angles less than 15°.
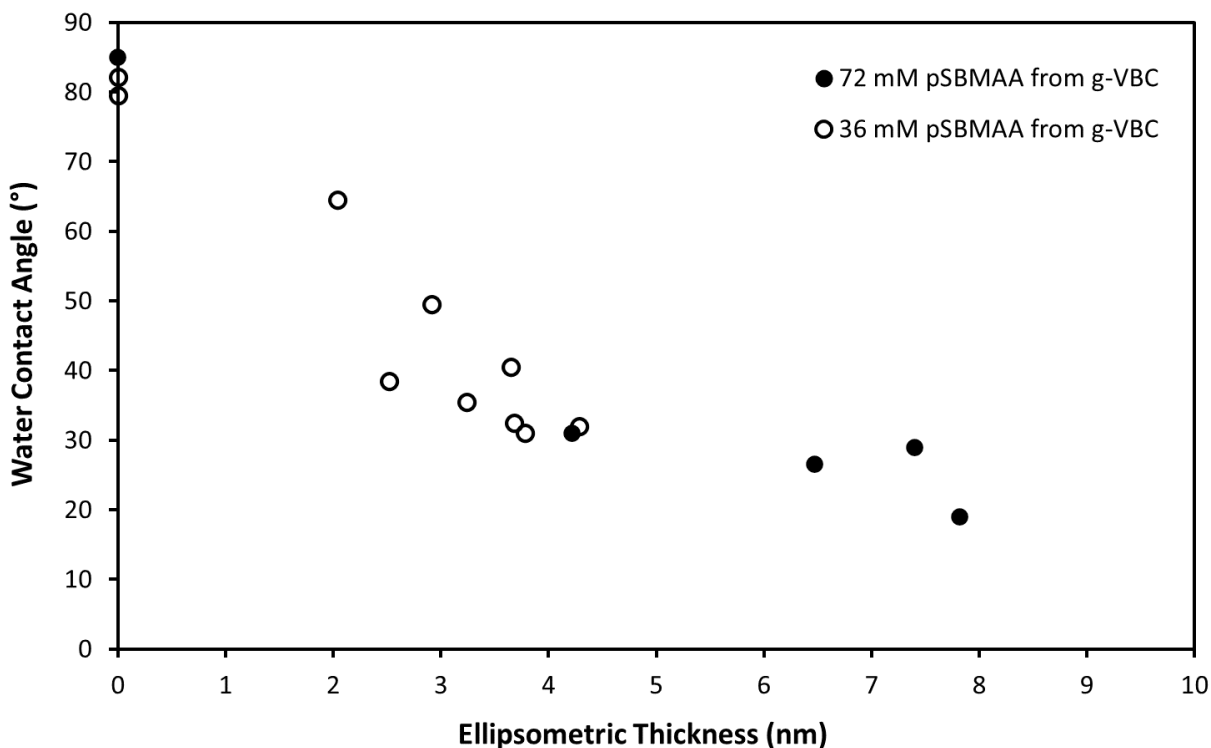
Figure 2.25. Water contact angle vs ellipsometric thickness of g-pSBMAA films formed from 36 and 72 mM SBMAA solutions using ARGET from g-VBC initiator surfaces. The molar ratios of SBMAA:CuBr$_2$:TPMA:AA were 500:1:5:160 and 1000:1:5:160 for the 36 and 72 mM SBMAA solutions respectively.

Another zwitterionic monomer, sulfobetaine acrylate (SBA), was synthesized via ring-opening reaction of 2-(dimethylamino)ethyl acrylate (DMAEA) with 1,3-PS (Figure 2.26). Efforts to graft g-pSBA via ARGET yielded films that were consistently highly wettable (water contact angles less than 15°). These films possessed a mirror-like, uniform surface appearance. Figure 2.27 shows the thickness growth for the ARGET polymerization of SBA from g-VBC formed from 18, 90, and 180 mM SBA solutions. While controlled growth of pSBA from g-VBC was demonstrated for 18 mM and 90 mM SBA monomer solutions, at 180 mM, many of the monomer solution would turn cloudy, likely due to excessive polymerization of SBA in solution. I was not able to produce controlled growth of g-pSBA at 180 mM.
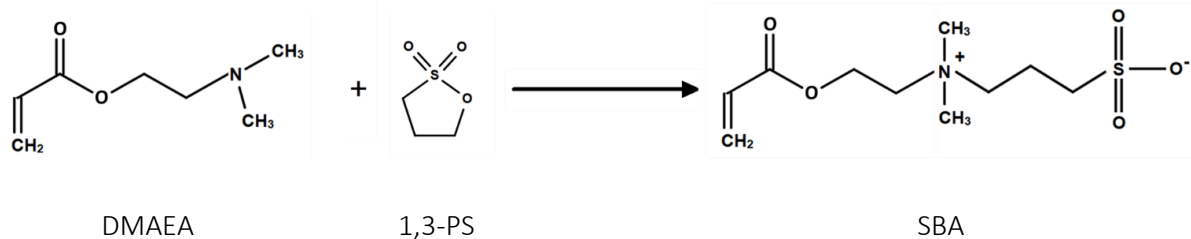
Figure 2.26. Reaction scheme for synthesis of SBA.
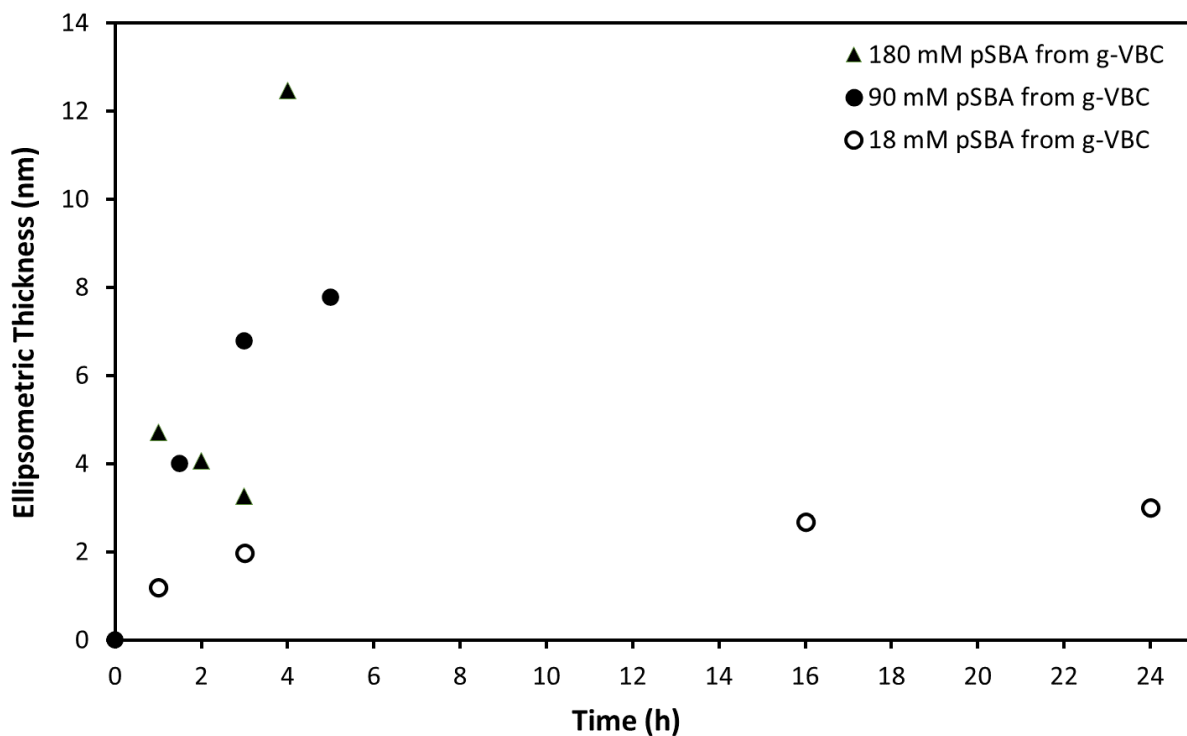
Figure 2.27. Ellipsometric thickness vs reaction time of g-pSBA films formed from 18, 90, and 180 mM SBA solutions using ARGET from g-VBC initiator surfaces. The molar ratios of SBA:CuBr$_2$:TPMA:AA were 250:1:5:160, 1250:1:5:160, and 2500:1:5:160 for the 18, 90, and 180 mM SBA solutions respectively.

Figure 2.28 shows the advancing water contact angles for the samples in shown Figure 2.27 against the increase in ellipsometric thicknesses due to added pSBA. The measured contact angles decreased from the higher values of g-VBC initiator slides to lower values as the zwitterionic polymer increased in

thickness, similar with data demonstrated in previous g-VBC-pSBMA experiments. Compared to g-VBC-pSBMA films, the g-VBC-pSBA films seemed to require a slightly higher ellipsometric thickness before exhibiting contact angles less than 15°. Based on these experiments, the pSBA films would likely need to be at least 5-6 nm in ellipsometric thickness before reaching below a 15° water contact angle. In addition, SBA is synthesized from 2-(dimethylamino)ethyl acrylate which is considered fatal if inhaled, further making it a less ideal zwitterionic monomer to work with as compared to SBMA.
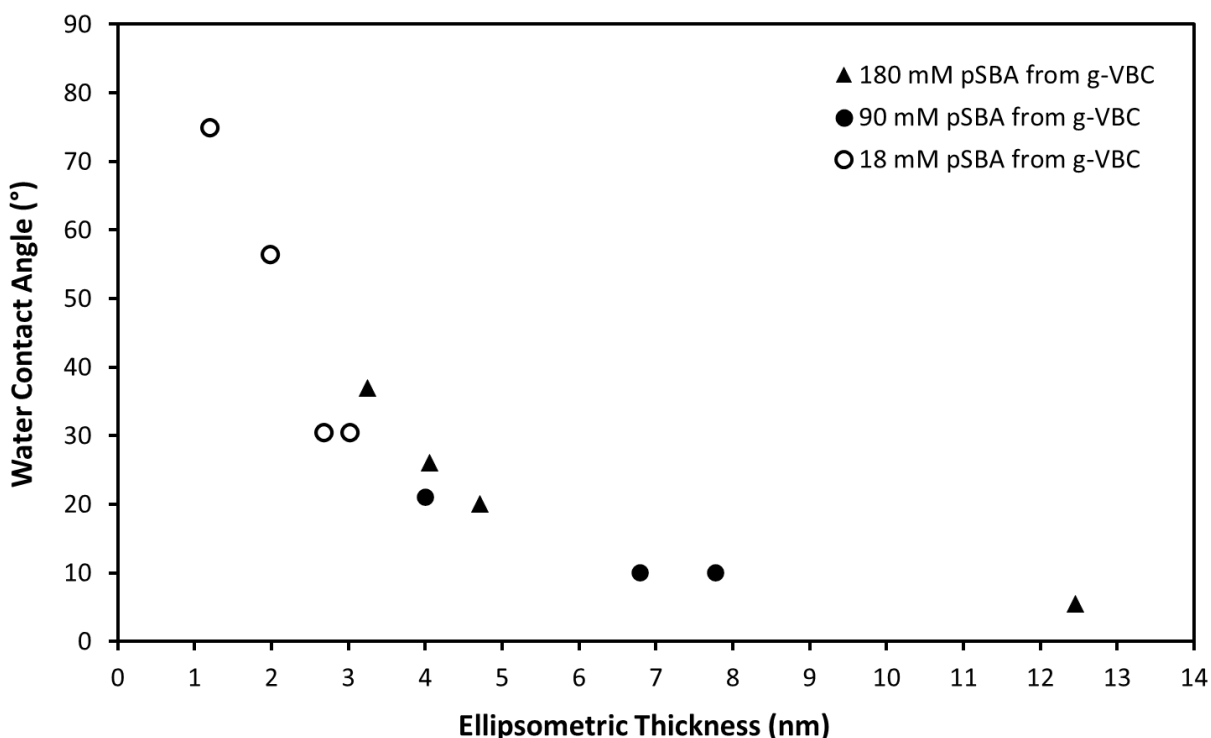
Figure 2.28. Contact angle vs ellipsometric thickness of g-pSBA films formed from 18, 90, and 180 mM SBA solutions using ARGET from g-VBC initiator surfaces. The molar ratios of SBA:CuBr$_2$:TPMA:AA were 250:1:5:160, 1250:1:5:160, and 2500:1:5:160 for the 18, 90, and 180 mM SBA solutions respectively.

Utilization of Membrane Geometry to Pattern via Combined Silanization/UV-Hydrosilylation Method

A future opportunity that arises from my work with UV-hydrosilylation and silane-monolayer research is to combine these two methods in a unique manner that utilizes the geometry of our collaborators' kidney nanopore membranes. Although resist-free patterning of silicon has been demonstrated by Kang et

65

al. on flat silicon substrates using a combined UV-induced linkage/silane approach, a mask was still required.[44] I propose the possibility of a resist-free/mask-free patterning technique for the silicon membranes using this combined UV-linkage and silane approach. Patterning could be accomplished by utilizing the pre-existing geometry of the nanopore membranes by the steps illustrated in Figure 2.29. After removal of the native oxide via HF etch, the initiator VBC (or any other desired alkene) would be covalently attached (step A) to the top surface of the silicon substrate via Si-C linkage using UV-hydrosilylation. As the UV light should only generate radical sites on the exposed outer surface of the nanofilter membrane, the pore walls should be left unmodified. After regrowth of the oxide on the unmodified pore walls (step B), a silane ("Z" in Figure 2.29) would be attached within the pores (step C). A chosen polymer would then be grafted from the attached initiator, g-VBC, via ARGET or ATRP (step D).
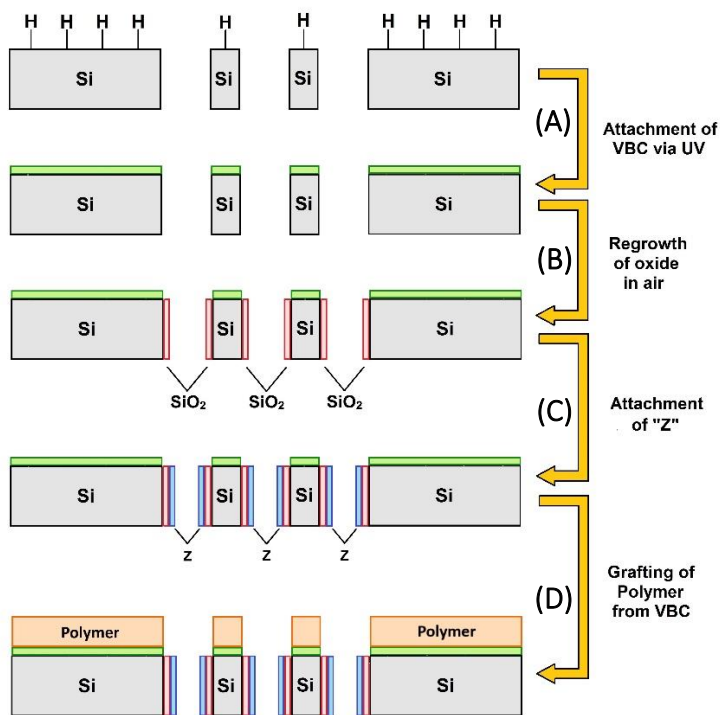
Figure 2.29. Reaction scheme for geometry-based pattering of nanopore membranes.

This process would tailor the surface properties of the exposed top (and bottom surfaces)

independently from the surface of the pore walls. As the pores of the nanofilter membranes can be ~7 nm across, the ability to independently control the modification occurring in the pores could prove crucial. This approach is designed to avoid clogging the pores while grafting a relatively thick polymer such as pSBMA from the top surface. A very thin monolayer of SBSi could be grafted from the pore walls to provide a highly wettable coating with minimal change in the cross-sectional area of the pores.

Conclusions

The procedures and techniques developed as part of my research have resulted in well-controlled surface-initiated ARGET polymerizations of a hydrophilic monomers including pPEGMA and pHEMA along with hydrophilic zwitterionic monomers including pSBMA, pSBMAA, pSBA, and others that are candidates to provide antifouling properties. Under the ARGET polymerization conditions developed here, the grafted film thicknesses of these polymer films increased in a manner consistent with well-controlled growth within the thickness range evaluated here. In addition to the siloxane-bound initiators typically used with surface-initiated polymerization, we also utilized Si-C bound initiators (g-VBC) formed through UV-induced hydrosilylation. The g-VBC proved successful for the initiation of ARGET polymerizations of the desired zwitterionic monomers and should provide improved hydrolytic stability as compared to the siloxane-bound initiator films. The polymer films produced here exhibited a uniform appearance and low variation in ellipsometric film thickness across each slide. This ability to produce films of predictable thickness and high uniformity are invaluable in situations, such as with the nanopore membranes, where precise control of film thickness may be required. In addition to these grafted polymers, covalently attached monolayers including g-PEGsilane and g-SBSi were produced. Based on results from fluorescence microscopy, multiple coatings produced to date, including g-pSBMA and g-SBSi, showed promise as fouling resistant coatings. Of the zwitterionc polymer films explored here, pSBMA seemed to be the most practical zwitterionic polymer coating system in terms of wettability, controllable growth kinetics, ease of use, and safety.

References:

(1)   Zoppe, J. O.; Ataman, N. C.; Mocny, P.; Wang, J.; Moraes, J.; Klok, H. A. Surface-Initiated Controlled Radical Polymerization: State-of-the-Art, Opportunities, and Challenges in Surface and Interface Engineering with Polymer Brushes. *Chemical Reviews* **2017**, *117* (3), 1105–1318. https://doi.org/10.1021/acs.chemrev.6b00314.

(2)   Blaszykowski, C.; Sheikh, S.; Thompson, M. A Survey of State-of-the-Art Surface Chemistries to Minimize Fouling from Human and Animal Biofluids. *Biomaterials Science* **2015**, *3* (10), 1335–1370. https://doi.org/10.1039/c5bm00085h.

(3)   Matyjaszewski, K. Atom Transfer Radical Polymerization (ATRP): Current Status and Future Perspectives. *Macromolecules* **2012**, *45* (10), 4015–4039. https://doi.org/10.1021/ma3001719.

(4)   Matyjaszewski, K.; Hongchen, D.; Jakubowski, W.; Pietrasik, J.; Kusumo, A. Grafting from Surfaces for "Everyone": ARGET ATRP in the Presence of Air. *Langmuir* **2007**, *23* (8), 4528–4531. https://doi.org/10.1021/la063402e.

(5)   Blaszykowski, C.; Sheikh, S.; Thompson, M. Surface Chemistry to Minimize Fouling from Blood-Based Fluids. *Chemical Society Reviews* **2012**, *41* (17), 5599–5612. https://doi.org/10.1039/c2cs35170f.

(6)   Sin, M. C.; Chen, S. H.; Chang, Y. Hemocompatibility of Zwitterionic Interfaces and Membranes. *Polymer Journal*. Nature Publishing Group June 18, **2014**, pp 436–443. https://doi.org/10.1038/pj.2014.46.

(7)   Quintana, R.; Gosa, M.; Jańczewski, D.; Kutnyanszky, E.; Vancso, G. J. Enhanced Stability of Low Fouling Zwitterionic Polymer Brushes in Seawater with Diblock Architecture. *Langmuir* **2013**, *29* (34), 10859–10867. https://doi.org/10.1021/la402287a.

(8)   Fissell, W. H.; Dubnisheva, A.; Eldridge, A. N.; Fleischman, A. J.; Zydney, A. L.; Roy, S. High-Performance Silicon Nanopore Hemofiltration Membranes. *Journal of Membrane Science* **2009**, *326* (1), 58–63. https://doi.org/10.1016/j.memsci.2008.09.039.

(9)   Kanani, D. M.; Fissell, W. H.; Roy, S.; Dubnisheva, A.; Fleischman, A.; Zydney, A. L. Permeability-Selectivity Analysis for Ultrafiltration: Effect of Pore Geometry. *Journal of Membrane Science* **2010**, *349* (1–2), 405–410. https://doi.org/10.1016/j.memsci.2009.12.003.

(10)   System, U. S. R. D. *2017 Annual Data Report*; 2017.

(11)   Ostuni, E.; Chapman, R. G.; Holmlin, R. E.; Takayama, S.; Whitesides, G. M. A Survey of Structure-Property Relationships of Surfaces That Resist the Adsorption of Protein. *Langmuir*. American Chemical Society September 4, **2001**, pp 5605–5620. https://doi.org/10.1021/la010384m.

(12)   Sharma, S.; Johnson, R. W.; Desai, T. A. Evaluation of the Stability of Nonfouling Ultrathin Poly(Ethylene Glycol) Films for Silicon-Based Microdevices. *Langmuir* **2004**, *20* (2), 348–356. https://doi.org/10.1021/la034753l.

(13)   Han, S.; Kim, C.; Kwon, D. Thermal/Oxidative Degradation and Stabilization of Polyethylene Glycol. *Polymer* **1997**, *38* (2), 317–323. https://doi.org/10.1016/S0032-3861(97)88175-X.

(14)   Kane, R. S.; Deschatelets, P.; Whitesides, G. M. Kosmotropes Form the Basis of Protein-Resistant Surfaces. *Langmuir* **2003**, *19* (6), 2388–2391. https://doi.org/10.1021/la020737x.

(15)   Herold, D. A.; Keil, K.; Bruns, D. E. Oxidation of Polyethylene Glycols by Alcohol Dehydrogenase. *Biochemical Pharmacology* **1989**, *38* (1), 73–76. https://doi.org/10.1016/0006-2952(89)90151-2.

(16)   Nguyen, A. T.; Baggerman, J.; Paulusse, J. M. J.; van Rijn, C. J. M.; Zuilhof, H. Stable Protein-Repellent Zwitterionic Polymer Brushes Grafted from Silicon Nitride. *Langmuir* **2011**, *27* (6), 2587–2594. https://doi.org/10.1021/la104657c.

(17)   Nguyen, A. T.; Baggerman, J.; Paulusse, J. M. J.; Zuilhof, H.; van Rijn, C. J. M. Bioconjugation of Protein-Repellent Zwitterionic Polymer Brushes Grafted from Silicon Nitride. *Langmuir* **2012**, *28* (1), 604–610. https://doi.org/10.1021/la2031363.

(18)   Zhang, Z.; Chao, T.; Chen, S.; Jiang, S. Superlow Fouling Sulfobetaine and Carboxybetaine Polymers on Glass Slides. *Langmuir* **2006**, *22* (24), 10072–10077. https://doi.org/10.1021/la062175d.

(19)   Zhang, Z.; Chen, S.; Chang, Y.; Jiang, S. Surface Grafted Sulfobetaine Polymers via Atom Transfer Radical Polymerization as Superlow Fouling Coatings. *Journal of Physical Chemistry B* **2006**, *110* (22), 10799–10804. https://doi.org/10.1021/jp057266i.

(20)   Li, L.; Marchant, R. E.; Dubnisheva, A.; Roy, S.; Fissell, W. H. Anti-Biofouling Sulfobetaine Polymer Thin Films on Silicon and Silicon Nanopore Membranes. *Journal of Biomaterials Science, Polymer Edition* **2011**, *22* (1–3), 91–106. https://doi.org/10.1163/092050609X12578498982998.

(21)   Sun, J.; Zeng, F.; Jian, H.; Wu, S. Conjugation with Betaine: A Facile and Effective Approach to Significant Improvement of Gene Delivery Properties of PEI. *Biomacromolecules* **2013**, *14* (3), 728–736. https://doi.org/10.1021/bm301826m.

(22)   Ezzat, M.; Huang, C. J. Zwitterionic Polymer Brush Coatings with Excellent Anti-Fog and Anti-Frost Properties. *RSC Advances* **2016**, *6* (66), 61695–61702. https://doi.org/10.1039/c6ra12399f.

(23)   Papra, A.; Gadegaard, N.; Larsen, N. B. Characterization of Ultrathin Poly(Ethylene Glycol) Monolayers on Silicon Substrates. **2001**. https://doi.org/10.1021/la000609d.

(24)   Yeh, S. B.; Chen, C. S.; Chen, W. Y.; Huang, C. J. Modification of Silicone Elastomer with Zwitterionic Silane for Durable Antifouling Properties. *Langmuir* **2014**, *30* (38), 11386–11393. https://doi.org/10.1021/la502486e.

(25)   Cheng, G.; Li, G.; Xue, H.; Chen, S.; Bryers, J. D.; Jiang, S. Zwitterionic Carboxybetaine Polymer Surfaces and Their Resistance to Long-Term Biofilm Formation. *Biomaterials* **2009**, *30* (28), 5234–5240. https://doi.org/10.1016/j.biomaterials.2009.05.058.

(26)   Laurent, P.; Souharce, G.; Duchet-Rumeau, J.; Portinha, D.; Charlot, A. "Pancake" vs. Brush-like Regime of Quaternizable Polymer Grafts: An Efficient Tool for Nano-Templating Polyelectrolyte Self-Assembly. *Soft Matter* **2012**, *8* (3), 715–725. https://doi.org/10.1039/c1sm06362f.

(27)   Christau, S.; Thurandt, S.; Yenice, Z.; von Klitzing, R. Stimuli-Responsive Polyelectrolyte Brushes As a Matrix for the Attachment of Gold Nanoparticles: The Effect of Brush Thickness on Particle Distribution. *Polymers* **2014**, *6* (7), 1877–1896. https://doi.org/10.3390/polym6071877.

(28)   Yang, W.; He, X. J.; Gao, J. Z.; Guo, H.; He, X. Y.; Wan, F.; Zhao, X. L.; Yu, Y.; Pei, B. Synthesis, Characterization, and Tunable Wettability of Poly(Ionic Liquid) Brushes via Nitroxide-Mediated Radical Polymerization (NMP). *Chinese Science Bulletin* **2010**, *55* (31), 3562–3568. https://doi.org/10.1007/s11434-010-3288-z.

(29)   Martins, M. C. L.; Wang, D.; Ji, J.; Feng, L.; Barbosa, M. A. Albumin and Fibrinogen Adsorption on PU-PHEMA Surfaces. *Biomaterials* **2003**, *24* (12), 2067–2076. https://doi.org/10.1016/S0142-9612(03)00002-4.

(30)   Zhao, Y. H.; Wee, K. H.; Bai, R. Highly Hydrophilic and Low-Protein-Fouling Polypropylene Membrane Prepared by Surface Modification with Sulfobetaine-Based Zwitterionic Polymer through a Combined Surface Polymerization Method. *Journal of Membrane Science* **2010**, *362* (1–2), 326–333. https://doi.org/10.1016/j.memsci.2010.06.037.

(31)   Lowe, S.; O'Brien-Simpson, N. M.; Connal, L. A. Antibiofouling Polymer Interfaces: Poly(Ethylene Glycol) and Other Promising Candidates. *Polymer Chemistry*. Royal Society of Chemistry January 14, **2015**, pp 198–212. https://doi.org/10.1039/c4py01356e.

(32)   Dong, H.; Matyjaszewski, K. ARGET ATRP of 2-(Dimethylamino)Ethyl Methacrylate as an Intrinsic Reducing Agent. *Macromolecules* **2008**, *41* (19), 6868–6870. https://doi.org/10.1021/ma8017553.

(33)   Bhairamadgi, N. S.; Pujari, S. P.; Trovela, F. G.; Debrassi, A.; Khamis, A. A.; Alonso, J. M.; al Zahrani, A. A.; Wennekes, T.; Al-Turaif, H. A.; van Rijn, C.; Alhamed, Y. A.; Zuilhof, H. Hydrolytic and Thermal Stability of Organic Monolayers on Various Inorganic Substrates. *Langmuir* **2014**, *30* (20), 5829–5839. https://doi.org/10.1021/la500533f.

(34)   Sano, H.; Maeda, H.; Ichii, T.; Murase, K.; Noda, K.; Matsushige, K.; Sugimura, H. Alkyl and Alkoxyl Monolayers Directly Attached to Silicon: Chemical Durability in Aqueous Solutions. *Langmuir* **2009**, *25* (10), 5516–5525. https://doi.org/10.1021/la804080g.

(35)   Xu, F. J.; Kang, E. T.; Neoh, K. G. UV-Induced Coupling of 4-Vinylbenzyl Chloride on Hydrogen-Terminated Si(100) Surfaces for the Preparation of Well-Defined Polymer-Si Hybrids via Surface-Initiated ATRP. *Macromolecules* **2005**, *38* (5), 1573–1580. https://doi.org/10.1021/ma049225a.

(36)   Yu, W. H.; Kang, E. T.; Neoh, K. G.; Zhu, S. Controlled Grafting of Well-Defined Polymers on Hydrogen-Terminated Silicon Substrates by Surface-Initiated Atom Transfer Radical Polymerization. **2003**. https://doi.org/10.1021/jp034330s.

(37)   Buriak, J. M. Organometallic Chemistry on Silicon and Germanium Surfaces. *Chem. Rev*. **2002**, 102, 5, 1271–1308. https://doi.org/10.1021/cr000064s.

(38)   Stewart, M. P.; Buriak, J. M. Photopatterned Hydrosilylation on Porous Silicon. *Angewandte Chemie - International Edition* **1998**, *37* (23), 3257–3260. https://doi.org/10.1002/(SICI)1521-3773(19981217)37:23<3257::AID-ANIE3257>3.0.CO;2-1.

(39)   Huck, L. A.; Buriak, J. M. UV-Initiated Hydrosilylation on Hydrogen-Terminated Silicon (111): Rate Coefficient Increase of Two Orders of Magnitude in the Presence of Aromatic Electron Acceptors. **2012**. https://doi.org/10.1021/la3035819.

(40) Effenberger, F.; Götz, G.; Bidlingmaier, B.; Wezstein, M. Photoactivated Preparation and Patterning of Self-Assembled Monolayers with 1-Alkenes and Aldehydes on Silicon Hydride Surfaces. *Angewandte Chemie - International Edition* **1998**, *37* (18), 2462–2464. https://doi.org/10.1002/(SICI)1521-3773(19981002)37:18<2462::AID-ANIE2462>3.0.CO;2-R.

(41) Terry, J.; Mo, R.; Wigren, C.; Cao, R.; Mount, G.; Pianetta, P.; Linford, M. R.; Chidsey, C. E. D. Reactivity of the H-Si (111) Surface. *Nuclear Instruments and Methods in Physics Research, Section B: Beam Interactions with Materials and Atoms* **1997**, *133* (1–4), 94–101. https://doi.org/10.1016/S0168-583X(97)00467-9.

(42) Cicero, R. L.; Linford, M. R.; Chidsey, C. E. D. Photoreactivity of Unsaturated Compounds with Hydrogen-Terminated Silicon(111). *Langmuir* **2000**, *16* (13), 5688–5695. https://doi.org/10.1021/la9911990.

(43) Xu, F. J.; Cai, Q. J.; Kang, E. T.; Neoh, K. G. Surface-Initiated Atom Transfer Radical Polymerization from Halogen-Terminated Si(111) (Si-X, X = Cl, Br) Surfaces for the Preparation of Well-Defined Polymer-Si Hybrids. *Langmuir* **2005**, *21* (8), 3221–3225. https://doi.org/10.1021/la0473714.

(44) Xu, F. J.; Kang, E. T.; Neoh, K. G. Resist-Free Micropatterning of Binary Polymer Brushes on Si(100) via Surface-Initiated Living Radical Polymerizations. *Journal of Materials Chemistry* **2006**, *16* (28), 2948–2952. https://doi.org/10.1039/b604410g.

(45) Xu, F. J.; Li, Y. L.; Kang, E. T.; Neoh, K. G. Heparin-Coupled Poly(Poly(Ethylene Glycol) Monomethacrylate)-Si(111) Hybrids and Their Blood Compatible Surfaces. *Biomacromolecules* **2005**, *6* (3), 1759–1768. https://doi.org/10.1021/bm050071w.

Chapter III

METHOD FOR DETERMINING SURFACE ENERGY COMPONENTS OF

SUPERHYDROPHILIC ZWITTERIONIC POLYMER FILMS

Introduction

For practical applications such as medical implants and devices exposed to marine environments, coatings are needed that can resist fouling.[1–3] Surface coatings expressing zwitterionic functionality are of high interest as they have been shown to exhibit exceptional antifouling properties.[1–5] Zwitterionic coatings are hypothesized to offer these exceptional antifouling properties via formation of an electrostatically-bound hydration layer (see Figure 3.1).[2] The strong binding of hydration layers makes zwitterionic coatings more promising than many current surface modification schemes that similarly rely on hydration layers albeit by weaker hydrogen-bonding interactions. Surface energy values can provide a measure of a surface's ability to form a hydration layer – a key to prevent fouling, and as such, is of great interest to my research.
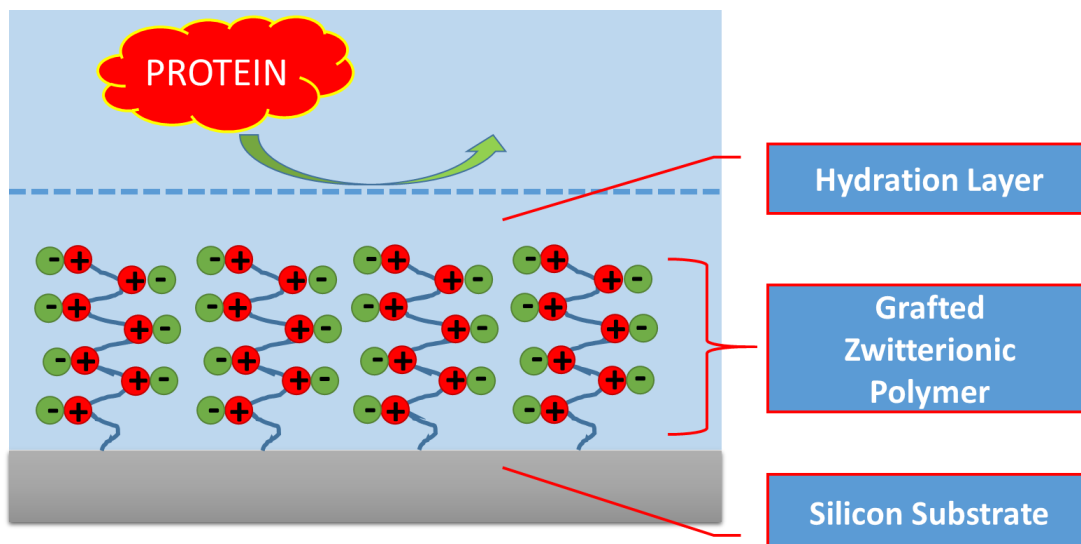
Figure 3.1. Hydration layer bound to surface via electrostatic interaction with grafted zwitterionic polymer coating.

Typically, the dispersive and polar components of a coating's surface energy are determined by conducting a pair of contact angle measurements on the surface with two different probe liquids, with one being a polar liquid (typically water) and the other being a dispersive liquid (such as diiodomethane or hexadecane); one such strategy is commonly known as the Fowkes method.[6–8] As wettability of many superhydrophilic zwitterionic polymer films are difficult to measure directly (i.e. possessing 0° or near-0° contact angles), a different analysis method must be utilized to assess such films. In this chapter, I present a method for analyzing these surface energy components using a model developed based upon the Cassie[9–13], Fowkes[14–20], and Young[21–24] equations, and also relative rate expressions to relate the surface properties of grafted copolymer surfaces to the composition of the comonomers in the forming solutions. This surface modification strategy is illustrated in Figure 3.2. Here, we first modified silicon substrates with an initiator group. Subsequently, a random copolymer of a zwitterionic (very hydrophilic) and a non-zwitterionic (less hydrophilic) monomer species was grafted from the initiator surface by ARGET polymerization. This model is unique in that it can provide the surface energy parameters of these superhydrophilic polymers by studying the wettability of the grafted mixed copolymers where the less-hydrophilic comonomer was included to raise the contact angles to more readily measured values.
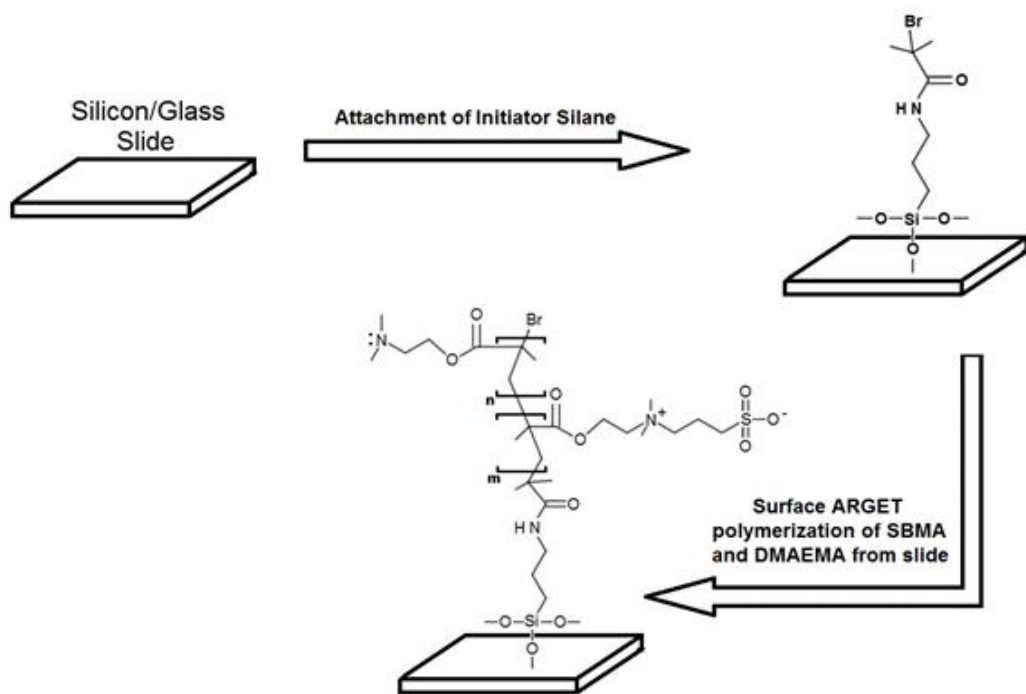
Figure 3.2. Scheme for grafting a g-p[(SBMA)-ran-(DMAEMA)] copolymer via ARGET polymerization from a g-BrTMOS initiator surface.

Experimental Methods

Materials: Copper(II) bromide, L-ascorbic acid, tris(2-pyridylmethyl)amine (TPMA), α-bromoisobutyryl bromide (BIBB), (3-aminopropyl) trimethoxysilane (APTMOS), 2-(dimethylamino)ethyl methacrylate (DMAEMA), 2-(Dimethylamino)ethyl acrylate (DMAEA), methyl methacrylate (MMA), 4-vinylbenzyl chloride (VBC), triethylamine (TEA), and 1,3-propanesultone were obtained from Aldrich. SBMA ([2-(methacryloyloxy)ethyl]dimethyl-(3-sulfopropyl)ammonium hydroxide) was obtained from both Aldrich and Fisher. 2-[methoxy(polyethyleneoxy) 6-9 propyl]trimethoxysilane (PEGsilane) was obtained from Gelest. All compounds were used as received. Silicon wafers <100> were purchased from Pure Wafer and cut into 1x1 cm^2 pieces using a dicing saw.

BrTMOS Initiator Synthesis: The initiator molecule, 3-(trimethoxysilyl)propyl 2-bromo-2-

methylpropanoate (BrTMOS), was synthesized as follows.[25,26] A stir bar and 3.49 mL (20.0 mmol) of APTMOS were placed in a 100 mL round bottom flask. The flask was sealed via septum and sparged with nitrogen. Subsequently, 50 mL of anhydrous THF and 2.79 mL of TEA (20.0 mmol) were added to the flask via syringe and then stirred for 30 min with nitrogen bubbled through it. Then, 3.00 mL of BIBB (24.0 mmol) was added dropwise to the solution via syringe over 30 min with continued stirring, nitrogen bubbling, and chilling via ice bath. The reaction was then allowed to proceed overnight at room temperature. The precipitate was removed via frit filtration, and THF was removed from the remaining solution using rotary evaporation. The resulting yellowish oil was redissolved in 40 mL of CH_2Cl_2, washed twice with 0.01 N HCl, and washed twice more with ice-cold water. The organic phase was dried over anhydrous $CaCl_2$ before removal of the CH_2Cl_2 by rotary evaporation. The remaining product was re-dissolved in hexane and precipitate removed via gravity filtration. The hexane was removed via rotary evaporation, yielding the product as a light-yellow colored oil that was placed under vacuum for 12 h to remove remaining solvent.

Fabrication of BrTMOS-modified silicon slides: Silicon slides were exposed to a piranha solution (7:3 mixture of sulfuric acid and 30% hydrogen peroxide) for 30 minutes. Caution: piranha solutions can be quite dangerous if not following proper safety precautions. Slides were triple rinsed in DI water, and then in ethanol before addition to the BrTMOS solution. The piranha-cleaned slides were immersed into an initiator solution consisting of 250 µL (1.72 mmol) of BrTMOS dissolved in 10 mL of ethanol. Samples were allowed to react with the solution overnight. After removal from the BrTMOS solution, the slides were rinsed with ethanol, dried with N_2, and placed in a 100 °C vacuum oven for 5 h. Initiator-modified slides were stored in foil-wrapped containers to prevent exposure to light.

Attachment of VBC via UV-Hydrosilylation: For modification of flat silicon, 1 x 1 cm^2 samples were placed in an 800 °C oven for 4 h. After cooling, the samples were soaked in a 2.5% solution of HF in a 7:3

ethanol-water mixture to remove the oxide, rinsed with DI water, and dried. For irradiation, samples consisted of 15 μL of VBC sandwiched between the silicon surface and a No. 1 thickness coverslide. Samples were irradiated with UV light in a DYMAX 5000-EC UV curing lamp system. Total exposure times were typically 100 s. After removal of the coverslides, the samples were immersed in acetone for 1 h and then dried before use.

Synthesis of Sulfobetaine Acrylate (SBA): First, 5.18 mL (34.1 mmol) of DMAEA (caution: fatal if inhaled) and 30 mL of dried acetone were added to a RB flask, sealed via septum, and sparged for 30 min with N_2. In a separate RB flask, 4.00 g or 2.8 mL (32.8 mmol) of 1,3-PS was dissolved in 30 mL of dried acetone and sparged with N_2 for 30 min. The 1,3-PS solution was added to the stirred DMAEA solution dropwise via canula over 30 min. The reaction was allowed to proceed overnight. The crude solid product was collected via filtration and washed with acetone before drying under reduced pressure. The product was then further purified via recrystallization. Briefly, the lumpy, crude product was dissolved in ethanol (~100 mL ethanol per gram of crude product) with heating and stirring. The solution was hot filtered to remove undissolved materials, and then allowed to cool in the refrigerator. The recrystallized product was collected via vacuum filtration, thoroughly rinsing with acetone after the ethanol was removed. The product was then dried under vacuum, yielding a fine white powder.

Surface initiated ARGET polymerization: A general procedure for surface-initiated ARGET polymerization of g-p[(SBMA)-ran-(DMAEMA)] is first described. For the 0.358 M SBMA-DMAEMA monomer solutions, the molar ratios of monomer:Cu(II):ligand:reducing agent were 5000:1:5:30 for the N_2-sparged systems in a 1:1 methanol:water mixture. Note that all SBMA-DMAEMA mixtures utilized a combined monomer concentration of 0.358 M. To begin a 0.358 M monomer solution containing appropriate quantity of CuBr$_2$/TPMA stock solution was made for each pure monomer, and the mixed monomer systems were formed by combination of appropriate ratios of the two solutions. Two stock

solutions were used in the synthesis: CuBr$_2$/TPMA in methanol (18 mM in CuBr$_2$; 86 mM in TPMA) and ascorbic acid in methanol (25 mg per mL methanol). First, 5 mL of pure or mixed monomer solution were added to a 10 mL RB flask containing an g-BrTMOS initiator slide. The flask was sealed via septum, and then N$_2$ was sparged through the solution for 30 min via syringe. Polymerization was initiated by injecting 100 μL of the ascorbic acid stock solution through the septum. Polymerizations were terminated by removal of the septum. The resulting polymer-grafted slides were submerged in 1:1 methanol/DI water, rinsed with DI water, and dried in a stream of N$_2$.

Later ARGET experiments (those for making g-p[(SBMA)-ran-(MMA)] and for making g-p[(SBA)-ran-(MMA)]) used a modified version of the previous procedure with lower monomer concentrations, higher reducing agent (ascorbic acid) concentration, and our newer g-VBC initiator surfaces. A general procedure for the revised surface-initiated ARGET polymerization experiments is described as follows. For 0.018 M SBMA-MMA monomer solutions, the molar ratios of monomer:Cu(II):ligand:reducing agent were 250:1:5:40 in a 1:1 methanol water mixture. The procedure for making the g-p[(SBA)-ran-(MMA)]) utilized a 0.100 M total monomer concentration, but was otherwise the same in regards to all other species concentrations. Two stock solutions were used in the synthesis: CuBr$_2$/TPMA in methanol (18 mM in CuBr$_2$; 86 mM in TPMA) and ascorbic acid in methanol (25 mg per mL methanol). In a 20mL vial, the following were added to form the monomer solution: 0.075g SBMA, 7.5 mL H$_2$O, 7.5 mL methanol, and 60 μL of CuBr$_2$/TPMA stock solution; in the case of the MMA solution, 0.027 g of MMA was included in place of SBMA. These monomer solutions were combined to yield the desired SBMA:MMA ratios, sealed via septum, and sparged with nitrogen for 30 minutes. Simultaneously, the initiator-modified silicon samplers were placed in vials, sealed via septum, and sparged with nitrogen for 30 minutes. After a mixed monomer solution was allowed to sparge for 30 minutes, 0.3 mL of the ascorbic acid stock solution was injected to the monomer solution before allowing the resulting solution to sparge for an additional 5 minutes. The monomer solution was then transferred to slide-containing vials via syringe to begin the surface-initiated ARGET polymerization. After the desired reaction time, samples were

removed from the monomer solution, soaked in a 50:50 DI H$_2$O:methanol mixture to remove unbound materials, rinsed with additional methanol and water, and finally dried with compressed nitrogen.

PEGsilane Monolayers: PEGsilane monolayers were produced using a procedure described by Papra et al.[27] Diced silicon slides were soaked in a 1:1 mixture of DI water and ethanol for at least 4 hours before rinsing with DI water and drying with stream of nitrogen. Subsequently, slides were soaked in a piranha solution for 30 minutes. The piranha-cleaned slides were triple rinsed with DI water, ethanol, and then toluene before addition to the PEGsilane solution consisting of22 μL of the PEGsilane and 12 μL of HCl in 15 mL of toluene for 18 h, then washed with toluene ethanol, and water, before drying in a steam of nitrogen.

Analytical Techniques: Film thicknesses were measured using an M-2000VI spectroscopic ellipsometer (J.A. Woollam Co.). Each sample was measured at angles of incidence of 60° and 70°. CompleteEASE software was used to analyze the measurements using the built-in transparent Cauchy film on silicon substrate model. A refractive index of 1.45 was assumed.

Advancing and receding water contact angles were measured on static drops. Contact angles measured under hexadecane were obtained using a custom-made solvent vessel/sample platform.

Fluorescence Fouling Assay: Each sample was first soaked in PBS at room temperature for 1 h, and then incubated in a well of a twelve well plate containing 2 mL of a 0.5 mg/mL solution of FITC-albumin in PBS at 37 °C for 1 h. Slides were removed from solution, triple rinsed with PBS, triple rinsed with DI water, then dried in a stream of N$_2$. Each sample was mounted on a microscope slide with SlowFade mounting medium and a coverslip, and then analyzed using a fluorescent microscope at various exposure times at 2x magnification. To evaluate changes in background fluorescence, untreated slides were mounted

and evaluated at regular intervals at the same microscope settings. Images were analyzed in ImageJ to obtain the mean intensity and standard deviation across each slide for the green channel on a scale of 0-255. Data were normalized to the background fluorescence from blank samples not exposed to FITC-albumin.

Model Derivation

As wettability of superhydrophilic polymer films are difficult to measure directly, due to the inherent challenge of accurately measuring values of 0° or near-0° contact angles via goniometer, a method is needed to assess the wettability of such films. The model presented here can provide surface energy parameters of superhydrophilic polymers by studying the wettability of grafted copolymers where a less-hydrophilic comonomer is included to raise the contact angles to more readily measured values. Further, as many of these copolymer samples still exhibited difficult-to-measure advancing water-in-air contact angles of less than 15°, I also measured water contact angles under a hexadecane environment. The increased interfacial interaction between the sample surface and the hexadecane environment (which lowers the interfacial tension γ_{SE} as compared to an air environment) effectively increases the water contact angle to a more easily measured value. Further, as high-energy zwitterionic surfaces could have a $\cos(\theta)$ value greater than 1, measurement of water contact angles in hexadecane allowed differentiation between surfaces that would otherwise show similar water contact angles of ~0° in an air environment. In addition, the use of two different environments (air and hexadecane) when measuring the water contact angles enabled determination of two individual components (dispersive and polar) contributing to the surface energy of the copolymer surfaces.

I began the derivation of this model by first taking into consideration the fraction of each co-monomer (*M1* and *M2*) present in a surface-grafted copolymer based on the composition of its forming solution. To do so, I first defined and rearranged the ratio of the relative rate expressions for the

polymerization of each monomer to produce (Eq. 1) and subsequently expressed this as the fraction of *M1* in the two-component grafted polymer (Eq. 2). In these equations, the "m" and "p" subscripts refer to a monomer found in the forming solution and in the grafted polymer, respectively. The term "α" represents the ratio of the rate constants.

$$\frac{[M1]_p}{[M2]_p} = \frac{k_{M1}[M1]_m}{k_{M2}[M2]_m} = \alpha\frac{[M1]_m}{[M2]_m} \tag{Eq. 1}$$

$$X_{M1} = \frac{[M1]_p}{[M1]_p + [M2]_p} = \frac{\alpha\frac{[M1]_m}{[M2]_m}}{\alpha\frac{[M1]_m}{[M2]_m}+1} = \frac{\alpha[M1]_m}{\alpha[M1]_m + [M2]_m} \tag{Eq. 2}$$

The Cassie equation (Eq. 3) relates the fractional surface area contribution and the wettability contribution of the two different monomers to the overall wettability of the grafted copolymer surface. In Eq. 4, we defined β as a proportionality constant to represent the ratio of exposed surface area per molecule of *M1* to that of *M2* at the substrate surface. This allowed us to account for size differences between the two monomer species in the copolymer. Substitution of Eq. 2 and Eq. 4 into the Cassie equation (Eq. 3) yielded Eq. 5 that relates wettability to monomer composition in solution. For simplification, we then defined φ as the product of α and β to yield Eq. 6.

$$\cos(\theta_{measured}) = f_{M1}\cos(\theta_{M1}) + f_{M2}\cos(\theta_{M2}) \tag{Eq. 3}$$

$$\beta = \frac{Surface\ area\ per\ M1\ molecule}{Surface\ area\ per\ M2\ molecule} \tag{Eq. 4}$$

$$\cos(\theta_{measured}) = [\frac{\alpha\beta[M1]_m}{\alpha\beta[M1]_m + [M2]_m}]\cos(\theta_{M1}) + [1 - \frac{\alpha\beta[M1]_m}{\alpha\beta[M1]_m + [M2]_m}]\cos(\theta_{M2}) \tag{Eq. 5}$$

$$\cos(\theta_{measured}) = [\frac{\varphi[M1]_m}{\varphi[M1]_m + [M2]_m}]\cos(\theta_{M1}) + [1 - \frac{\varphi[M1]_m}{\varphi[M1]_m + [M2]_m}]\cos(\theta_{M2}) \tag{Eq. 6}$$

The Young equation (Eq. 7) relates the interfacial tensions of the three phases present in our system: surface (S), probe liquid (L), and the environment (E) to surface wettability. Figure 3.3 depicts the notation scheme I used to represent this system where the environment can either be air, or in the case of Figure 3.3b, hexadecane. Substitution of the Young equation (Eq. 7) into Eq. 6 yields Eq. 8.
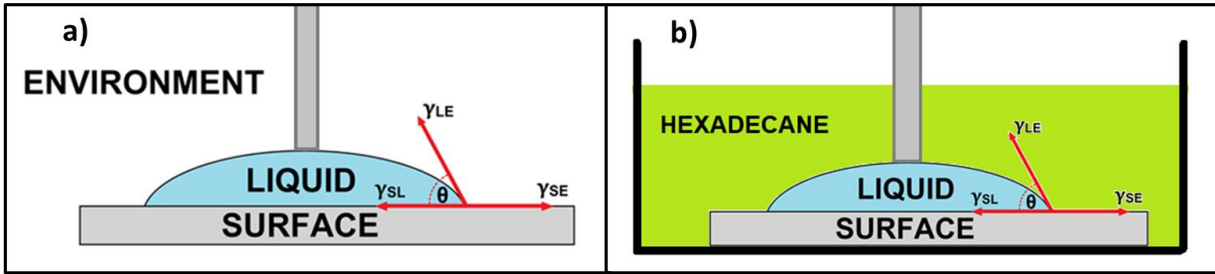
Figure 3.3. a) Labeling convention used in this dissertation when describing the interfacial tensions analyzed as part of these advancing water contact angle experiments. b) Although air is typically the environment in which water contact angles are measured, the samples were also submerged in a hexadecane environment when measuring contact angles as seen in the right image.

$$\cos(\theta) = [\frac{\gamma_{SE} - \gamma_{SL}}{\gamma_{LE}}] \tag{Eq. 7}$$

$$\cos(\theta_{measured}) = [\frac{\varphi[M1]_m}{\varphi[M1]_m + [M2]_m}] [\frac{\gamma_{SE}^{M1} - \gamma_{SL}^{M1}}{\gamma_{LE}}] + [1 - \frac{\varphi[M1]_m}{\varphi[M1]_m + [M2]_m}] [\frac{\gamma_{SE}^{M2} - \gamma_{SL}^{M2}}{\gamma_{LE}}] \tag{Eq. 8}$$

The Fowkes equation (Eq. 9) allows the various interfacial tensions to be determined in terms of the dispersive "D" and polar "P" components of the surface tension parameters of the two contacting phases. Note that for simplification purposes, the non-dispersive interactions have all been combined into the "P" components in our model. Substitution of Eq. 9 into Eq. 8 yields the relationship between the rate, surface tension, and wetting properties (Eq. 10).

$$\gamma_{AB} = \gamma_A + \gamma_B - 2\left[(\gamma_A^D)^{\frac{1}{2}}(\gamma_B^D)^{\frac{1}{2}} + (\gamma_A^P)^{\frac{1}{2}}(\gamma_B^P)^{\frac{1}{2}}\right] \tag{Eq. 9}$$
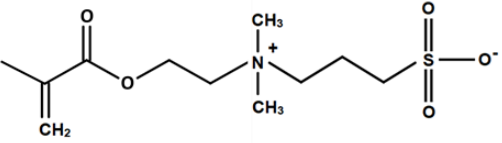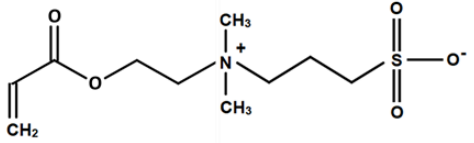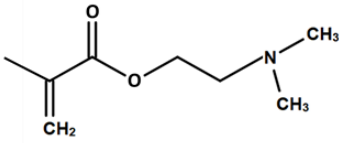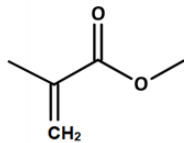
$$\cos(\theta_{measured}) = \left[\frac{\alpha[M1]_m}{\alpha[M1]_m + [M2]_m}\right]\frac{\left[\gamma_{M1} + \gamma_E - 2\{(\gamma_{M1}^D)^{\frac{1}{2}}(\gamma_E^D)^{\frac{1}{2}} + (\gamma_{M1}^P)^{\frac{1}{2}}(\gamma_E^P)^{\frac{1}{2}}\}\right] - \left[\gamma_{M1} + \gamma_L - 2\{(\gamma_{M1}^D)^{\frac{1}{2}}(\gamma_L^D)^{\frac{1}{2}} + (\gamma_{M1}^P)^{\frac{1}{2}}(\gamma_L^P)^{\frac{1}{2}}\}\right]}{\left[\gamma_L + \gamma_E - 2\{(\gamma_L^D)^{\frac{1}{2}}(\gamma_E^D)^{\frac{1}{2}} + (\gamma_L^P)^{\frac{1}{2}}(\gamma_E^P)^{\frac{1}{2}}\}\right]} \tag{Eq. 10}$$

$$+ \left[1 - \frac{\alpha[M1]_m}{\alpha[M1]_m + [M2]_m}\right]\frac{\left[\gamma_{M2} + \gamma_E - 2\{(\gamma_{M2}^D)^{\frac{1}{2}}(\gamma_E^D)^{\frac{1}{2}} + (\gamma_{M2}^P)^{\frac{1}{2}}(\gamma_E^P)^{\frac{1}{2}}\}\right] - \left[\gamma_{M2} + \gamma_L - 2\{(\gamma_{M2}^D)^{\frac{1}{2}}(\gamma_L^D)^{\frac{1}{2}} + (\gamma_{M2}^P)^{\frac{1}{2}}(\gamma_L^P)^{\frac{1}{2}}\}\right]}{\left[\gamma_L + \gamma_E - 2\{(\gamma_L^D)^{\frac{1}{2}}(\gamma_E^D)^{\frac{1}{2}} + (\gamma_L^P)^{\frac{1}{2}}(\gamma_E^P)^{\frac{1}{2}}\}\right]}$$

Table 3.1 summarizes the surface tension parameters, as reported by Accu Dyne Test and others, used in this model.[28–30] The γ^P and γ^H terms have been combined via addition to yield the γ^P term in Table 3.1. The incorporation of the hydrogen-bonding contribution into the polar contribution term was performed to reduce the complexity of Eq. 10. Table 3.2 depicts the structure of the monomers examined in these experiments.

Table 3.1. Surface tension values and their polar and dispersive components as reported by Accu Dyne Test.[28]

	γ (mN/m)	γ^P (mN/m)	γ^D (mN/m)
Water	72.8	51	21.8
Hexadecane	27.5	0	27.5

Table 3.2. Structures of the four monomers examined in this chapter.

Monomer	Structure
SBMA	
SBA	
DMAEMA	
MMA	

Results and Discussion

SBMA-DMAEMA Copolymer System

Figure 3.4 displays the advancing water contact angles in air and under hexadecane on the g-p[(SBMA)-ran-(DMAEMA)] copolymer-modified slides prepared from mixed sulfobetaine methacrylate (SBMA) and 2-(dimethylamino)ethyl methacrylate (DMAEMA) monomer solutions differing in their SBMA fraction. To analyze the results in Figure 3.4, the developed model (Eq. 10) was used which incorporates the Cassie, Fowkes, and Young equations, and rate expressions to relate the surface properties of g-p[(SBMA)-ran-(DMAEMA)] slides to the monomer composition of the polymerization solutions.
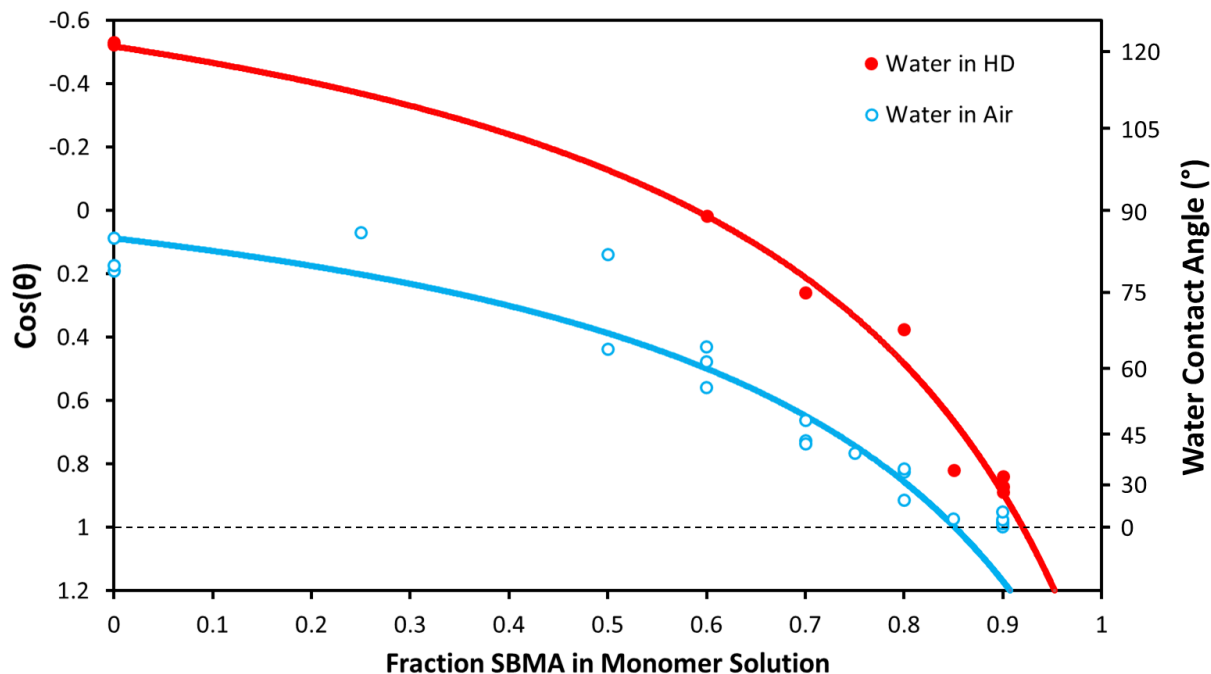
Figure 3.4. Wetting results and derived model for the g-p[(SBMA)-ran-(DMAEMA)] ARGET copolymerization system prepared from solutions with a 0.358 M total monomer concentration from a g-BrTMOS initiator surface. Note that the 90% SBMA water-in-air data were omitted from fit.

The model was used to calculate the surface composition of the grafted copolymer films and relate the wetting properties of the films to the monomer solution composition. Matlab's "Curve Fitting" application was utilized to simultaneously fit the water-in-air and water-in-hexadecane contact angle data sets shown here. Note that the 90% SBMA water-in-air data were omitted from the fit as the water contact angles appeared to have already reached near-0° minimum/floor values at lower monomer compositions; as the water-in-hexadecane contact angles were still in an easily measured regime, the 90% SBMA water-in-hexadecane contact angle data were not omitted from this fit. The fit of Eq. 10 to this data set yielded values found in Table 3.3 provided with 95% confidence intervals.

Table 3.3. Parameters resulting from a fit of the model (Eq. 10) to the g-p[(SBMA)-ran-(DMAEMA)] data presented in Figure 3.4. Data presented with 95% confidence intervals.

Parameter	Fitted Results
ϕ	0.23 ± 0.12
γ^D_{SBMA}	45 ± 25 mN/m
γ^P_{SBMA}	88 ± 30 mN/m
γ^D_{DMAEMA}	33 ± 10 mN/m
γ^P_{DMAEMA}	3.1 ± 1.5 mN/m

The φ value of 0.23 ± 0.12 expressed that the SBMA composition in the grafted polymer was less than in the forming monomer solution. As a result, DMAEMA was enriched in the grafted copolymer relative to the forming solution. We can illustrate this by plotting the monomer fraction of SBMA in solution against the surface area fraction for SBMA predicted by our model as shown in Figure 3.5. The included dotted line demonstrates the theoretical situation where $\varphi = 1$; in this situation there would be a 1:1 correspondence between the fraction of a monomer in solution and its fractional area at the resulting surface. Higher fractions of SBMA in the monomer solution produced films that were more hydrophilic, consistent with an increased fraction of SBMA present in the grafted copolymer. Importantly, grafted films with low water contact angles represent good candidates for antifouling coatings as such surfaces better form surface-bound hydration layers that impede adsorption. As evident in Figure 3.4 by the model predicting $\cos(\theta)$ values greater than 1 (see dotted line) at high SBMA fractions, the γ^p_{SBMA} and γ^d_{SBMA} parameters likely could not have been directly calculated or measured for a pure g-pSBMA surface. The obtained γ^p_{SBMA} value of 88 ± 30 mN/m is consistent with that of a high surface energy zwitterionic polymer film.
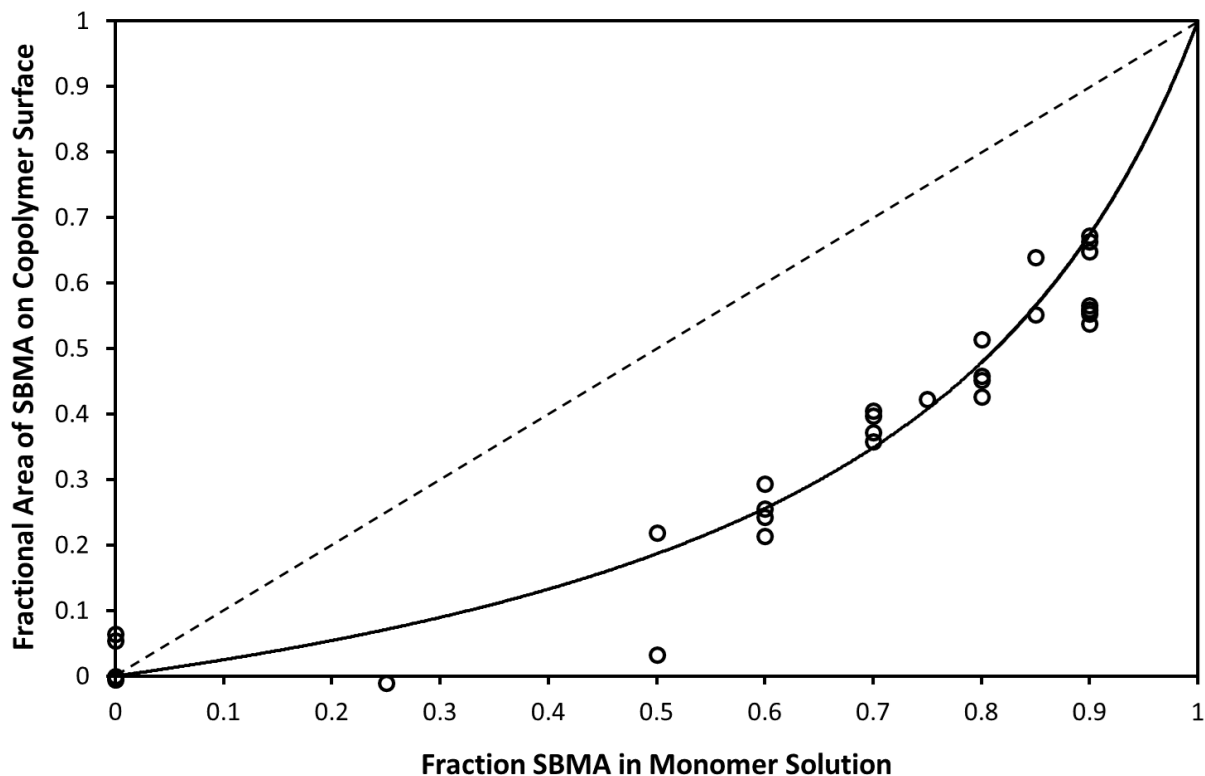
Figure 3.5. Predicted fractional area of SBMA at the g-p[(SBMA)-ran-(DMAEMA)] copolymer surface for various mixed monomer forming solutions using the determined $\varphi = 0.23$ parameter. Note the dotted line represents the theoretical situation if $\varphi = 1$ for comparison.

To evaluate the ability of these surfaces to resist fouling, samples were incubated in a solution of fluorescently-labeled albumin (FITC-albumin). A fluorescence microscope was used to evaluate the changes in fluorescence of each sample resulting from adsorbed FITC-albumin. Background fluorescence was evaluated by collecting microscopy images of untreated slides at regular intervals using the same microscope settings. A grafted film showing little to no increase in fluorescence from background would imply that the coating exhibits a higher degree of fouling resistance. Images were analyzed using ImageJ to obtain the mean intensity and standard deviation across each slide for the green light channel. Data were normalized to the background fluorescence of blank samples not exposed to FITC-albumin.

Figure 3.6 summarizes the fluorescence data obtained for the g-p[(SBMA)-ran-(DMAEMA)] copolymers and compares them to the fluorescence increases on the BrTMOS initiator and PEG-modified

surfaces. While Figure 3.6 shows that the ability of a surface to resist fouling improved with increasing

SBMA fraction and hydrophilicity, all of the grafted SBMA-DMAEMA copolymers exhibited significantly

greater increases in fluorescence (i.e. greater fouling) than the g-PEGsilane monolayers. As grafted, the

pDMAEMA homopolymer exhibited a very high increase in fluorescence (data not shown); DMAEMA's

presence in relatively small quantities in the grafted g-poly[(SBMA)-ran-(DMAEMA)] copolymers

suggested a level of fouling that would make these copolymer surfaces unusable for antifouling purposes.
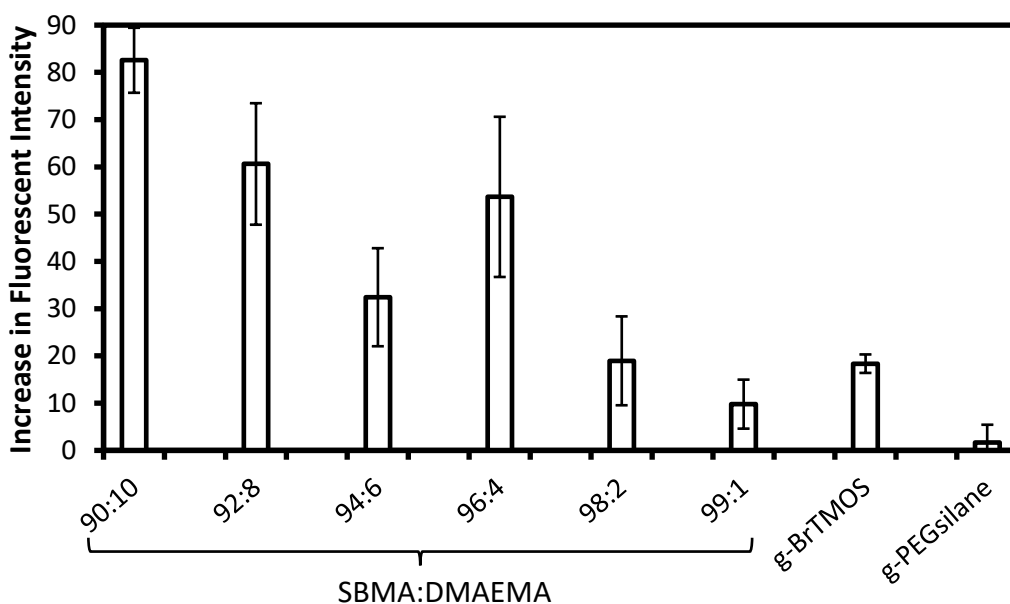
Figure 3.6. Fluorescence increases from adsorbed FITC-labelled albumin on various surfaces. Fluorescence increases due to protein adsorption onto grafted SBMA-DMAEMA surfaces are compared to that on g-BrTMOS and g-PEGsilane slides. Fluorescence data were normalized to the background fluorescence of blank samples not exposed to FITC-albumin. Exposure time = 5000 ms.

Other Copolymer Systems

In addition to the g-p[(SBMA)-ran-(DMAEMA)] system discussed above, I also looked at two

additional systems. These systems used methyl methacrylate (MMA) in place of DMAEMA as the "less-

hydrophilic" comonomer. In one of the systems a different zwitterionic monomer, sulfobetaine acrylate

(SBA) which differed from SBMA in having one less methyl group on the polymerizeable group, was used

for the purpose of comparing the calculated surface energy parameters to that of SBMA. First, the g-p[(SBMA)-ran-(MMA)] system was examined to compare how similar the determined surface energy parameters of SBMA were between it and the g-p[(SBMA)-ran-(DMAEMA)] system, where we would expect agreement between the two. Figure 3.7 shows the advancing water contact angles in air and under hexadecane on the g-p[(SBMA)-ran-(MMA)] copolymer-modified slides prepared from mixed SBMA-MMA monomer solutions differing in their SBMA fraction. Note that both the 90% SBMA water-in-air data and 90% SBMA water-in-hexadecane data were omitted from the fit as these water contact angles appeared to have already reached near-0° minimum/floor values at lower monomer compositions.
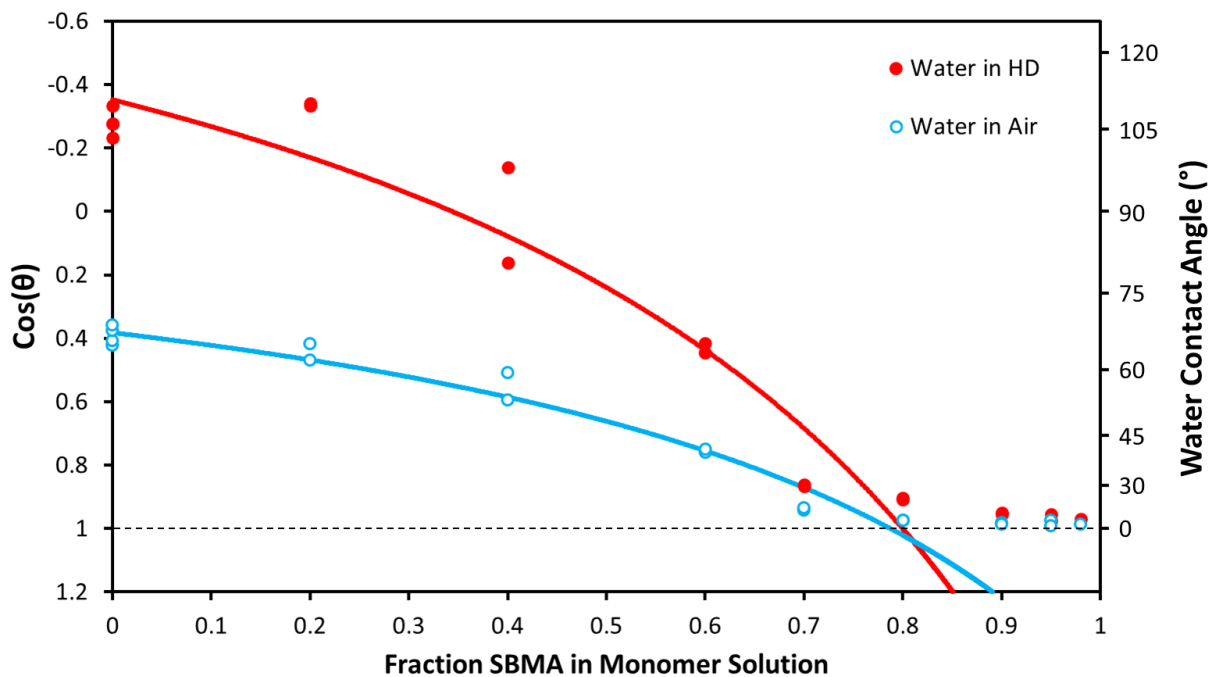
Figure 3.7. Wetting results and derived model for the g-p[(SBMA)-ran-(MMA)] ARGET copolymerization system prepared from solutions with a 0.018 M total monomer concentration from a g-VBC initiator surface. Note that the ≥ 90% SBMA contact angle data sets were omitted from the fit.

The fit of Eq. 10 to this data set yielded values found in Table 3.4 provided with 95% confidence intervals. The φ value of 0.33 ± 0.23 expresses that the fractional area contribution of SBMA at the grafted copolymer surface is less than in the forming monomer solution. Accordingly, the fractional area

contribution of MMA is enriched in the grafted copolymer relative to forming solution composition. As with the previous system, higher fractions of SBMA in the forming monomer solution produced films that were more hydrophilic, consistent with an increased fraction of SBMA present in the grafted copolymer. As evident in Figure 3.7 by the model predicting cos(θ) values greater than 1 (see dotted line) at high SBMA fractions, the γ^p_{SBMA} and γ^d_{SBMA} parameters likely could not have been directly calculated or measured for a pure g-pSBMA surface. The obtained γ^p_{SBMA} value of 114 ± 60 mN/m is consistent with that of a high surface energy zwitterionic polymer film. This is consistent with the prior SBMA-DMAEMA system. The g-p[(SBMA)-ran-(DMAEMA)] and g-p[(SBMA)-ran-(MMA)] data are both consistent in that the polar contribution to the surface energy of SBMA is quite large. However, we can see that the 95% confidence intervals are too large to accurately pin down values for φ and the surface energy component values. When evaluating this model, I observed that it was quite sensitive to changes in the φ value, resulting in the larger uncertainty in the surface energy component values. Thus, φ needs to be determined through other means, rather than being a fitted term in future experiments. As φ is the product of α (the ratio of rate constants for *M1* and *M2*) and β (the ratio of exposed surface area per molecule of *M1* to that of *M2*), surface analysis techniques such as FT-IR or XPS should allow determination of the surface composition of the copolymer surfaces, thus allowing φ to no longer be needed as a fitted term.

Table 3.4. Parameters resulting from a fit of the model (Eq. 10) to the g-p[(SBMA)-ran-(MMA)] data presented in Figure 3.7. Data presented with 95% confidence intervals.

Parameter	Fitted Results
φ	0.33 ± 0.23
γ_{SBMA}^{D}	10 ± 12 mN/m
γ_{SBMA}^{P}	114 ± 60 mN/m
γ_{MMA}^{D}	49 ± 10 mN/m
γ_{MMA}^{P}	6.1 ± 1.5 mN/m

Next, I examined the g-p[(SBA)-ran-(MMA)] system to compare the surface energy parameters of SBMA to that of SBA, with the goal of determining which zwitterionic polymer was the higher energy surface. It was expected that since the structures of these two monomers were the same with the exception that SBA contained one less methyl group (i.e. one less hydrophobic group), that SBA would be a slightly higher energy, slightly more hydrophilic surface than SBMA. Figure 3.8 shows the advancing water contact angles in air and under hexadecane on the g-p[(SBA)-ran-(MMA)] copolymer-modified slides prepared from mixed SBA-MMA monomer solutions differing in their SBA fraction.
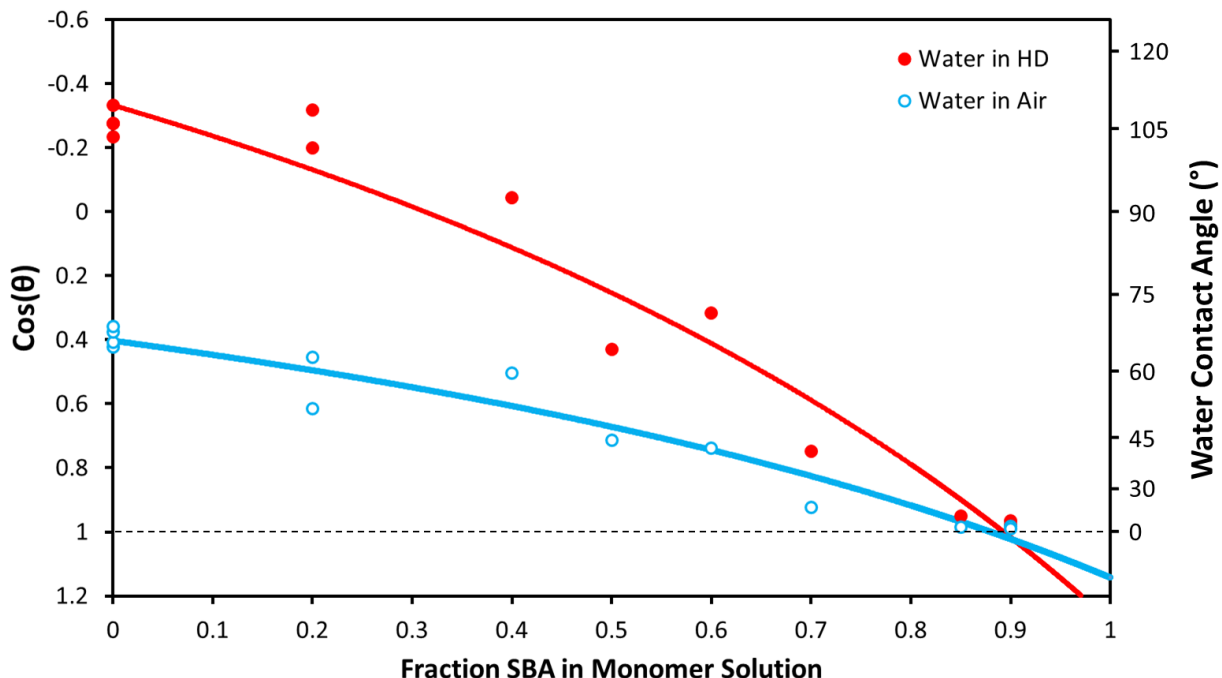
Figure 3.8. Wetting results and derived model for the g-p[(SBA)-ran-(MMA)] ARGET copolymerization system prepared from solutions with a 0.100 M total monomer concentration from a g-VBC initiator surface.

The fit of Eq. 10 to this data set yielded values found in Table 3.5 provided with 95% confidence intervals. The φ value of 0.57 ± 0.26 expresses that the fractional area contribution of SBA at the grafted copolymer surface was less than in the forming monomer solution. Accordingly, the fractional area contribution of MMA was enriched in the grafted copolymer relative to forming solution composition. As with both of the previous systems, higher fractions of zwitterionic monomer, in this case SBA, in the forming monomer solution produced films that were more hydrophilic, consistent with an increased fraction of SBA present in the grafted copolymer. As evident in Figure 3.8 by the model predicting cos(θ) values greater than 1 (see dotted line) at high SBA fractions, the γ^{p}_{SBA} and γ^{d}_{SBA} parameters likely could not have been directly calculated or measured for a pure g-pSBA surface. The obtained γ^{p}_{SBA} value of 66 ± 12 mN/m is consistent with that of a high surface energy zwitterionic polymer film. This is consistent with the two prior SBMA copolymer systems. The g-p[(SBMA)-ran-(MMA)] and g-p[(SBA)-ran-(MMA)] data are both

93

consistent in that the polar contributions to the surface energy of the zwitterionic species are quite large, as would be expected. However, we can see that the 95% confidence intervals are again too large to differentiate between the two zwitterionic species in terms of their surface energy component values. Once again, we see that, φ needs to be determined through other means such as FT-IR or XPS, rather than being a fitted term.

Table 3.5. Parameters resulting from a fit of the model (Eq. 10) to the g-p[(SBA)-ran-(MMA)] data presented in Figure 3.8. Data presented with 95% confidence intervals.

Parameter	Fitted Results
φ	0.57 ± 0.26
γ_{SBA}^{D}	18 ± 10 mN/m
γ_{SBA}^{P}	66 ± 12 mN/m
γ_{MMA}^{D}	50 ± 10 mN/m
γ_{MMA}^{P}	6.5 ± 1.5 mN/m

Conclusions

In this chapter, I presented a method for analyzing the surface energy components of superhydrophilic species using a model developed based upon the Cassie, Fowkes, Young equations, and also the relative rate expressions for grafted copolymer surfaces containing a less-hydrophilic comonomer. This method is significant in that the wettability of many superhydrophilic zwitterionic polymer films are difficult to measure directly due to their inherent 0° or near-0° contact angles, data that typical methods for determining surface energy components rely upon. A collection of zwitterionic-monomer containing

copolymers was produced by surface-initiated ARGET polymerization and used to evaluate the usefulness of the developed model. Although it was evident that the model was able to provide values for surface energy components that were consistent with the grafted copolymers' structures and their functionality, we observed that the confidence intervals for these values were too large to differentiate between the two studied zwitterionic monomer species. When evaluating this model, it was observed that the model was quite sensitive to changes in the φ value, resulting in the higher uncertainty in the calculated surface energy component values. Consequently, future work in evaluating this model would involve determining the φ term through other means such as FT-IR or XPS, rather than φ being fitted; this should reduce the uncertainty of the model's predictions.

References:

(1) Blaszykowski, C.; Sheikh, S.; Thompson, M. A Survey of State-of-the-Art Surface Chemistries to Minimize Fouling from Human and Animal Biofluids. *Biomaterials Science* **2015**, *3* (10), 1335–1370. https://doi.org/10.1039/c5bm00085h.

(2) Blaszykowski, C.; Sheikh, S.; Thompson, M. Surface Chemistry to Minimize Fouling from Blood-Based Fluids. *Chemical Society Reviews* **2012**, *41* (17), 5599–5612. https://doi.org/10.1039/c2cs35170f.

(3) Quintana, R.; Gosa, M.; Jańczewski, D.; Kutnyanszky, E.; Vancso, G. J. Enhanced Stability of Low Fouling Zwitterionic Polymer Brushes in Seawater with Diblock Architecture. *Langmuir* **2013**, *29* (34), 10859–10867. https://doi.org/10.1021/la402287a.

(4) Zoppe, J. O.; Ataman, N. C.; Mocny, P.; Wang, J.; Moraes, J.; Klok, H. A. Surface-Initiated Controlled Radical Polymerization: State-of-the-Art, Opportunities, and Challenges in Surface and Interface Engineering with Polymer Brushes. *Chemical Reviews* **2017**, *117* (3), 1105–1318. https://doi.org/10.1021/acs.chemrev.6b00314.

(5) Sin, M. C.; Chen, S. H.; Chang, Y. Hemocompatibility of Zwitterionic Interfaces and Membranes. *Polymer Journal*. Nature Publishing Group June 18, **2014**, pp 436–443. https://doi.org/10.1038/pj.2014.46.

(6) Żenkiewicz, M. Methods for the Calculation of Surface Free Energy of Solids. *Journal of Achievements in Materials and Manufacturing Engineering* **2007**, *24* (1), 137–145.

(7)   Law, K.-Y.; Zhao, H. Determination of Solid Surface Tension by Contact Angle. In *Surface Wetting*; Springer International Publishing, **2016**; pp 135–148. https://doi.org/10.1007/978-3-319-25214-8_7.

(8)   Rhee, S. K. A Method for Determining Surface Energy of Solids. *Materials Science and Engineering* **1973**, *11* (6), 311–318. https://doi.org/10.1016/0025-5416(73)90121-3.

(9)   Cassie, A. B. D. Contact Angles. *Discussions of the Faraday Society*. The Royal Society of Chemistry January 1, **1948**, pp 11–16. https://doi.org/10.1039/DF9480300011.

(10)   McHale, G. Cassie and Wenzel: Were They Really so Wrong? *Langmuir* **2007**, *23* (15), 8200–8205. https://doi.org/10.1021/la7011167.

(11)   Gao, L.; McCarthy, T. J. How Wenzel and Cassie Were Wrong. *Langmuir* **2007**, *23* (7), 3762–3765. https://doi.org/10.1021/la062634a.

(12)   Marmur, A.; Bittoun, E. When Wenzel and Cassie Are Right: Reconciling Local and Global Considerations. *Langmuir* **2009**, *25* (3), 1277–1281. https://doi.org/10.1021/la802667b.

(13)   Milne, A. J. B.; Amirfazli, A. The Cassie Equation: How It Is Meant to Be Used. *Advances in Colloid and Interface Science*. Elsevier January 15, **2012**, pp 48–55. https://doi.org/10.1016/j.cis.2011.12.001.

(14)   Kwok, D. Y.; Li, D.; Neumann, A. W. Fowkes' Surface Tension Component Approach Revisited. *Colloids and Surfaces A: Physicochemical and Engineering Aspects* **1994**, *89* (2–3), 181–191. https://doi.org/10.1016/0927-7757(94)80117-7.

(15)   Owens, D. K.; Wendt, R. C. Estimation of the Surface Free Energy of Polymers. *Journal of Applied Polymer Science* **1969**, *13* (8), 1741–1747. https://doi.org/10.1002/app.1969.070130815.

(16)   Fowkes, F. M. Determination of Interfacial Tensions, Contact Angles, and Dispersion Forces in Surfaces by Assuming Additivity of Intermolecular Interactions in Surfaces [5]. *Journal of Physical Chemistry*. UTC **1962**, p 382. https://doi.org/10.1021/j100808a524.

(17)   Fowkes, F. M. ATTRACTIVE FORCES AT INTERFACES. *Industrial & Engineering Chemistry* **1964**, *56* (12), 40–52. https://doi.org/10.1021/ie50660a008.

(18)   Saito, M.; Yabe, A. Dispersion and Polar Force Components of Surface Tension of Oily Soils. *Textile Research Journal* **1984**, *54* (1), 18–22. https://doi.org/10.1177/004051758405400104.

(19)   Fowkes, F. M.; Riddle, F. L.; Pastore, W. E.; Weber, A. A. Interfacial Interactions between Self-Associated Polar Liquids and Squalane Used to Test Equations for Solid-Liquid Interfacial Interactions. *Colloids and Surfaces* **1990**, *43* (2), 367–387. https://doi.org/10.1016/0166-6622(90)80298-I.

(20)   Jie-Rong, C.; Wakida, T. Studies on the Surface Free Energy and Surface Structure of PTFE Film Treated with Low Temperature Plasma. *Journal of Applied Polymer Science* **1997**, *63* (13), 1733–1739. https://doi.org/10.1002/(SICI)1097-4628(19970328)63:13<1733::AID-APP4>3.0.CO;2-H.

(21)   Thomas Young, B.; For Sec, M. D. III. An Essay on the Cohesion of Fluids. *Philosophical Transactions of the Royal Society of London* **1805**, *95*, 65–87. https://doi.org/10.1098/rstl.1805.0005.

(22)   White, L. R. On Deviations from Young's Equation. *Journal of the Chemical Society, Faraday Transactions 1: Physical Chemistry in Condensed Phases* **1977**, *73* (0), 390–398. https://doi.org/10.1039/F19777300390.

(23)   Adam, N. K. Use of the Term "Young's Equation" for Contact Angles. *Nature* **1957**, *180*, 809-810. https://doi.org/10.1038/180809a0

(24)   Whyman, G.; Bormashenko, E.; Stein, T. The Rigorous Derivation of Young, Cassie-Baxter and Wenzel Equations and the Analysis of the Contact Angle Hysteresis Phenomenon. *Chemical Physics Letters* **2008**, *450* (4–6), 355–359. https://doi.org/10.1016/j.cplett.2007.11.033.

(25)   Zhang, Z.; Chen, S.; Chang, Y.; Jiang, S. Surface Grafted Sulfobetaine Polymers via Atom Transfer Radical Polymerization as Superlow Fouling Coatings. *Journal of Physical Chemistry B* **2006**, *110* (22), 10799–10804. https://doi.org/10.1021/jp057266i.

(26)   Li, L.; Marchant, R. E.; Dubnisheva, A.; Roy, S.; Fissell, W. H. Anti-Biofouling Sulfobetaine Polymer Thin Films on Silicon and Silicon Nanopore Membranes. *Journal of Biomaterials Science, Polymer Edition* **2011**, *22* (1–3), 91–106. https://doi.org/10.1163/092050609X12578498982998.

(27)   Papra, A.; Gadegaard, N.; Larsen, N. B. Characterization of Ultrathin Poly(Ethylene Glycol) Monolayers on Silicon Substrates. **2001**. https://doi.org/10.1021/la000609d.

(28)   Surface Tension Components and Molecular Weight of Selected Liquids http://www.accudynetest.com/surface_tension_table.html (accessed Apr 30, 2021).

(29)   van Oss, C. J.; Good, R. J.; Chaudhury, M. K. Additive and Nonadditive Surface Tension Components and the Interpretation of Contact Angles. *Langmuir* **1988**, *4* (4), 884–891. https://doi.org/10.1021/la00082a018.

(30)   Jańczuk, B.; Wójcik, W.; Zdziennicka, A. Determination of the Components of the Surface Tension of Some Liquids from Interfacial Liquid-Liquid Tension Measurements. *Journal of Colloid And Interface Science* **1993**, *157* (2), 384–393. https://doi.org/10.1006/jcis.1993.1200.

Chapter IV

FORMATION OF SILICA COATINGS ON ZWITTERIONIC SURFACES

Introduction

While developing zwitterionic polymer and monolayer coatings on silicon substrates to study the antifouling capabilities of these coatings, we observed that when these samples were placed in phosphate-buffered saline (PBS) solutions under certain conditions, a thick layer (usually hundreds of nanometers in thickness) of what appeared to be SiO_2 would form on the surface of these samples. We found that we could more reliably replicate and also accelerate this SiO_2 coating formation by placing the zwitterion-modified silicon substrates into refluxing PBS in a glass round-bottom flask under a condenser. Figure 4.1 below shows one of the thick SiO_2 films that formed on a zwitterionic sulfobetaine silane (SBSi) modified surface.
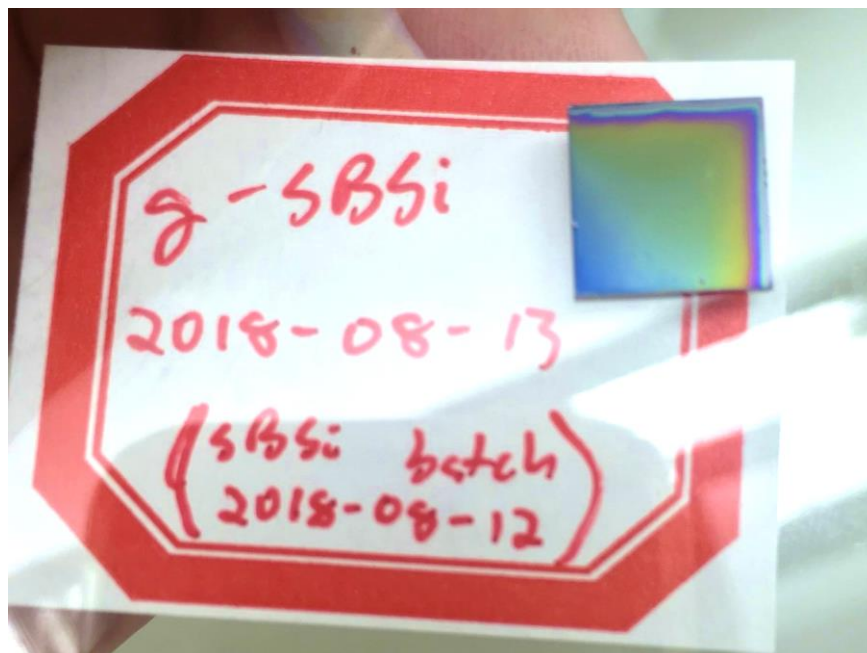
Figure 4.1. SiO$_2$ coating formed on a g-SBSi sample after 1 day exposure to refluxing PBS.

We characterized these formed coatings with ellipsometry and profilometry to assess their thickness, and further, we used FTIR to further demonstrate that the coatings were consistent with silica. Based on literature reports, we suspect that the PBS slowly etched the walls of the glass round-bottom flask (and potentially also the uncoated bottom of our samples) to form soluble silicic acid. It is then expected that the silica coating was formed via the polycondensation of silicic acid, nucleated at the zwitterionic surface. This process is illustrated in Figure 4.2 below. Although the conditions we used to make these silica coatings have not been previously reported in an "all-in-one" experimental setup, others have demonstrated, separately, the different aspects that comprise our approach: 1. the etching of Si/SiO$_2$ to form silicic acid and 2. the polycondensation of silicic acid to form an SiO$_2$ coating.
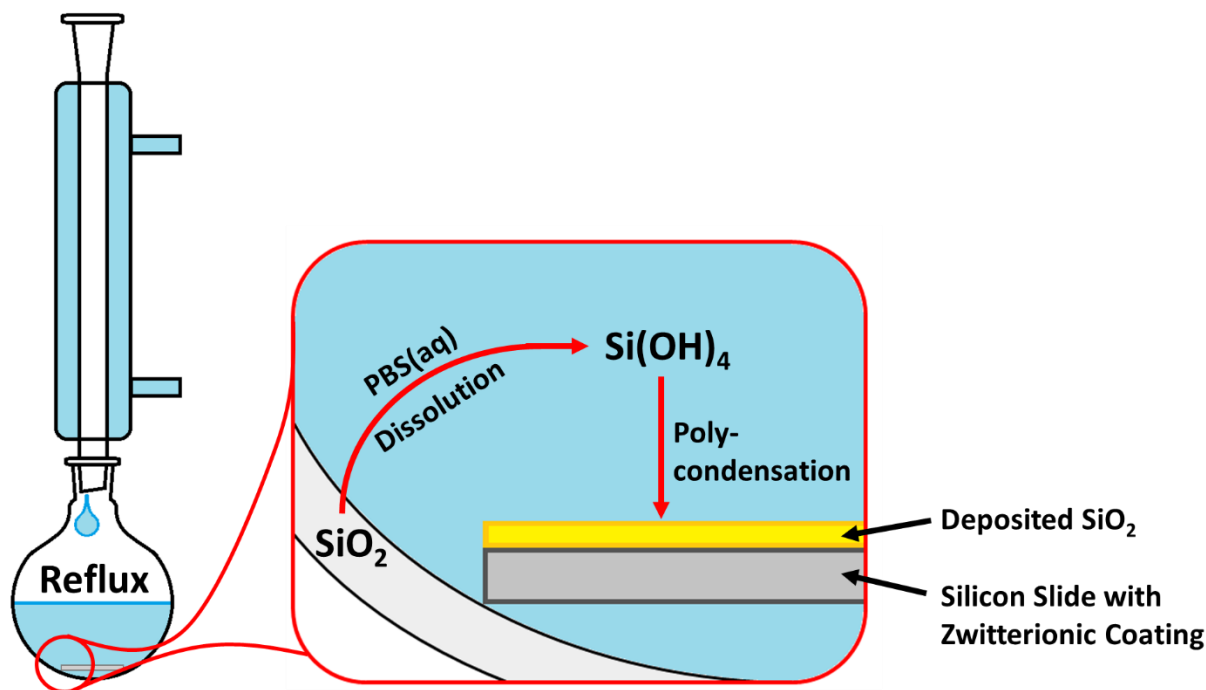
Figure 4.2. The suspected process of SiO_2 dissolution to form silicic acid and subsequent polycondensation/deposition on a substrate possessing a zwitterionic polymer coating.

Many have demonstrated the etching and dissolution of Si and SiO_2 in PBS to form silicic acid $(Si(OH)_4)$. Ahn et al. reported an etch rate of around 5.5 pm/h for an SiO_2 surface in 1x PBS at room temperature.[1] Further, the Rogers group reported a dissolution rate of their thermally grown SiO_2 of 0.07 nm/day at 37 °C and approximately 80 nm/day at 96 °C, describing the dissolution reaction follows: SiO_2 + 2 H_2O → H_4SiO_4.[2,3] As for Si substrates, Peled et al. studied the stability of silicon nanostructures in PBS and reported a Si nanowire dissolution at a rate of approximately 2.15 nm/day in 37 °C PBS.[4] The Rogers group found a dissolution rate of their silicon nanomembranes of 4 nm/day at 37 °C and 2 nm/day at 25 °C; they described the dissolution reaction via hydrolysis as follows where $Si + 4H_2O$ → $Si(OH)_4 + 2H_2$ with SiO_2 as a possible intermediate.[5] Literature reports point to the phosphate anion in PBS as the etchant for these Si and SiO_2 surfaces/interfaces.[6] The Rogers group has leveraged the phenomenon of silicon dissolution in PBS (to simulate physiological conditions) to develop implantable "transient" electronics for

use as sensors and therapeutic devices.[5] Further, they have conducted molecular simulations studying the processes and mechanisms of dissolution of Si and SiO_2 in both PBS and chloride solutions at multiple temperatures and concentrations.[3,7] Some have reported preventing dissolution of their PEG-trichlorosilane layer on silicon substrates via inclusion of a hydrophobic carbon spacer group, suggesting that this spacer is needed to prevent substrate dissolution/detachment.[6]

Also well reported is the formation of silica films from solutions containing silicic acid. One example of this phenomena occurring in nature is the formation of diatom shells and sponges.[8] Here, natural mechanisms exist by which organisms use "protein templating" to generate controlled structure of the precipitated silica.[8] Wenzl et al. studied the process of silica biomineralization in these diatoms (Thalassiosira pseudonana); they demonstrated the precipitation of spherical silica particles from a silicic acid solution when polyamines (cationic region) and silacidin (anionic region) were introduced.[9] Silacidin is a peptide rich in anionic phosphate groups found in this variety of diatom's shells that Wenzyl et al. showed serves as a cross-linking agent with polyamines to guide silica formation.[9] Also mentioned in this paper was that silaffins ("highly zwitterionic" proteins) have also been shown to guide silica formation in silicic acid solutions.[9]

Formation of silica films from synthetic surfaces has also been reported. Kim et al. reported the formation of a ~600 nm thick silica film by submerging a pDMAEMA coated substrate in a PH 5.5 phosphate buffer solution to which silicic acid was added; further, silica did not form in the absence of phosphate ions.[10] Wallace et al. studied silica nucleation rates on amine ($R-NH_3^+$), carboxyl ($R-COO^-$), and mixed surfaces using tapping-mode atomic force microscopy.[11] Here, forming solutions studied were at pH=5 and the silicic acid concentration varied.[11] Their amine surfaces resisted silica deposition, while the carboxyl surfaces exhibited silica deposition; mixed surfaces showed up to 18 times the rate of silica nucleation as compared to carboxyl surfaces.[11] They also patterned a substrate with alternating stripes of amine and carboxyl coatings, and they observed the greatest amount of silica deposition occurring at the interface between stripes (i.e. where carboxyl and amine groups were both present).[11] Helmecke et al.

demonstrated patterning of deposited silica.[12] To accomplish this, they patterned silicon wafers with regions of two different polymers where the hydrophilic polymer (PEI) and was surrounded by a hydrophobic polymer (poly(acrylic acid 2-ethyl-hexylester)).[12] Silicic acid solutions in pH 5.5 phosphate buffer were spin-coated onto the patterned surfaces which resulted in silica deposition occurring on the PEI-coated areas.[12] In addition to silica growth from planar surfaces, this phenomena has also been demonstrated on nanoparticles and membranes. Cornelissen et al. used latex nanoparticles with positively charged, negatively charged, and mixed charge (i.e. zwitterionic) surfaces and created silica shells via dispersion of the particles in silicic acid solutions.[13] They showed that these shells could be made hollow via heating to remove latex, and the resulting hollow shells demonstrated thicknesses up to 10nm.[13]

Although the silica coating formation on zwitterionic surfaces was not an anticipated focus of my research, the phenomena we observed regarding the formation of these silica layers by this "all-in-one" refluxing-PBS method are certainly worth documenting. These results and observations are reported here. As the data and results for this topic are preliminary in nature, this project presents an excellent opportunity for future development/research to better understand and characterize this interesting system.

Experimental Methods

Chemicals and Materials: 4-Vinylbenzyl chloride, copper(II) bromide, L-ascorbic acid, tris(2-pyridylmethyl)amine (TPMA), α-bromoisobutyryl bromide (BIBB), (3-aminopropyl) trimethoxysilane (APTMOS), triethylamine (TEA), and 1,3-propanesultone were obtained from Aldrich. SBMA ([2-(methacryloyloxy)ethyl]dimethyl-(3-sulfopropyl)ammonium hydroxide) and phosphate buffered saline (PBS) tablets were obtained from Fisher. N,N-Dimethyl-3-(trimethoxysilyl)propylamine (DMASi) and 2-[methoxy(polyethyleneoxy) 6-9 propyl]trimethoxysilane (PEGsilane) were obtained from TCI America and Gelest, respectively. All compounds were used as received. Single-sided polished, boron-doped, p-type silicon wafers (⟨100⟩, 0.01–0.02 Ω cm, 500–550 μm) were purchased from Pure Wafer Inc.

BrTMOS Initiator Synthesis: This procedure was adapted from that reported by the Shaoyi Jiang group.[14] The initiator molecule, 3-(trimethoxysilyl)propyl 2-bromo-2-methylpropanoate (BrTMOS), was synthesized as follows.[10] A stir bar and 3.49 mL (20.0 mmol) of APTMOS were placed in a 100 mL round bottom flask. The flask was sealed via septum and sparged with nitrogen. Subsequently, 50 mL of anhydrous THF and 2.79 mL of TEA (20.0 mmol) were added to the flask via syringe and then stirred for 30 min with nitrogen bubbled through it. Then, 3.00 mL of BIBB (24.0 mmol) was added dropwise to the solution via syringe over 30 min with continued stirring, nitrogen bubbling, and chilling via ice bath. The reaction was allowed to proceed overnight. The precipitate was removed via frit filtration, and THF was removed from the remaining solution using rotary evaporation. The resulting yellowish oil was redissolved in 40 mL of CH_2Cl_2, washed twice with 0.01 N HCl, and washed twice more with ice-cold water. The organic phase was dried over anhydrous $CaCl_2$ before removal of the CH_2Cl_2 by rotary evaporation. The remaining product was re-dissolved in hexane and precipitate removed via gravity filtration. The hexane was removed via rotary evaporation, yielding the product as a light-yellow colored oil that was placed under vacuum for 12 h to remove remaining solvent.

Fabrication of BrTMOS-modified silicon slides: Silicon slides were exposed to a piranha solution (7:3 mixture of sulfuric acid and 30% hydrogen peroxide) for 30 minutes. Caution: piranha solution can dangerous if not following proper safety precautions. Slides were triple rinsed in DI water, and then in ethanol before addition to the BrTMOS solution. The piranha-cleaned slides were immersed into an initiator solution consisting of 250 µL (1.72 mmol) of BrTMOS dissolved in 10 mL of ethanol. Samples were allowed to react with the solution overnight. After removal from the BrTMOS solution, the slides were rinsed with ethanol, dried with N_2, and placed in a 100 °C vacuum oven for 5 h. Initiator-modified slides were stored in foil-wrapped containers to prevent exposure to light.

Attachment of VBC via Hydrosilylation: For modification of flat silicon, 1 x 1 cm^2 samples were placed in an 800 °C oven for 4 h. After cooling, the samples were soaked in a 2.5% solution of HF in a 7:3 ethanol-water mixture to remove the oxide, rinsed with DI water, and dried. For irradiation, samples consisted of 15 µL of VBC sandwiched between the silicon surface and a No. 1 thickness coverslide. Samples were irradiated with UV light in a DYMAX 5000-EC UV curing lamp system. Total exposure times were typically 100 s. After removal of the coverslides, the samples were immersed in acetone for 1 h and then dried before use.

PEG-Silane attachment procedure flat silicon: Diced silicon slides were soaked in a 1:1 mixture of DI water and ethanol for at least 4 hours before rinsing with DI water and drying with stream of nitrogen. Subsequently, slides were soaked in a piranha solution for 30 minutes. The piranha-cleaned slides were triple rinsed with DI water, ethanol, and then toluene before addition to the PEGsilane solution consisting of 22 µL of the PEGsilane and 12 µL of HCl in 15 mL of toluene for 18 h, then washed with toluene ethanol, and water, before drying in a steam of nitrogen.

SBSi Monolayers: SBSi was synthesized based on a method described by Yeh et al.[10] To a N$_2$-sparged round-bottom flask, 0.600 g (4.91 mmol) of 1,3-PS, 5 mL of dried acetone, and 1.00 mL (4.57 mmol) of DMASi were each injected via syringe. After 12 h reaction under N$_2$ with stirring, the resulting white solid product was collected by filtration, washed with acetone, and dried under reduced pressure for 1 hour.

To form the g-SBSi monolayer, piranha-cleaned slides were placed in a solution containing 50 mg of SBSi, 20 mL of EtOH, and 40 µL of DI water for 12 h, rinsed with EtOH, and cured in an 80 °C vacuum oven for 30 min.

Surface-Initiated ARGET Polymerization of SBMA: A general procedure for surface-initiated ARGET

polymerization is described as follows. For 0.018 M SBMA monomer solutions, the molar ratios of monomer:Cu(II):ligand:reducing agent were 250:1:5:160 in a 1:1 methanol water mixture. Two stock solutions were used in the synthesis: $CuBr_2$/TPMA in methanol (18 mM in $CuBr_2$; 86 mM in TPMA) and ascorbic acid in methanol (25 mg per mL methanol). In a 20mL vial, the following were added to form the monomer solution: 0.075g SBMA, 7.5 mL H_2O, 7.5 mL methanol, and 60 µL of $CuBr_2$/TPMA stock solution. This was sealed via septum and sparged with nitrogen for 30 minutes. Simultaneously, the initiator-modified silicon samplers were placed in vials, sealed via septum, and sparged with nitrogen for 30 minutes. After the monomer solution was allowed to sparge for 30 minutes, 1.2 mL of the ascorbic acid stock solution was injected to the monomer solution before allowing the resulting solution to sparge for an additional 5 minutes. The monomer solution was then transferred to slide-containing vials via syringe to begin the surface-initiated ARGET polymerization. After the desired reaction time, samples were removed from the monomer solution, soaked in a 50:50 DI H_2O:methanol mixture to remove unbound materials, rinsed with additional methanol and water, and finally dried with compressed nitrogen.

PBS Soak for Silica Growth: PBS tablets from fisher were dissolved in 200 mL of deionized water per tablet to form a 0.01M (1x) phosphate buffer solution. For samples exposed to 37 °C PBS, each sample was placed in a well of a polystyrene 12-well plate with 3 mL of PBS per well. The well plate was wrapped with parafilm and foil before placing in a 37 °C incubation chamber.

For samples exposed to refluxing PBS, approximately 30 mL of PBS was placed in a multi-neck glass round-bottom flask and equipped with a reflux condenser. The PBS was then heated to reflux (~100 °C). Depending on the experiment, samples were either immediately to added to the flask, or after the solution was first allowed to reflux for 24 hours. After samples soaked in the refluxing PBS for the allotted exposure time, they were then removed, rinsed with deionized water, and then dried with a stream of nitrogen before analysis.

Analytical Techniques: Infrared data were obtained using a Thermo Nicolet 6700 FT-IR Spectrometer with Smart iTR™ Attenuated Total Reflectance (ATR) attachment with diamond crystal plate.

Film thicknesses were measured using an M-2000VI spectroscopic ellipsometer (J.A. Woollam Co.). Each sample was measured at angles of incidence of 60° and 70°. CompleteEASE software was used to analyze the measurements using the built-in transparent Cauchy film on silicon substrate model. A refractive index of 1.45 was assumed. A Veeco Dektak 150 profilometer was also used to analyze thicknesses of SiO_2 coatings.

Advancing and receding water contact angles were measured on static drops with the dispensing needle remaining in the drop using a Rame Hart goniometer.

Scanning electron microscopy images were obtained using a Zeiss Merlin SEM instrument with a GEMINI II column provided through the Vanderbilt Institute of Nanoscale Science and Engineering (VINSE).

Results and Discussion

While developing zwitterionic polymer (g-pSBMA) and monolayer (g-SBSi) coatings on silicon substrates to study the antifouling capabilities of these coatings, an interesting and unexpected phenomenon was observed when these samples were placed in phosphate-buffered saline (PBS) solutions under certain conditions. In many cases where the samples were placed in PBS at the physiological temperature of 37 °C, a thick layer (usually hundreds of nanometers in thickness) of what appeared to be SiO_2 would form on the surface of these samples. This SiO_2-like coating would often take multiple days or even weeks to appear at 37 °C. This thick coating was stable to 0.1M HCl even after 24 hours of exposure, showing negligible loss of thickness. However, the coating was quickly etched/dissolved in a 2.5% solution of HF in a 7:3 ethanol-water mixture, as would be expected of a silica coating. As shown in Figure 4.3 below, profilometry

experiments showed that these silica coatings could possess thicknesses around the 1 μm range for these g-VBC-pSBMA samples exposed to 37 °C PBS for 3 weeks.
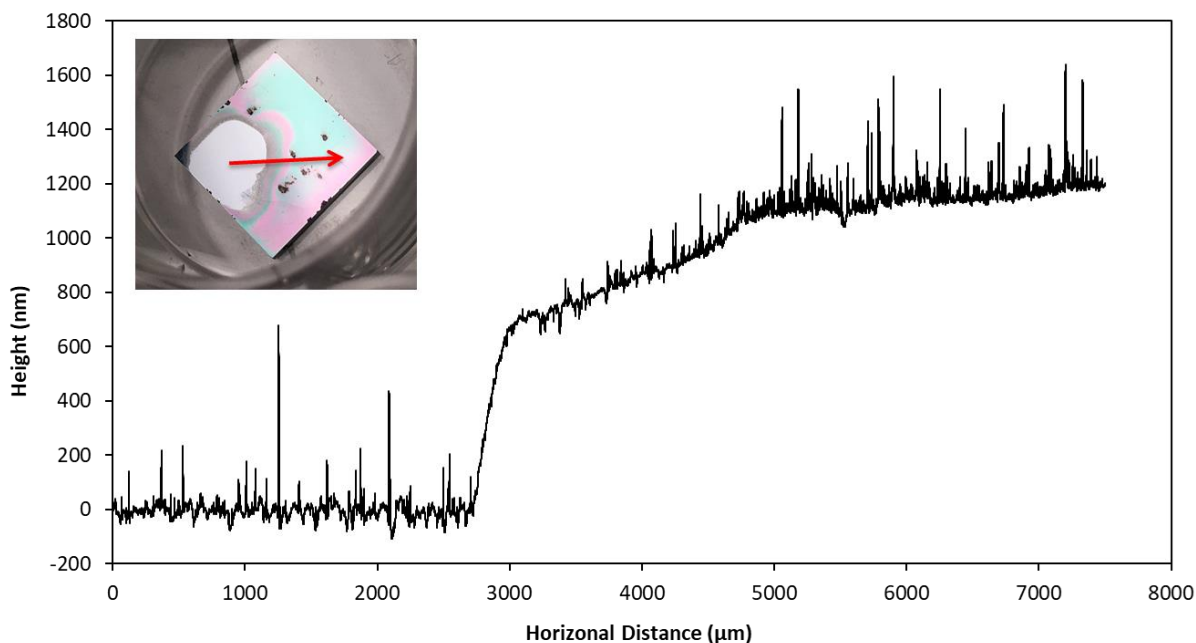
Figure 4.3. Profilometry trace of SiO$_2$ formed on sample surface, starting from HF-etched corner to provide zero value. Inset image: SiO$_2$ from the measured g-BrTMOS-pSBMA sample after 3 weeks in PBS at 37 °C. Profilometry trace includes a baseline correction to compensate for stage leveling irregularities.

We further characterized these same SiO$_2$-coated g-VBC-pSBMA samples via scanning electron microscopy (SEM). Figure 4.4 shows SEM images after cleaving these samples to expose the cross-section. The figure shows the thickness of the SiO$_2$ coating at various locations (and magnifications) on the cleaved sample's edge. Note that in Figure 4.4, along with Figure 4.5 which shows a top-down view, the SiO$_2$ coating appears to possibly be porous in nature.
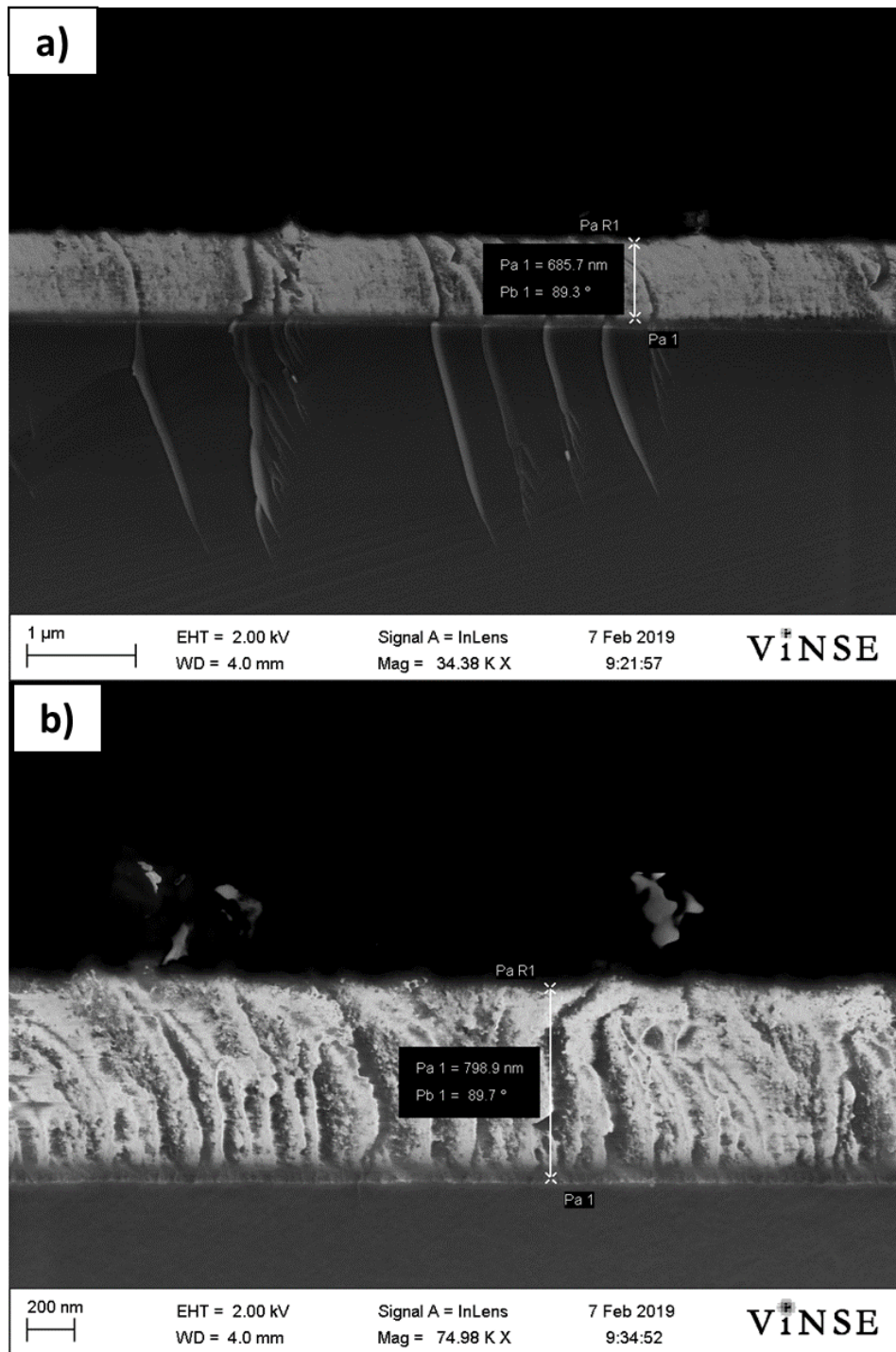
Figure 4.4. Scanning electron microscopy images of SiO_2 coatings formed on g-VBC-pSBMA samples after 3 weeks exposure to PBS at 37 °C. Shown above are cross-sections of cleaved samples to illustrate thickness. Note the images above are from two different samples and at two different magnifications.
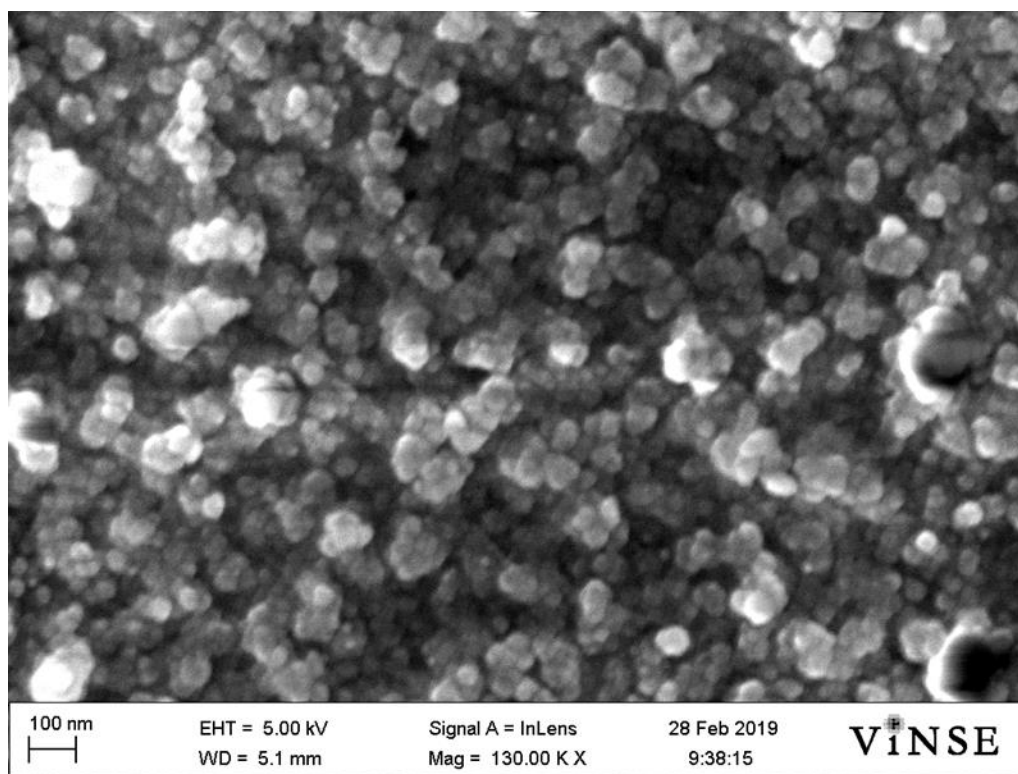
Figure 4.5. Scanning electron microscopy images of SiO$_2$ coatings formed on g-VBC-pSBMA samples after 3 weeks exposure to PBS at 37 °C. Shown above is a top-down image to demonstrate surface topography/texture.

In order to more reliably replicate this occurrence, and also accelerate the occurrence via the faster kinetics afforded by the elevated temperature, we placed silicon substrates modified with a zwitterionic polymer (g-pSBMA) or monolayer (g-SBSi) films into refluxing PBS in a glass round-bottom flask under a condenser. Here we found that we could reliably induce the formation of the silica coating in a matter of 2 days or even less under these conditions. Figure 4.6 and 4.7 demonstrate the increase in thickness as measured by ellipsometry and profilometry, respectively, due to SiO$_2$ film formation. Figure 4.6 shows the ellipsometric thickness versus exposure time to refluxing PBS for both zwitterionic g-VBC-pSBMA samples and for unmodified "blank" silicon samples as controls. As can be seen in Figure 4.6, no significant film thickness increase was observed for either sample type after the first day of exposure; however, the zwitterion-modified samples showed a large increase in thickness after two or more days of exposure to refluxing PBS, reaching thicknesses of around 600 nm. The blank silicon controls continued to experience

minimal change in thickness over the same period. We suspect that the freshy-prepared PBS had not been given sufficient time to form silicic acid via etching of the glassware at day one. We found in later experiments that refluxing the PBS for multiple days prior to introduction of the zwitterion-modified samples eliminated this delay in SiO_2 coating formation, and the SiO_2 coatings would form on zwitterion-modified samples in less than a day. Figure 4.7 shows the profilometry trace measured across one of these g-VBC-pSBMA samples where the trace was measured from one HF-etched corner (i.e. a zero thickness region) to the opposite HF-etched corner, showing the SiO_2 thickness in the region between the two corners. Thicknesses of 500 – 600 nm were apparent for this sample, similar to that observed via ellipsometry.
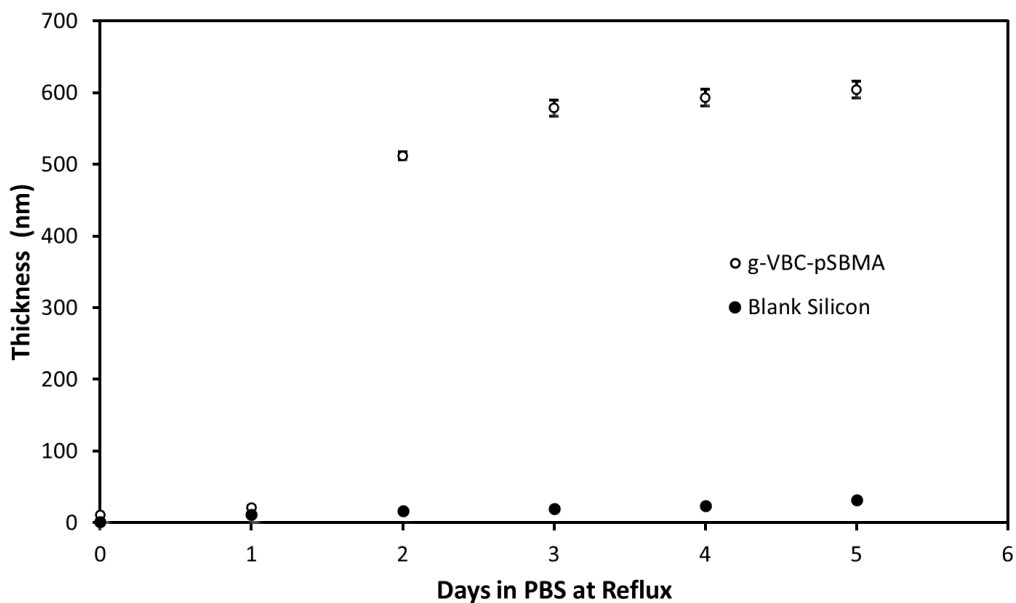
Figure 4.6. Ellipsometric thickness of samples exposed to refluxing PBS versus time. Compared are silica growth on g-VBC-SBMA samples versus that on blank (i.e. uncoated) silicon samples.
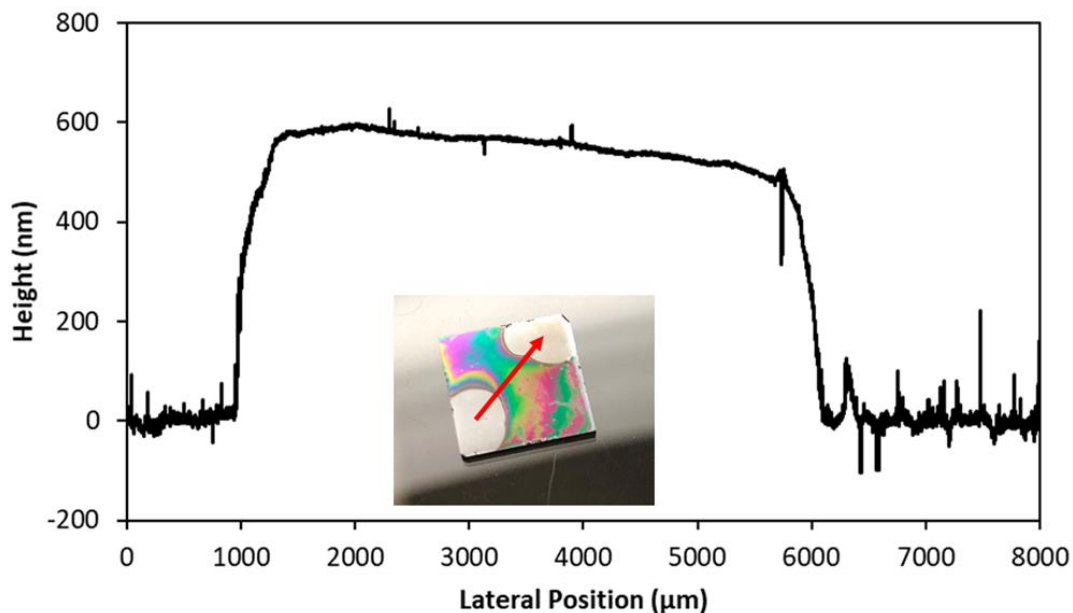
Figure 4.7. Profilometry trace of SiO_2 formed on sample surface, starting and ending at HF-etched corners to provide zero values. Inset image: SiO_2 coating on the measured g-VBC-pSBMA after 1 day in refluxing PBS. Profilometry trace includes a baseline correction to compensate for stage leveling irregularities.

Further, we used FTIR to further support that the coating was indeed silica. As seen in Figure 4.8, the coatings demonstrated spectra consistent with SiO_2 films reported in literature.[10,15,16]
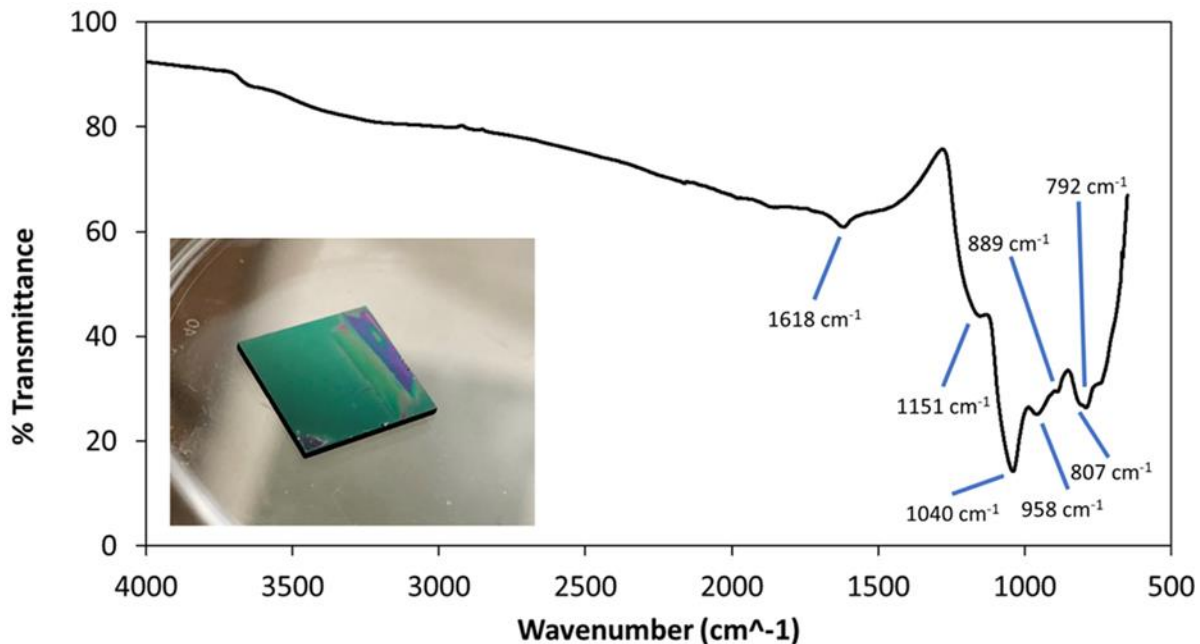
Figure 4.8. FT-IR ATR spectra of SiO_2 formed on g-VBC-pSBMA sample surface after 5 days in refluxing PBS. Inset image: Photograph of sample that was analyzed in this figure.

We also attempted to form SiO_2 coatings on other polymer-modified and monolayer-modified silicon substrates; however, these did not prove successful. Silicon samples modified with a poly(HEMA) coating and silicon samples modified with a g-VBC molecular film were both exposed to the refluxing PBS. Gas/steam bubbles formed at the surface of these samples when submerged in the refluxing PBS, and once removed from the solution, a very-nonuniform, scale-like material was evident. This was vastly different than the more uniform coatings that formed on the zwitterion-modified substrates. Of note, gas/steam bubbles did not form on the more hydrophilic zwitterion-modified samples, as these are expected to be better wetted than the less hydrophilic poly(HEMA) and g-VBC modified silicon substrates.

114

Conclusions

Here, we demonstrated the reliable formation of a thick coating of SiO_2 at/near the 1 μm scale on the surface of zwitterionic polymer (g-VBC-pSBMA) and monolayer (g-SBSi) coatings on silicon substrates by exposure to 37 °C phosphate buffered saline (PBS) solutions. Further, we demonstrated the ability to accelerate this SiO_2 coating formation by placing the zwitterion-modified silicon substrates into refluxing PBS in a glass round-bottom flask under a condenser. We characterized the coating with ellipsometry, profilometry, and scanning electron microscopy to assess its thickness, and further, we used FTIR to demonstrate that the coating was consistent with silica. Based on literature reports and our experiments shown here, we suspect that the PBS slowly etches the walls of the glass round-bottom flask (and potentially also the uncoated bottom of our samples) to form soluble silicic acid. It is then expected that the silica coating is formed via the polycondensation of silicic acid, nucleated at the zwitterion-modified surface. Once again, these results and observations are quite preliminary in nature, allowing an excellent opportunity for future development/research of this interesting system.

References:

(1)   Ahn, S.; Spuhler, P. S.; Chiari, M.; Cabodi, M.; Selim¨unï, M.; Selim¨unï, S. Quantification of Surface Etching by Common Buffers and Implications on the Accuracy of Label-Free Biological Assays. *Biosensors and Bioelectronics* **2012,** *36* (1), 222-229. https://doi.org/10.1016/j.bios.2012.04.020.

(2)   Kyeung Lee, Y.; Jun Yu, K.; Kim, Y.; Yoon, Y.; Xie, Z.; Song, E.; Luan, H.; Feng, X.; Huang, Y.; Rogers, J. A. Kinetics and Chemistry of Hydrolysis of Ultrathin, Thermally Grown Layers of Silicon Oxide as Biofluid Barriers in Flexible Electronic Systems. *ACS Appl. Mater. Interfaces* **2017** *9* (49), 42633–42638. https://doi.org/10.1021/acsami.7b15302.

(3)   Fang, H.; Zhao, J.; Yu, K. J.; Song, E.; Farimani, A. B.; Chiang, C. H.; Jin, X.; Xue, Y.; Xu, D.; Du, W.; Seo, K. J.; Zhong, Y.; Yang, Z.; Won, S. M.; Fang, G.; Choi, S. W.; Chaudhuri, S.; Huang, Y.; Alam, M. A.; Viventi, J.; Aluru, N. R.; Rogers, J. A. Ultrathin, Transferred Layers of Thermally Grown Silicon Dioxide as Biofluid Barriers for Biointegrated Flexible Electronic Systems. *Proceedings of the National Academy of Sciences of the United States of America* **2016**, *113* (42), 11682–11687. https://doi.org/10.1073/pnas.1605269113.

(4)   Peled, A.; Pevzner, A.; Peretz Soroka, H.; Patolsky, F. Morphological and Chemical Stability of Silicon Nanostructures and Their Molecular Overlayers under Physiological Conditions: Towards Long-Term Implantable Nanoelectronic Biosensors. *Journal of Nanobiotechnology* **2014**, 12. https://doi.org/10.1186/1477-3155-12-7.

(5)   Hwang, S. W.; Tao, H.; Kim, D. H.; Cheng, H.; Song, J. K.; Rill, E.; Brenckle, M. A.; Panilaitis, B.; Won, S. M.; Kim, Y. S.; Song, Y. M.; Yu, K. J.; Ameen, A. A.; Li, R.; Su, Y.; Yang, M.; Kaplan, D. L.; Zakin, M. R.; Slepian, M. J.; Huang, Y.; Omenetto, F. G.; Rogers, J. A. A Physically Transient

Form of Silicon Electronics. *Science* **2012**, *337* (6102), 1640–1644. https://doi.org/10.1126/science.1226325.

(6)   Dekeyser, C. M.; Buron, C. C.; Derclaye, S. R.; Jonas, A. M.; Marchand-Brynaert, J.; Rouxhet ⇑, P. G. Degradation of Bare and Silanized Silicon Wafer Surfaces by Constituents of Biological Fluids. **2012**. https://doi.org/10.1016/j.jcis.2012.04.022.

(7)   Yin, L.; Farimani, A. B.; Min, K.; Vishal, N.; Lam, J.; Lee, Y. K.; Aluru, N. R.; Rogers, J. A. Mechanisms for Hydrolysis of Silicon Nanomembranes as Used in Bioresorbable Electronics. *Advanced Materials* **2015**, *27* (11), 1857–1864. https://doi.org/10.1002/adma.201404579.

(8)   Wong, C.; Foo, P.; Huang, J.; Kaplan, D. L. Lessons from Seashells: Silica Mineralization via Protein Templating. *Trends in Biotechnology* **2004**, *22* (11), 577-585. https://doi.org/10.1016/j.tibtech.2004.09.011.

(9)   Wenzl, S.; Hett, R.; Richthammer, P.; Sumper, M. Silacidins: Highly Acidic Phosphopeptides from Diatom Shells Assist in Silica Precipitation In Vitro. *Angewandte Chemie International Edition* **2008**, *47* (9), 1729–1732. https://doi.org/10.1002/anie.200704994.

(10)   Kim, D. J.; Lee, K.-B.; Chi, Y. S.; Kim, W.-J.; Paik, H.-J.; Choi, I. S. Biomimetic Formation of Silica Thin Films by Surface-Initiated Polymerization of 2-(Dimethylamino)Ethyl Methacrylate and Silicic Acid. **2004**. https://doi.org/10.1021/la048657b.

(11)   Wallace, A. F.; Deyoreo, J. J.; Dove, P. M. Kinetics of Silica Nucleation on Carboxyl-and Amine-Terminated Surfaces: Insights for Biomineralization. *J. Am. Chem. Soc*. **2009**, 131, 14, 5244–5250. https://doi.org/10.1021/ja809486b.

(12)   Helmecke, O.; Hirsch, A.; Behrens, P.; Menzel, H. Influence of Polymeric Additives on Biomimetic Silica Deposition on Patterned Microstructures. *Journal of Colloid and Interface Science* **2008**, *321*, 44–51. https://doi.org/10.1016/j.jcis.2008.01.006.

(13)   Cornelissen, J. J. L. M.; Connor, E. F.; Kim, H. C.; Lee, V. Y.; Magibitang, T.; Rice, P. M.; Volksen, W.; Sundberg, L. K.; Miller, R. D. Versatile Synthesis of Nanometer Sized Hollow Silica Spheres. *Chemical Communications* **2003**, *3* (8), 1010–1011. https://doi.org/10.1039/b212811j.

(14)   Zhang, Z.; Chao, T.; Chen, S.; Jiang, S. Superlow Fouling Sulfobetaine and Carboxybetaine Polymers on Glass Slides. *Langmuir* **2006**, *22* (24), 10072–10077. https://doi.org/10.1021/la062175d.

(15)   Socrates, G. *Infrared and Raman Characteristic Group Frequencies: Tables and Charts*, 3rd ed.; John Wiley & Sons Ltd: Chichester, **2001**.

(16)   Almeida, R. M.; Marques, A. C. Characterization of Sol-Gel Materials by Infrared Spectroscopy. In *Handbook of Sol-Gel Science and Technology: Processing, Characterization and Applications*; **2018**; pp 1121–1151. https://doi.org/10.1007/978-3-319-32101-1_33.

Chapter V

NUCLEOPHILIC SUBSTITUTION REACTIONS AT BENZYL CHLORIDE SURFACES

Introduction

A surface modification strategy utilizing nucleophilic substitution can provide researchers the ability to tailor interfacial properties by attaching moieties possessing desirable characteristics from surfaces. This work demonstrated the versatility of benzyl chloride molecular films as a platform for surface modification via nucleophilic substitution. Rather than using siloxane-based methods for attachment, this research investigated an approach that employed more hydrolytically stable Si-C linkages to form benzyl chloride molecular films. The method of grafting vinyl compounds from silicon utilizing a UV-induced silicon-carbon linkage has been demonstrated by the Buriak and Chidsey groups, among others.[1–8] As compared to Si-O-Si linkages, Si-C linkages are more stable and less susceptible to failure in aqueous environments as they avoid the hydrolytic instability associated with Si-O-Si linkages.[9–12]

Figure 5.1 illustrates the general scheme for the studied routes to covalently attach the benzyl chloride group to a H-terminated silicon substrate and subsequently modify via substitution. Xu et al. demonstrated UV-induced hydrosilylation for attachment of 4-vinylbenzyl chloride to H-terminated silicon for use as an ATRP initiator for grafting polymers from silicon surfaces, but this surface's ability to provide sites for further modification via nucleophilic substitution has not, until this point, been explored or reported.[13,14] Demonstrated here is the ability to utilize these grafted benzyl chloride moieties (g-VBC) to perform substitution reactions with a variety of molecules to yield potentially useful surface coatings. First, substitution reactions of alkoxides with g-VBC to yield hydrophobic alkyl-terminated surfaces or more hydrophilic PEG-terminated surfaces were demonstrated. Also shown was the ability to perform a quaternization reaction to convert the g-VBC surfaces to ones possessing zwitterionic moieties. Another

route was explored reacting dimethylamine with g-VBC surfaces to produce tertiary-amine terminated surfaces; these were subsequently converted to zwitterionic surfaces upon reaction with 1,3-propane sultone. Finally demonstrated was a substitution reaction with NaN₃ to yield azide-modified surfaces potentially useful for "click" chemistry. In addition to flat silicon substrates, we attached VBC to porous silicon (PSi) substrates where the inherent high surface area of PSi provided higher signal for attenuated total reflectance (ATR) FT-IR analysis of the substitution-modified surfaces.
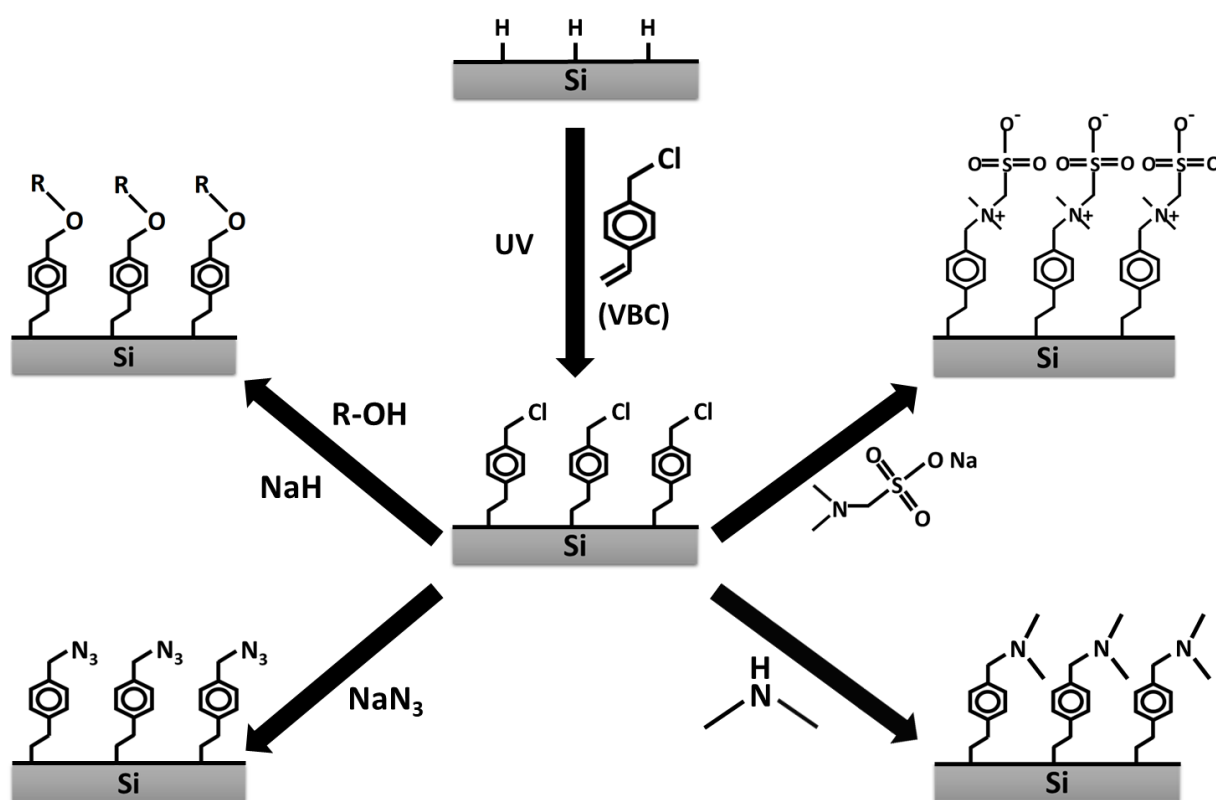
Figure 5.1. Strategy for introducing surface-bound benzyl chloride groups to a H-terminated silicon surface. VBC introduced onto the surface of the freshly HF-etched silicon substrate was then irradiated with UV to induce attachment. Nucleophilic substitution reactions between the surface-bound benzyl chloride moiety and a chosen nucleophilic compound was then performed.

Experimental Methods

Chemicals and Materials: 4-Vinylbenzyl chloride, sodium hydride (60% dispersion in mineral oil), dimethylamine (40% solution in water), dimethylamine (2M solution in THF), formaldehyde-sodium bisulfite adduct, and 1-dodecanol were purchased from Sigma-Aldrich and used as received. Sodium azide, 1,3-propanesultone, and polyethylene glycol monomethyl ether 2000 (PEG2000) were purchased from TCI and used as received. Single-sided polished, boron-doped, p-type silicon wafers (⟨100⟩, 0.01–0.02 Ω cm, 500–550 μm) were purchased from Pure Wafer Inc.

PEG-Silane attachment procedure flat silicon: Diced silicon sliders were soaked in a 1:1 mixture of DI water and ethanol for at least 4 hours before rinsing with DI water and drying with stream of nitrogen. Subsequently, slides were soaked in a piranha solution (7:3 mixture of Sulfuric acid and 30% hydrogen peroxide; caution dangerous) for 30 minutes. Slides were triple rinsed with DI water, ethanol, and then toluene before addition to the PEGsilane solution. These piranha-cleaned slides were placed into a solution containing 22 μL of PEGsilane and 12 μL of HCl in 15 mL of toluene for 18 h, then washed with toluene ethanol, and water, before drying in a steam of nitrogen.

Producing Porous Silicon Wafers: Si wafers were sequentially washed with acetone, isopropanol, and ethanol, and then dried with nitrogen before use. A layer of PSi was formed by electrochemical etching Si in a 15% HF solution in ethanol at a current density of 70 mA/cm^2 for 100 s. The substrates were then thoroughly washed with ethanol and dried with nitrogen. The PSi layer was 3.65 μm thick and had a porosity of 80%.

Attachment of VBC via Hydrosilylation: For modification of flat silicon, 1 x 1 cm^2 samples were placed in an 800 °C oven for 4 h. After cooling, the samples were soaked in a 2.5% solution of HF in a 7:3 ethanol-

water mixture to remove the oxide, rinsed with DI water, and dried. For irradiation, samples consisted of 15 µL of VBC sandwiched between the silicon surface and a No. 1 thickness coverslide. Samples were irradiated with UV light in a DYMAX 5000-EC UV curing lamp system. Total exposure times were typically 100 s. After removal of the coverslides, the samples were immersed in acetone for 1 h and then dried before use.

For modification of porous silicon: Porous silicon samples were similarly soaked in the HF solution as for flat silicon, but rinsed with water and then ethanol before drying. They were similarly contacted with VBC and irradiated with UV, except that a total exposure time of 400 s was used.

For all samples, exposure times over 100 s consisted of sequential 100-s irradiations with intermediate pauses to avoid excessive heating.

Synthesis of N,N-dimethylamino methanesulfonate (DMAMS): DMAMS was synthesized as described previously[15,16]; briefly, the procedure was as follows. Formaldehyde-sodium bisulfite adduct (2.7 g, 20 mmol) was dissolved in 10 mL of DI water and then cooled over an ice bath. To this, 2.94 mL of 40% aqueous dimethylamine solution (23 mmol) was added dropwise with stirring. The solution was allowed to rise to room temperature and then react for an additional hour. Water and excess dimethylamine were removed via vacuum and collected in a liquid nitrogen cooled trap. The obtained product was a white powder with a yield of 90%. NMR and ATR FT-IR spectra may be found in Appendix B (Figure B.1 and B.2 respectively).

Zwitterionic Modification of g-VBC Samples via Substitution with DMAMS: Grafted VBC samples (flat or porous silicon) were submerged in 186 mM solution of DMAMS in a 1:1 water and ethanol mixture. The samples were allowed to react in the solution at 50 °C. After allowing to react for a predetermined period of time, the samples were rinsed and soaked in an ethanol/water mixture overnight before drying.

Azide Modification of g-VBC Samples via Substitution: In a small vial, 0.01 g of NaN$_3$ and a g-VBC sample were added, sealed with septum, and sparged with nitrogen. Subsequently, 2 mL of anhydrous DMF was added via syringe. The g-VBC slide was then allowed to react in the resulting solution at 70 °C for 18 h. After reaction, the sample was soaked in DMF for 24 hours, rinsed with water and ethanol, and then dried with nitrogen.

Substitution Reactions with Dimethylamine at g-VBC Surfaces and Subsequent Quaternization: A two-neck flask was equipped with a reflux condenser, the apparatus was purged with nitrogen for 30 minutes, and the apparatus was protected via bubbler for maintaining a nitrogen atmosphere throughout the following reaction steps. The reflux condenser was then chilled to approximately -5 °C using a cooled water circulator/pump containing a 50/50 mix of water and ethylene glycol (this sub-zero coolant temperature was to condense the volatile dimethyl amine and prevent its loss from reaction apparatus). Once chilled, g-VBC samples and approximately 20 mL of a 2M dimethylamine/THF solution were added into the RB flask through the 2nd neck and re-sealed via glass stopper. The solution was then heated to 60 °C and allowed to react 18 h. The solution was then allowed to cool back to room temperature, and the samples were removed before rinsing with THF, EtOH, and drying with nitrogen. The resulting dimethylamine-modified samples were then placed in 5 mL of a 1.64 M solution of 1,3-propanesultone in acetone. Samples were allowed to react for 18 h at room temperature before rinsing with acetone and drying with nitrogen.

Substitution Reactions with PEG2000 at g-VBC Surface of PSi: For reactions 18 mM in concentration of PEG2000, the procedure was as follows. First, NaH (0.03 g, 0.75 mmol, NaH 60% dispersion in mineral oil) was added to a flask which was then sealed via septum and sparged with nitrogen. After allowing sufficient time for nitrogen to displace the air in the flask, the NaH was washed three times with pentane to

remove mineral oil. Caution: NaH needs to be kept under an inert atmosphere during and after removal of mineral oil to prevent ignition upon contact with moisture present in air. Subsequently, 10 mL of anhydrous THF was injected into the flask. In a separate flask, 1.5 g (0.75 mmol) of PEG2000 was added and the flask was sealed and sparged with nitrogen before injecting 30 mL of anhydrous THF. Both solutions were chilled via ice bath before transferring the PEG2000-containing solution to the NaH solution via cannula with stirring; the resulting mixture was allowed to warm room temperature and react for 1 h with continued stirring. The mixture was then transferred via cannula to a nitrogen-sparged reflux condenser apparatus protected by a nitrogen bubbler. Grafted 4-vinylbenzyl chloride (g-VBC) silicon slides were added to the reaction vessel and allowed to react under refluxing THF conditions for the prescribed period of time. Flat silicon samples were removed from the condenser, washed in toluene, ethanol, and water, and then dried via a nitrogen. Porous silicon samples were soaked in THF for 24 hours before washing with toluene, ethanol, water, and again with ethanol before drying via nitrogen.

Substitution Reactions with n-Dodecanol at g-VBC Surface of PSi: For reactions 720 mM in concentration of the alkoxide, the procedure was as follows. First, NaH (0.258 g, 6.45 mmol, NaH 60% dispersion in mineral oil) was added to a flask which was then sealed via septum and sparged with nitrogen. Subsequently, 5 mL of anhydrous THF was injected into the flask. In a separate flask, 2.0 g (11 mmol) of n-dodecanol was added, and the flask was sealed and sparged with nitrogen before injecting 10 mL of anhydrous THF. Both solutions were chilled via ice bath before transferring the alcohol-containing solution to the NaH solution via cannula with stirring; the resulting mixture was allowed to warm room temperature and react for 1 h with continued stirring. The mixture was then transferred via cannula to a nitrogen-sparged reflux condenser apparatus protected by a nitrogen bubbler. Grafted 4-vinylbenzyl chloride (g-VBC) silicon slides were added to the reaction vessel and allowed to react under refluxing THF conditions for the prescribed period of time. The flat silicon samples were removed from the condenser, washed in toluene, ethanol, and water, and then dried via a nitrogen.

Analytical Techniques: Infrared data were obtained using a Thermo Nicolet 6700 FT-IR Spectrometer with Smart iTR™ Attenuated Total Reflectance (ATR) attachment with diamond crystal plate. Due to the need to clamp samples to the diamond crystal for analysis, this method was destructive to PSi surface; thus measurements taken after each reaction step were taken at different locations, albeit on the same sample.

Film thicknesses were measured using an M-2000VI spectroscopic ellipsometer (J.A. Woollam Co.). Each sample was measured at angles of incidence of 60° and 70°. CompleteEASE software was used to analyze the measurements using the built-in transparent Cauchy film on silicon substrate model. A refractive index of 1.45 was assumed.

Advancing and receding water contact angles were measured on static drops with the dispensing needle remaining in the drop using a Rame Hart goniometer.

Results and Discussion

DMAMS Substitution Reaction at g-VBC Surface of Porous Silicon

To increase ATR FT-IR signal over that of surface modifications applied to flat silicon, the coating strategies were also applied to porous silicon (PSi). As shown in Figure 5.2, upon 18 h reaction of DMAMS with the g-VBC surface, appearance of the peak at 1475 cm^{-1} commonly associated with C-H bending of methyl groups of the quaternary nitrogen of the zwitterionic group was observed.[17–21] Adsorbed water on the hydrophilically-modified surface and oxidation of the silicon (creating surface Si-OH hydroxyl groups) could both contribute to the broad peak centered at around 3455 cm^{-1} and the broad peak at 1630 cm^{-1} assigned to O-H stretching and bending respectively.[22] The sharp peaks at 1214 cm^{-1} and 1046 cm^{-1}, corresponds to S=O asymmetric and symmetric stretching respectively of the sulfobetaine group. Further, the loss of the peaks at 2782 cm^{-1} and 2828 cm^{-1}, associated with C-H stretching of the methyl groups of the tertiary amine, when comparing the FTIR spectra of the pure DMAMS powder to that of the modified

surface, was consistent with successful quaternization reaction of DMAMS at the g-VBC surface.[22] In addition, the 1265 cm^{-1} peak assigned to the C-H bending vibration of the Ar-CH$_2$Cl group of the g-VBC surface was no longer apparent after reaction with DMAMS, further consistent with conversion of surface benzyl chloride groups to the zwitterionic groups.[22–24]
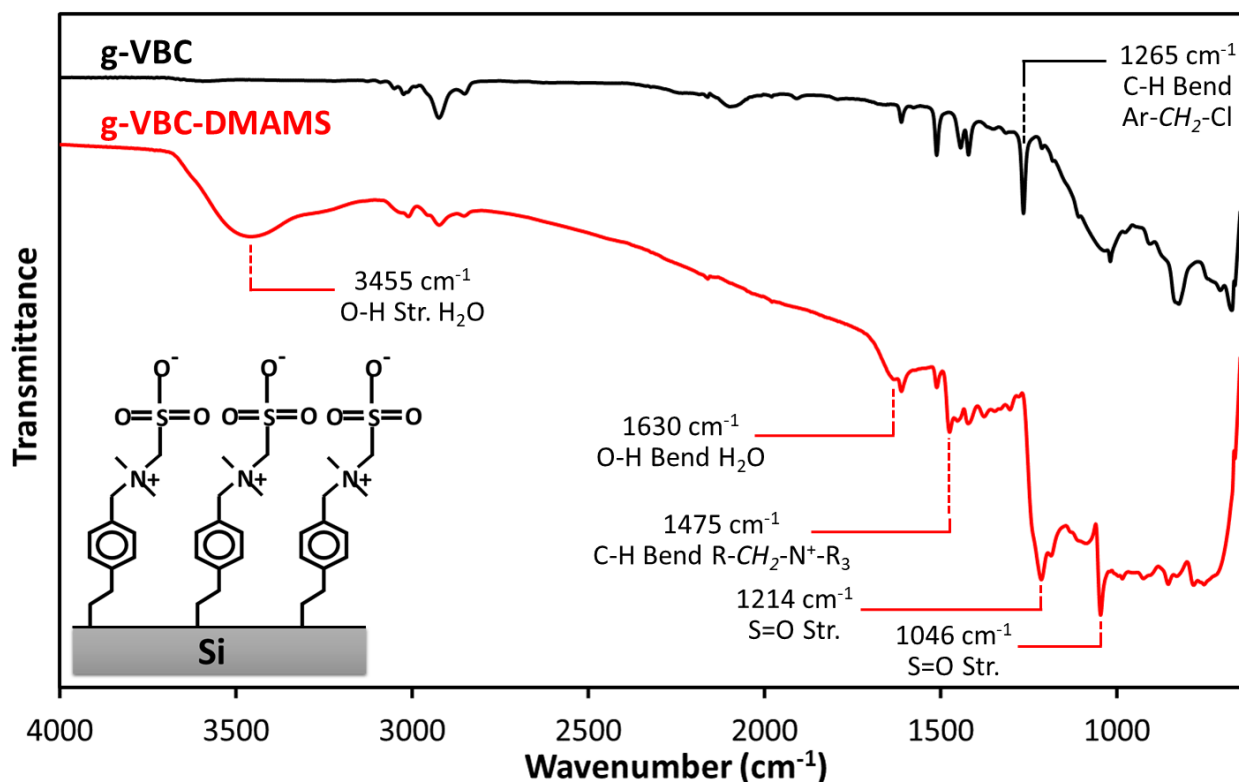
Figure 5.2. Comparison of the FTIR spectra of VBC-modified porous silicon before and after substitution reaction with DMAMS.

DMAMS Substitution Reaction at g-VBC Surface of Flat Silicon

Obtained g-VBC surfaces on flat silicon possessed advancing contact angles of approximately 70° before modification. Figure 5.3 illustrates that upon reaction with DMAMS, the measured advancing contact angle dropped significantly, decreasing to below 20° after 5 days reaction. This increase in

hydrophilicity was consistent with conversion of surface benzyl chloride groups to zwitterionic groups. As a control, g-VBC samples were also exposed to the same conditions except with DMAMS omitted from the solution. As seen in the figure, the control samples did not experience the same increase in hydrophilicity as samples exposed to DMAMS and maintained advancing contact angles over 60° after 4 days.
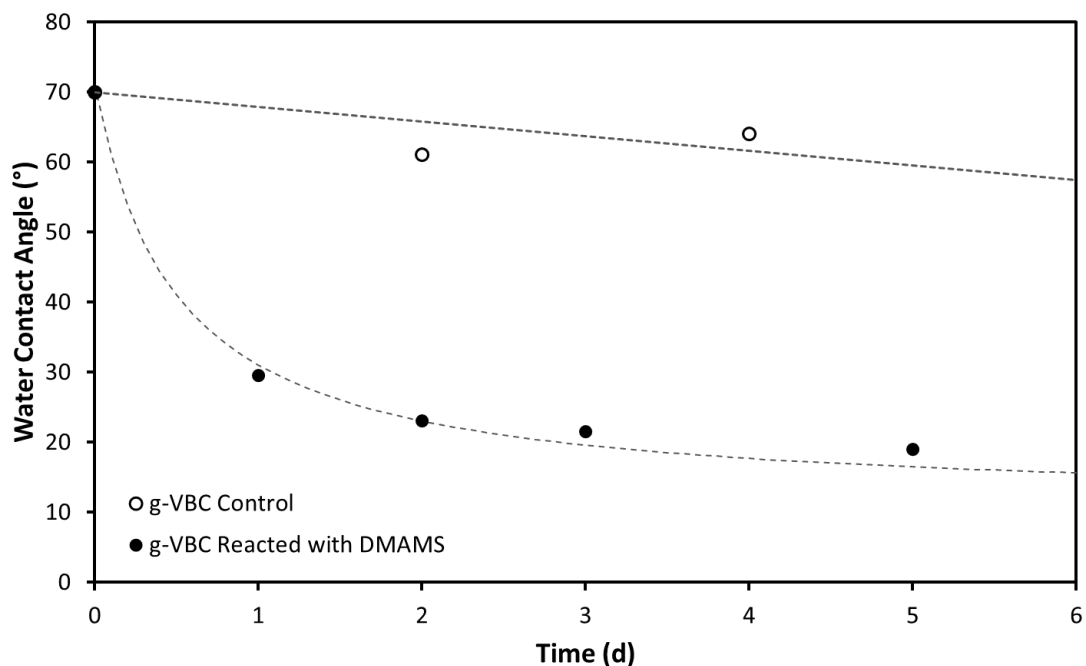
Figure 5.3. Comparison of average advancing water contact angles of g-VBC samples reacted with DMAMS to those exposed only to solvent as a control.

Substitution Reactions with Alkoxides at g-VBC Surface of PSi

First, substitution of the benzyl chloride surfaces with PEG2000 was examined. To perform this modification, NaH was utilized to deprotonate the terminal hydroxyl group of each PEG2000 chain, and the g-VBC samples were subsequently added to the PEG2000 solution at THF reflux. The resulting PEG-alkoxide would then displace the surface-bound benzyl chloride via nucleophilic substitution resulting in

covalently-bound PEG2000 chains. Figure 5.4 provides the FT-IR data obtained for these PEG-modified g-VBC surfaces. Upon reaction of the g-VBC surface in the PEG2000 solution at reflux for 2 h and 24 h, the appearance of the peak at 1113 cm^{-1}, characteristic of C-O stretching of ethers, suggested conversion of the g-VBC substrate to form a PEG-modified surface; the prominence of this peak increased with reaction time. Further, the peak at 2893 cm^{-1} and the shoulder at 2862 cm^{-1}, assigned to the C-H asymmetric and C-H symmetric stretches respectively of the PEG2000's methylene groups, demonstrated conversion of benzyl chloride sites with PEG2000. In addition, the 1265 cm^{-1} peak assigned to the C-H bending vibration of the Ar-CH$_2$Cl group of the g-VBC surface diminished with increasing reaction time, further consistent with conversion of surface benzyl chloride moieties to the desired PEG2000 moieties.[22–24] A comparison of these spectra with that of bulk PEG2000 powder is found in Appendix B (Figure B.3). Further, the presence of the 1344, 1113, and 964 cm^{-1} peaks was consistent with literature reports of PEG existing in a helical conformation; likewise, the lack of peak near 1325 cm^{-1} associated with trans-extended confirmation was further consistent with the bulk of the grafted PEG2000 possibly having assumed a helical conformation.[25]
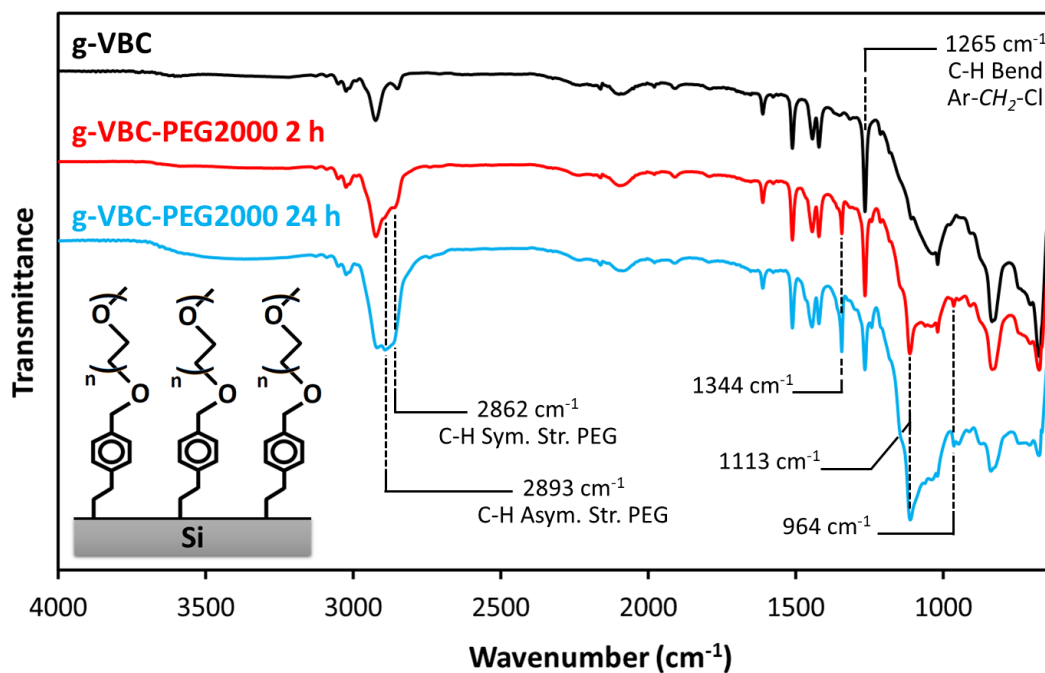
Figure 5.4. Comparison of the FTIR spectra of VBC-modified porous silicon before and after 2 h and 24 h reaction with PEG2000-MME.

Substitution Reactions with Alkoxides at g-VBC Surface of flat Silicon

Modification of g-VBC surfaces with PEG2000 on flat silicon was also examined. Figure 5.5a demonstrates that the ellipsometric thickness of the samples increased rapidly in the first 4 hours before reaching a maximum thickness of 8.1 ± 0.8 nm after 24 h reaction. This reaction was performed at a concentration of 18 mM in the PEG2000 species. At much higher concentrations than used here, incomplete dissolution of the reactive species was noted. Reactions at a lower concentration (6 mM) were also explored, but resulting films were ultimately thinner than desired even after 24 h reaction (see Figure B.4 in Appendix B). Based upon a trans-extended PEG repeat-unit length of 0.358 nm and its average molecular weight of 2000 g/mol, a total PEG2000-length of around 16 nm could easily be calculated which represented the maximum theoretical thickness of a PEG2000-derived monolayer.[26] As PEG has a tendency to exist in an amorphous form or in a helical conformation rather than trans-extended unless very closely packed[25], PEG2000-derived monolayers reported in literature tend to be a fraction of this amount.[27,28] For a helical

129

PEG with a repeat-unit length of 0.278 nm and average molecular weight of 2000 g/mol, a total PEG2000-length of around 12.5 nm could be estimated which represents a maximum theoretical thickness more applicable to the kind of PEG2000-derived molecular film made in this experiment.[27] Based upon the thickness of 8.1 nm, an assumed density of 1 g/cm^3, and a cross-sectional area of 0.213 nm^2 per PEG chain (in the helical conformation[25]), the grafting density could be estimated to be 2.4 molecules/nm^2 or a grafting distance of 0.64 nm/molecule. Again, this assumed that the grafted PEG2000 existed in the helical conformation as suggested by the ATR FT-IR results from the PEG2000-grafted porous silicon samples.
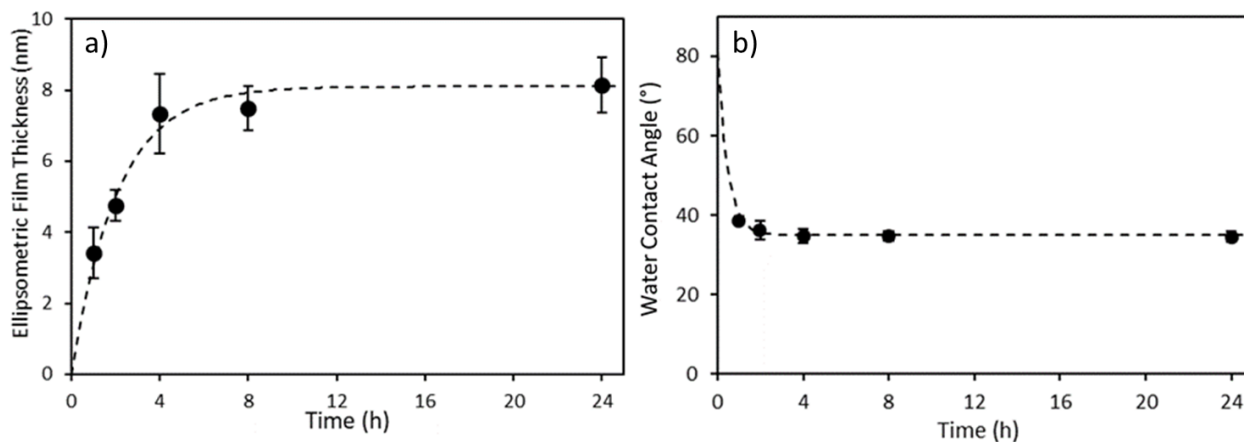
Figure 5.5. Modification of g-VBC surfaces with 18 mM PEG2000. a) The ellipsometric film thickness of the PEG2000 modification with increasing time normalized to initial g-VBC thickness. b) The advancing water contact change with increasing reaction time.

Before modification, these g-VBC surfaces on flat silicon possessed advancing contact angles of approximately 80 ± 4°. As seen in Figure 5.5b, upon reaction with PEG2000, the measured advancing contact angle dropped significantly within the first few hours, with a contact angle of 34.7 ± 1.2° after 24 h exposure to the PEG2000 reaction solution. These contact angles were consistent with the formation of a PEG-modified surface as shown in literature, and further, these contact angles were also consistent with those of PEG-silane monolayers (35.8 ± 0.8°) produced in our lab using commonly reported methods.[29]

Further, these advancing contact angles were consistent with good substrate coverage, which is essential for antifouling applications. As controls, g-VBC samples were also exposed to refluxing THF, omitting the PEG2000 and NaH; after 24 h reaction, resulting contact angles ($77 \pm 2°$) remained similar to that of unmodified g-VBC samples with negligible change in thickness. Further, blank silicon showed no increase in thickness after exposure to the same refluxing PEG2000/NaH/THF reaction mixture, further demonstrating the need for the surface benzyl chloride groups for successful conversion to PEG2000 groups via nucleophilic substitution.

In order to demonstrate that we could also make surfaces more hydrophobic, modification of g-VBC surfaces with n-dodecanol on flat silicon was also examined. This reaction was performed at a concentration of 720 mM of the alcohol species. Before modification, g-VBC surfaces on flat silicon possessed advancing contact angles of approximately 80°. As seen in Figure 5.6, upon reaction with n-dodecanol, the measured advancing water contact angle increased significantly to around 95° after 18 h exposure to the reaction solution. This increase in contact angles was consistent with the addition of a more hydrophobic group, such as the alkyl tail of n-dodecanol, to the g-VBC surface. As controls, g-VBC samples were also exposed to refluxing THF, omitting the alcohol and NaH; after the 24 h reaction, resulting contact angles remained similar to that of unmodified g-VBC samples. In addition, unmodified (i.e. "blank") silicon samples exposed to the n-dodecanol/NaH solution did not exhibit an increase in contact angle, further demonstrating the need for the surface benzyl chloride groups for successful reaction via nucleophilic substitution.
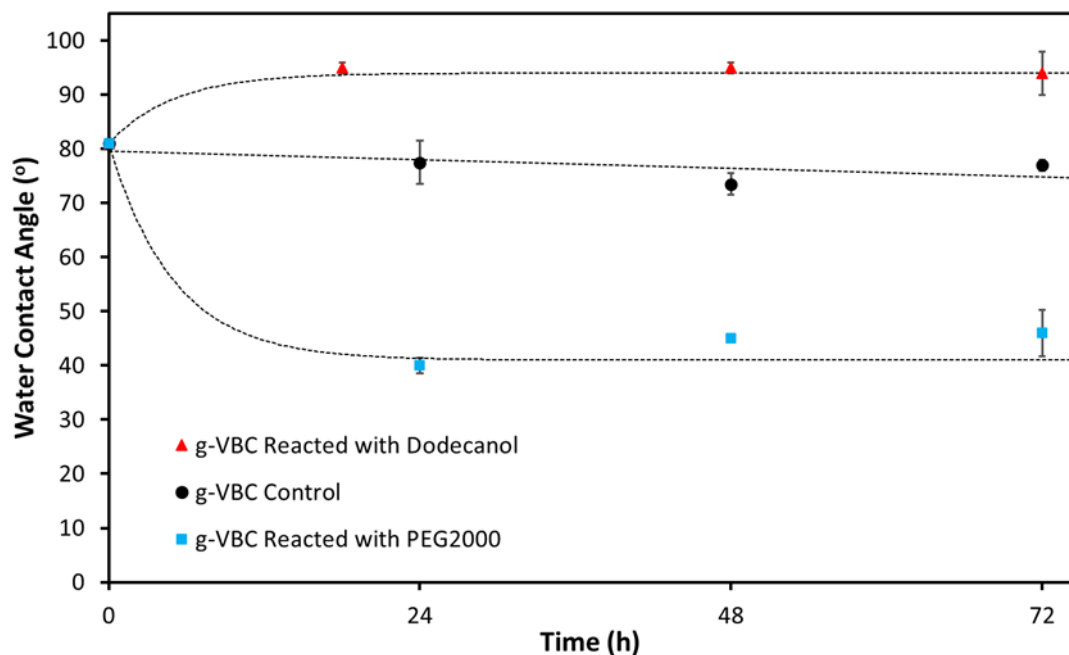
Figure 5.6. The change in water contact angle with increasing reaction time for the modification of g-VBC surfaces with n-dodecanol from a 720 mM solution. For comparison, g-VBC samples exposed to 18 mM PEG2000 and g-VBC exposed only to THF (as a control) are included.

Substitution Reactions with Dimethylamine at g-VBC Surfaces and Subsequent Quaternization

Figure 5.7 provides the FT-IR data obtained for PSi-g-VBC surfaces modified with dimethylamine and then with 1,3-propanesultone. Upon reaction of the g-VBC surface in a 2 M dimethylamine in THF solution at 60 °C for 18 h, appearance of the FT-IR peaks at 2815 cm^{-1} and 2772 cm^{-1} assigned to the C-H stretching of the methyl and methylene groups of newly-formed tertiary amine were observed.[22] In addition, the 1265 cm^{-1} peak assigned to the C-H bending vibration of the Ar-CH$_2$Cl group of the g-VBC surface was greatly diminished after reaction with dimethylamine, further consistent with conversion of surface benzyl chloride moieties to the desired tertiary amine.[22–24] This dimethylbenzylamine-terminated surface was then reacted with 1,3-propanesultone in acetone for 18 h in order to produce a zwitterionic sulfobetaine surface. The resulting surface exhibited new peaks at 1166 cm^{-1} and 1035 cm^{-1} assigned to the S=O stretching of the sulfobetaine group. Further, the 2815 cm^{-1} and 2772 cm^{-1} peaks of the methyl and methylene groups of the

132

tertiary amine mostly diminished as would be consistent with a fairly high conversion to a quaternary amine in the desired zwitterionic sulfobetaine moiety.
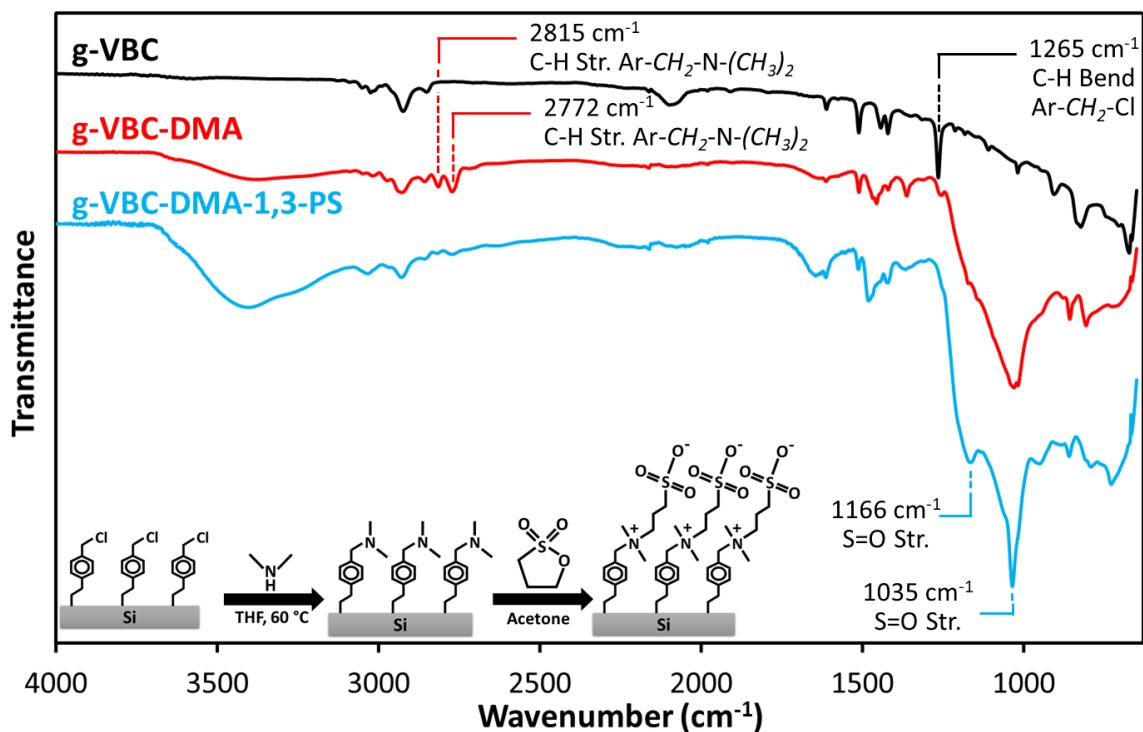
Figure 5.7. Comparison of FTIR spectra of a PSi-g-VBC surface and a PSi-g-VBC surface reacted with dimethylamine. Also shown, the spectra for the resulting dimethylbenzylamine-terminated surface reacted with 1,3-propanesultone to generate a zwitterionic sulfobetaine surface.

NaN$_3$ Substitution Reaction at g-VBC Surface of PSi

Figure 5.8 provides the FT-IR data obtained for PSi-g-VBC surfaces modified with sodium azide to produce an azide-terminated surface. Upon reaction of the g-VBC surface in the NaN$_3$ solution at 70 °C for 18 h, appearance of the sharp peak at 2097 cm^{-1} characteristic of -N$_3$ stretching suggested successful reaction of the g-VBC substrate with NaN$_3$ to form a benzyl azide surface. In addition, the 1265 cm^{-1} peak assigned to the C-H bending vibration of the Ar-CH$_2$Cl group of the g-VBC surface was no longer apparent

after reaction with NaN$_3$, further consistent with conversion of surface benzyl chloride moieties to the desired benzyl azide moieties.[22–24] These azide modified surfaces provide the opportunity to be further utilized for Copper(I)-catalyzed azide alkyne cycloaddition (CuAAC) reactions, the most common variety of "click" reaction; this technique provides an efficient method for the linking of a diverse collection of organic moieties to one another, including at surfaces such as this benzyl azide surface.[30,31]
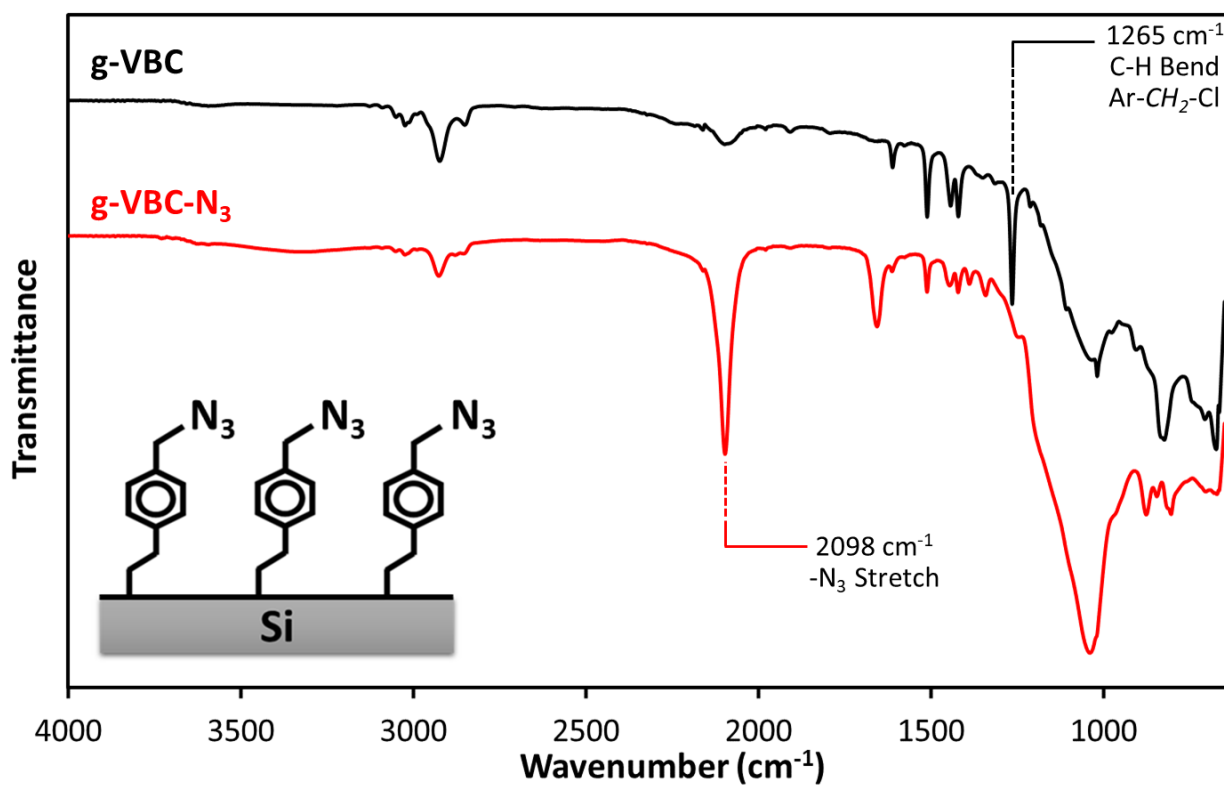
Figure 5.8. Comparison of FTIR spectra of a PSi-g-VBC surface, and a PSi-g-VBC surface reacted with sodium azide.

Conclusions

This work demonstrated both the successful attachment of 4-vinylbenzyl chloride to H-terminated silicon to create g-VBC surfaces by UV-induced hydrosilylation and also the usefulness of this surface for subsequent modification via nucleophilic substitution reactions. Attachment of VBC to flat and porous silicon substates was performed and subsequent substitution reactions were verified via wetting, ellipsomety, and FT-IR analysis. Specifically, substitution with sodium azide, alkoxides (n-dodecanol and PEG2000-MME), and amines (dimethylamine and DMAMS) were shown. In addition, ellipsometric thickness results for the much thicker PEG2000-modified g-VBC surfaces further demonstrated successful attachment/conversion and provided the ability to estimate a grafting density.

References:

(1)   Xu, F. J.; Kang, E. T.; Neoh, K. G. UV-Induced Coupling of 4-Vinylbenzyl Chloride on Hydrogen-Terminated Si(100) Surfaces for the Preparation of Well-Defined Polymer-Si Hybrids via Surface-Initiated ATRP. *Macromolecules* **2005**, *38* (5), 1573–1580. https://doi.org/10.1021/ma049225a.

(2)   Yu, W. H.; Kang, E. T.; Neoh, K. G.; Zhu, S. Controlled Grafting of Well-Defined Polymers on Hydrogen-Terminated Silicon Substrates by Surface-Initiated Atom Transfer Radical Polymerization. *J. Phys. Chem. B* **2003**, *107* (37), 10198–10205. https://doi.org/10.1021/jp034330s.

(3)   Buriak, J. M. Organometallic Chemistry on Silicon and Germanium Surfaces. *Chem. Rev*. **2002**, *102* (5), 1271–1308. https://doi.org/10.1021/cr000064s.

(4)   Stewart, M. P.; Buriak, J. M. Photopatterned Hydrosilylation on Porous Silicon. *Angewandte Chemie - International Edition* **1998**, *37* (23), 3257–3260. https://doi.org/10.1002/(SICI)1521-3773(19981217)37:23<3257::AID-ANIE3257>3.0.CO;2-1.

(5)   Huck, L. A.; Buriak, J. M. UV-Initiated Hydrosilylation on Hydrogen-Terminated Silicon (111): Rate Coefficient Increase of Two Orders of Magnitude in the Presence of Aromatic Electron Acceptors. *Langmuir* **2012** *28* (47), 16285–16293. https://doi.org/10.1021/la3035819.

(6)   Effenberger, F.; Götz, G.; Bidlingmaier, B.; Wezstein, M. Photoactivated Preparation and Patterning of Self-Assembled Monolayers with 1-Alkenes and Aldehydes on Silicon Hydride Surfaces. *Angewandte Chemie - International Edition* **1998**, *37* (18), 2462–2464. https://doi.org/10.1002/(SICI)1521-3773(19981002)37:18<2462::AID-ANIE2462>3.0.CO;2-R.

(7)   Terry, J.; Mo, R.; Wigren, C.; Cao, R.; Mount, G.; Pianetta, P.; Linford, M. R.; Chidsey, C. E. D. Reactivity of the H-Si (111) Surface. *Nuclear Instruments and Methods in Physics Research, Section B: Beam Interactions with Materials and Atoms* **1997**, *133* (1–4), 94–101. https://doi.org/10.1016/S0168-583X(97)00467-9.

(8)   Cicero, R. L.; Linford, M. R.; Chidsey, C. E. D. Photoreactivity of Unsaturated Compounds with Hydrogen-Terminated Silicon(111). *Langmuir* **2000**, *16* (13), 5688–5695. https://doi.org/10.1021/la9911990.

(9)   Nguyen, A. T.; Baggerman, J.; Paulusse, J. M. J.; Zuilhof, H.; van Rijn, C. J. M. Bioconjugation of Protein-Repellent Zwitterionic Polymer Brushes Grafted from Silicon Nitride. *Langmuir* **2012**, *28* (1), 604–610. https://doi.org/10.1021/la2031363.

(10)   Nguyen, A. T.; Baggerman, J.; Paulusse, J. M. J.; van Rijn, C. J. M.; Zuilhof, H. Stable Protein-Repellent Zwitterionic Polymer Brushes Grafted from Silicon Nitride. *Langmuir* **2011**, *27* (6), 2587–2594. https://doi.org/10.1021/la104657c.

(11)   Sano, H.; Maeda, H.; Ichii, T.; Murase, K.; Noda, K.; Matsushige, K.; Sugimura, H. Alkyl and Alkoxyl Monolayers Directly Attached to Silicon: Chemical Durability in Aqueous Solutions. *Langmuir* **2009**, *25* (10), 5516–5525. https://doi.org/10.1021/la804080g.

(12)   Bhairamadgi, N. S.; Pujari, S. P.; Trovela, F. G.; Debrassi, A.; Khamis, A. A.; Alonso, J. M.; al Zahrani, A. A.; Wennekes, T.; Al-Turaif, H. A.; van Rijn, C.; Alhamed, Y. A.; Zuilhof, H. Hydrolytic and Thermal Stability of Organic Monolayers on Various Inorganic Substrates. *Langmuir* **2014**, *30* (20), 5829–5839. https://doi.org/10.1021/la500533f.

(13)   Xu, F. J.; Kang, E. T.; Neoh, K. G. UV-Induced Coupling of 4-Vinylbenzyl Chloride on Hydrogen-Terminated Si(100) Surfaces for the Preparation of Well-Defined Polymer-Si Hybrids via Surface-Initiated ATRP. *Macromolecules* **2005**, *38* (5), 1573–1580. https://doi.org/10.1021/ma049225a.

(14)   Xu, F. J.; Li, Y. L.; Kang, E. T.; Neoh, K. G. Heparin-Coupled Poly(Poly(Ethylene Glycol) Monomethacrylate)-Si(111) Hybrids and Their Blood Compatible Surfaces. *Biomacromolecules* **2005**, *6* (3), 1759–1768. https://doi.org/10.1021/bm050071w.

(15)   King, J. F.; Skonieczny, S. TRIMETHYLAMMONIOMETHANESULFINATE AND TRIMETHYLAMMONIOMETHANESULFONATE, THE SIMPLEST SULFINIC AND SULFONIC ACID BETAINES. REVISION OF THE STRUCTURE OF THE TRIMETHYLAMINE OXIDE–SULFUR DIOXIDE PRODUCT. *Phosphorus and Sulfur and the Related Elements* **1985**, *25* (1), 11–20. https://doi.org/10.1080/03086648508074251.

(16)   Sonnenschein, L.; Seubert, A. Synthesis of a Series of Monomeric Styrene Sulfobetaine Precursors. *Tetrahedron Letters* **2011**, *52* (10), 1101–1104. https://doi.org/10.1016/j.tetlet.2010.12.100.

(17)   Pigorsch, E. Spectroscopic Characterisation of Cationic Quaternary Ammonium Starches. *Starch - Stärke* **2009**, *61* (3–4), 129–138. https://doi.org/10.1002/star.200800090.

(18)   Sánchez, J.; Rivas, B. L. Cationic Hydrophilic Polymers Coupled to Ultrafiltration Membranes to Remove Chromium (VI) from Aqueous Solution. *Desalination* **2011**, *279* (1–3), 338–343. https://doi.org/10.1016/j.desal.2011.06.029.

(19)   Palacio, D. A.; Rivas, B. L.; Urbano, B. F. Ultrafiltration Membranes with Three Water-Soluble Polyelectrolyte Copolymers to Remove Ciprofloxacin from Aqueous Systems. *Chemical Engineering Journal* **2018**, *351*, 85–93. https://doi.org/10.1016/j.cej.2018.06.099.

(20)   Loubaki, E.; Ourevitch, M.; Sicsic, S. Chemical Modification of Chitosan by Glycidyl Trimethylammonium Chloride. Characterization of Modified Chitosan by 13C- and 1H-NMR Spectroscopy. *European Polymer Journal* **1991**, *27* (3), 311–317. https://doi.org/10.1016/0014-3057(91)90111-Z.

(21)   Sajomsang, W.; Gonil, P.; Tantayanon, S. Antibacterial Activity of Quaternary Ammonium Chitosan Containing Mono or Disaccharide Moieties: Preparation and Characterization.

International Journal of Biological Macromolecules **2009**, *44* (5), 419–427. https://doi.org/10.1016/j.ijbiomac.2009.03.003.

(22) Socrates, G. *Infrared and Raman Characteristic Group Frequencies: Tables and Charts*, 3rd ed.; John Wiley & Sons Ltd: Chichester, 2001.

(23) Chen, Q.; Zheng, L.; Chen, B.; He, J.; Huang, H.; Lin, J. Highly Efficient Phase Transfer Catalyst Supported on Janus Composite Particles: Synthesis, Characterization, and Applications. *Journal of Materials Research* **2014**, *29* (11), 1231–1236. https://doi.org/10.1557/jmr.2014.117.

(24) Kim, S. H.; Park, Y. C.; Jung, G. H.; Cho, C. G. Characterization of Poly(Styrene-b-Vinylbenzylphosphonic Acid) Copolymer by Titration and Thermal Analysis. *Macromolecular Research* **2007**, *15* (6), 587–594. https://doi.org/10.1007/BF03218835.

(25) Harder, P.; Grunze, M.; Dahint, R.; Whitesides, G. M.; Laibinis, P. E. Molecular Conformation in Oligo(Ethylene Glycol)-Terminated Self-Assembled Monolayers on Gold and Silver Surfaces Determines Their Ability To Resist Protein Adsorption. *J. Phys. Chem. B* **1998**, *102* (2), 426–436. https://doi.org/10.1021/jp972635z

(26) Oesterhelt, F.; Rief, M.; Gaub, H. E. Single Molecule Force Spectroscopy by AFM Indicates Helical Structure of Poly(Ethylene-Glycol) in Water. *New Journal of Physics* **1999**, *1* (1), 6. https://doi.org/10.1088/1367-2630/1/1/006.

(27) Tokumitsu, S.; Liebich, A.; Herrwerth, S.; Eck, W.; Himmelhaus, M.; Grunze, M. Grafting of Alkanethiol-Terminated Poly(Ethylene Glycol) on Gold. *Langmuir* **2002**, *18* (23), 8862–8870. https://doi.org/10.1021/la0258953.

(28) Zhu, X. Y.; Jun, Y.; Staarup, D. R.; Major, R. C.; Danielson, S.; Boiadjiev, V.; Gladfelter, W. L.; Bunker, B. C.; Guo, A. Grafting of High-Density Poly(Ethylene Glycol) Monolayers on Si(111). *Langmuir* **2001**, *17* (25), 7798–7803. https://doi.org/10.1021/la010672i.

(29)   Papra, A.; Gadegaard, N.; Larsen, N. B. Characterization of Ultrathin Poly(Ethylene Glycol) Monolayers on Silicon Substrates. *Langmuir* **2001**, *17* (5), 1457–1460. https://doi.org/10.1021/la000609d.

(30)   Liang, L.; Astruc, D. The Copper(I)-Catalyzed Alkyne-Azide Cycloaddition (CuAAC) "Click" Reaction and Its Applications. An Overview. *Coordination Chemistry Reviews*. December **2011**, pp 2933–2945. https://doi.org/10.1016/j.ccr.2011.06.028.

(31)   Castro, V.; Rodríguez, H.; Albericio, F. CuAAC: An Efficient Click Chemistry Reaction on Solid Phase. *ACS Comb. Sci.* **2016**, *18* (1), 1–14. https://doi.org/10.1021/acscombsci.5b00087.

Chapter VI

ONE-STEP ATTACHMENT OF 4-VINYLBENZYL AZIDE TO H-TERMINATED SILICON SURFACES FOR CLICK CHEMISTRY APPLICATIONS

Introduction

Copper(I)-catalyzed azide-alkyne cycloaddition (CuAAC) represents the most commonly used variety of "click" reaction and provides an efficient method for the linking of a diverse collection of organic moieties to one another, including at surfaces.[1–3] CuAAC has found wide use in many areas of research including solid-phase peptide synthesis,[2,4] cross-linking of polymers,[5] introducing/tailoring polymer architecture,[3–6] and surface modification.[1,6,7] For use in surface modification, once either an alkyne or azide group has been attached to a desired substrate (nanoparticles, flat surfaces, porous surfaces, CNT's, fibers, etc.), CuAAC can be an efficient strategy for introducing other functionalities, molecular species, biomolecules, and polymers with the corresponding azide or alkyne group to these solid supports/surfaces.[1,2,8,9] In this paper, we present a straightforward method to attach an organic azide to H-terminated silicon surfaces by a one-step hydrosilylation approach using 4-vinylbenzyl azide (VBA) for use in CuAAC click chemistry. In addition to traditional CuAAC click chemistry, this grafted VBA (g-VBA) surface also allows utilization of copper-free click chemistry, a technique that leverages ring-strained alkynes to alleviate the need to include catalysts such as copper, for surface attachment.[10] To demonstrate the presence of the attached azide and its usefulness for both of these variations of click chemistry, we investigated the reactions between a collection of alkynes with g-VBA surfaces and analyzed their products by FT-IR, water contact angles, and ellipsometry.

Typically, azide-terminated monolayers are attached to silicon surfaces via silane chemistry[8,11,12] or via a multi-step modification of an existing hydrosilylation-derived monolayer.[13] For example, Zheng et

al., Heise et al., and Balachander et al. all demonstrated the modification Si/SiO$_2$ substrates with various bromide-terminated alkyltrichlorosilane compounds and subsequent conversion to azide-terminated monolayers via substitution with sodium azide.[8,14,15] Meanwhile Paoprasert et al. and Vos et al. formed azide-terminated monolayers directly onto Si/SiO$_2$ substrates using azide-terminated trimethoxysilane molecules that were deposited through a vapor or solution-phase process, respectively.[11,12] In contrast, others have investigated approaches that employ more hydrolytically stable Si-C linkages to form monolayers and to provide sites for further modification via CuAAC and also copper-free click reactions. The method of grafting vinyl compounds from silicon utilizing a UV-induced silicon-carbon linkage has been demonstrated by the Buriak and Chidsey groups, among others.[16–23] As compared to Si-O-Si linkages, Si-C linkages are more stable and less susceptible to failure in aqueous environments as they avoid the hydrolytic instability associated with Si-O-Si linkages.[24–27] Gouget-Laemmel et al. demonstrated formation of azide-terminated films from silicon by first attaching undecylenic acid by hydrosilylation and then converting this acid-terminated monolayer to an NHS ester using EDC coupling before finally obtaining the desired azide functionality by reaction with an azido-PEG8-amine compound.[13] While the method presented by Gouget-Laemmel et al. was successful, their multi-step approach is more complicated than the more "straight-forward" approach to obtain azide-modified silicon via hydrosilylation that we demonstrate here.

Figure 6.1 illustrates the general scheme for the route presented in this paper for covalently attaching an organic azide to a H-terminated silicon substrate via a one-step, UV-induced hydrosilylation reaction. In addition to flat silicon substrates, we attached VBA to porous silicon (PSi) substrates where the inherent high surface area of PSi provided higher signal for FT-IR analysis. Porous silicon (PSi) also provides a useful platform for sensing applications. Porous silicon has been demonstrated to be a highly effective platform for sensing applications as the presence of captured target molecules can be quantified via analysis of changes in position of interference fringes obtained through reflectance experiments.[28] The biotin-streptavidin interaction system represents one of the most common coupling strategies for binding

bioreceptor systems to surfaces for capturing analytes in biosensing applications. [28–33] To illustrate the potential utility of our azide-modified porous silicon samples for biosensing applications, we demonstrated biotinylation of the substrates using a copper-free click reaction between an alkyne-containing biotin compound and the g-VBA surface.
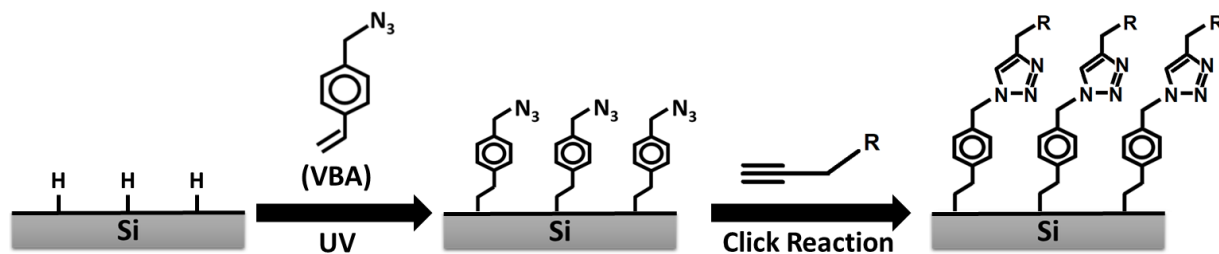
Figure 6.1. Strategy for introducing surface-bound azide groups to a H-terminated silicon surface. VBA was irradiated with UV to induce attachment to a freshly HF-etched silicon substrate. In a second step, a click reaction between the surface-bound azide and an alkyne was performed.

Experimental Methods

Chemicals and Materials: 4-Vinylbenzyl chloride, propargyl bromide (80% soln. in toluene), sodium hydride (60% dispersion in mineral oil), dibenzocyclooctyne-PEG4-biotin conjugate (DBCO-PEG4-biotin), N,N,N′,N″,N″-pentamethyldiethylenetriamine (PMDETA), potassium carbonate, 4-hydroxybenzaldehyde, and copper(II) sulfate pentahydrate were purchased from Sigma-Aldrich and used as received. Sodium azide, N,N-dimethylpropargylamine, 1,3-propanesultone, sodium ascorbate (NaAsc), and polyethylene glycol monomethyl ether 2000 (PEG2000) were purchased from TCI and used as received. 5-Hexynoic acid was purchased from Acros Organics and used as received. Single-sided polished, boron-doped, p-type silicon wafers (⟨100⟩, 0.01–0.02 Ω cm, 500–550 μm) were purchased from Pure Wafer Inc.

4-Vinylbenzyl Azide (VBA): This synthesis was conducted in a manner similar to that described previously.[34] 4-Vinylbenzyl chloride (0.84 mL, 6 mmol) was added dropwise with stirring to a solution containing 1.95 g (30 mmol) of sodium azide in 7.5 mL of anhydrous DMF. After stirring for 2 days, the solution was combined with 30 mL of DI water and then extracted with diethyl ether (3 x 30 mL). The ether phases were combined, washed with DI water (3 x 100 mL), and were dried over sodium sulfate. Concentration by rotary evaporation provided the title compound as a light-yellow oil in 80% yield. NMR and FT-IR spectra are provided as Figures C.1 and C.2 in Appendix C. ^{1}H-NMR (400 MHz, DMSO-d_6) δ/ppm = 7.52–7.50 (m, 2 H, Ar*H*), 7.36–7.34 (m, 2 H, Ar*H*), 6.75 (dd, 1 H, J = 17.7 Hz, J = 10.9 Hz, Ar–C*H*=CH$_2$), 5.86 (dd, 1 H, J = 17.7 Hz, J = 0.9 Hz, Ar–CH=C*H*$_2$), 5.28 (dd, 1 H, J = 10.9 Hz, J = 0.8 Hz, Ar–CH=C*H*$_2$), 4.44 (s, 2H, Ar–C*H*$_2$-N$_3$). *CAUTION: Sodium azide (NaN$_3$) is known to present an explosion hazard. Exposure to halogenated solvents or some organohalides can lead to the formation of explosive organic azides. Sodium azide can also react with water to form hydrazoic acid, a toxic and explosive gas. Sodium azide should be handled with non-metal utensils to prevent formation of unintended shock-sensitive products. To further minimize potential risks, it is recommended that synthesis of organic azides are conducted in small batch sizes as the organic azides can also be explosion hazards. Appropriate safety protocols should be established before attempting any synthesis involving sodium azide or its derivatives.*

Porous Silicon: Si wafers were sequentially washed with acetone, isopropanol, and ethanol, and then dried with nitrogen before use. A layer of PSi was formed by electrochemical etching Si in a 15% HF solution in ethanol at a current density of 70 mA/cm^2 for 100 s. The substrates were then thoroughly washed with ethanol and dried with nitrogen. The PSi layer was 3.65 µm thick and had a porosity of 80%.

Methoxy-PEG2000-propyne. This synthesis was conducted based on that described by Zill et al.[35] In a round-bottom flask, 5.0 g (2.5 mmol) of polyethylene glycol monomethyl ether (average M.W. ~2000) was added, sealed via septum, and sparged with N_2 for approximately 30 min before adding 100 mL of anhydrous THF. In a separate flask, 0.1 g of NaH (2.5 mmol, 60% dispersion in mineral oil) was added along with a stir bar, and sparged with N_2 for approximately 30 min before adding 35 mL of anhydrous THF. The NaH/THF solution was chilled over ice bath before adding the PEG2000/THF solution via cannula transfer dropwise and with stirring. After 30 min, 0.334 mL of propargyl bromide (3.0 mmol, 80% solution in toluene) was added dropwise to the solution with stirring over an ice bath. The reaction solution was then allowed to warm to room temperature and react overnight. The solution was then gravity filtered, rinsing the filter paper with DCM. The filtrate was diluted with 75 mL of DI water and the solution was extracted 3x with 75 mL of DCM. The organic layers were combined and then concentrated to approximately 25 mL via rotary evaporation before precipitating into 250 mL of cold ether overnight in a freezer. The white powder product was collected via filtration with a 74.9% yield.

3-[Dimethyl(2-propyn-1-yl)ammonio]-1-propanesulfonate (SB-Alkyne): In a round-bottom flask, 0.5 mL (4.6 mmol) of n,n-dimethylpropargylamine was dissolved in 5 mL of dry acetone. In a separate round-bottom flask 0.44 mL (5.0 mmol) of 1,3-propanesultone was dissolved 5 mL of dry acetone. Both solutions were sparged with nitrogen before transferring the 1,3-propanesultone solution to the N,N-dimethylpropargylamine solution dropwise over 30 min with stirring. The reaction was allowed to proceed for 18 h and the solid product was collected via filtration, washing with acetone to obtain a 68.4% yield.

4-(Prop-2-ynyloxy)benzaldehyde. This synthesis was conducted based on that described by Darroudi et al.[36] In a round-bottom flask, 0.611 g (5 mmol) of 4-hydroxybenzaldehyde and 0.691 g (5 mmol) of potassium carbonate were dissolved in 15 mL of anhydrous DMF. With stirring, 0.668 mL (6 mmol) of

propargyl bromide solution (80% wt. in toluene) was added dropwise. The reaction was allowed to proceed for 24 hours before precipitating the product into 40 mL of deionized H_2O. The product was collected via filtration, washed very thoroughly with water, and dried via vacuum. The product was an off-white powder with a yield of 66.2%. FT-IR spectra of the product is available in Appendix C (Figure C.3).

Attachment of VBA via Hydrosilylation: For modification of flat silicon, 1 x 1 cm^2 samples were placed in an 800 °C oven for 4 h. After cooling, the samples were soaked in a 2.5% solution of HF in a 7:3 ethanol-water mixture to remove the oxide, rinsed with DI water, and dried. For irradiation, samples consisted of 15 µL of VBA sandwiched between the silicon surface and a No. 1 thickness coverslide. Samples were irradiated with UV light in a DYMAX 5000-EC UV curing lamp system. Total exposure times were typically 200 s. After removal of the coverslides, the samples were immersed in acetone for 1 h and then dried before use.

For modification of porous silicon: Porous silicon samples were similarly soaked in the HF solution as for flat silicon, but rinsed with water and then ethanol before drying. They were similarly contacted with VBA and irradiated with UV, except that a total exposure time of 400 s was used.

For all samples, exposure times over 100 s consisted of sequential 100-s irradiations with intermediate pauses to avoid excessive heating.

CuAAC Reactions with VBA: For VBA-modified porous and flat silicon samples reacted with SB-alkyne: A VBA-modified sample and 10 mg of SB-alkyne were placed in a vial, sealed via septum, and sparged with nitrogen. A solution containing 8 mg of CuSO$_4$·5H$_2$O and 6.3 µL of PMDETA in 5 mL of deionized H_2O was produced and sparged with nitrogen. A second solution containing 12 mg of sodium ascorbate in 5 mL of deionized H_2O was produced and sparged with nitrogen. Both solutions (1 mL each) were then injected into the slide-containing vial to start the click reaction. Concentrations in the final reaction solution

were as follows: SB-alkyne (25 mM), $CuSO_4 \cdot 5H_2O$ (3 mM), PMDETA (3 mM), NaAsc (6 mM). After 18 h reaction completion, samples were soaked in water for 24 hours to remove unbound material, rinsed with EtOH, and dried with nitrogen.

For VBA-modified samples reacted with 4-(prop-2-ynyloxy)benzaldehyde: This process was the same as for SB-alkyne, except 8 mg (25 mM in final solution) of 4-(prop-2-ynyloxy)benzaldehyde was placed in each vial. Additionally, the reaction solvent was a 50/50 mix of ethanol and water, rather than just water as with SB-alkyne experiments.

For VBA-modified samples reacted with PEG2000-alkyne: This process was the same as for SB-alkyne, except 50 mg of PEG2000-alkyne was placed in each vial resulting in a final concentration of 12.5 mM of the alkyne. Additionally, the reaction solvent was a 50/50 mix of ethanol and water, rather than just water as with SB-alkyne experiments.

For VBA-modified porous silicon samples reacted with 5-hexynoic acid: A 100 µL solution containing 5-hexynoic acid (85 mM), $CuSO_4 \cdot 5H_2O$ (3 mM), PMDETA (3 mM), and sodium ascorbate (6 mM) in a 1:1 $EtOH:H_2O$ mixture was dispensed onto the surface of a VBA-modified porous silicon slide and covered to prevent evaporation of solvent. After 18 h reaction, the samples were removed from reaction mixture then soaked for 24 h in a 50/50 mix of ethanol and water to remove unbound material, rinsed with EtOH, and then dried with nitrogen

Biotinylation of g-VBA Surfaces via Copper-Free Click Chemistry: To modify g-VBA surfaces with biotin via copper-free click chemistry, a 20 mM solution of DBCO-PEG4-biotin in DMSO was dispensed onto the g-VBA surface, covering the sample. The samples were then allowed to react with the DBCO-PEG4-biotin solution at room temperature for 24 h. The samples were then rinsed with DMSO, ethanol, water, and again with ethanol before drying with a stream of nitrogen.

Analytical Techniques: Infrared data were obtained using a Thermo Nicolet 6700 FT-IR Spectrometer with Smart iTR™ Attenuated Total Reflectance (ATR) attachment with diamond crystal plate. Due to the need to clamp samples to the diamond crystal for analysis, this method is destructive to PSi surface; thus measurements taken after each reaction step were taken at different locations, albeit on the same sample.

Film thicknesses were measured using an M-2000VI spectroscopic ellipsometer (J.A. Woollam Co.). Each sample was measured at angles of incidence of 60° and 70°. CompleteEASE software was used to analyze the measurements using the built-in transparent Cauchy film on silicon substrate model. A refractive index of 1.45 was assumed.

Advancing and receding water contact angles were measured on static drops with the dispensing needle remaining in the drop using a Rame Hart goniometer.

Results and Discussion

Synthesis of VBA and Optimizing Attachment to Flat Silicon

Although the synthesis of 4-vinylbenzyl azide and its attachment to H-terminated silicon as described here were quite simple and straightforward, one must still be aware of the hazards of working with sodium azide and organic azides in general as described in the Experimental Methods section. The synthesis of VBA has been described previously for its use as a monomer to introduce azide groups in styrene-based copolymers[34,37,38]; however, it has not been used to create molecular films such as those described here. Once the liquid VBA compound had been synthesized, an azide-modified silicon substrate could be made in a single reaction step in just a matter of minutes. To do so, the liquid was simply deposited onto H-terminated silicon wafers, covered with a coverslip, and then exposed to a UV source. As each UV-source's power and emission spectrum along with the coverglass's thickness and material (i.e. glass vs quartz) will all likely impact the hydrosilylation reaction progress differently, it is likely necessary to

determine an ideal UV-exposure time for one's individual setup. To determine these ideal conditions, water

contact angles on the g-VBA samples and subsequent thickness after click reaction were examined.

Figure 6.2. a) Average advancing contact angles of water on g-VBA surfaces with varying UV exposure time. b) Ellipsometric thickness change of the g-VBA samples in "a)" after click reaction with a PEG2000-alkyne.

With our DYMAX 5000-EC UV curing lamp system and No. 1 thickness glass coverslides, we

determined 200 s exposure to be appropriate for flat silicon samples. The resulting samples modified with

VBA produced via this UV hydrosilylation technique resulted in films with water contact angles of

approximately 75°, consistent with literature reports for azide-terminated monolayers.[11,39] As evident in Figure 6.2a, shorter exposure times (50 s and 100 s) were also examined, but these conditions resulted in water contact angles less than that expected of an azide coating, suggesting incomplete substrate coverage. Longer times yielded minimal change in water contact angle or thickening/hardening of the VBA liquid (likely a polymerization process) that would result in the coverglass becoming stuck to the sample surface, and thus were avoided.

Subsequently, modification of g-VBA surfaces with PEG2000-alkyne via click reaction on flat silicon was examined to further assess the effect of UV exposure time on the g-VBA surfaces. PEG2000-alkyne was chosen as this linear polyether's much larger molecular weight and resulting length, as compared to the other alkynes discussed later, produced coatings of ample thickness as to more easily be evaluated via ellipsometry. As shown in Figure 6.2b, the ellipsometric thickness of the added PEG was 4.2 $\pm$ 0.3 nm after 18 h reaction for g-VBA slides produced with 200 s exposure. Shorter exposure times resulted in the grafted PEG thickness being lower, further consistent with a lesser availability of surface azide sites due to lesser or incomplete substrate coverage. Based upon a trans-extended PEG repeat-unit length of 0.358 nm and its average molecular weight of 2000 g/mol, a total PEG-length of around 16 nm can easily be estimated which represents the maximum theoretical thickness of a PEG2000-derived monolayer.[40] As PEG has a tendency to exist in an amorphous form or in a helical conformation rather than trans-extended unless very closely packed[41], PEG2000-derived monolayers reported in literature tend to be a fraction of this amount.[42,43] For a helical PEG with a repeat-unit length of 0.278 nm and average molecular weight of 2000 g/mol, a total PEG-length of around 12.5 nm can be estimated which represents a maximum theoretical monolayer thickness more applicable to the kind of PEG2000-derived molecular coating made in this experiment.[42] Based upon the obtained thickness of 4.2 nm and an assumed density of 1 g/cm^3, the grafting density could be estimated to be approximately 1.3 molecules/nm^2. Based upon the assumption that each individual PEG2000-alkyne molecule attached to the surface during the click reaction corresponded to an available surface azide site, this suggested that azide coverage must have been at least 1.3 molecules/nm^2

also. As PEG2000-alkyne represents a fairly large molecule, the inability to reach the theoretical thickness may have resulted from steric limitations. Also of note, little difference in water contact angles between the various PEG-grafted samples was observed after the modification of the g-VBA samples prepared with different exposure times, with all water contact angles being in the 30° - 40° range after click reaction with the PEG. This decrease in water contact angle from the ~75° of a g-VBA surface before click reaction was consistent with successful conversion of an azide-modified silicon surface to a PEG-modified surface. Further, these water contact angles were consistent with PEG modified surfaces shown in literature.[44]
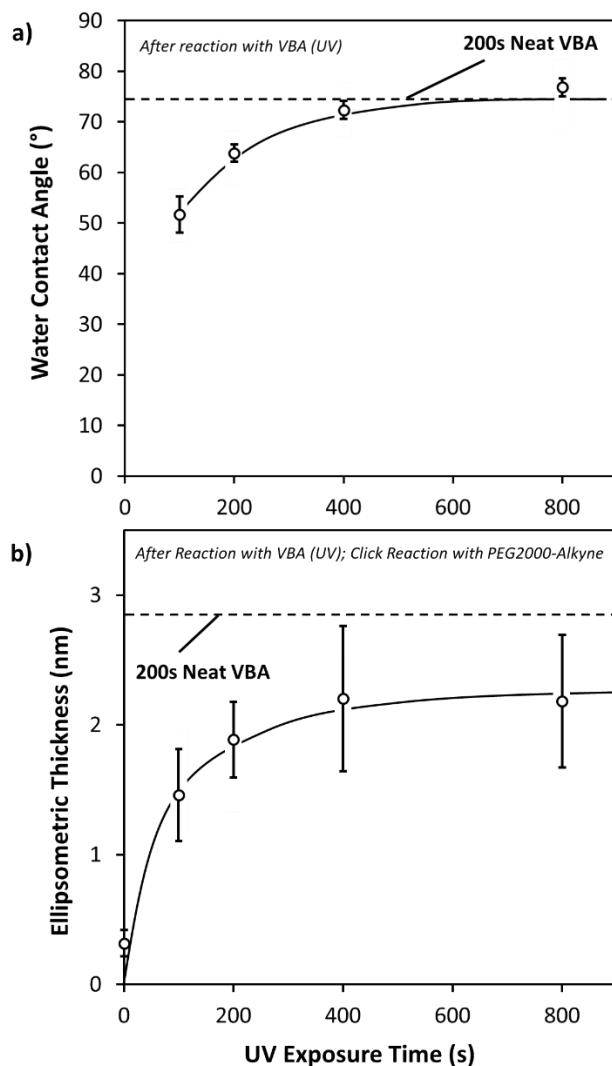
Figure 6.3. Comparison of g-VBA samples prepared via "dilute" preparation method (i.e. 10% v/v VBA in o-Xylene) to those prepared from "neat" VBA (average values for "neat" samples denoted by dotted l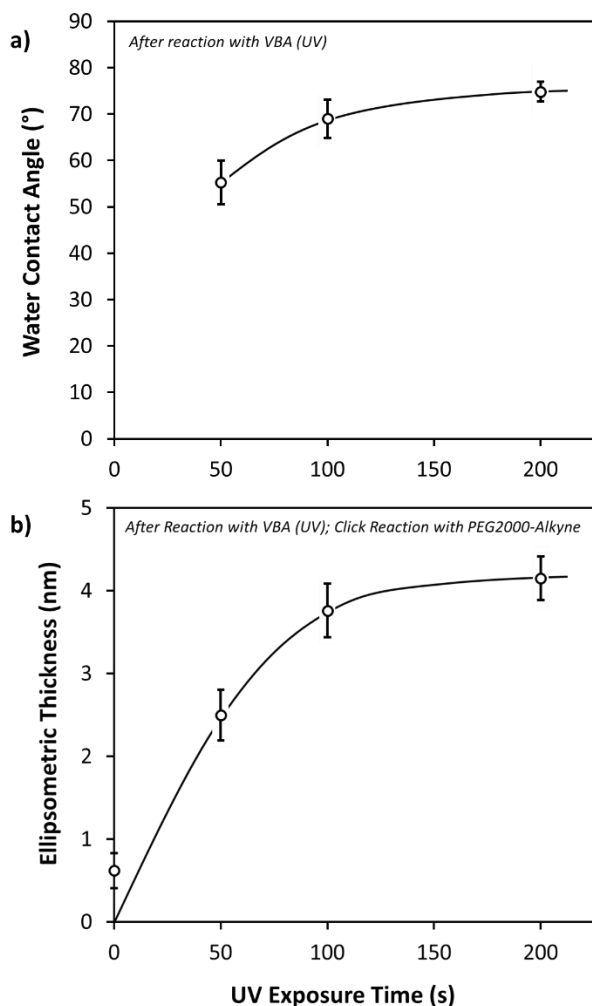ine). a) Average advancing contact angles of water on g-VBA surfaces with varying UV exposure time. b) Ellipsometric thickness change to the g-VBA samples in "a)" after click reaction with a PEG2000-alkyne.

To evaluate whether g-VBA modified silicon surfaces could be obtained using dilute VBA solutions, as opposed to the "neat" VBA discussed above, we repeated the same experiments except with the VBA diluted in a solvent during the UV-exposure step. Being able to obtain g-VBA surfaces from dilute VBA solutions would reduce VBA consumption during the preparation of the samples. Solvent choice was

important here as the desired solvent needed to possess the following properties: being able dissolve the VBA effectively, exhibiting no reactivity with the H-terminated silicon surface during the UV exposure, and also being relatively low in volatility to avoid evaporation. Xylene was found to fit these needs, and 10% (v/v) solutions of VBA in o-xylene were utilized for the UV-hydrosilylation step. Figure 6.3 shows the water contact angles of g-VBA surfaces prepared with different exposure times and also the thickness of PEG2000-alkyne "clicked" to each of the different surfaces. Also included were controls where o-xylene was introduced to the H-terminated silicon surface with VBA omitted during the UV exposure step. Further included for reference were g-VBA surfaces prepared from "neat" VBA. As seen in the figure, increasing the exposure time resulted in higher water contact angles for the g-VBA modified surface by this dilute method, with exposure times of 400 s and longer comparable to that of the "neat" g-VBA samples. The shortest exposure (100 s) exhibited the lowest water contact angle as seen in Figure 6.3, being similar to that of the VBA-omitted controls (50.1 ± 2.6° for 200 s; 45.0 ± 2.7° for 800 s). After click reaction with PEG2000-alkyne, all of the g-VBA samples prepared from dilute VBA solutions possessed PEG coating thicknesses much greater than that measured for the controls (0.4 ± 0.3 nm for 200 s; 0.2 ± 0.1 nm for 800 s), which had no reactive azide sites available for attachment via click chemistry. What little increase in thickness that was observed for the controls after exposure to the click solution was likely due to oxidation of the Si surface to a thin layer of SiO_2. Even after 800 s of UV exposure, the g-VBA samples produced by this dilute method were unable to produce PEG coating thicknesses matching that of those prepared via the "neat" VBA method. Like the PEG2000 coatings produced from "neat" g-VBA samples, little difference was observed in the water contact angles of the PEG-grafted "dilute" g-VBA substrates with different exposure times, with all water contact angles being in the 30-40° range. Based upon these results, using "neat" VBA solutions and 200 s of UV exposure to produce the g-VBA silicon substrates was determined to be the most ideal preparation conditions.

Attachment of VBA to Porous Silicon for FT-IR Analysis

Another strategy utilized to verify the presence of the surface-bound azide moeities on silicon samples by this hydrosilylation process was infrared analysis. Coatings on flat silicon were much too thin to be analyzed via ATR FT-IR. To increase the measurable IR signal of these surface modifications, the same VBA coating strategy was also applied to H-terminated porous silicon (PSi) to take advantage of the much higher surface area available for modification. As shown in Figure 6.4, the appearance of the sharp peak at 2098 cm^{-1} characteristic of -N_3 stretching suggested successful attachment of VBA to the PSi substrate. Figure 6.5 shows a comparison of the FT-IR spectra of g-VBA samples to that of liquid VBA. The loss in intensity of the 3087 cm^{-1} peak attributed to C-H asymmetric stretching of the vinyl group after UV surface treatment as compared to the pure VBA liquid, was consistent with successful attachment of VBA via hydrosilylation. Further, the relative increase in intensity of the peak at 2926 cm^{-1} associated with antisymmetric C-H stretching due to the vinyl group converting to methylene groups upon hydrosilylation further supported successful attachment of VBA. The loss of the 1629 cm^{-1} and 1406 cm^{-1} peaks attributed to C=C stretching and C-H bending, respectively, of the vinyl group after UV surface treatment as compared to the pure VBA liquid, was once again consistent with successful attachment of VBA via hydrosilylation. To ensure the loss of the peaks assigned to the vinyl group did simply not occur as a result of a UV-induced polymerization/oligimerization of the liquid VBA, a sample of the liquid was exposed to the same UV source for 400 s and then analyzed via FT-IR (see Figure C.4 in Appendix C). Spectra for the UV-irradiated VBA displayed no changes, particularly those that would be associated with loss of a vinyl group due to polymerization, further supporting that the spectral changes observed at the VBA-grafted surface were due to successful attachment of VBA via hydrosilylation. Further, NMR spectra collected for VBA before and after 400s of UV-irradiation also showed no change (see Figure C.5 in Appendix C). The stability of these g-VBA films on PSi was also assessed by exposure to a 2.5% solution of HF in a 7:3 ethanol-water mixture. In the FT-IR spectra of the resulting HF-exposed sample (Figure C.6 in Appendix C) only signal associated with SiO_2 was diminished, with the grafted VBA clearly remaining present on the substrate.
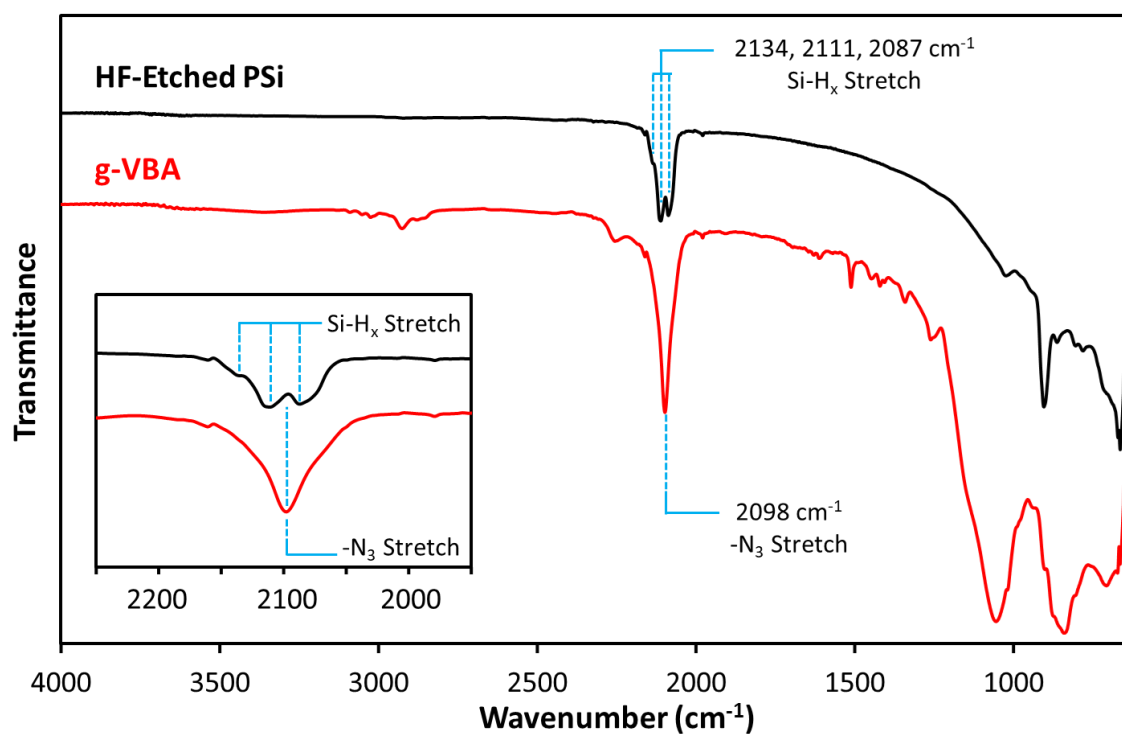
Figure 6.4. Comparison of the FT-IR spectra of HF-etched porous silicon to VBA-modified porous silicon produced by 200s exposure to UV with VBA.
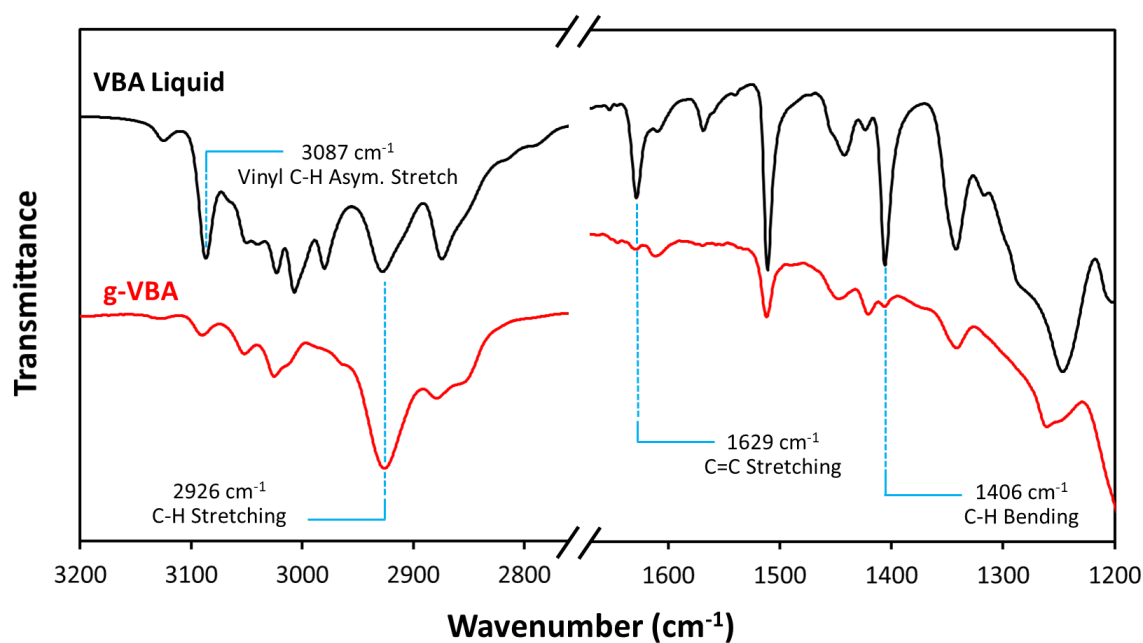
Figure 6.5. Comparison of the FT-IR spectra of liquid VBA to VBA-modified porous silicon.

Looking at the same reaction we previously examined on flat silicon surfaces, g-PSi-VBA surfaces were allowed to react in the PEG2000-akyne click solutions for 18 h. Figure 6.6 shows the FT-IR spectra before and after click reaction with PEG2000-alkyne. Appearance of the peak at 1062 cm^{-1} characteristic of C-O stretching of ethers suggested some conversion of the g-VBA substrate to form a PEG2000-modified surface. It is worth noting that Si-O stretching appears in the same region of FT-IR spectra as the C-O stretching of PEG, and thus was difficult to differentiate here. For further evidence of added PEG moieties, the shoulder at approximately 2900 cm^{-1} and the peak at 2872 cm^{-1}, assigned to the C-H asymmetric and C-H symmetric stretches respectively of the PEG2000's methylene groups, demonstrated conversion of azide sites with PEG2000-alkyne. Further, the appearance of the 1348 and 946 cm^{-1} peaks characteristic of PEG moieties suggested successful incorporation of the PEG2000-alkyne.[41] In addition, the 2098 cm^{-1} peak assigned to -N$_3$ stretching of the azide groups of the g-PSi-VBA surface diminished, further consistent with conversion of some of the surface azide moieties to the desired PEG2000 moieties. As with the click reactions performed on flat substrates, the FT-IR spectra suggested that complete conversion was, once again, not achieved as evidenced by the azide peak not being fully diminished after the reaction. Due to the large size of the approximately 2000 molecular weight PEG compound, steric limitations may have played a role in the lack of full conversion. Samples were also allowed to react for 48 h, but these did not show evidence of further reaction as compared to 18 h samples. A comparison of these spectra with that of bulk PEG2000-alkyne powder is found in Appendix C (Figure C.7).

Figure 6.6. Comparison of the FT-IR spectra of VBA-modified porous silicon before and after click reaction with PEG2000-alkyne.

Other CuAAC Click Reactions on Azide-Grafted Porous Silicon

Upon 18 h click reaction of the zwitterionic SB-alkyne with the PSi-g-VBA surface, appearance of the peak at 1479 cm^{-1} commonly associated with C-H bending of methyl groups of the quaternary nitrogen of the zwitterionic group was observed as shown in Figure 6.7.[45–49] Adsorbed water on the hydrophilically-modified surface and oxidation of the silicon (creating surface Si-OH hydroxyl groups) could both have contributed to the broad peak centered at 3390 cm^{-1} and the peak at 1628 cm^{-1} assigned to O-H stretching and bending respectively. The sharp peak at 1035 cm^{-1}, which protrudes from the broader Si-O stretching in the same region, corresponded to S=O stretching of the sulfobetaine group. The loss of the azide peak at 2098 cm^{-1} and the absence of the 3189 cm^{-1} and 2123 cm^{-1} peaks associated with the C-H stretching and C≡C stretching respectively of the alkyne group further suggested successful attachment of SB-alkyne through triazole formation. A comparison of this FT-IR spectra to that of VBA reacted with SB-alkyne in

the solution phase is found in Appendix C (Figure C.8). Further, NMR spectra of VBA reacted with SB-alkyne in the solution phase demonstrated successful click reaction and is also found in Appendix C (Figure C.9). With the successful click reaction of SB-alkyne, a novel symmetric dual zwitterionic alkyne (DZA) was synthesized in an effort to increase density of zwitterionic groups clicked to the g-VBA surfaces as compared to SB-alkyne. However, click reaction attempts with DZA proved unsuccessful; interestingly, DZA in the presence of the copper catalyst would precipitate from the aqueous solution, possibly removing the copper from solution with it, and no attachment to the g-VBA surfaces was observed. A summary of the synthesis of the novel DZA compound and related experimental observations is found in the "Dual Zwitterionic Alkyne Experiments" section of Appendix C.
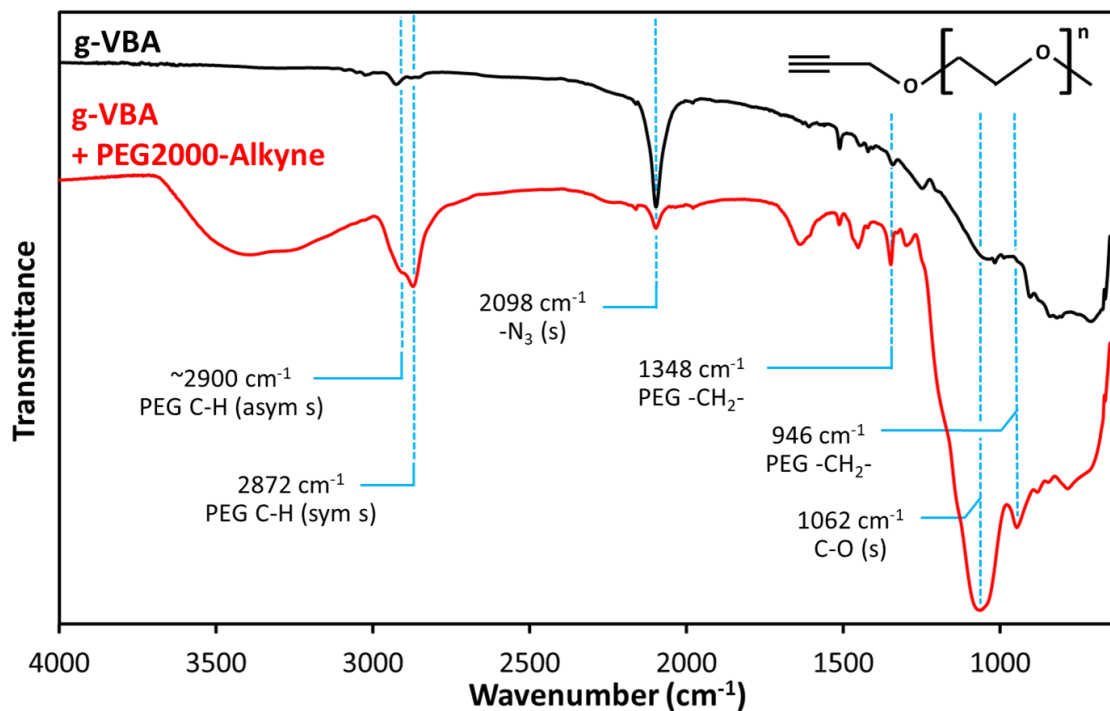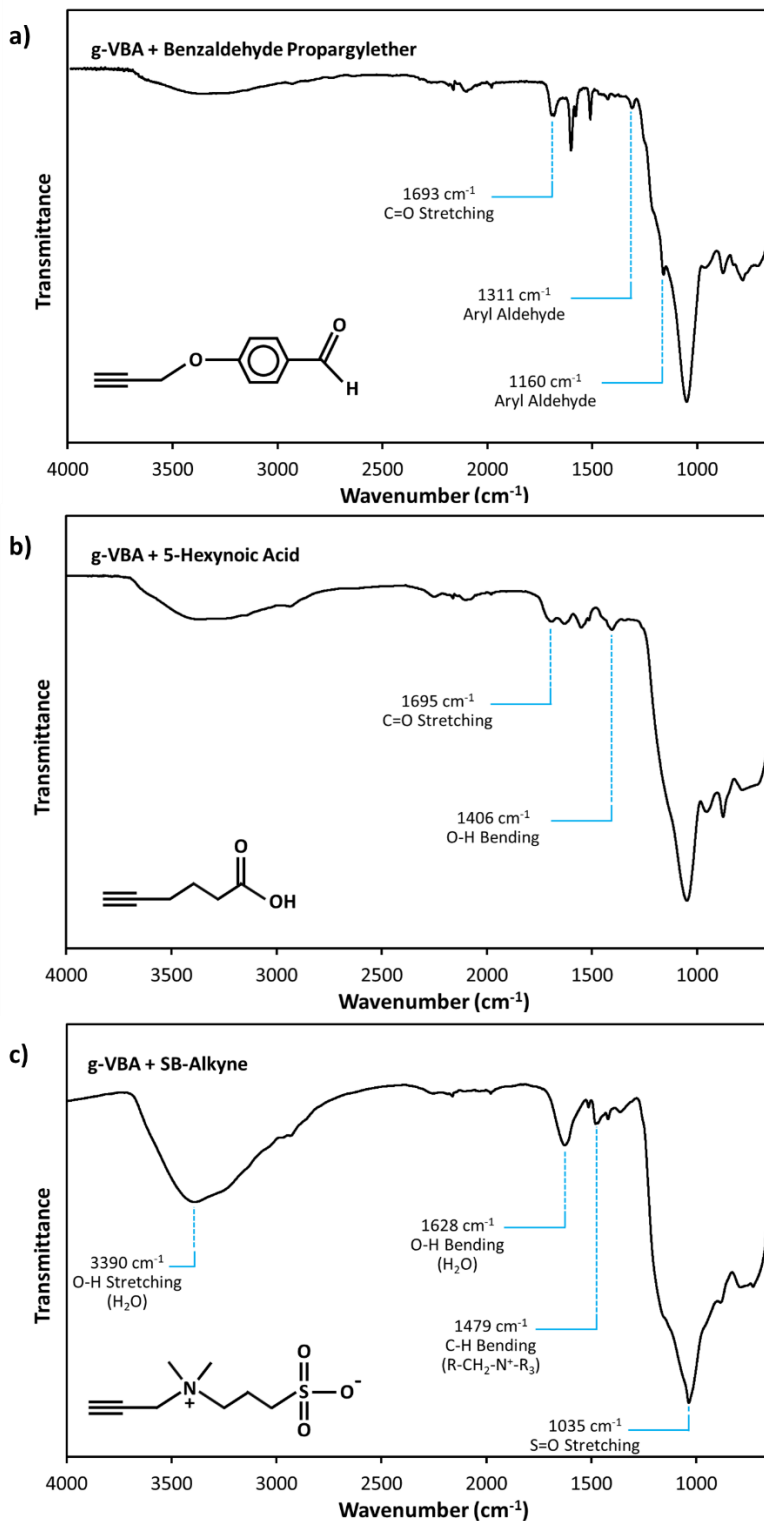
Figure 6.7. Comparison of the FT-IR spectra of VBA-modified porous silicon before and after click reaction with benzaldehyde propargylether, 5-hexynoic acid, and SB-Alkyne.

Upon 18 h click reaction of 5-hexynoic acid with the PSi-g-VBA surface, appearance of peaks at 1695 cm^{-1} and 1406 cm^{-1} associated with C=O stretching and OH bending of the carboxylic acid were observed. Once again, adsorbed water on the hydrophilically-modified surface and oxidation of the silicon (creating surface Si-OH hydroxyl groups) could have both contributed to the broad peak centered at 3390 cm^{-1} and the peak at 1628 cm^{-1} assigned to O-H stretching and bending respectively. The loss of the azide peak at 2098 cm^{-1} and the absence of the 3295 cm^{-1} and 2118 cm^{-1} peaks associated with the C-H stretching and C$\equiv$C stretching respectively of the alkyne group further suggested successful attachment of 5-hexynoic acid through triazole formation.

Upon 18 h click reaction of 4-(prop-2-ynyloxy)benzaldehyde (benzaldehyde propargylether) with the PSi-g-VBA surface, appearance of the peak at 1693 cm^{-1} associated with C=O stretching of the aldehyde group was observed. In addition, peaks at 1160 cm^{-1} and 1311 cm^{-1} characteristic of aryl aldehydes were observed.[50] The loss of the azide peak at 2098 cm^{-1} and the absence of the 3203 cm^{-1} and 2122 cm^{-1} peaks associated with the C-H stretching and C$\equiv$C stretching respectively of any unreacted alkyne group further suggested successful attachment of benzaldehyde propargylether by click chemistry.

Copper-free Click Reactions with Azide-Grafted Porous Silicon for Biotinylation

Upon 24 h click reaction of DBCO-PEG4-biotin with the PSi-g-VBA surface in DMSO, appearance of peaks at 1696 cm^{-1} and 1655 cm^{-1} associated with the Amide I bands of the cyclic urea group in biotin and the secondary amides respectively within the DBCO-PEG4-biotin structure were observed as shown in Figure 6.8.[50] Further, the appearance of peak at 1549 cm^{-1} could be assigned to the Amide II band for the attached DBCO-PEG4-biotin.[50] The diminishing of the azide peak at 2098 cm^{-1} further suggested successful click attachment of DBCO-PEG4-biotin to the porous silicon surface. As a control, PSi-g-VBA surfaces were exposed to the same reaction solvent (DMSO) for 24 h, omitting only the DBCO-PEG4-biotin. As expected, no change to azide peak was observed when the alkyne was omitted; the FT-IR spectra for this control experiment is found in Appendix C (Figure C.10).

160
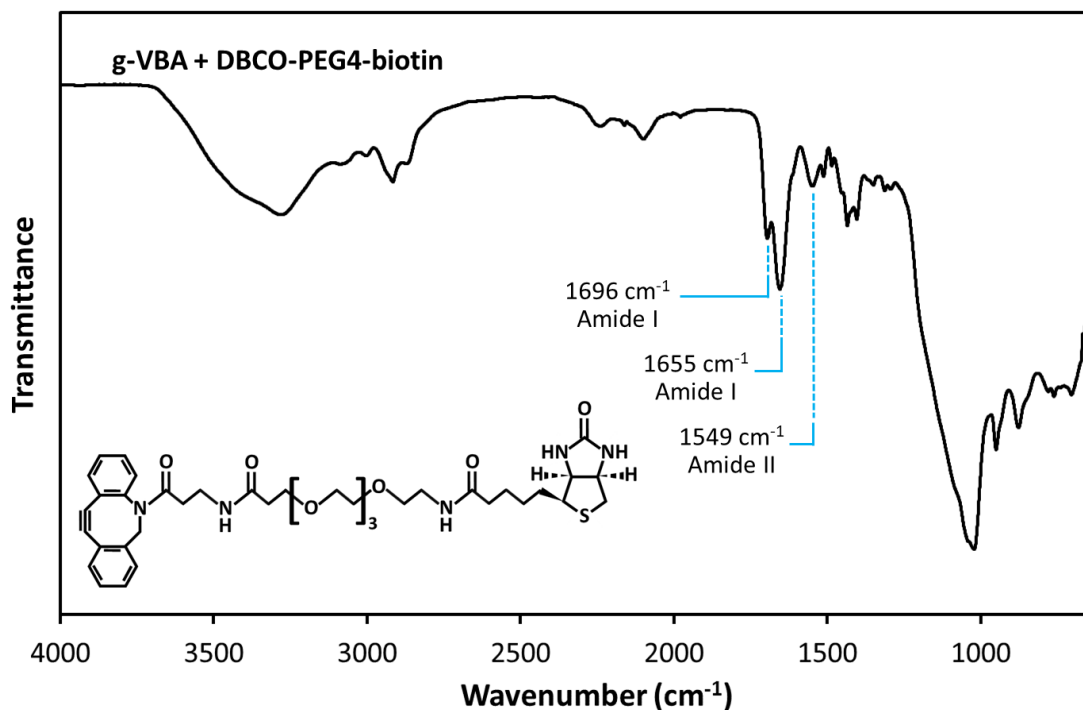
Figure 6.8. Comparison of the FT-IR spectra of VBA-modified porous silicon before and after copper-free click reaction with DBCO-PEG4-biotin.

Conclusions

This work demonstrated the successful attachment of an organic azide (VBA) to H-terminated silicon surfaces by a novel one-step UV-induced hydrosilylation method. In addition to flat silicon substrates, attachment of VBA to porous silicon (PSi) substates was performed and verified via FT-IR analysis. We further demonstrated the presence of the attached azide to PSi surfaces and its usefulness for click chemistry by "clicking" an assortment of alkynes to azide surface via both copper(I)-catalyzed azide alkyne cycloaddition (CuAAC) and also copper-free click chemistry using a ring-strained alkyne, verifying successful attachment via FT-IR in each case. Biotinylation of the substrates was performed via the aforementioned copper-free click reaction between an alkyne-containing biotin compound and the g-VBA surface to demonstrate the potential utility of the azide-modified porous silicon samples for biosensing applications afforded by the porous substrate.

References:

(1)   Liang, L.; Astruc, D. The Copper(I)-Catalyzed Alkyne-Azide Cycloaddition (CuAAC) "Click" Reaction and Its Applications. An Overview. *Coordination Chemistry Reviews*. December **2011**, pp 2933–2945. https://doi.org/10.1016/j.ccr.2011.06.028.

(2)   Castro, V.; Rodríguez, H.; Albericio, F. CuAAC: An Efficient Click Chemistry Reaction on Solid Phase. *ACS Comb. Sci.* **2016**, *18* (1), 1–14. https://doi.org/10.1021/acscombsci.5b00087.

(3)   Neumann, S.; Biewend, M.; Rana, S.; Binder, W. H. The CuAAC: Principles, Homogeneous and Heterogeneous Catalysts, and Novel Developments and Applications. *Macromolecular Rapid Communications* **2020**, *41* (1), 1900359. https://doi.org/10.1002/marc.201900359.

(4)   Martens, S.; Holloway, J. O.; du Prez, Filip. E. Click and Click-Inspired Chemistry for the Design of Sequence-Controlled Polymers. *Macromolecular Rapid Communications* **2017**, *38* (24), 1700469. https://doi.org/10.1002/marc.201700469.

(5)   Arslan, M.; Tasdelen, M. A. Click Chemistry in Macromolecular Design: Complex Architectures from Functional Polymers. *Chemistry Africa* **2019**, *2* (2), 195–214. https://doi.org/10.1007/s42250-018-0030-8.

(6)   Arslan, M.; Tasdelen, M. A. Polymer Nanocomposites via Click Chemistry Reactions. *Polymers*. MDPI AG October 11, **2017**. https://doi.org/10.3390/polym9100499.

(7)   Yáñez-Sedeño, P.; González-Cortés, A.; Campuzano, S.; Pingarrón, J. M. Copper(I)-Catalyzed Click Chemistry as a Tool for the Functionalization of Nanomaterials and the Preparation of Electrochemical (Bio)Sensors. *Sensors* **2019**, *19* (10), 2379. https://doi.org/10.3390/s19102379.

(8)   Zheng, S.; Yang, Q.; Mi, B. Novel Antifouling Surface with Improved Hemocompatibility by Immobilization of Polyzwitterions onto Silicon via Click Chemistry. *Applied Surface Science* **2016**, *363*, 619–626. https://doi.org/10.1016/j.apsusc.2015.12.081.

(9)   Li, N.; Binder, W. H. Click-Chemistry for Nanoparticle-Modification. *J. Mater. Chem.,* **2011**, *21,* 16717-16734, https://doi.org/10.1039/c1jm11558h.

(10)   Jewett, J. C.; Bertozzi, C. R. Cu-Free Click Cycloaddition Reactions in Chemical Biology. *Chem. Soc. Rev.*, **2010**, *39*, 1272-1279. https://doi.org/10.1039/b901970g.

(11)   Vos, R.; Rolin, C.; Rip, J.; Conard, T.; Steylaerts, T.; Cabanilles, M. V.; Levrie, K.; Jans, K.; Stakenborg, T. Chemical Vapor Deposition of Azidoalkylsilane Monolayer Films. *Langmuir* **2018**, *34* (4), 1400–1409. https://doi.org/10.1021/acs.langmuir.7b04011.

(12)   Paoprasert, P.; Spalenka, J. W.; Peterson, D. L.; Ruther, R. E.; Hamers, R. J.; Evans, P. G.; Gopalan, P. Grafting of Poly(3-Hexylthiophene) Brushes on Oxides Using Click Chemistry. *J. Mater. Chem*., **2010**, *20*, 2651-2658 . https://doi.org/10.1039/b920233a.

(13)   Gouget-Laemmel, A. C.; Yang, J.; Lodhi, M. A.; Siriwardena, A.; Aureau, D.; Boukherroub, R.; Chazalviel, J.; Ozanam, F.; Szunerits, S. Functionalization of Azide-Terminated Silicon Surfaces with Glycans Using Click Chemistry: XPS and FTIR Study. *J. Phys. Chem. C* **2013**, *117* (1), 368–375. https://doi.org/10.1021/jp309866d.

(14)   Heise, A.; Menzel, H.; Yim, H.; Foster, M. D.; Wieringa, R. H.; Schouten, A. J.; Erb, V.; Stamm, M. Grafting of Polypeptides on Solid Substrates by Initiation of N-Carboxyanhydride Polymerization by Amino-Terminated Self-Assembled Monolayers. *Langmuir* **1997**, *13* (4), 723–728. https://doi.org/10.1021/la960467g.

(15)   Balachander, N.; Sukenik, C. N. Functionalized Siloxy-Anchored Monolayers with Exposed Amino, Azido, Bromo, or Cyano Groups. *Tetrahedron Letters* **1988**, *29* (44), 5593–5594. https://doi.org/10.1016/S0040-4039(00)80820-5.

(16)   Xu, F. J.; Kang, E. T.; Neoh, K. G. UV-Induced Coupling of 4-Vinylbenzyl Chloride on Hydrogen-Terminated Si(100) Surfaces for the Preparation of Well-Defined Polymer-Si Hybrids via Surface-Initiated ATRP. *Macromolecules* **2005**, *38* (5), 1573–1580. https://doi.org/10.1021/ma049225a.

(17)   Yu, W. H.; Kang, E. T.; Neoh, K. G.; Zhu, S. Controlled Grafting of Well-Defined Polymers on Hydrogen-Terminated Silicon Substrates by Surface-Initiated Atom Transfer Radical Polymerization. *J. Phys. Chem. B* **2003**, *107* (37), 10198–10205. https://doi.org/10.1021/jp034330s.

(18)   Buriak, J. M. Organometallic Chemistry on Silicon and Germanium Surfaces. *Chem. Rev.* **2002**, *102* (5), 1271–1308. https://doi.org/10.1021/cr000064s.

(19)   Stewart, M. P.; Buriak, J. M. Photopatterned Hydrosilylation on Porous Silicon. *Angewandte Chemie - International Edition* **1998**, *37* (23), 3257–3260. https://doi.org/10.1002/(SICI)1521-3773(19981217)37:23<3257::AID-ANIE3257>3.0.CO;2-1.

(20)   Huck, L. A.; Buriak, J. M. UV-Initiated Hydrosilylation on Hydrogen-Terminated Silicon (111): Rate Coefficient Increase of Two Orders of Magnitude in the Presence of Aromatic Electron Acceptors. *Langmuir* **2012**, *28* (47), 16285–16293. https://doi.org/10.1021/la3035819.

(21)   Effenberger, F.; Götz, G.; Bidlingmaier, B.; Wezstein, M. Photoactivated Preparation and Patterning of Self-Assembled Monolayers with 1-Alkenes and Aldehydes on Silicon Hydride Surfaces. *Angewandte Chemie - International Edition* **1998**, *37* (18), 2462–2464. https://doi.org/10.1002/(SICI)1521-3773(19981002)37:18<2462::AID-ANIE2462>3.0.CO;2-R.

(22)   Terry, J.; Mo, R.; Wigren, C.; Cao, R.; Mount, G.; Pianetta, P.; Linford, M. R.; Chidsey, C. E. D. Reactivity of the H-Si (111) Surface. *Nuclear Instruments and Methods in Physics Research, Section B: Beam Interactions with Materials and Atoms* **1997**, *133* (1–4), 94–101. https://doi.org/10.1016/S0168-583X(97)00467-9.

(23)   Cicero, R. L.; Linford, M. R.; Chidsey, C. E. D. Photoreactivity of Unsaturated Compounds with Hydrogen-Terminated Silicon(111). *Langmuir* **2000**, *16* (13), 5688–5695. https://doi.org/10.1021/la9911990.

(24)   Nguyen, A. T.; Baggerman, J.; Paulusse, J. M. J.; Zuilhof, H.; van Rijn, C. J. M. Bioconjugation of Protein-Repellent Zwitterionic Polymer Brushes Grafted from Silicon Nitride. *Langmuir* **2012**, *28* (1), 604–610. https://doi.org/10.1021/la2031363.

(25)   Nguyen, A. T.; Baggerman, J.; Paulusse, J. M. J.; van Rijn, C. J. M.; Zuilhof, H. Stable Protein-Repellent Zwitterionic Polymer Brushes Grafted from Silicon Nitride. *Langmuir* **2011**, *27* (6), 2587–2594. https://doi.org/10.1021/la104657c.

(26)   Sano, H.; Maeda, H.; Ichii, T.; Murase, K.; Noda, K.; Matsushige, K.; Sugimura, H. Alkyl and Alkoxyl Monolayers Directly Attached to Silicon: Chemical Durability in Aqueous Solutions. *Langmuir* **2009**, *25* (10), 5516–5525. https://doi.org/10.1021/la804080g.

(27)   Bhairamadgi, N. S.; Pujari, S. P.; Trovela, F. G.; Debrassi, A.; Khamis, A. A.; Alonso, J. M.; al Zahrani, A. A.; Wennekes, T.; Al-Turaif, H. A.; van Rijn, C.; Alhamed, Y. A.; Zuilhof, H. Hydrolytic and Thermal Stability of Organic Monolayers on Various Inorganic Substrates. *Langmuir* **2014**, *30* (20), 5829–5839. https://doi.org/10.1021/la500533f.

(28)   Arshavsky-Graham, S.; Massad-Ivanir, N.; Segal, E.; Weiss, S. Porous Silicon-Based Photonic Biosensors: Current Status and Emerging Applications. *Anal. Chem.* **2019**, *91* (1), 441–467. https://doi.org/10.1021/acs.analchem.8b05028.

(29)   Bañ, M.-J.; Puchades, R.; Maquieira, Á. Chemical Surface Modifications for the Development of Silicon-Based Label-Free Integrated Optical (IO) Biosensors: A Review. *Analytica Chimica Acta* **2013**, *777*, 1–16. https://doi.org/10.1016/j.aca.2013.01.025.

(30)   Lowe, B. M.; Sun, K.; Zeimpekis, I.; Skylaris, C.-K.; Green, N. G. Analyst CRITICAL REVIEW Field-Effect Sensors-from PH Sensing to Biosensing: Sensitivity Enhancement Using Streptavidin-Biotin as a Model System †. *Analyst* **2017**, *142*, 4173. https://doi.org/10.1039/c7an00455a.

(31)   Chaki, N. K.; Vijayamohanan, K. Self-Assembled Monolayers as a Tunable Platform for Biosensor Applications. *Biosensors and Bioelectronics* **2002** *17* (1-2) 1-12. https://doi.org/10.1016/S0956-5663(01)00277-9

(32)   Mooney, J. F.; Huntt, A. J.; Mcintosht, J. R.; Liberkot, C. A.; Walbat, D. M.; Rogers, C. T.; Prescott, D. M. *Patterning of Functional Antibodies and Other Proteins by Photolithography of Silane Monolayers (Self-Assembled Monolayers/Biotin/Streptavidin/Adsorption Isotherms)*; 1996; Vol. 93.

(33)   Williams, E. H.; Davydov, A. v; Motayed, A.; Sundaresan, S. G.; Bocchini, P.; Richter, L. J.; Stan, G.; Steffens, K.; Zangmeister, R.; Schreifels, J. A.; Rao, V. Immobilization of Streptavidin on 4H-SiC for Biosensor Development. *Applied Surface Science* **2012**, *258*, 6056–6063. https://doi.org/10.1016/j.apsusc.2012.02.137.

(34)   Albuszis, M.; Roth, P. J.; Exnowitz, F.; Wong, D. L.; Pauer, W.; Moritz, H. U. Synthesis and In-Depth Characterization of Reactive, Uniform, Crosslinked Microparticles Based on Free Radical Copolymerization of 4-Vinylbenzyl Azide. *Polymer Chemistry* **2016**, *7* (5), 1168–1180. https://doi.org/10.1039/c5py01848j.

(35)   Zill, A. T.; Licha, K.; Haag, R.; Zimmerman, S. C. Synthesis and Properties of Fluorescent Dyes Conjugated to Hyperbranched Polyglycerols. *New Journal of Chemistry* **2012**, *36* (2), 419–427. https://doi.org/10.1039/c1nj20476a.

(36)   Darroudi, M.; Sarrafi, Y.; Hamzehloueian, M. An Efficient Synthesis of Novel Triazoles Incorporating Barbituric Motifs via [3+2] Cycloaddition Reactions: An Experimental and Theoretical Study. *Journal of the Serbian Chemical Society* **2018**, *83* (7–8), 821–835. https://doi.org/10.2298/JSC170618038D.

(37)   Li, S. X.; Feng, L. R.; Guo, X. J.; Zhang, Q. Application of Thermal Azide-Alkyne Cycloaddition (TAAC) Reaction as a Low Temperature Cross-Linking Method in Polymer Gate Dielectrics for Organic Field-Effect Transistors. *Journal of Materials Chemistry C* **2014**, *2* (18), 3517–3520. https://doi.org/10.1039/c4tc00116h.

(38)   Albuszis, M.; Roth, P. J.; Pauer, W.; Moritz, H. U. Two in One: Use of Azide Functionality for Controlled Photo-Crosslinking and Click-Modification of Polymer Microspheres. *Polymer Chemistry* **2016**, *7* (34), 5414–5425. https://doi.org/10.1039/c6py00937a.

(39)   Collman, J. P.; Devaraj, N. K.; Eberspacher, T. P. A.; Chidsey, C. E. D. Mixed Azide-Terminated Monolayers: A Platform for Modifying Electrode Surfaces. *Langmuir* **2006**, *22* (6), 2457–2464. https://doi.org/10.1021/la052947q.

(40)   Oesterhelt, F.; Rief, M.; Gaub, H. E. Single Molecule Force Spectroscopy by AFM Indicates Helical Structure of Poly(Ethylene-Glycol) in Water. *New Journal of Physics* **1999**, *1* (1), 6. https://doi.org/10.1088/1367-2630/1/1/006.

(41)   Harder, P.; Grunze, M.; Dahint, R.; Whitesides, G. M.; Laibinis, P. E. Molecular Conformation in Oligo(Ethylene Glycol)-Terminated Self-Assembled Monolayers on Gold and Silver Surfaces Determines Their Ability To Resist Protein Adsorption. *J. Phys. Chem. B* **1998**, *102* (2), 426–436. https://doi.org/10.1021/jp972635z

(42)   Tokumitsu, S.; Liebich, A.; Herrwerth, S.; Eck, W.; Himmelhaus, M.; Grunze, M. Grafting of Alkanethiol-Terminated Poly(Ethylene Glycol) on Gold. *Langmuir* **2002**, *18* (23), 8862–8870. https://doi.org/10.1021/la0258953.

(43)   Zhu, X. Y.; Jun, Y.; Staarup, D. R.; Major, R. C.; Danielson, S.; Boiadjiev, V.; Gladfelter, W. L.; Bunker, B. C.; Guo, A. Grafting of High-Density Poly(Ethylene Glycol) Monolayers on Si(111). *Langmuir* **2001**, *17* (25), 7798–7803. https://doi.org/10.1021/la010672i.

(44) Papra, A.; Gadegaard, N.; Larsen, N. B. Characterization of Ultrathin Poly(Ethylene Glycol) Monolayers on Silicon Substrates. *Langmuir* **2001**, *17* (5), 1457–1460. https://doi.org/10.1021/la000609d.

(45) Pigorsch, E. Spectroscopic Characterisation of Cationic Quaternary Ammonium Starches. *Starch - Stärke* **2009**, *61* (3–4), 129–138. https://doi.org/10.1002/star.200800090.

(46) Sánchez, J.; Rivas, B. L. Cationic Hydrophilic Polymers Coupled to Ultrafiltration Membranes to Remove Chromium (VI) from Aqueous Solution. *Desalination* **2011**, *279* (1–3), 338–343. https://doi.org/10.1016/j.desal.2011.06.029.

(47) Palacio, D. A.; Rivas, B. L.; Urbano, B. F. Ultrafiltration Membranes with Three Water-Soluble Polyelectrolyte Copolymers to Remove Ciprofloxacin from Aqueous Systems. *Chemical Engineering Journal* **2018**, *351*, 85–93. https://doi.org/10.1016/j.cej.2018.06.099.

(48) Loubaki, E.; Ourevitch, M.; Sicsic, S. Chemical Modification of Chitosan by Glycidyl Trimethylammonium Chloride. Characterization of Modified Chitosan by 13C- and 1H-NMR Spectroscopy. *European Polymer Journal* **1991**, *27* (3), 311–317. https://doi.org/10.1016/0014-3057(91)90111-Z.

(49) Sajomsang, W.; Gonil, P.; Tantayanon, S. Antibacterial Activity of Quaternary Ammonium Chitosan Containing Mono or Disaccharide Moieties: Preparation and Characterization. *International Journal of Biological Macromolecules* **2009**, *44* (5), 419–427. https://doi.org/10.1016/j.ijbiomac.2009.03.003.

(50) Socrates, G. *Infrared and Raman Characteristic Group Frequencies: Tables and Charts*, 3rd ed.; John Wiley & Sons Ltd: Chichester, 2001.

(51) Collman, J. P.; Devaraj, N. K.; Eberspacher, T. P. A.; Chidsey, C. E. D. Mixed Azide-Terminated Monolayers: A Platform for Modifying Electrode Surfaces. *Langmuir* **2006**, *22* (6), 2457–2464. https://doi.org/10.1021/la052947q.

(52)   Vos, R.; Rolin, C.; Rip, J.; Conard, T.; Steylaerts, T.; Cabanilles, M. V.; Levrie, K.; Jans, K.; Stakenborg, T. Chemical Vapor Deposition of Azidoalkylsilane Monolayer Films. *Langmuir* **2018**, *34* (4), 1400–1409. https://doi.org/10.1021/acs.langmuir.7b04011.

(53)   Gouget-Laemmel, A. C.; Yang, J.; Lodhi, M. A.; Siriwardena, A.; Aureau, D.; Boukherroub, R.; Chazalviel, J. N.; Ozanam, F.; Szunerits, S. Functionalization of Azide-Terminated Silicon Surfaces with Glycans Using Click Chemistry: XPS and FTIR Study. *Journal of Physical Chemistry C* **2013**, *117* (1), 368–375. https://doi.org/10.1021/jp309866d.

CHAPTER VII

CONCLUSIONS AND FUTURE WORK

Conclusions

The results I have presented in this dissertation demonstrate the use of ARGET polymerization to generate various grafted polar polymers, particularly zwitterionic polymers, from silicon surfaces. I developed experimental conditions and procedures that provided reliable control of a grafted polymer film's thickness for preparing ultrathin coatings. Using these conditions, multiple polymers with potential antifouling properties, including zwitterionic polymers, were successfully grafted from silicon substrates. In addition to these grafted polymer coatings, several strategies to modify surfaces with molecular films were studied. A variety of methods were investigated for producing fouling-resistant molecular films including by silanization, "click" chemistry, and substitution reactions. Grafting methods based on the UV-induced attachment of alkene-containing compounds, as opposed to the grafting using silanes, were investigated to address the long-term film stability issues associated with siloxane attachment chemistries. These Si-C bound surfaces were used for polymer initiation, substitution reactions, and "click" chemistry. Of particular importance was the development of novel, one-step attachment strategies utilizing either UV-hydrosilylation or thermal hydrosilylation to obtain "clickable" azide-terminated molecular films. Surface coatings discussed in this dissertation were characterized by a variety of methods including ellipsometry, wetting, FT-IR (for coatings on porous Si substrates), profilometry, SEM, among other techniques. Further, the fouling resistances of promising coatings on planar Si surfaces were examined via fluorescence microscopy to quantify the non-specific adsorption of fluorescently-labeled albumin.

In Chapter II, I demonstrated the procedures and techniques needed to conduct well-controlled surface-initiated ARGET polymerizations of hydrophilic monomers including pPEGMA and pHEMA

along with hydrophilic zwitterionic monomers including pSBMA, pSBMAA, pSBA, and others that are candidates to provide antifouling properties. Under the ARGET polymerization conditions developed here, the grafted film thicknesses of these polymer films increased in a manner consistent with well-controlled growth within the thickness range of interest. In addition to the siloxane-bound initiators typically used with surface-initiated polymerization, we also utilized Si-C bound initiators (g-VBC) formed through UV-induced hydrosilylation. The g-VBC proved successful for the initiation of ARGET polymerizations of the desired zwitterionic monomers and should provide improved hydrolytic stability as compared to the siloxane-bound films. The polymer films produced here exhibited a uniform appearance and low variation in ellipsometric film thickness across each slide. This ability to produce films of predictable thickness and high uniformity are invaluable in situations, such as with the nanopore membranes, where precise control of film thickness is required. In addition to these grafted polymers, covalently attached monolayers including g-PEGsilane and g-SBSi were produced. Based on results from fluorescence microscopy, multiple coatings produced to date, including g-pSBMA and g-SBSi, showed promise as fouling resistant coatings. Of the zwitterionc polymer films explored here, pSBMA seemed to be the most practical zwitterionic polymer coating system in terms of wettability, controllable growth kinetics, ease of use, and safety of synthesis.

In Chapter III, I presented a method for analyzing the surface energy components of superhydrophilic species using a model developed based upon the Cassie, Fowkes, Young equations, and also the relative rate expressions for grafted copolymer surfaces containing a less-hydrophilic comonomer. This method is significant in that the wettability of many superhydrophilic zwitterionic polymer films are difficult to measure directly due to their inherent 0° or near-0° contact angles, data that typical methods for determining surface energy components rely upon. A collection of zwitterionic-monomer containing copolymers was produced by surface-initiated ARGET polymerization and used to evaluate the usefulness of the developed model. Although it was evident that the model was able to provide values for surface energy components that were consistent with the grafted copolymers' structures and their functionality, we

171

observed that the confidence intervals for these values were too large to differentiate between the two studied zwitterionic monomer species. When evaluating this model, it was observed that the model was quite sensitive to changes in the φ value, resulting in the higher uncertainty in the calculated surface energy component values. Consequently, future work in evaluating this model would involve determining the φ term through other means such as FT-IR or XPS, rather than φ being fitted; this should reduce the uncertainty of the model's predictions.

In Chapter IV, I demonstrated the reliable formation of a thick coating of SiO_2 at/near the 1 μm scale on the surface of zwitterionic polymer (g-VBC-pSBMA) and monolayer (g-SBSi) coatings on silicon substrates by exposure to 37 °C phosphate buffered saline (PBS) solutions. Further, we demonstrated the ability to accelerate this SiO_2 coating formation by placing the zwitterion-modified silicon substrates into refluxing PBS in a glass round-bottom flask under a condenser. We characterized the coating with ellipsometry, profilometry, and scanning electron microscopy to assess its thickness, and further, we used FTIR to further demonstrate that the coating was consistent with silica. Based on literature reports and the experiments shown here, we suspect that the PBS slowly etched the walls of the glass round-bottom flask (and potentially also the uncoated bottom of our samples) to form soluble silicic acid. It is then expected that the silica coating was formed via the polycondensation of silicic acid, nucleated at the zwitterion-modified surface.

The work in Chapter V demonstrated both the successful attachment of 4-vinylbenzyl chloride to H-terminated silicon to create g-VBC surfaces by UV-induced hydrosilylation and also the usefulness of this surface for subsequent modification via substitution reactions. Attachment of VBC to flat and porous silicon substates was performed and subsequent substitution reactions were verified via wetting, ellipsomety, and FT-IR analysis. Specifically, substitution with sodium azide, alkoxides (n-dodecanol and PEG2000-MME), and amines (dimethylamine and DMAMS) were shown. In addition, ellipsometric thickness results for the much thicker PEG2000-modified g-VBC surfaces further demonstrated successful attachment/conversion and provided the ability to estimate a grafting density.

In Chapter VI, my work demonstrated successful attachment of an organic azide (VBA) to H-terminated silicon surfaces by a one-step UV-induced hydrosilylation method. In addition to flat silicon substrates, attachment of VBA to porous silicon (PSi) substates was performed and verified via FT-IR analysis. We further demonstrated the presence of the attached azide to PSi surfaces and its usefulness for click chemistry by "clicking" an assortment of alkynes to azide surface via both copper(I)-catalyzed azide alkyne cycloaddition (CuAAC) and also copper-free click chemistry using a ring-strained alkyne, verifying successful attachment via FTIR in each case. Biotinylation of the substrates was performed via the aforementioned copper-free click reaction between an alkyne-containing biotin compound and the g-VBA surface to demonstrate the potential utility of the azide-modified porous silicon samples for biosensing applications afforded by the porous substrate.

Future Work

This dissertation demonstrates a breadth of strategies including surface-initiated polymerization, "click" chemistry, and nucleophilic substitution at molecular films, all of which were investigated in order to produce thin, stable, and potentially fouling-resistant coating architectures. In order to further the utility and understanding of the coating strategies I have presented in this document, I propose the following future research topics that could expand on the results shown here.

In Chapter II, I demonstrated the procedures and techniques needed to conduct well-controlled surface-initiated ARGET polymerizations of antifouling polymers including pPEGMA, pHEMA, pSBMA, pSBMAA, and pSBA. These were grafted from both siloxane-bound initiators and also Si-C bound initiators (g-VBC) formed through UV-induced hydrosilylation. In addition to these grafted polymers, covalently attached monolayers including g-PEGsilane and g-SBSi were produced. A logical continuation of the work presented in Chapter II would be to more thoroughly evaluate the antifouling abilities of the of the coatings developed in this dissertation. The fouling resistance experiments that I conducted were limited to fluorescence microscopy analysis of FITC-albumin exposed polymer and monolayer modified samples;

further, some of the coatings I produced have not yet been compared by these fluorescence experiments. In addition, other fouling measurement techniques and long-term stability testing would provide further insight for choosing an ideal antifouling coating architecture from those I investigated.[1–4]

A future opportunity that arises from my work with UV-hydrosilylation and silane-monolayers would be to combine these two methods in a unique manner that utilizes the geometry of our collaborators' silicon kidney nanopore membranes. Although resist-free patterning of silicon has been demonstrated by Kang et al. on flat silicon substrates using a combined UV-induced linkage/silane approach, a mask was still required.[5] In Chapter II, I detailed a possible resist-free/mask-free patterning technique for the silicon membranes using this combined UV-linkage and silane approach. Patterning could be accomplished by utilizing the pre-existing geometry of the nanopore membranes by the steps illustrated in Figure 2.29. The attachment of the VBC initiator to the top surface of the membranes could first be conducted via the UV-hydrosilyation methods I have presented in this document, and as the UV light should only generate radical sites on the exposed outer surface of the nanopore membrane, the pore walls should be left unmodified by the alkene initiator. After regrowth of the oxide on the inner unmodified pore walls, a silane of desired functionality could then be attached within the pores. Finally, the desired antifouling polymer would then be grafted from the attached initiator at the membrane's top surface via ARGET or ATRP. This process would tailor the surface properties of the exposed top (and bottom) surfaces independently from the surface of the pore walls. As the pores of the nanofilter membranes are ~7 nm across, the ability to independently control the modification occurring in the pores could prove crucial. This approach is designed to avoid clogging the pores while grafting a relatively thick polymer such as pSBMA from the top surface. A very thin monolayer of SBSi, or other comparable silane, could be grafted from the pore walls to provide a highly wettable coating with minimal change in the pore size.

In Chapter III, I presented a method for analyzing the surface energy components of superhydrophilic species using a model developed based upon the Cassie, Fowkes, Young equations, and also the relative rate expressions for grafted copolymer surfaces containing a less-hydrophilic comonomer.

174

When evaluating this model, I observed that it was quite sensitive to changes in the φ value, resulting in larger than desired confidence intervals for the calculated surface energy component values. As such, φ could be determined through other means, rather than being a fitted term. As φ is the product of α (the ratio of rate constants for *M1* and *M2*) and β (the ratio of exposed surface area per molecule of *M1* to that of *M2*), surface analysis techniques such as FT-IR or XPS should allow determination of the surface composition of the copolymer surfaces, thus allowing φ to no longer be needed as a fitted term. Once an appropriate strategy for evaluating φ is determined, the model should prove useful in the evaluation and comparison of surface energy parameters for a variety of superhydrophilic polymer coatings. Further, the model should also be applicable to superhydrophilic molecular films or monolayer coatings such as g-SBSi. For such an experiment examining a superhydrophilic silane monolayer or molecular film, one should choose a less-hydrophilic "companion" silane to produce mixed monolayers with higher, more easily measured contact angles as compared to the pure superhydrophilic monolayer. In choosing this "companion" silane, one should ideally match, or at least take into account, the height/area of the "companion" silane to the height/area of the superhydrophilic silane of interest in order to satisfy the Cassie relationship that exists within this model.[6–8]

In Chapter IV, we demonstrated the formation of thick of SiO_2 coatings on the surface of zwitterionic polymer (g-VBC-pSBMA) and monolayer (g-SBSi) coatings on silicon substrates by exposing these samples to either 37 °C PBS or also refluxing PBS in a glass round-bottom flask under a condenser. Based on literature reports and our experimental results from Chapter IV, we suspected that the PBS slowly etched the walls of the glass round-bottom flask (and potentially also the uncoated bottom of our silicon samples) to form soluble silicic acid, and subsequently, the silica coating formed via the polycondensation of silicic acid, nucleated at the zwitterion-modified surface. Firstly, future work could involve FT-IR analysis of dried PBS solutions that were refluxed within glassware; this would be performed to demonstrate the presence of the anticipated silicic acid. As I noted in this chapter, there was a delay in silica coating formation when samples were exposed to freshly prepared refluxing PBS; this delay was

circumvented by allowing the PBS solution to reflux for multiple days before introduction of the zwitterion-modified sample. This process of "building-up" of the water-soluble silicic acid could be better understood by conducting a kinetic study of the formation of the silicic acid in the PBS solution with increasing time at reflux. Further, a kinetic study of the formation of the SiO_2 coating itself using ellipsometry and/or profilometry should enable future researchers to better understand and control of the thickness of this deposited/grown silica film.

In Chapter V, I demonstrated that the g-VBC on flat and porous silicon substates made by UV-induced hydrosilylation was useful for subsequent modification via nucleophilic substitution reactions. The primary motivation of Chapter V was to demonstrate the utility of g-VBC for substitution reactions to form thin molecular films, a purpose other than its typical use as an initiator for ATRP.[9] As such, I performed multiple substitution reactions at this g-VBC surface to showcase the kind of functionality one could obtain via this reaction scheme. The utility of these surfaces, however, was not demonstrated and provides an opportunity for future researchers to examine the utility of these surfaces for uses such as fouling resistance (in the case of the PEG2000-MME or zwitterion modified g-VBC substrates) or also for "click" chemistry (in the case of the azide-modified g-VBC substrates). Further, although literature reports suggest that films such as g-VBC that are anchored by Si-C attachments should be more hydrolytically stable than similar films anchored by siloxane chemistries,[4] this was an area that I did not experimentally visit during my research, and thus would provide an excellent opportunity for future researchers to conduct a stability comparison between the two attachment chemistries.

Chapter VI demonstrates a novel method to attach an organic azide to H-terminated silicon surfaces by a one-step hydrosilylation approach using 4-vinylbenzyl azide (VBA). In addition to flat silicon substrates, we also attached VBA to porous silicon (PSi) which could provide a potentially useful platform for sensing applications. Porous silicon has been demonstrated to be a highly effective platform for sensing applications as the presence of captured target molecules can be quantified via analysis of changes in position of interference fringes obtained through reflectance experiments.[10] The biotin-streptavidin

interaction system represents one of the most common coupling strategies for binding bioreceptor systems to such surfaces for capturing analytes in biosensing applications.[10–15] To demonstrate the potential utility of our azide-modified porous silicon samples for biosensing applications, we demonstrated biotinylation of the substrates using a copper-free click reaction between an alkyne-containing biotin compound and the g-VBA surface. However, we did not proceed further than attaching the alkyne-biotin molecule to our azide surface. The logical continuation and expansion of the work presented in this chapter would involve introducing a streptavidin-containing molecule or bio-capture agent in order to utilize these g-VBA modified PSi substrates for the sensing of biomolecules. Doing so would underscore the utility of these simple-to-manufacture g-VBA surfaces for a practical, and possibly commercialize-able, application. Further, as VBA is attached to H-terminated silicon via a UV-light process, the opportunity arises to perform patterning of a surface with g-VBA by controlling UV exposure by a simple masking step such as that demonstrated with a g-VBC surface in Figure 2.13. This would enable the simple and straight-forward manufacture of arrays of g-VBA sites needed for "clicking on" of specific molecules for purposes such as capture; the substrate could subsequently be modified in the un-exposed/un-reacted areas with a second molecule, possibly a silane, possessing another desired moiety, such as for fouling resistance. Finally, I only explored the attachment of VBA to flat and porous silicon substrates; however, there are many other Si-H containing substrates/materials available that should be compatible with the UV-attachment of VBA. Specifically, commercially-available siloxane polymers are available which contain Si-H groups either along the backbone (such as Dow's XIAMETER™ MHX-1107) or at the ends of the polymer chains (such as the "hydrogen-terminated silicone fluids" available from Genesee Polymers Corporation). These polymers should be able to be modified using UV-attachment of VBA for a variety of purposes including attachment to alkyne-modified substrates or particles via "click" reactions. Further, cross-linking of VBA-modified polymers with those decorated with alkyne groups is another possibility, along with end-to-end linking of the terminal Si-H/g-VBA modified siloxane polymer chains with alkyne-terminated polymer chains would be of potential interest.

References:

(1)   Chan, R.; Chen, V. Characterization of Protein Fouling on Membranes: Opportunities and Challenges. *Journal of Membrane Science* **2004**, *242* (1–2), 169–188. https://doi.org/10.1016/j.memsci.2004.01.029.

(2)   Hedayati, M.; Faulón Marruecos, D.; Krapf, D.; Kaar, J. L.; Kipper, M. J. Protein Adsorption Measurements on Low Fouling and Ultralow Fouling Surfaces: A Critical Comparison of Surface Characterization Techniques. *Acta Biomaterialia* **2020**, *102*, 169–180. https://doi.org/10.1016/j.actbio.2019.11.019.

(3)   Zhang, Z.; Chao, T.; Chen, S.; Jiang, S. Superlow Fouling Sulfobetaine and Carboxybetaine Polymers on Glass Slides. *Langmuir* **2006**, *22* (24), 10072–10077. https://doi.org/10.1021/la062175d.

(4)   Bhairamadgi, N. S.; Pujari, S. P.; Trovela, F. G.; Debrassi, A.; Khamis, A. A.; Alonso, J. M.; al Zahrani, A. A.; Wennekes, T.; Al-Turaif, H. A.; van Rijn, C.; Alhamed, Y. A.; Zuilhof, H. Hydrolytic and Thermal Stability of Organic Monolayers on Various Inorganic Substrates. *Langmuir* **2014**, *30* (20), 5829–5839. https://doi.org/10.1021/la500533f.

(5)   Xu, F. J.; Kang, E. T.; Neoh, K. G. Resist-Free Micropatterning of Binary Polymer Brushes on Si(100) via Surface-Initiated Living Radical Polymerizations. *Journal of Materials Chemistry* **2006**, *16* (28), 2948–2952. https://doi.org/10.1039/b604410g.

(6)   Laibinis, P. E.; Whitesides, G. M. ω-Terminated Alkanethiolate Monolayers on Surfaces of Copper, Silver, and Gold Have Similar Wettabilities. *Journal of the American Chemical Society* **1992**, *114* (6), 1990–1995. https://doi.org/10.1021/ja00032a009.

(7)   Israelachvili, J. N.; Gee, M. L. Contact Angles on Chemically Heterogeneous Surfaces. *Langmuir* **1989**, *5* (1), 288–289. https://doi.org/10.1021/la00085a059.

(8)   Halverson, J. D.; Maldarelli, C.; Couzis, A.; Koplik, J. Atomistic Simulations of the Wetting Behavior of Nanodroplets of Water on Homogeneous and Phase Separated Self-Assembled Monolayers. *Soft Matter* **2010**, *6* (6), 1297–1307. https://doi.org/10.1039/b921840h.

(9)   Xu, F. J.; Kang, E. T.; Neoh, K. G. UV-Induced Coupling of 4-Vinylbenzyl Chloride on Hydrogen-Terminated Si(100) Surfaces for the Preparation of Well-Defined Polymer-Si Hybrids via Surface-Initiated ATRP. *Macromolecules* **2005**, *38* (5), 1573–1580. https://doi.org/10.1021/ma049225a.

(10)   Arshavsky-Graham, S.; Massad-Ivanir, N.; Segal, E.; Weiss, S. Porous Silicon-Based Photonic Biosensors: Current Status and Emerging Applications. *Anal. Chem.* **2019**, *91* (1), 441–467. https://doi.org/10.1021/acs.analchem.8b05028.

(11)   Bã, M.-J.; Puchades, R.; Maquieira, Á. Chemical Surface Modifications for the Development of Silicon-Based Label-Free Integrated Optical (IO) Biosensors: A Review. *Analytica Chimica Acta* **2013**, *777*, 1–16. https://doi.org/10.1016/j.aca.2013.01.025.

(12)   Lowe, B. M.; Sun, K.; Zeimpekis, I.; Skylaris, C.-K.; Green, N. G. Analyst CRITICAL REVIEW Field-Effect Sensors-from PH Sensing to Biosensing: Sensitivity Enhancement Using Streptavidin-Biotin as a Model System †. *Analyst* **2017**, *142*, 4173. https://doi.org/10.1039/c7an00455a.

(13)   Chaki, N. K.; Vijayamohanan, K. Self-Assembled Monolayers as a Tunable Platform for Biosensor Applications. *Biosensors and Bioelectronics*. Elsevier January 1, **2002**, pp 1–12. https://doi.org/10.1016/S0956-5663(01)00277-9.

(14)   Mooney, J. F.; Huntt, A. J.; Mcintosht, J. R.; Liberkot, C. A.; Walbat, D. M.; Rogers, C. T.; Prescott, D. M. Patterning of Functional Antibodies and Other Proteins by Photolithography of Silane Monolayers. *Proc Natl Acad Sci U S A.* **1996** Oct 29; *93* (22): 12287–12291. https://doi.org/10.1073/pnas.93.22.12287

(15)   Williams, E. H.; Davydov, A. v; Motayed, A.; Sundaresan, S. G.; Bocchini, P.; Richter, L. J.; Stan, G.; Steffens, K.; Zangmeister, R.; Schreifels, J. A.; Rao, V. Immobilization of Streptavidin on 4H-SiC for Biosensor Development. *Applied Surface Science* **2012**, *258*, 6056–6063. https://doi.org/10.1016/j.apsusc.2012.02.137.

APPENDIX A

SUPPLEMENTARY INFORMATION FOR CHAPTER III

Matlab Code: Below is the equation used for the simultaneous fitting of both the water-in-air and water-in-hexadecane contact angle data sets for the zwitterionic copolymer systems:

Cos(theta) = (1-y)* ((1/(72.8+0-2*(sqrt(21.8)*sqrt(0) + sqrt(51.0)*sqrt(0))))*((((B*(x))/(B*(x)+(1-(x)))))*(0-72.8 + 2*(sqrt(M)*sqrt(21.8)+sqrt(N)*sqrt(51.0)-sqrt(M)*sqrt(0)-sqrt(N)*sqrt(0)))+(1-(((B*(x))/(B*(x)+(1-(x))))))*(0-72.8 + 2*(sqrt(O)*sqrt(21.8)+sqrt(P)*sqrt(51.0)-sqrt(O)*sqrt(0)-sqrt(P)*sqrt(0)))))

+

y*((1/(72.8+27.5-2*(sqrt(21.8)*sqrt(27.5) + sqrt(51.0)*sqrt(0))))*((((B*(x))/(B*(x)+(1-(x)))))*(27.5-72.8 + 2*(sqrt(M)*sqrt(21.8)+sqrt(N)*sqrt(51.0)-sqrt(M)*sqrt(27.5)-sqrt(N)*sqrt(0)))+(1-(((B*(x))/(B*(x)+(1-(x))))))*(27.5-72.8 + 2*(sqrt(O)*sqrt(21.8)+sqrt(P)*sqrt(51.0)-sqrt(O)*sqrt(27.5)-sqrt(P)*sqrt(0)))))

Below are the terms from the Matlab fitting equation and their descriptions:

$x = f_{M1}$

y = air/HD environment "switch" (If air environment, then y = 0; If HD environment, then y = 1)

$z = Cos(\theta)$

$B = \varphi$

$M = \gamma_{M1}$ (dispersive component)

$N = \gamma_{M1}$ (polar component)

$O = \gamma_{M2}$ (dispersive component)

$P = \gamma_{M2}$ (polar component)

For SBMA-DMAEMA system: The following arrays were the data used for analysis of the g-p[(SBMA)-ran-(DMAEMA)] ARGET copolymerization system.

SBMA_fraction = [0 0.25 0.5 0.6 0.7 0.75 0.8 0.5 0.6 0.7 0.8 0.85 0 0 0.6 0.7 0.8 0.6 0.7 0.8 0.9 0.85 0.9 0.9 0 0];

HD_switch = [0 0 0 0 0 0 0 0 0 0 0 0 0 0 0 0 0 0 0 1 1 1 1 1 1 1 1 1];

Cos_theta = [0.087155768 0.069756499 0.139173125 0.430511114 0.72537438 0.766044451 0.824126194 0.438371164 0.559192917 0.737277345 0.913545461 0.974370066 0.190809018 0.173648201 0.477158776 0.662620059 0.814115524 0.017452433 0.258819067 0.374606612 0.838670573 0.81915205 0.8703557 0.887010837 -0.529919233 -0.522498534];

Figure A.1. Screen-capture of the Matlab "Curve Fitting" application's fit of the g-p[(SBMA)-ran-(DMAEMA)] ARGET copolymerization system data.

For SBMA-MMA system: The following arrays were the data used for analysis of the g-p[(SBMA)-ran-(MMA)] ARGET copolymerization system.

monomerfrac_SBMA = [0.8 0.6 0.4 0.2 0.7 0 0 0 0 0 0.8 0.6 0.4 0.2 0.7 0 0 0 0 0 0.2 0.4 0.6 0.7 0.8 0.2 0.4 0.6 0.7 0.8]

Air_HD_Switch = [0 0 0 0 0 0 0 0 0 0 1 1 1 1 1 1 1 1 1 1 0 0 0 0 0 0 1 1 1 1 1]

Cos_Theta = [0.973379259 0.760405973 0.507538378 0.417338472 0.942641493 0.422618279 0.406736661 0.374606612 0.358367969 0.908143177 0.41469326 -0.139173072 -0.342020113 0.861629165 -0.233445334 -0.275637325 -0.275637325 -0.333806829 0.469471579 0.5948228 0.748955729 0.933580429 0.974370066 -0.333806829 0.160742589 0.44619783 0.866025408 0.902585288]
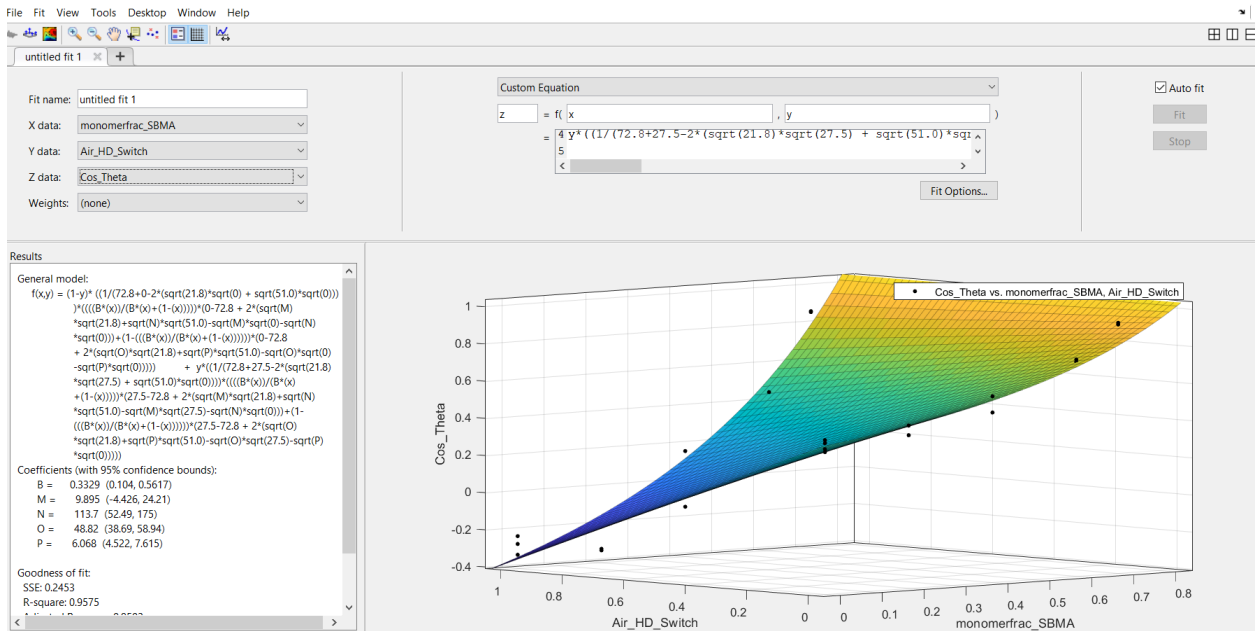
Figure A.2. Screen-capture of the Matlab "Curve Fitting" application's fit of the g-p[(SBMA)-ran-(MMA)] ARGET copolymerization system data.

For SBA-MMA system: The following arrays were the data used for analysis of the g-p[(SBA)-ran-(MMA)] ARGET copolymerization system.

monomerfrac_SBA = [0 0 0 0 0 0 0 0 0.4 0.9 0.2 0.6 0.2 0.5 0.7 0.85 0.9 0.4 0.9 0.2 0.6 0.2 0.5 0.7 0.85 0.9]

Air_HD_Switch = [0 0 0 0 1 1 1 1 0 0 0 0 0 0 0 0 0 1 1 1 1 1 1 1 1 1]

Cos_Theta = [0.422618279 0.406736661 0.374606612 0.358367969 -0.233445334 -0.275637325 -0.275637325 -0.333806829 0.503773992 0.981627184 0.615661488 0.737277345 0.453990516 0.713250458 0.923879535 0.984807754 0.990268069 -0.04361936 0.965925827 -0.317304626 0.317304677 -0.199367905 0.430511114 0.748955729 0.951056518 0.978147601]
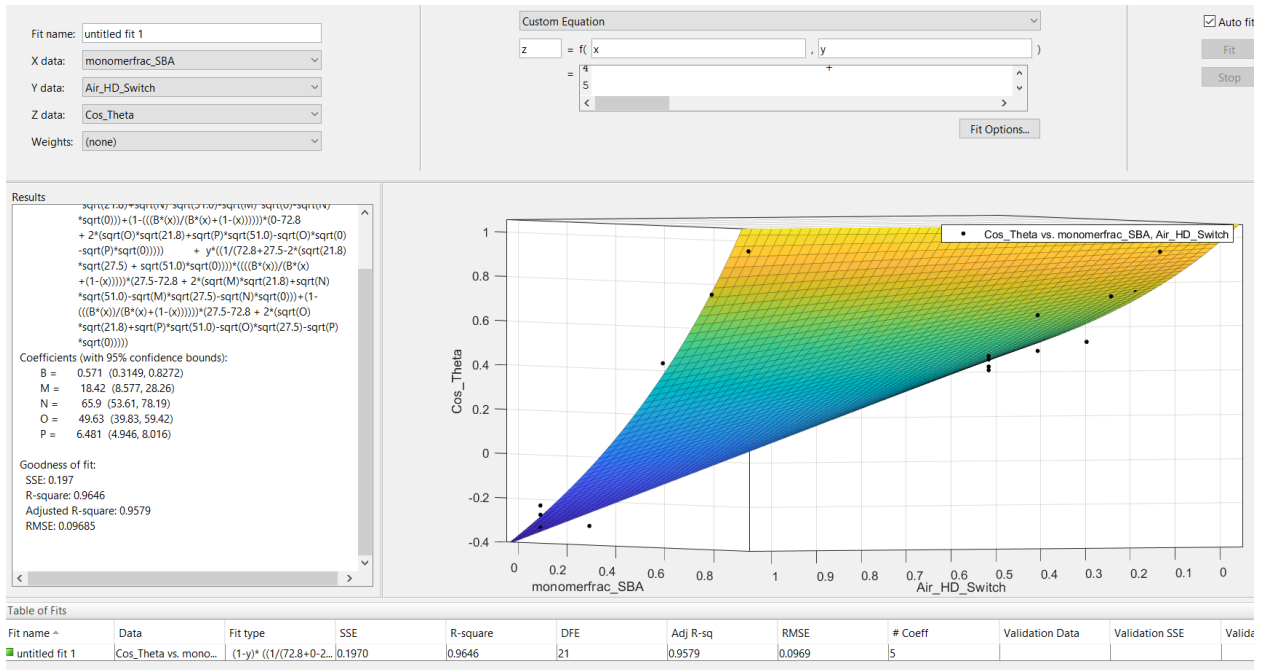
Figure A.3. Screen-capture of the Matlab "Curve Fitting" application's fit of the g-p[(SBA)-ran-(MMA)] ARGET copolymerization system data.

SUPPLEMENTARY INFORMATION FOR CHAPTER V
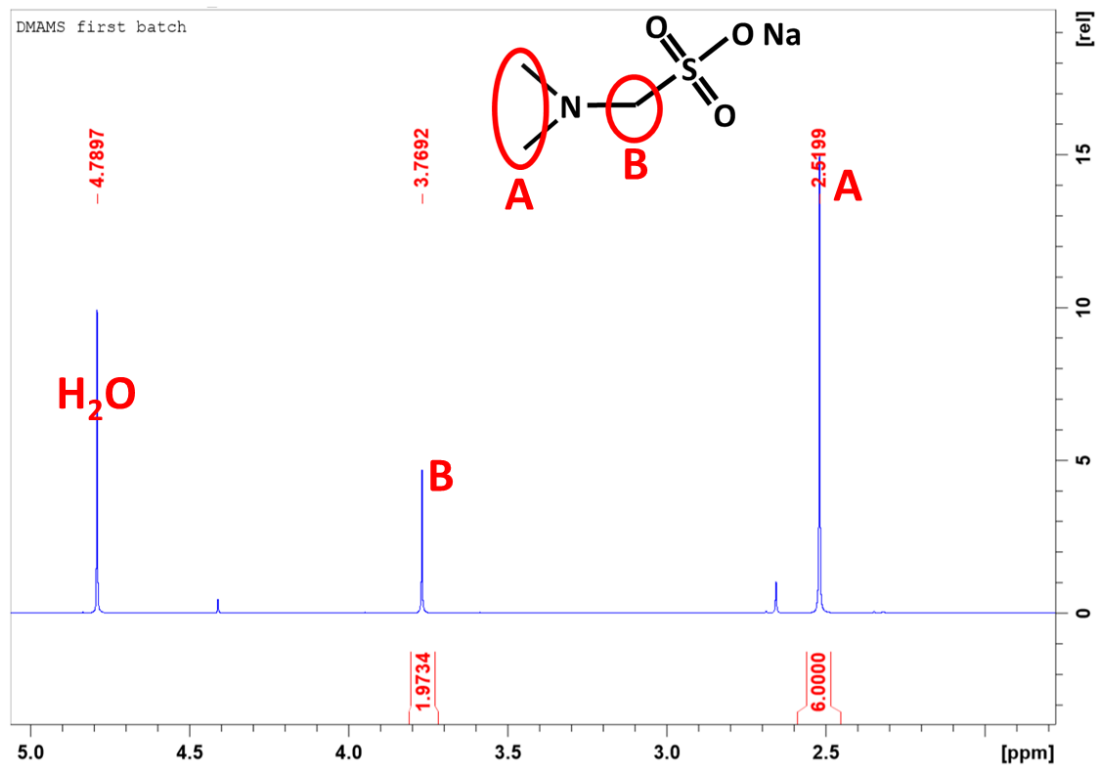
Figure B.1. NMR spectra of N,N-dimethylamino methanesulfonate (DMAMS).
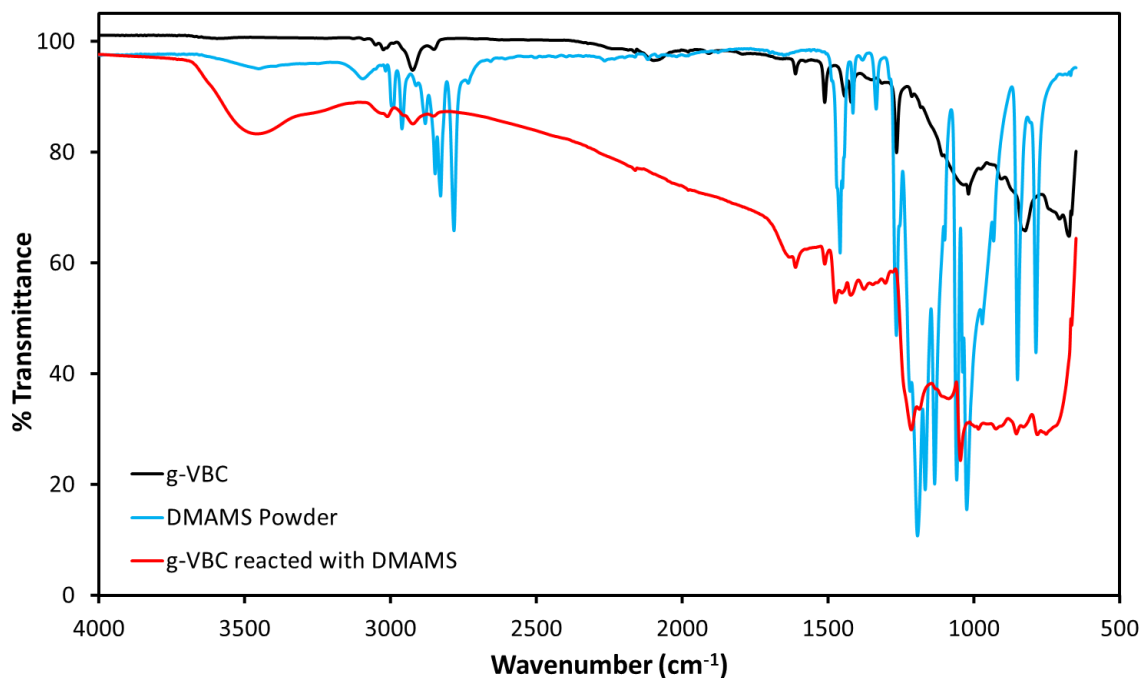
Figure B.2. FT-IR spectra of N,N-dimethylamino methanesulfonate (DMAMS). Also shown, an unmodified g-VBC surface and a DMAMS-modified g-VBC surface.
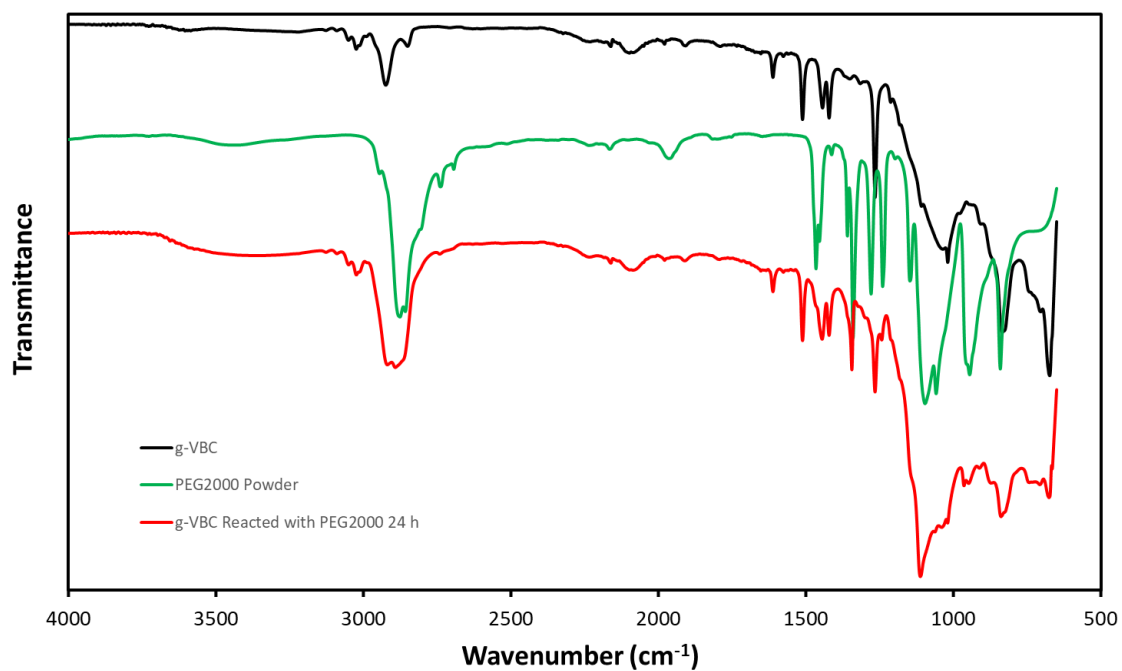
Figure B.3. FT-IR spectra of PEG2000-MME powder. Also shown, an unmodified g-VBC surface and a PEG2000-modified g-VBC surface.
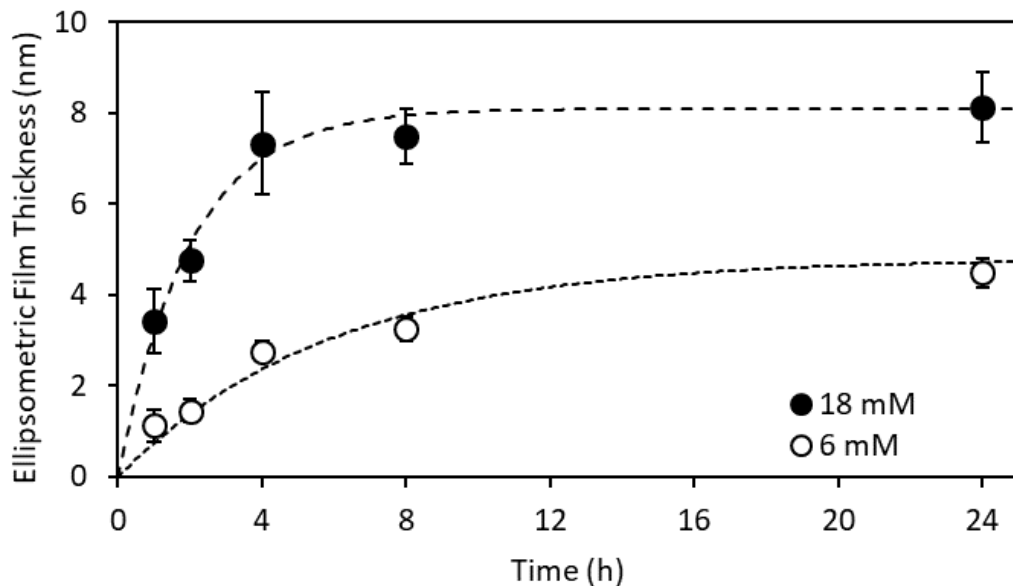
Figure B.4. Ellipsometric thickness results for PEG2000-modified g-VBC silicon substrates with varying reaction time. The reaction was conducted at two different concentration: 18 mM and 6 mM. The shown thickness values represent the difference in thickness of the g-VBC sample before and after PEG2000 substitution reaction. Note that the 18 mM experiments above were performed in triplicate (with 5 ellipsometric thickness measurements per sample), while the 6 mM data represents a single experiment (with 5 ellipsometric thickness measurements per sample).

SUPPLEMENTARY INFORMATION FOR CHAPTER VI
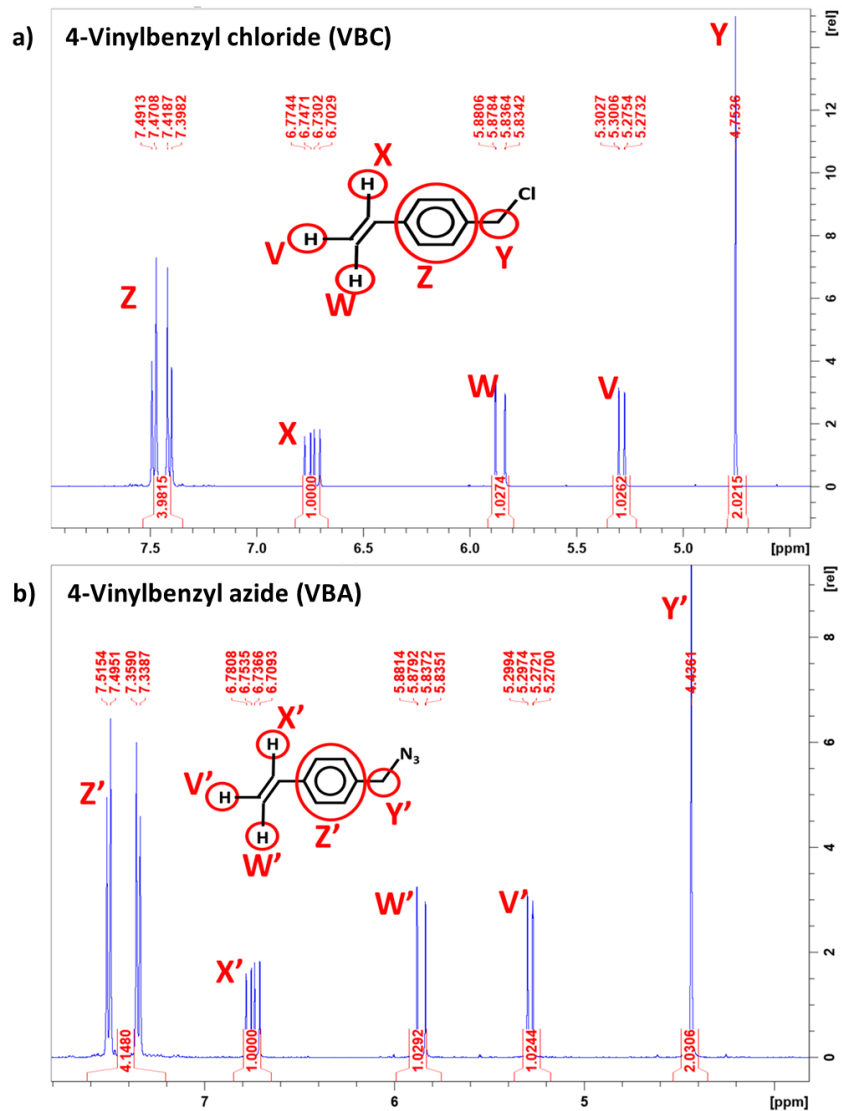
Figure C.1. a) NMR spectra of 4-vinylbenzyl chloride (starting material). b) NMR spectra of 4-vinylbenzyl azide (product).
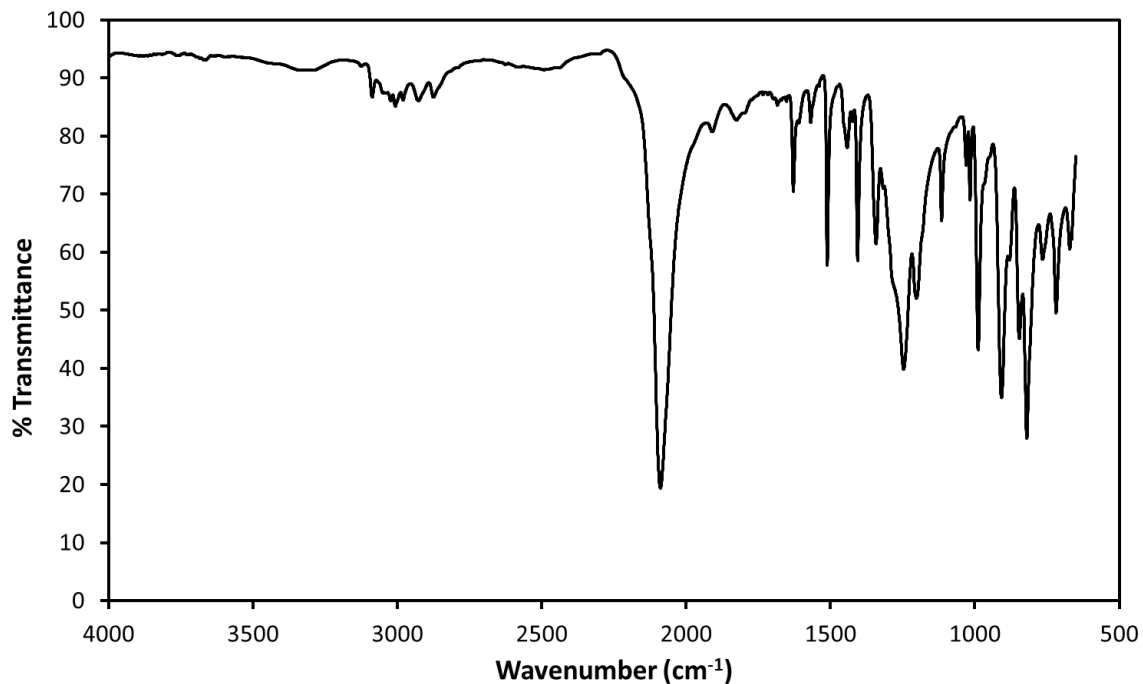
Figure C.2. FTIR spectra of 4-vinylbenzyl azide.
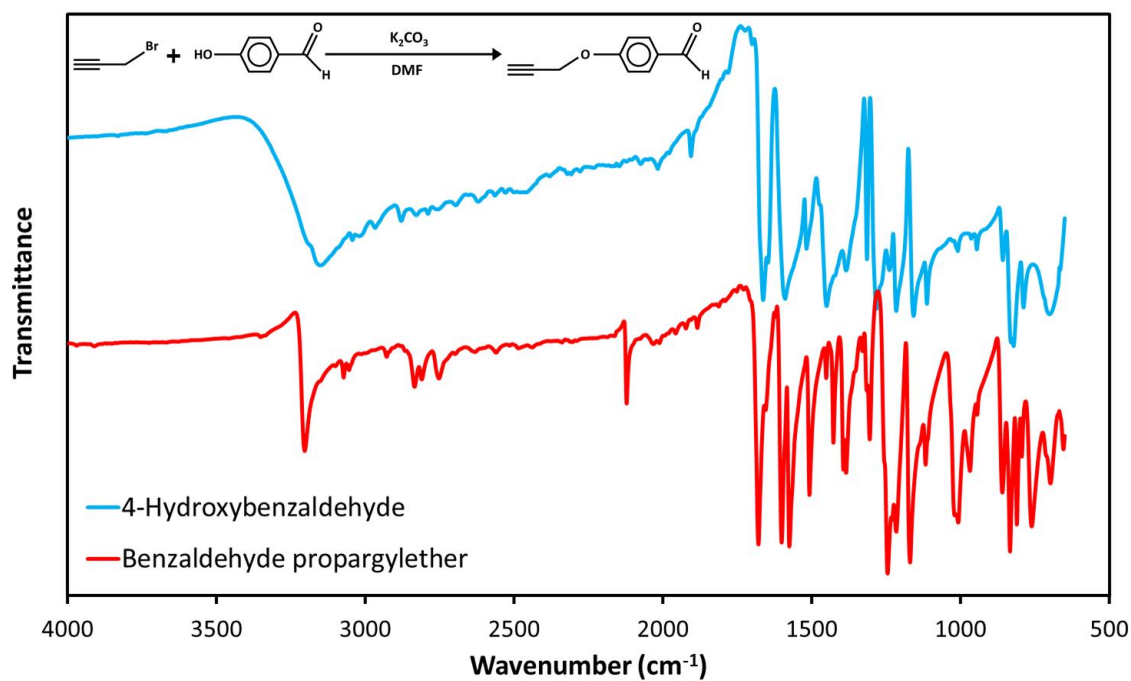
Figure C.3. FTIR spectra of 4-hydroxybenzaldehyde (starting material) and Benzaldehyde proparygylether (product).
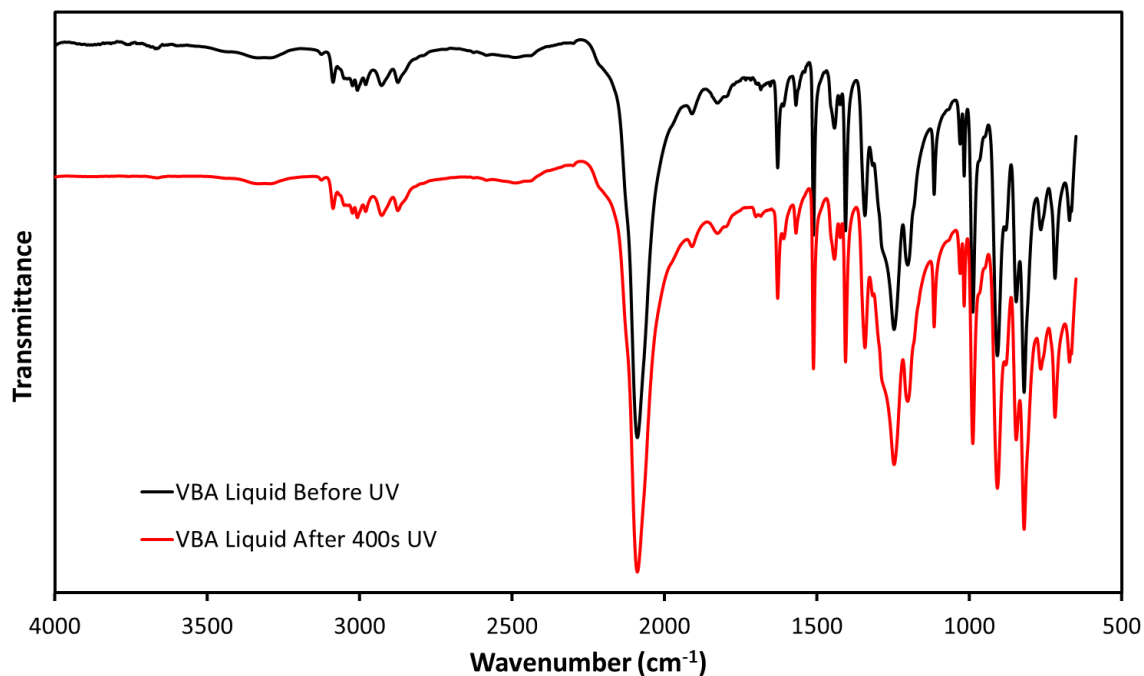
Figure C.4. Comparison of FTIR spectra of liquid 4-vinylbenzyl azide before and after 400 seconds of UV exposure.
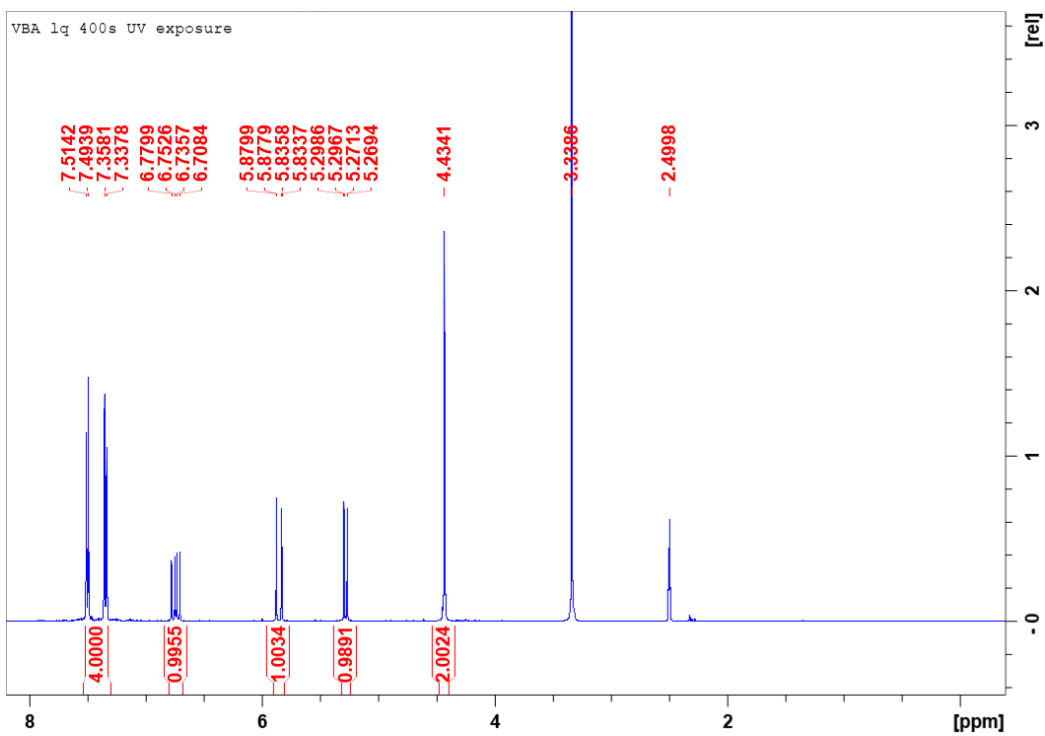
Figure C.5. NMR spectra of 4-vinylbenzyl azide after 400 seconds of exposure to UV.
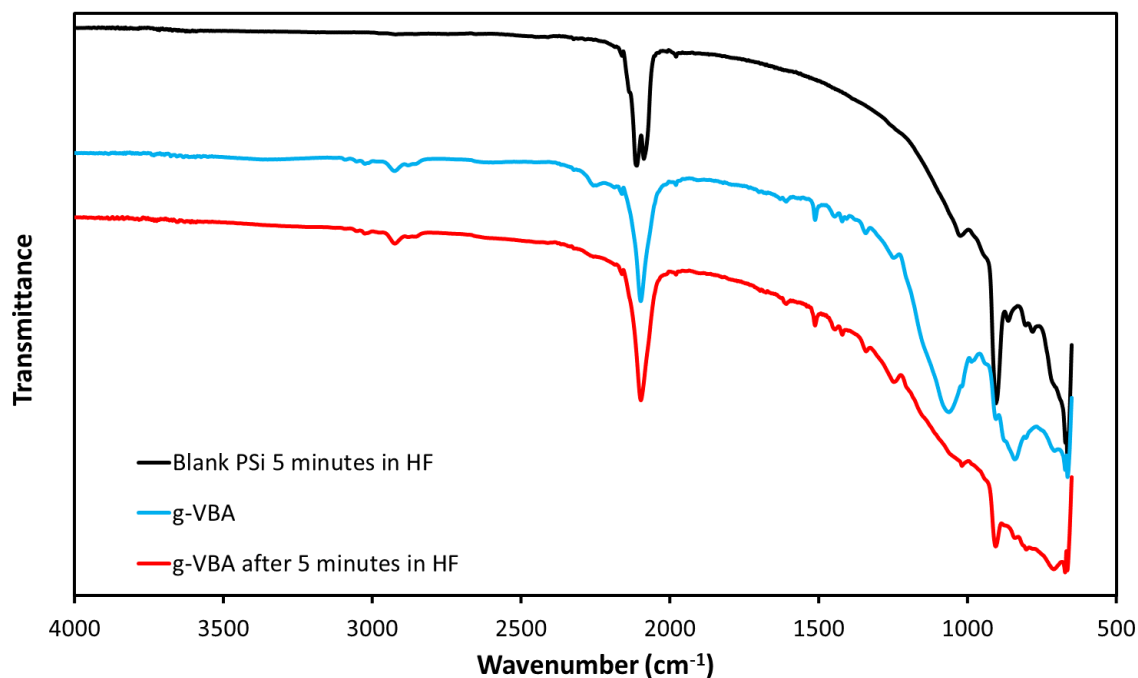
Figure C.6. Comparison of FTIR spectra of an HF-etched porous silicon surface before and after VBA attachment. To assess durability in HF, this PSi-g-VBA sample was also exposed to a 2.5% aqueous HF solution for 5 minutes.
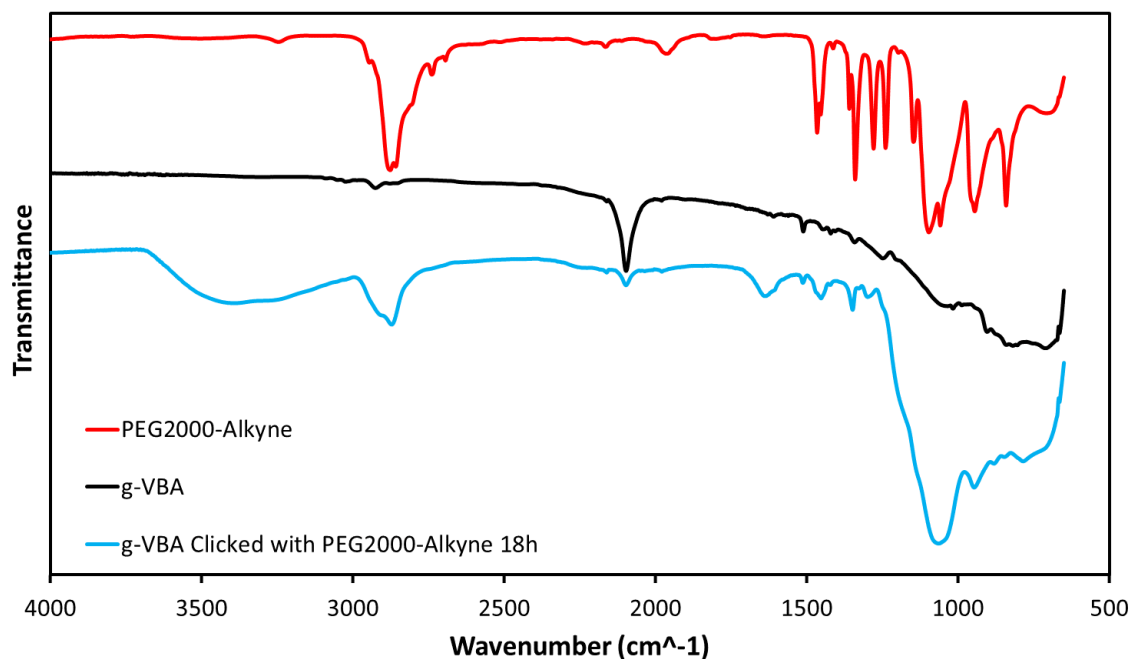
Figure C.7. Comparison of FTIR spectra of a PSi-g-VBA surface before and after click reaction with PEG2000-Alkyne. FTIR spectra of PEG2000-Alkyne powder is included for reference.
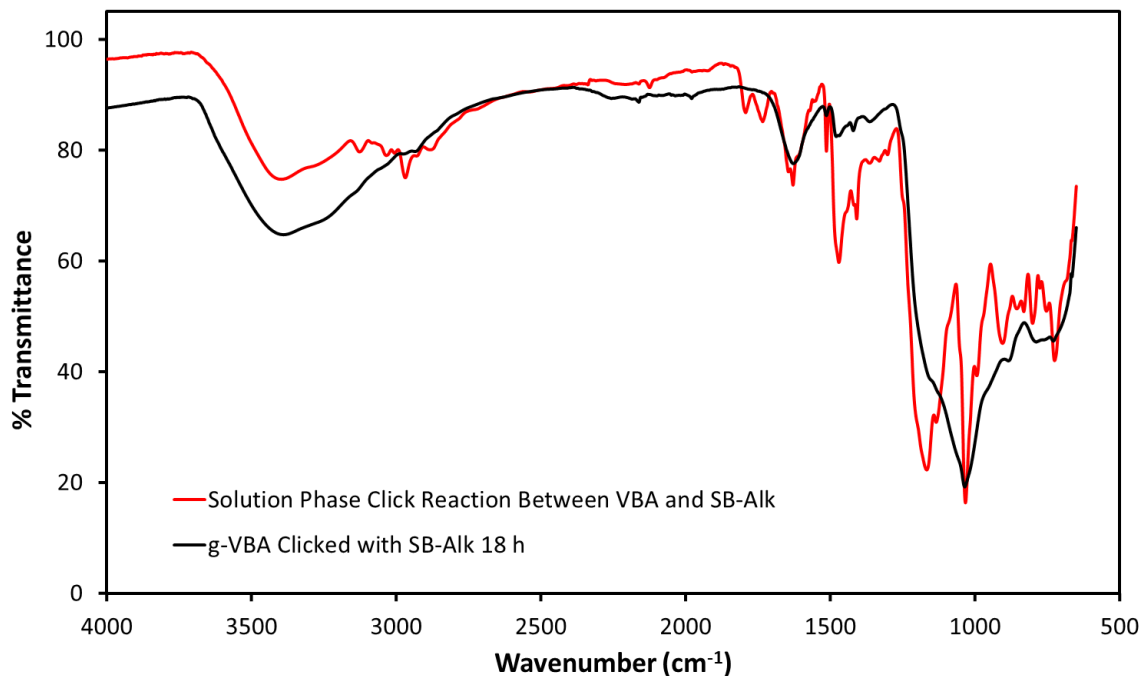
Figure C.8. Comparison of FTIR spectra of a PSi-g-VBA surface clicked with SB-Alkyne and the product of the liquid phase Click reaction of VBA and SB-Alkyne.
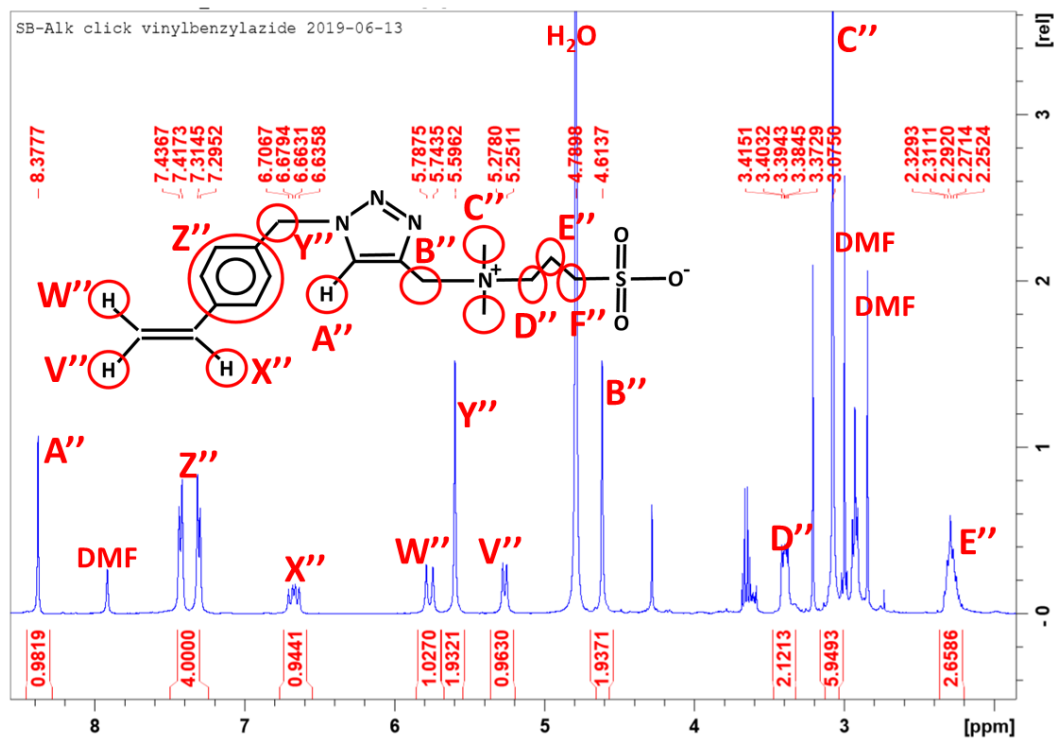
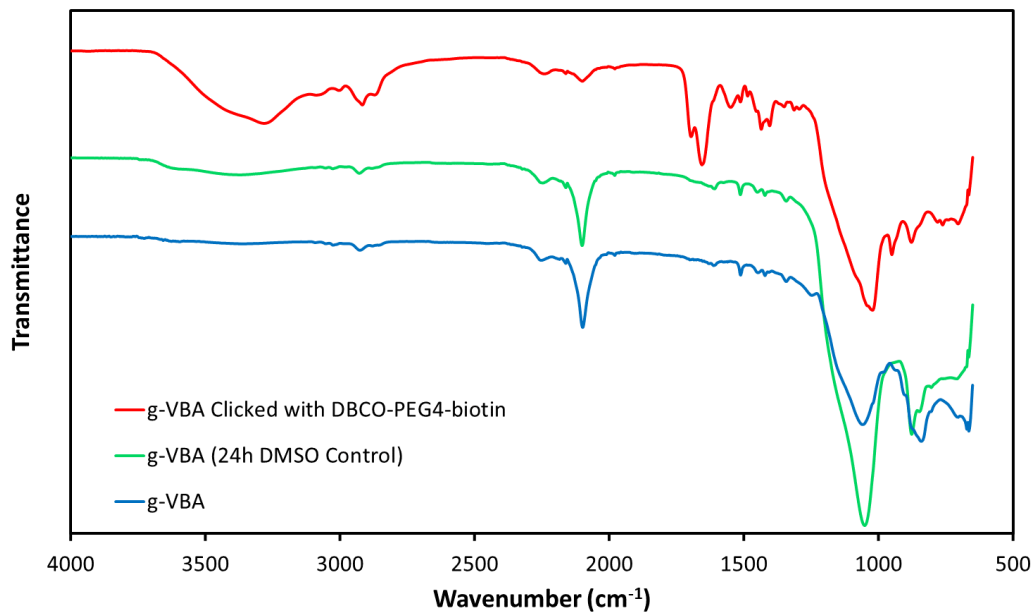**Figure C.9.** NMR spectra of SB-Alkyne.

Figure C.10. Comparison of FTIR spectra of a PSi-g-VBA surface before and after click reaction. An FTIR spectrum from a control experiment with the same reaction conditions, only omitting the DBCO-PEG4-biotin, is also included.
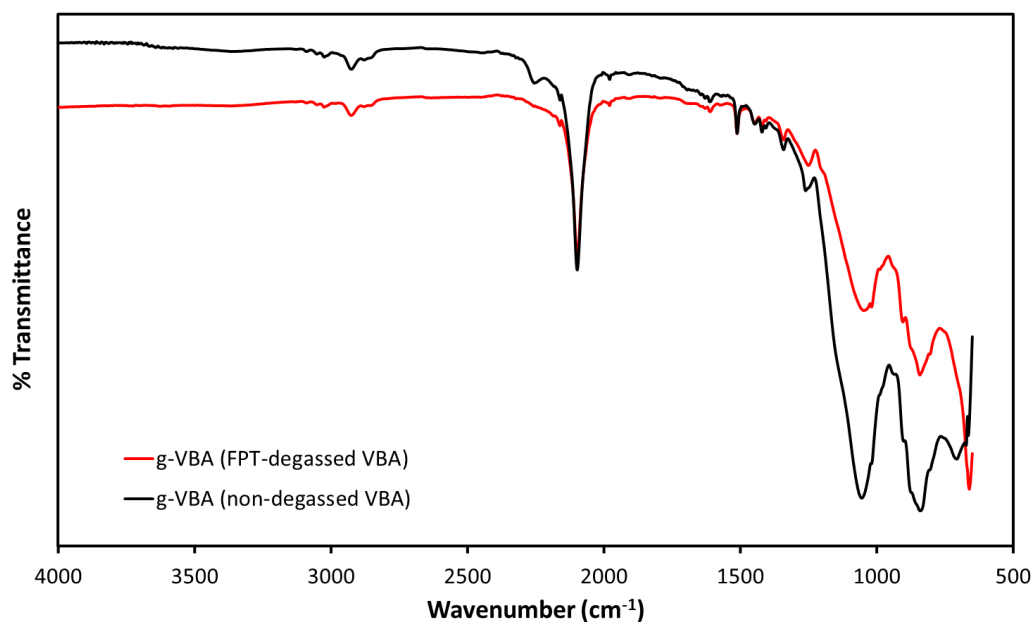

Figure C.11. Comparison of FTIR spectra of a PSI-g-VBA surfaces prepared with and without Freeze-Pump-Thaw degassing of the liquid VBA before UV exposure. (Note: the degassed spectra is scaled up to match azide peak size for easier comparison)
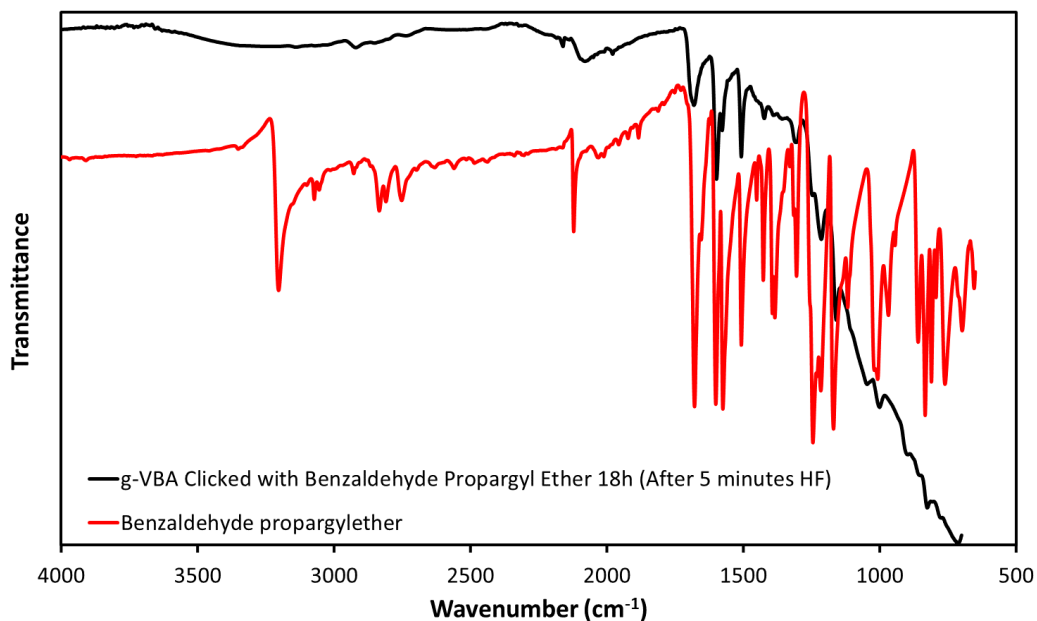
Figure C.12. FTIR spectra of a PSi-g-VBA reacted via Click chemistry with Benzaldehyde propargylether and then etched in HF for 5 minutes to remove oxidized silicon. This is compared to the FTIR spectra of Benzaldehyde propargyl ether.
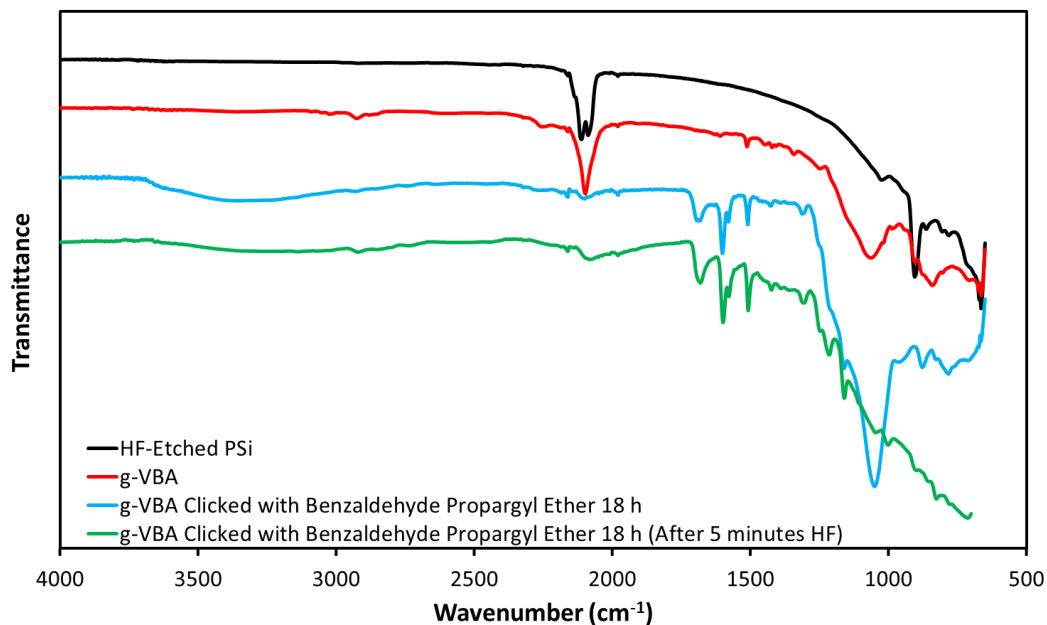

Figure C.13. FTIR spectra of a PSi-g-VBA before and after Click reaction with Benzaldehyde propargylether. This was then etched in HF for 5 minutes to remove oxidized silicon and analyzed again via FTIR. This is compared to the FTIR spectra of freshly HF-etched porous silicon.
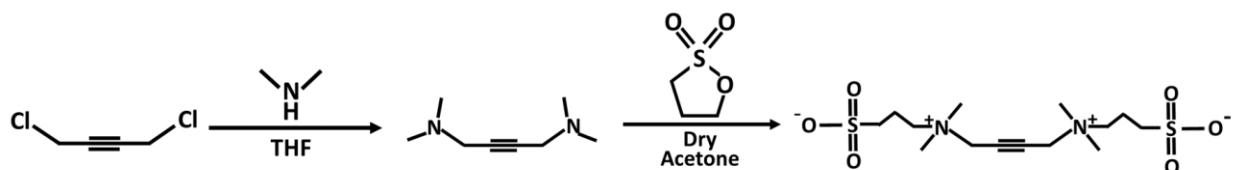
Figure C.14. Scheme for the synthesis of a dual-zwitterionic alkyne compound.

Synthesis Procedure for 1,4-Bis(dimethylamino)-2-butyne: This synthesis based upon the following

citations.[1-3] A three-neck flask was equipped with a reflux condenser, drop funnel, and stir bar as seen

below. The third neck of the RB flask was sealed via glass stopper. This apparatus was then purged with

nitrogen for at least 30 minutes with the nitrogen entering through the top of the condenser, flowing through

the 3-neck flask, and exiting through the top of the drop funnel. The nitrogen source line contained a "Y"

adapter before the condenser inlet for connection of a bubbler for maintaining a nitrogen atmosphere

throughout the following reaction steps. After the nitrogen purge, a septum was placed over the drop-funnel,

and the valve of the drop-funnel was then closed. Nitrogen flow was slowed to approximately 1-2 bubbles

per second through the bubbler upon sealing of the drop funnel. The reflux condenser was then chilled using

a cooled water circulator/pump containing a 50/50 mix of water and ethylene glycol. This cooling solution

for the condenser was maintained at -15 °C. (This subzero coolant temperature is to condense the volatile

dimethyl amine and prevent its loss from reaction apparatus.) Simultaneously the RB flask was pre-chilled

via ice bath. Once chilled, 76.5 mL of the 2M dimethylamine/THF solution (0.153 mol of dimethylamine)

was added into the RB flask through the 3rd neck and re-sealed via glass stopper. A solution of 3mL (0.031

mol) of 1,4-dichloro-2-butyne in 20mL of THF was prepared and injected into the drop funnel via syringe.

With stirring and over the ice bath, the 1,4-dichloro-2-butyne solution was dispensed from the drop funnel

over the course of 30 minutes. This was allowed to react for 4 hours while chilled via ice bath. The ice bath

was then removed and the mixture was allowed to reach room temperature and react for an additional 16

hours. The solution was then slowly heated (at a rate of approx. 10 °C per hour) to THF reflux and allowed

to react at reflux for 1 hour. The reaction mixture was allowed to cool back to room temperature, and the

THF was removed via rotary evaporation. The remaining contents of the flask were re-dissolved in 50 mL

of diethyl ether. This was poured over an aqueous solution of KOH (10g in 50mL water) in a separatory

funnel. After phase separation, the lower aqueous phase was collected and set aside. The upper ether phase

was then collected. The aqueous phase was then washed 4 times with diethyl ether (25 mL each) and then

all of the ether extracts were combined. The combined ether extracts were dried over K_2CO_3 for at least 30

minutes. The diethyl ether was removed via rotary evaporation. The product was collected with 2.574g
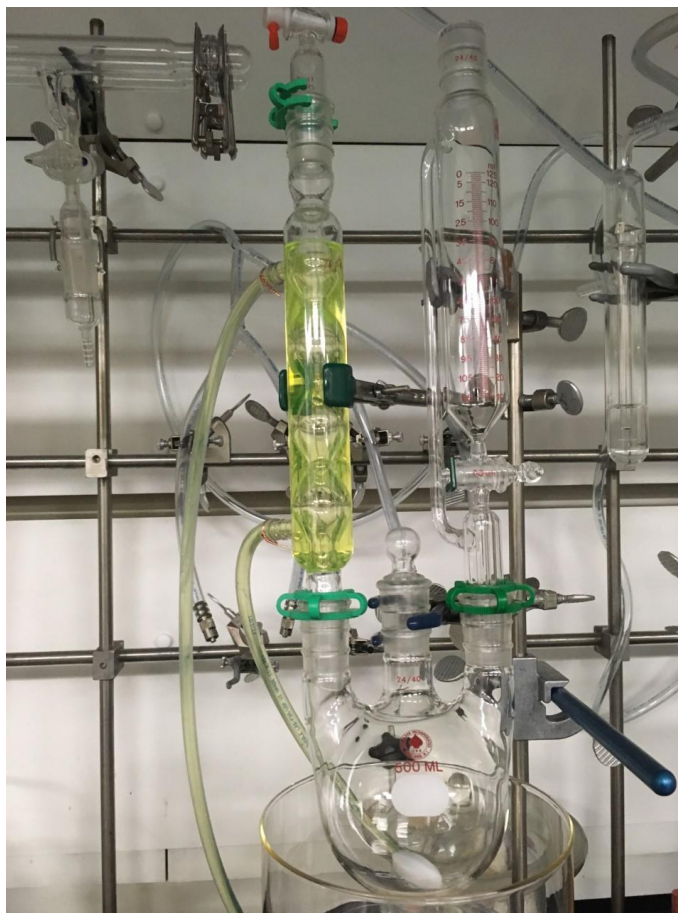
recovered (59.2% yield).

Figure C.15. Apparatus used for the synthesis of 1,4-bis(dimethylamino)-2-butyne.

Reaction of 1,4-Bis(dimethylamino)-2-butyne with 1,3-Propane sultone: To a RB flask, 2.22 g (15.8 mmol) of 1,4-bis(dimethylamino)-2-butyne was added and dissolved in 10 mL of dry acetone. In a separate flask, 4.25 g (34.8 mmol) of 1,3-propane sultone (1,3-PS) was added and dissolved in 15 mL of dry acetone. Both flasks were sealed and sparged with nitrogen. The 1,3-PS solution was then transferred via cannula to the first solution over the course of 30 minutes with stirring. This was allowed to react for 24 hours at room temperature. The product was collected via filtration, rinsed with an excess of acetone, and dried under vacuum. The product was collected with 4.25 g recovered (70.1% yield).
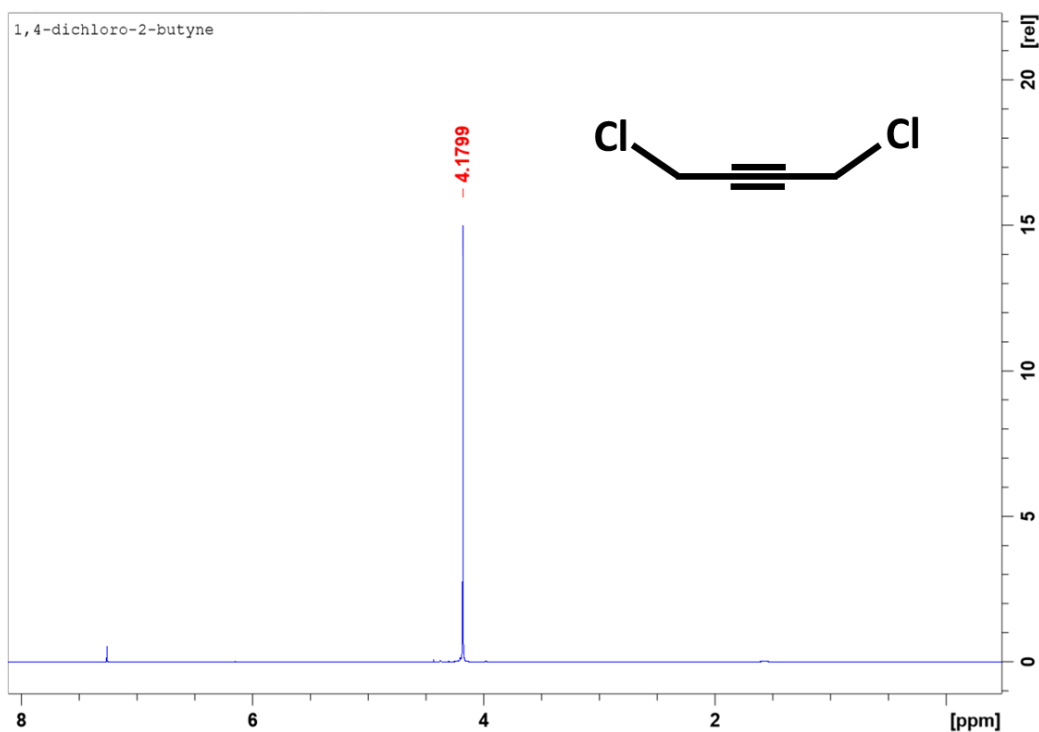

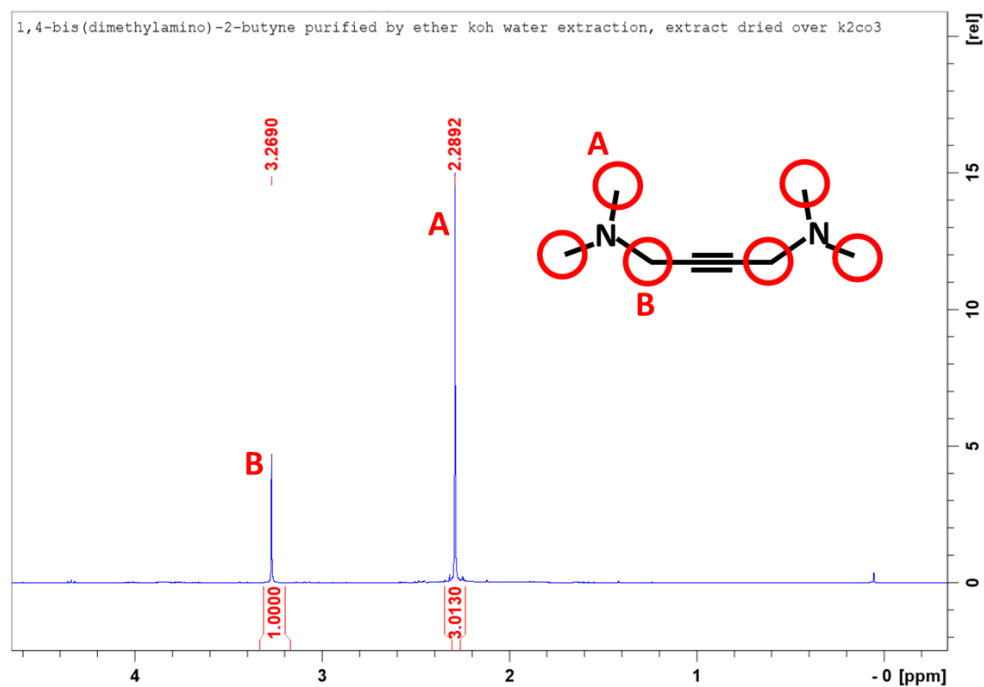**Figure C.16.** NMR spectra of 1,4-dichloro-2-butyne.

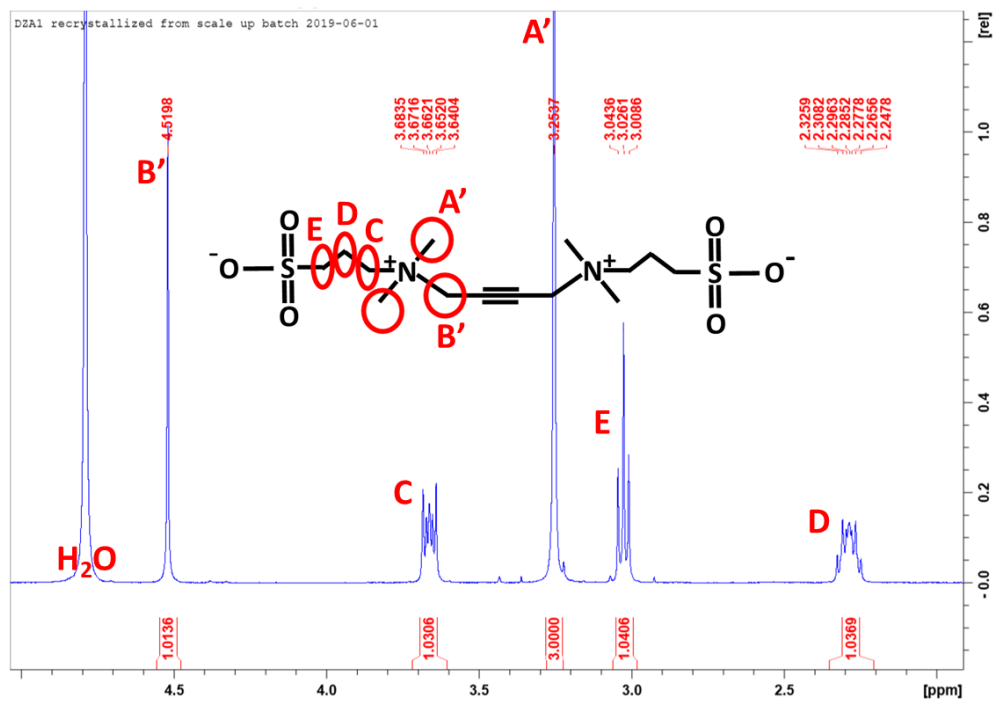**Figure C.17.** NMR spectra of 1,4-bis(dimethylamino)-2-butyne.

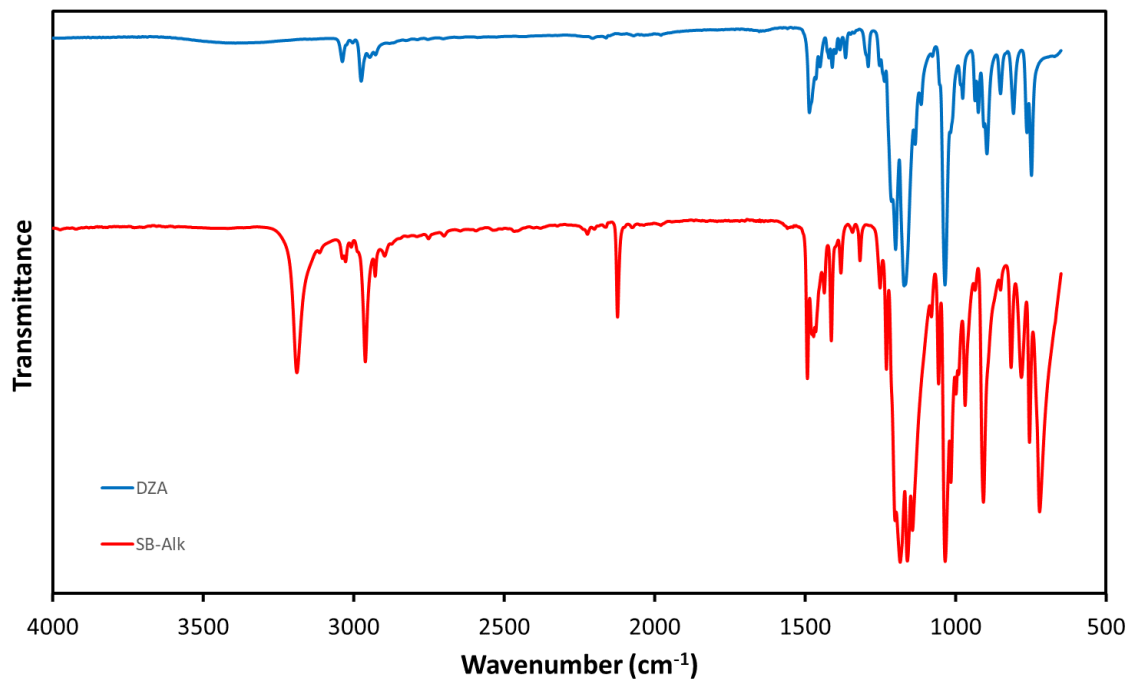**Figure C.18.** NMR spectra of the dual zwitterionic alkyne (DZA).

Figure C.19. Looking at the FTIR spectra for SB-Alk, a terminal alkyne, the peaks present at 3189 and 2123 cm^{-1} are associated with C-H and CΞC stretching respectively. As would be expected for an alkyne which is both internal and symmetric, these are not present in DZA.

Vial Number	Contents	Precipitation Observed?
1	- DZA (25mM)	NO
2	- DZA - NaAsc	NO
3	- DZA - $CuSO_4 \cdot 5H_2O$	YES
4	- DZA - $CuSO_4 \cdot 5H_2O$ - NaAsc	YES
5	- DZA - $CuSO_4 \cdot 5H_2O$ - NaAsc - PMDETA	YES

DZA : $CuSO_4 \cdot 5H_2O$: NaAsc : PMDETA
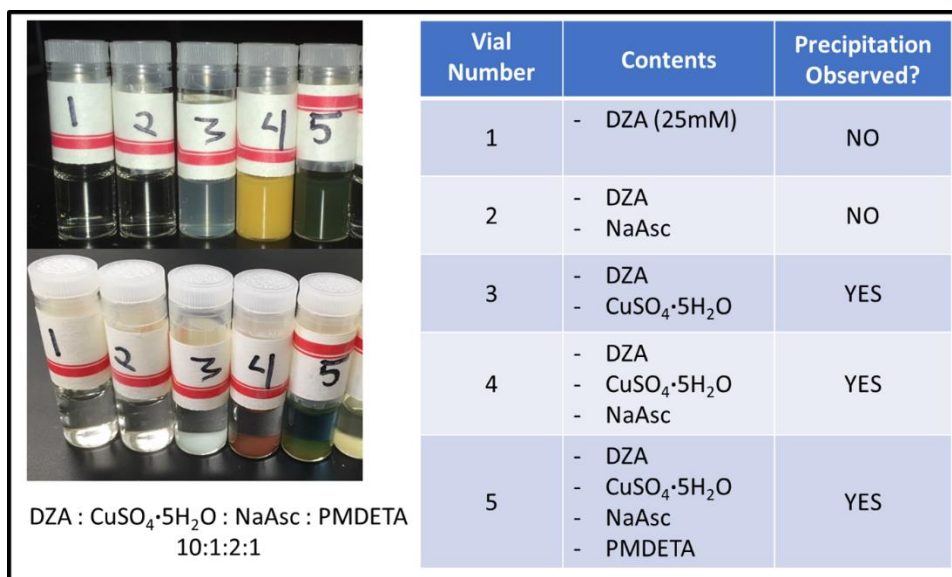10:1:2:1

Figure C.20. A summary of the conducted solubility experiments of 25 mM DZA mixtures in water. Note that the solutions all were comprised of the compounds typically used in our click chemistry reactions. The top image illustrates the state of the solutions at time of making/mixing. Meanwhile, the lower image illustrates the state of the solution after several hours. In all cases where DZA and the copper salt were both present, precipitation was observed.

References:

(1)   Barton, D. H. R.; Dawes, C. C.; Franceschi, G.; Foglio, M.; Ley, S. v; Magnus, P. D.; Mitchell, W. L.; Temperelli, A. A New Synthetic Approach towards Adriamycin. *J. Chem. Soc., Perkin Trans. 1,* **1980**, 643-647. https://doi.org/10.1039/P19800000643

(2)   Brandsma, L. *Preparative Acetylenic Chemistry.*, 2nd ed.; Elsevier Science, 1988. ISBN: 9780444429605.

(3)   Brandsma, L.; Verkruijsse, H. D. Synthesis of Acetylenes, Allenes and Cumulenes. In *Synthesis of Acetylenes, Allenes and Cumulenes*; Elsevier: Amsterdam, 1981. https://doi.org/10.1016/b978-0-12-125751-4.x5000-0.